Charles University

Faculty of Science

Study programme: Animal physiology

MUDr. Jakub Žiak

The role of CRMP2 in the nervous system development

Ph.D thesis

Supervisor: Mgr. Martin Balaštík, Ph.D

Prague, 2019

Dedicated to Katka, Saška and Max.

Declaration:

I hereby declare that the thesis has been written independently and with no other sources than quoted. Nor the thesis or its significant part has been used to get any academic degree.

Prohlášení:

Čestně prohlašuji, že práce ani její podstatná část nebyla předložena k získání jiného nebo stejného akademického titulu, byla zpracována samostatně a byly uvedeny všechny použité informační zdroje a literatura.

Jakub Žiak,
Prague, 2019

ACKNOWLEDGMENTS

Experiments may only work if the experimental conditions are balanced perfectly. This work would not have been possible without help and support from many people I had been fortunate to meet.

First, I want to express my gratefulness towards my wife Katka for her endless patience and encouragement. The plentiful source of happiness and fun are our kids, Saška&Max, especially important for mind refreshment. I also want to thank to my parents for their continuous support and preyers.

I believe I could hardly find better place to do my Ph.D then Martin Balastik's laboratory. Martin created a genuine and communicative environment for sharing and testing knowledge and ideas. I am grateful to Romana Weissova and Marie Kleisnerova, Martin's first students, for their advices and for sharing experimental protocols. I am grateful to Barbora Pukajova for teaching me *in utero* electroporation technique. I also want to thank Peter Buran for his inspiration. It's been a great time in this lab.

Special thanks belong to our collaborators from Israel and France, namely Roy Maimon, Eran Perlson, Magda Magiera and Carsten Janke. I was happy to collaborate with Martina Janikova, Tomas Petrasek and Ales Stuchlik from Institute of Physiology who tested behavior of our mice. I also thank to dr. Vyklicky for gene gun, dr. Palecek for vibratome and dr. Krusek for assistance with glass capillary preparation.

Solving a lot of scientific questions in neurobiology require advanced microscopy techniques. I am happy that in imaging facilities of both Institute of Physiology and Institute of Molecular Genetics there are helpful people with a great expertise. I want to thank Ivan Novotny, Ondrej Horvath, David Vondrasek and Daniel Hadraba for their kind assistance.

Finally, there are many almost invisible individuals yet crucial for doing science. I would like to thank to folks from animal facilities of both Institute of Physiology and Institute of Molecular Genetics and Zuzana Soukupova for her help with GAUK administration.

I would also like to thank to Charles University Grant Agency as this work was partially funded by GAUK no. 682217.

Abstract

Regulation of axon guidance and pruning of inappropriate synapses is key to development of neural circuits. Secreted semaphorins are integral part of both processes. Collapsin response mediator protein 2 (CRMP2) has been shown to regulate axon guidance by mediating Semaphorin 3A (Sema3A) signaling, however, nothing is known about its role in the synapse pruning. Similarly, it is also not known if CRMP2 mediates signals from other semaphorins. We herein studied CRMP2 protein and revealed its role in growth and pruning of selected axons and dendrites. In newly generated *crmp2*$^{-/-}$ and *crmp2a*$^{-/-}$ mice we demonstrate that CRMP2 has a moderate effect on Sema3A-dependent axon guidance *in vivo*, and its deficiency leads to a mild defect in axon guidance in peripheral nerves and corpus callosum. CRMP2A isoform is specifically involved in development of callosal axons. Surprisingly, we show that *crmp2*$^{-/-}$ mice display prominent defects in stereotyped axon pruning in hippocampus and visual cortex and altered dendritic spine remodeling, which are consistent with impaired Sema3F signaling and with models of autism spectrum disorder (ASD). Indeed, we demonstrate that CRMP2 mediates Sema3F signaling in primary neurons and that *crmp2*$^{-/-}$ mice display ASD-related social behavior changes in early postnatal period as well as in adults. Together, we demonstrate that CRMP2 mediates Sema3F-dependent synapse pruning and its dysfunction shares histological and behavioral features of ASD.

Abstrakt

Regulácia navádzania axónov a remodelácie synapsií je kľúčová pre vývoj nervových spojení. Semaforíny sekretované do prostredia sú neoddeliteľnou súčasťou oboch procesov. Proteín CRMP2 reguluje navádzanie axónov ako mediátor signalizácie semaforínu 3A (Sema3A), avšak nie je známe nič o jeho úlohe pri synaptickom pruningu, rovnako ako nie je známe, či je súčastou signalizácie iných semaforínov. V tejto práci sme študovali proteín CRMP2 a popísali sme jeho úlohu v raste a pruningu špecifických axónov a dendritov. Na mutantných *crmp2*$^{-/-}$ and *crmp2a*$^{-/-}$ myšiach demonštrujeme, že CRMP2 má mierny vplyv na navádzanie axónov regulovaných pomocou Sema3A *in vivo,* a že jeho nedostatok vedie k miernemu defektu navádzania axónov v periférnych nervoch a corpus callosum. CRMP2A izoforma sa špecificky podieľa na vývoji kalosálnych axónov. Prekvapivo sme zistili, že *crmp2*$^{-/-}$ myši majú značné defekty v stereotypickom pruningu axónov v hippocampe a zrakovej kôre a nedostatočnú remodeláciu dendritických tŕňov. Tieto defekty sú v súlade so zhoršenou Sema3F signalizáciou a modelmi autistického spektra (ASD). Potvrdili sme, že CRMP2 sprostredkuje signalizáciu Sema3F v primárnych neurónoch a že *crmp2*$^{-/-}$ myši vykazujú zmeny sociálneho správania súvisiace s ASD v skorom postnatálnom období, ako aj u dospelých. Celkovo demonštrujeme, že CRMP2 sprostredkuje Sema3F-riadený pruning synapsií a jeho dysfunkcia má histologické a behaviorálne znaky ASD.

Table of contents

1. Introduction

86 000 000 000. With a higher precision – 86.1 +/- 8.1 billion. This represents the total number of neurons in the human brain as calculated by Azevedo et al. 10 years ago (Azevedo et al., 2009). Estimated number of synapses – only in the cortex – is about 164 trillion (Jin et al., 1996). Even more astonishing fact than counts of neurons and synapses is that neuronal connections are not random, but precisely regulated. This extraordinary arrangement of the brain allows us to move, think, feel or write the thesis. How neurons interconnect themselves, how axons and dendrites are guided to their targets and how the neuronal network is maintained and refined are the big questions in neuroscience.

The growing tip of the axon, the growth cone, contains molecular machinery that translates extracellular signals into changes in cytoskeleton – as a consequence the growth cone may grow, turn or stop. In the first few decades of the 20th century neuroscientists suggested that growth of axons is regulated by mechanical forces from surroundings. This so called mechanistic theory was mostly based on observations from *in vitro* experiments (e.g. axons tended to grow in dents in a dish). In 40s, however, chemoaffinity theory was proposed after Sperry's experiments with a frog eye (the concept is reviewed in (Sperry, 1963)). In his experiments, neurons from a given eye quadrant always grew into their original targets in tectum, despite the surgical eye rotation (Fig 1).

In the next decades, neuroscientists were searching for such molecules that are capable to dictate axons were to grow. Finally, just few decades ago, four main classes of so called axon guidance molecules or cues were identified: Semaphorins, Netrins, Ephrins and Slits (Kolodkin and Tessier-Lavigne, 2011). They can be either secreted in exracellular space or bound to a membrane of cells surrounding the growth cone (Tessier-Lavigne and Goodman, 1996). The membrane of the growth cone possesses receptors for a given guidance cue(s). Signals from receptors are mediated through various kinases and small G proteins and finally change cytoskeletal dynamics.

Studying the principles of axon guidance is vital for understanding the pathophysiology of neurodevelopmental disorders with specific defects in axon and dendrite development as epilepsy, autism spectrum disorder, schizophrenia or a group of rare yet devastating syndromes (e.g. lissencephaly, polymicrogyria, Aicardi syndrome).

In this thesis, we studied the component of Semaphorin pathway, the protein named „collapsin response mediator protein 2" (CRMP2). Using newly developed mouse models of CRMP2 deficiency and multiple *in vitro*/*ex vivo* experiments, we provide evidence that CRMP2 regulates axon and dendritic spine rearrangements in the brain and its deletion associates with developmental behavioral defects in mice.

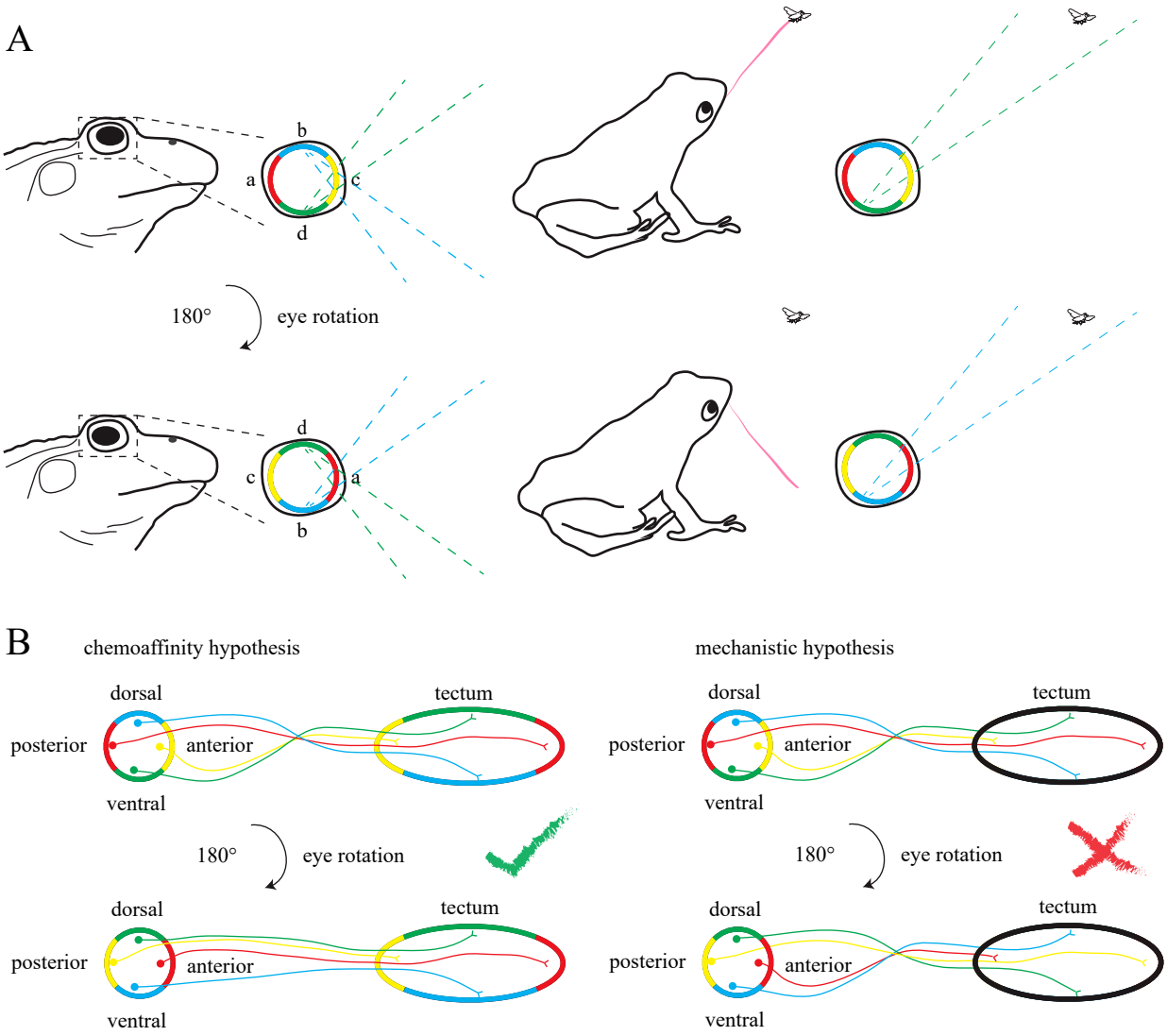

Figure 1. Sperry's experiments support chemoaffinity hypothesis. (A) Optic nerve regenerates well in frogs. In the experiment, eye was surgically rotated and after healing, behavioral responses were tested. The frog without rotated eye sees the fly in the air and catches it. After rotation, however, fly image is presented to the eye quadrant that has originally been responsible for the bottom of the visual field (the blue "b" segment of the eye). As a result, frog is trying to catch the fly on the ground. (B) The experiment tested whether axons are guided either by chemical substances in surrounding environment (chemoaffinity hypothesis) or by the varying tissue stiffness (mechanistic hypothesis). In the case of chemoaffinity hypothesis, axons would always target the same part of the tectum despite the eye rotation and as a result, representation of the visual field is also rotated. In the case of mechanistic hypothesis, axons would always grow by the path that interconnects respective regions of eye and tectum thus preserving the visual field. Observations from eye rotation experiments is in line with the chemoaffinity hypothesis. (modified after Kandel, ER. *Principles of Neural Science*, 5th ed.)

1.1 Patterning of the cerebral cortex

Cerebral cortex is a six-layered structure that originates from telencephalic vesicle. Cells migrate into the cortical wall (developing cortex) from embryonic day 11.5 (E11.5) to E18.5 (Dehay and Kennedy, 2007). Neurons in each cortical layer contain specific set of transcription factors that determine their fate (Molyneaux et al., 2007b, Arlotta and Pasca, 2019). The main input into cortex comes from thalamus that sorts relevant information and prevents from information overload. Axon projections from cortex include intrahemispheric collaterals, transhemispheric (callosal) projections into contralateral hemisphere and subcortical projections into many targets in CNS (thalamus, superior colliculus, spinal cord, etc.) (Molyneaux et al., 2007a).

Neurogenesis, neuronal migration

Neural plate, the embryonic precursor of the nervous system, contains just few hundred cells. It is clear that a massive proliferation is required to create billions of neurons. The major regions involved in the neurogenesis (production of neural cells) are small areas surrounding the ventricles, so called ventricular (VZ) and subventricular zones (SVZ) (Dehay and Kennedy, 2007). Cells residing there divide by symmetric or asymmetric divisions. Symmetric division causes expansion of the population of progenitors while asymmetric division produces one cell with properties of a stem cells and second, differentiated cell (Dehay and Kennedy, 2007).

During development, two main classes of neurons – excitatory and inhibitory – populate the cortical plate. Excitatory neurons originate either directly from radial glial cells (RGC) or from multipolar basal intermediate progenitors after asymmetric division (Campbell and Gotz, 2002, Namba et al., 2015). RGCs have a typical shape: cell body is located in the ventricular zone and the processes are attached to ventricular or pial surface, respectively (Fig. 2). The long, apical process serves as a scaffold for migrating neurons that originate in the ventricular zone. Beside this function in neuron migration, RGCs are also precursors of both neurons and astrocytes (Campbell and Gotz, 2002). Signals that direct RGC to differentiate into neurons or astrocytes include Delta-Notch signaling pathway (Grandbarbe et al., 2003). After Delta binding to Notch, cytoplasmic domain of Notch is cleaved and transported into nucleus. Newborn cells shift to multipolar stage and migrate randomly in the intermediate zone. Next, neurons undergo multipolar-to-bipolar transition and begin radial migration into the cortical plate, using radial glial cells as a scaffold. Transition to the bipolar stage is regulated by transcription factors (e.g. LIS1, DCX) and various cytoplasmic effectors and leads to cytoskeletal rearrangements (Shu et al., 2004). Early-born neurons migrate into deepest layers, which can be well documented by the *in utero* electroporation (Fig. 2C). The six-layered cortex thus forms in an inside-out manner.

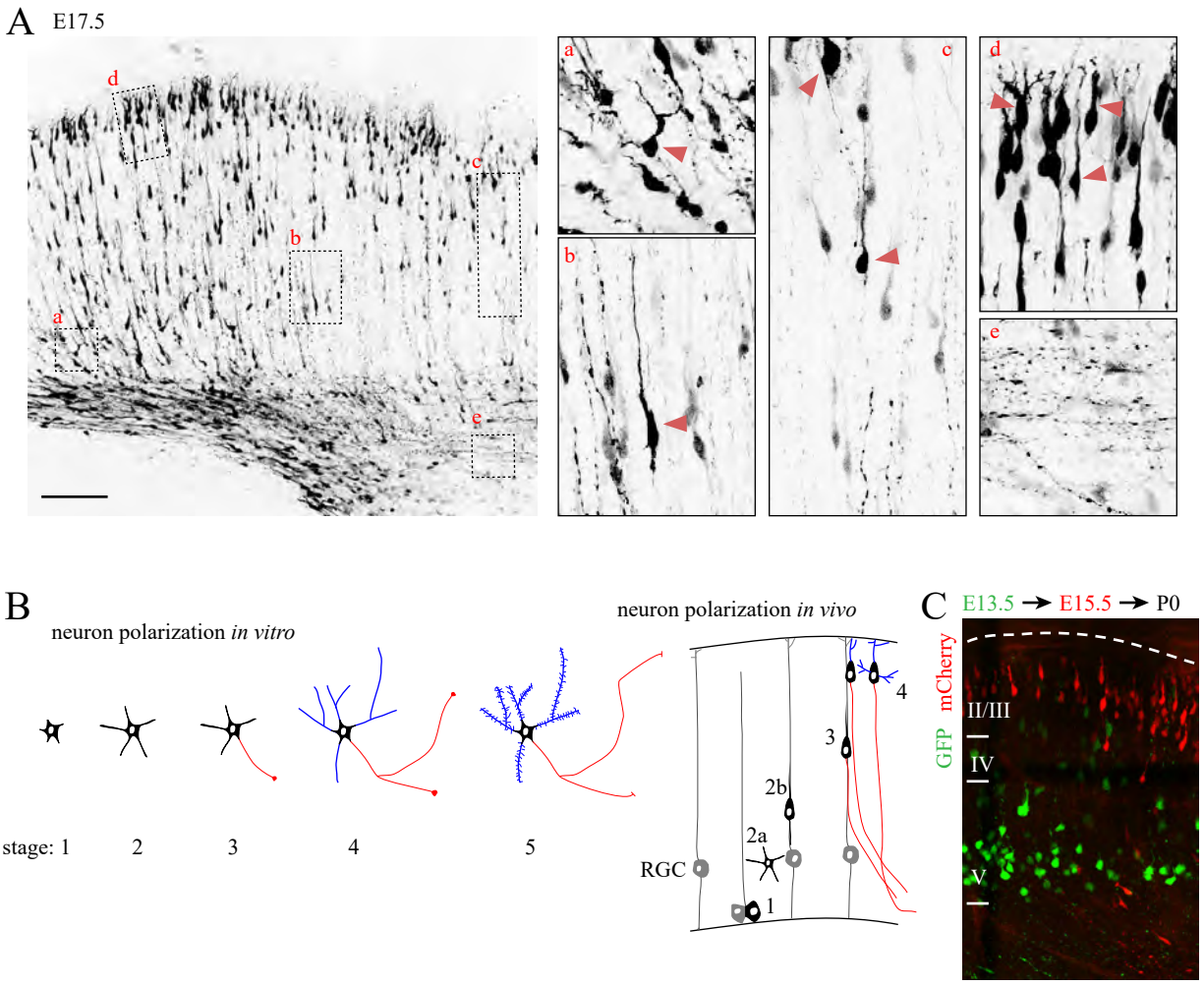

Figure 2. Neuronal polarization and axon initiation. One of the most important experimental approaches that significantly increased our knowledge about cortical development is the *in utero* electroporation technique. With this method, neural progenitor cells are randomly electroporated in the cortical ventricular zone by GFP expressing plasmid allowing to trace their future development. (A) Embryos electroporated at E14.5 were analyzed for neuronal migration two days later (E17.5). Different stages of neuron polarization can be observed (arrowheads). There are neurons at multipolar stage (a), bipolar migrating neurons (b), bipolar neurons with established axons that start to grow (c) and neurons in their final position in the upper layer where dendrites are visible (d). Growing axon tracts are also visualized (e). (B) Comparison of neuron polarization *in vitro* and *in vivo*. Left, *in vitro* situation. In stage 1, cells have multiple unspecific protrusions. These protrusions elongate (stage 2) and one of them later differentiate into axon (red, stage 3). In stage 4, other neurites become dendrites (blue), axon continues to grow and creates collaterals. Synapse formation at stage five is accompanied by generation of dendritic spines. Right, situation *in vivo*. Assymetric division of RGC generates another RGC and a neuron. Multipolar (2a) and further bipolar shape (2b) represents stage 2 *in vitro*. Other stages are similar. (C) Sequential *in utero* electroporation was performed at E13.5 (GFP) and E15.5 (mCherry) and brains were isolated after birth (P0). Later born neurons electroporated with mCherry migrate into the upper layers.

Inhibitory neurons are born in ganglionic eminences and originate from intermediate progenitors and subapical progenitors. These neurons migrate tangentially over long distances and then switch to radial mode of migration and populate cortical plate (Polleux et al., 2002). Neuronal migration control requires variety of signals that regulate the actin and microtubule cytoskeleton. For example, Slit1 and Netrin1 repel migrating interneurons from ganglionic eminences and neuregulin 1 attracts them (Stanco et al., 2009). The change from tangential to radial migration is regulated by Sonic hedgehog (SHH) gradient. Interestingly, interneurons use their primary cilia as a SHH detectors (Baudoin et al., 2012).

During radial migration, neurons interact with extracellular matrix and surrounding cells. Together with diffusible molecules that create gradients, these are cues that navigate neurons into appropriate position. Beside radial glial cells, there are other transient cell populations regulating migration: Cajal-Retzius cells (CR) and subplate neurons (SP) (Gil et al., 2014, Hoerder-Suabedissen and Molnar, 2015). Both of these neuronal classes emerge in the cortex before the migration starts, at E10.5. CR cells cover the surface of the cortical wall and SP neurons sit above the proliferative zone. SP neurons make transient glutamatergic synapses with migrating multipolar neurons – activation of NMDA receptors increases Ca^{2+} intake into multipolar neurons and participates in bipolar transition. CR cells are the source of reelin (Rugarli and Ballabio, 1995) that at its highest concentration instructs neurons to stop. Deletion of reelin in mice (mutant mouse *reeler*) causes severe lamination defects (Goffinet, 1984). Additionally, CR cells express nectin1 (adhesion molecule) which binds to nectin3 expressed by migrating cortical neurons. Nectin1 and nectin3 mediate interaction between CR cells and the leading processes of migrating neurons (Gil-Sanz et al., 2013).

Axon specification, growth, branching and differentiation

Specification of dendrites and axons starts already during migration. We can divide axon development into three main steps: 1) axon specification during neuronal polarization, 2) axon elongation and guidance, and 3) formation of branches and presynaptic differentiation (Lewis et al., 2013). As an example, we will follow the development of callosal axons since their growth is well described in rodents. Figure 3 demonstrates individual steps of callosal axon targeting as we have observed in our longitudinal *in utero* electroporation experiments. Neurons born at E15.5 in mice migrate into cortical layer 2/3. At E18.5, migration is finished and axons emerge (Fig. 3A). Original leading process of the migrating neuron becomes apical dendrite, trailing process is transformed into axon. Axons then grow towards the midline and after crossing it, they are further guided to upper layers in the contralateral cortex (Fig. 3B). Here, multiple branches and synaptic contacts are formed. Axon collaterals in the ipsilateral hemisphere also emerge and are mainly branching in the layer 5 (Fig. 3C, D). Molecular mechanisms that participate in axon development have been extensively studied in last decades.

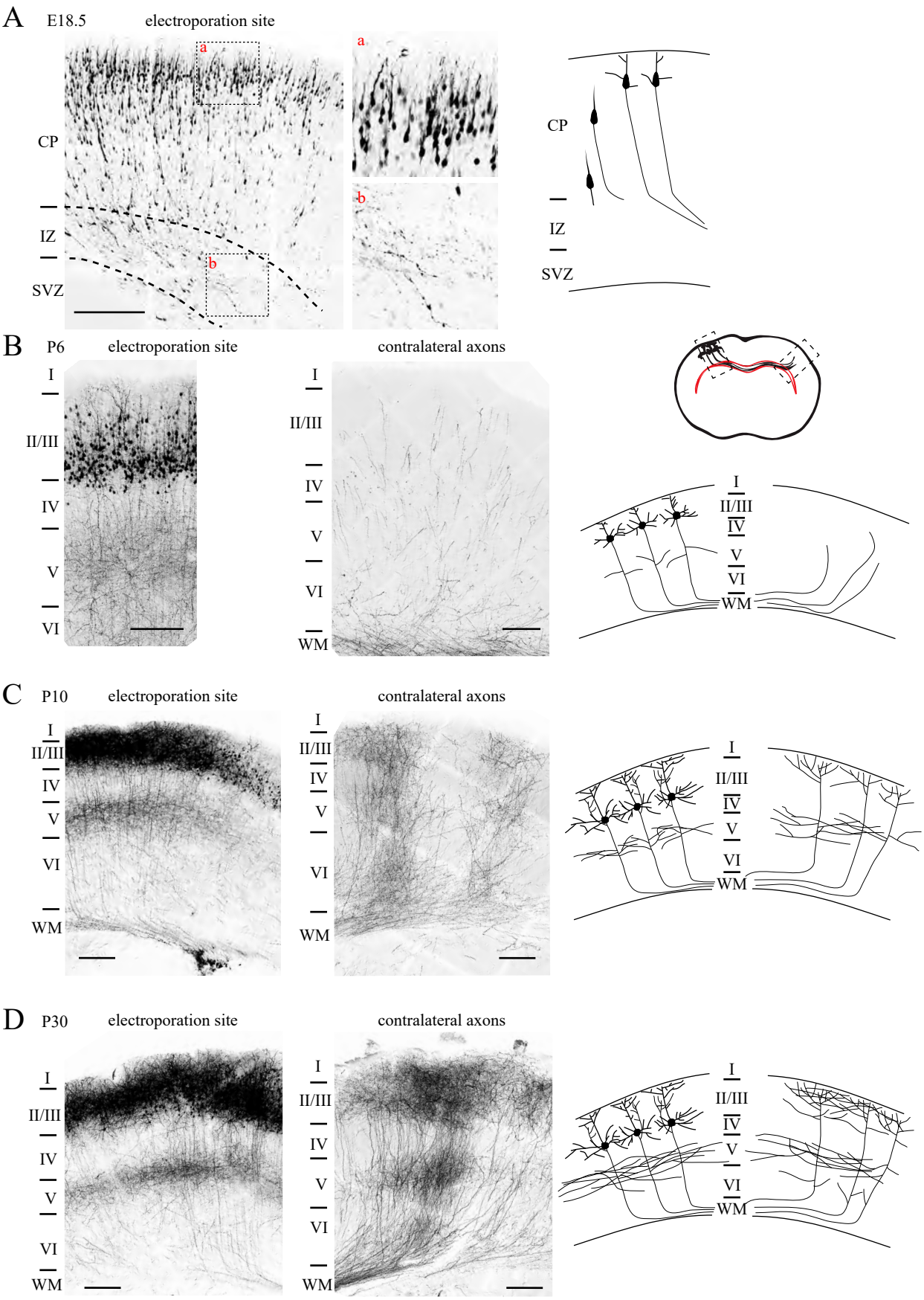
A
E18.5
electroporation site
a
b
CP
IZ
SVZ
B
P6
electroporation site
contralateral axons
I
II/III
IV
V
VI
WM
C
P10
electroporation site
contralateral axons
D
P30
electroporation site
contralateral axons

Neuronal polarization is an event of breaking the cell symmetry resulting in two distinct neuronal compartments – somatodendritic and axonal – regulated by intrinsic and extrinsic cues, as well as organelle distribution/localization (Dotti and Banker, 1987, Dotti et al., 1988, Bradke and Dotti, 2000, Namba et al., 2011). Unpolarized, developing neuron possesses multiple small neurites, of which only one is becoming an axon. In this one destabilization of actin network allows microtubule penetration and axon specification (Bradke and Dotti, 1999). On the other hand, actin in minor neurites is stabilized (e.g. by myosin II) preventing formation of multiple axons. Neurotrophins (such as BDNF and NT-3) and TGF-β signaling are the key molecular pathways required to establish polarization (Yi et al., 2010, Nakamuta et al., 2011). Signal from TGF- β receptor is mediated through PARs (partition-defective proteins), atypical protein kinase C (aPKC) and Rac1 (Nishimura et al., 2005). Rac1 (together with RhoA and Cdc42) is a master regulator of cytoskeletal dynamics (Hall and Lalli, 2010). Moreover, Rac1 activates PI3 kinase that is required for a subsequent Cdc42 activation. Cdc42 associates with PAR complexes – creating a positive-feedback loop that appears to be the crucial for polarization and axon specification (Arimura and Kaibuchi, 2007).

Signals from neurotrophin receptors (such as TrkA – C) are mediated through various pathways including again Rac1 (thus strengthening the feedback loop mentioned above), CAMKI (modulating microtubule dynamics), LKB1 (regulating Tau phosphorylation) and Ras/GSK3-β/CRMP2 (Takano et al., 2015). The role of organelle distribution is so far not clear although in vitro studies showed positive correlation between e.g. mitochondria or Golgi complex and future axon localization (Bradke and Dotti, 1997).

There are several differences in the cytoskeleton architecture and composition between axonal and somatodendritic compartment. First, axonal microtubules are plus-end oriented away from the neuron body while in dendrites there is a mixed polarity (Baas et al., 1988). Second, microtubule stabilization in axons is provided by tau (protects again microtubule severing) and MAP1B, while in dendrites MAP2 family proteins label microtubules. Mice deficient for both Tau and MAP1B display axon growth defects (Harada et al., 1994, Dawson et al., 2001, Takei et al., 2000). Another feature is a presence of dense F-actin meshwork in the proximal part of the axon that originates soon after axon specification. This structure functions as a diffusion barrier between soma and axon and directly precedes formation of an axon initial segment. Disruption of actin polymerization causes invasion of dendritic proteins into axon (Song et al., 2009).

Figure 3 (opposite). Axon guidance in the corpus callosum. (A) Callosal projection neurons start to develop at E15.5 in mice. Electroporation at this date, a subset of callosal neurons is visualized by GFP. At E18.5, neuron migration is almost complete and axons are guided into the interventricular zone (IVZ, developing white matter) towards the midline. (B) At P6, axons are entering contralateral cortex. On the electroporation site, axon collaterals emerge in the layer V. (C) Cell bodies together with their dendrites are densely labelled at P10. In the contralateral cortex, axon are branching mainly in the upper layers and in the layer V. (D) At P30, the tract is fully formed.

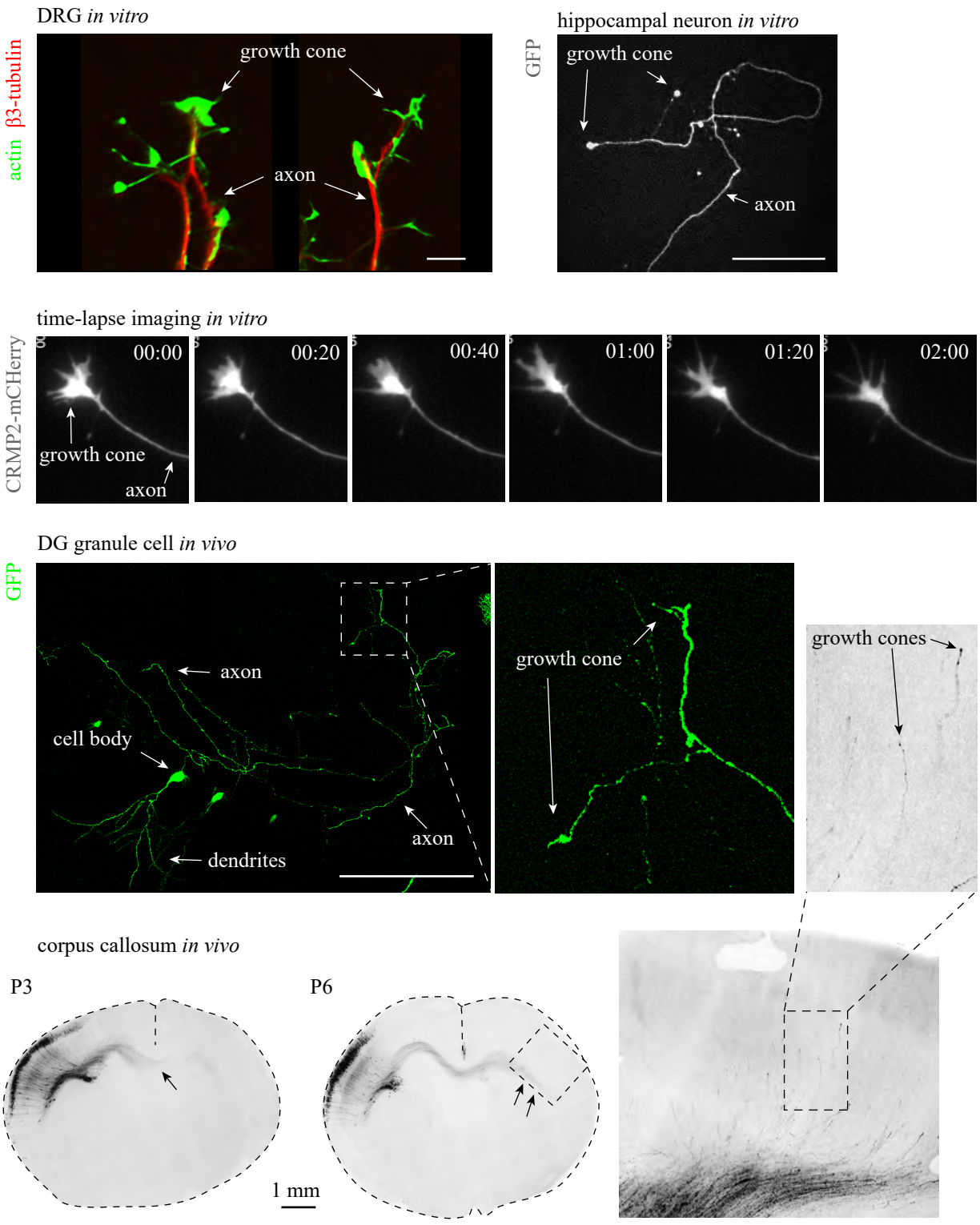

Figure 4. The growth cone. Multiple examples of growth cones (GC) of different types of neurons are present in this figure. In DIV1 DRGs, growth cones are stained with tubulin and actin. Note that it is mainly the actin that is localized inside the GC. Time lapse imaging (time stamp in min:sec) shows intriguing dynamic of the GC. Note also high variability of the growth cone shape. DG granule cells (middle) and callosal neurons (bottom) were visualized by *in utero* electroporation. In corpus callosum at P6, axons are entering the contralateral cortex with GCs easily identifiable.

Second step of the axon development is its growth and guidance towards the target. Axons sense an environment mainly through their leading parts, growth cones (GC). GCs are usually small, round-shaped axon endings with various number of processes (filopodia, lamellipodia). Fig. 4 demonstrates few examples of GC's appearance in both *in vitro* and *in vivo* neurons, as well as huge dynamic of GC filopodia observed during time-lapse imaging (see also video1). The central zone of the GC is fulfilled with microtubules and, conversely, actin filaments are located at the periphery. GCs are pushed forward by axonal microtubule polymerization in the region close to the GC's central zone (Letourneau et al., 1987). Impairing the pushing force by disruption of tubulin axonal transport negatively affects axon growth (Suter and Miller, 2011). Similarly, disruption of microtubule polymerization, e.g. by manipulation with plus-end binding molecules such as APC or EB3, causes axon growth defects (Zhou et al., 2004). Contrary, regulated actin dynamic seems to be involved mainly in axon guidance. Upstream from microtubules, Tiam1 and Tiam2 mediate axon elongation through activated Rac1 and Cdc42 (Kunda et al., 2001). Axon navigation by guidance cues is described in the next chapter.

Axon branching is the last step of axon development. There are two distinct mechanisms of branch formation: growth cone splitting/bifurcation and interstitial branching (Portera-Cailliau et al., 2005). Both modalities require reorganization of cytoskeleton in the nascent branch – first, transient protrusion filled with F-actin emerge, microtubules invade into it and the new branch elongates (Gallo, 2011). Together with cytoskeletal changes, axon branching is regulated through immobilization of mitochondria (Courchet et al., 2013). In the case of interstitial branching, microtubules are fragmented at the branch points before microtubule invasion and these fragments are transported into new branches to stabilize them (Courchet et al., 2013). Fragmentation of microtubules is mainly mediated by severing protein spastin (Yu et al., 2008). What is the exact mechanism of interstitial branching initiation is not clear, however, branches often occur at the place where the growth cone paused during growth, soon after it has started to move again. On the other hand, axons sometimes grow over the long distances without branching (e.g. callosal axons in the first postnatal week in mice, Fig. 3B) indicating that there are signals that actively prevent branch formation. Identity of this signal is not known. Neuronal activity also participates at terminal branching since various approaches of neuronal silencing cause decreased branching (e.g. inhibition of synaptic release by toxins or neuronal silencing by overexpression of hyperpolarizing potassium channel Kir2.1 (Wang et al., 2007)).

Axon pruning and synapse elimination

General strategy used to build the brain connectome is creation of more axon branches and synapses than needed – substantial part of them even with incorrect targets – and subsequent elimination of inappropriate axonal branches and dendritic spines. Thus, an embryonic template resulting from exuberant growth of axons must be refined later in development (Luo and O'Leary, 2005). The process

of refinement is called pruning. Generally, two types of pruning are recognized: 1) small-scale axon pruning, regulated by neural activity or trophic support and 2) large-scale stereotyped axon pruning, which depends on predetermined genetic program (Riccomagno and Kolodkin, 2015, Vanderhaeghen and Cheng, 2010). Examples of activity dependent pruning include elimination of axon collaterals in tectum and visual cortex during eye-opening period or pruning of peripheral motor axons during maturation of neuromuscular junctions. Stereotyped pruning has been so far described in few regions: (a) Infrapyramidal bundle (IPB) axons of hippocampal mossy fibers are retracted between P14 – P30 in mice (Riccomagno et al., 2012); (b) Excess of layer 2/3 callosal axons of motor, sensory and visual cortex is refined by P30 (Zhou et al., 2013); (c) Axonal branches to pyramidal tract from layer 5 visual cortex are eliminated between P9 – P25 (Low et al., 2008). Based on histological observations, stereotyped pruning can be further divided into degeneration-like (Yu and Schuldiner, 2014) and retraction-like, which has been described in rodent CNS (Portera-Cailliau et al., 2005) and linked to secreted semaphorins through their co-receptors e.g. Plexin-A4 and -A3 (Bagri et al., 2003, Low et al., 2008). Elimination of axons that were connected with their targets must include also elimination of its postsynaptic counterparts – e.g. dendritic spines (small protrusions that serve as postsynaptic side of excitatory synapses). Density of dendritic spines in various brain regions in mice peaks about 1 month and significant portion of them is eliminated until adulthood. In humans, postmortem studies showed similar profile of dendritic spines development (Petanjek et al., 2011). Excess of dendritic branches in DG newborn neurons is also retracted as they are becoming mature (Goncalves et al., 2016).

Molecules related to stereotyped pruning include Sema3A and its receptor complex (Nrp1/PlxnA4), Sema3F and its receptors (Nrp2/PlxnA3) and EphrinB3-Eph2 pair (Bagri et al., 2003), (Xu and Henkemeyer, 2009). Another recently discovered pruning regulator is C4 component of complement (Cocchi et al., 2016). Molecular mechanisms regulating axon refinement and synapse elimination are however far less understood in comparison with axon guidance biology. Nevertheless it appears that some signaling axon guidance molecules that were silenced after axon growing period are reexpressed again during pruning period. For example, Sema3F is present in hippocampus in early postnatal period preventing certain axons from entering the wrong hippocampal layers. Then, its expression is shut down, but between P20 – P40 it is expressed again triggering axon pruning (Bagri et al., 2003). Intracellular signals that translate extracellular signal to cytoskeleton are however poorly understood.

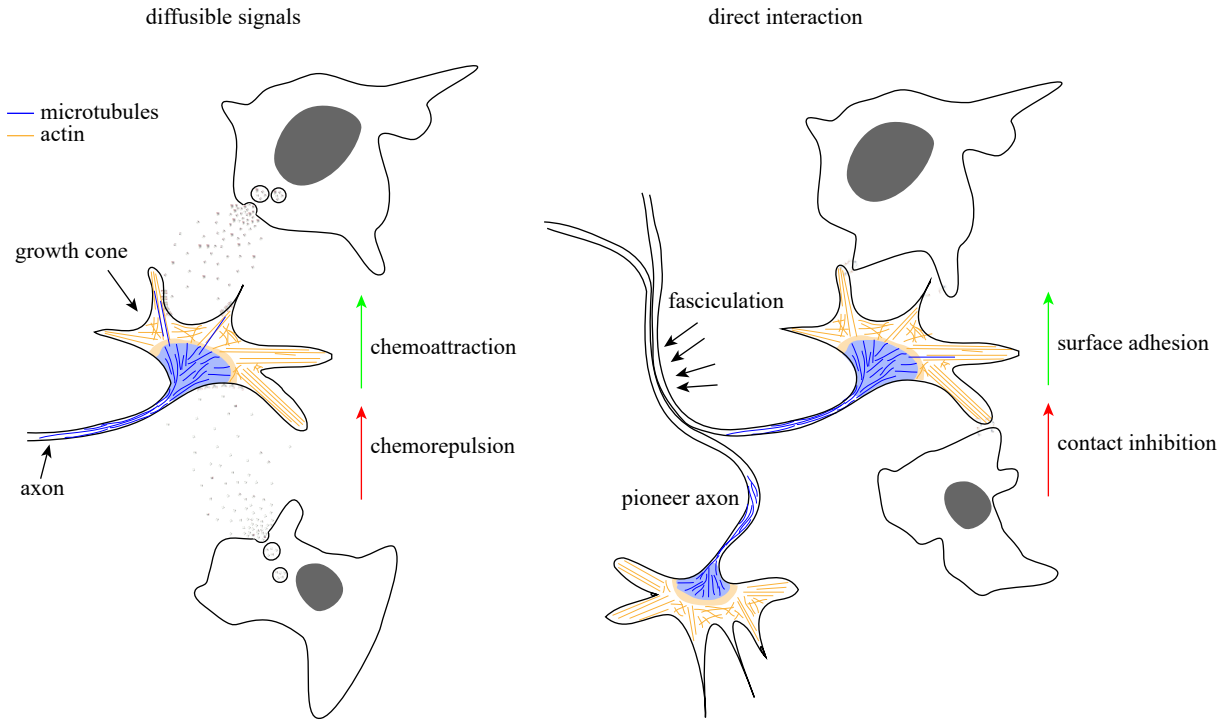

Figure 5. Principles of axon guidance by diffusible signals or physical interactions. Various strategies of axon guidance include diffusible signals (chemoattraction/repulsion) and interaction with surroundings (axon fasciculation, surface adhesion and contact inhibition).

1.2 Axon guidance molecules

Axons are using multiple strategies to get into target location. These include scaffolding (pioneer) axons, short- and long-range secreted attractive/repulsive cues, guidance by adhesion molecules and contact inhibition ((Tessier-Lavigne and Goodman, 1996), Fig. 5). In this chapter, I will introduce major functions of secreted and membrane-anchored guidance molecules. Beside the four main classes (Semaphorins, Netrins, Ephrins and Slits), trophic signals, morphogenes or adhesive factors may also act as a navigation cues ((Kolodkin and Tessier-Lavigne, 2011), Fig. 6). Importantly, axon guidance molecules possess different functions during nervous system development depending on temporal and spatial expression pattern of their ligand/receptor. For example, axon elimination may be triggered by the same molecule that in other conditions supports axon growth. Various cell types can be source of guidance cues, including pyramidal neurons, interneurons and glial cells.

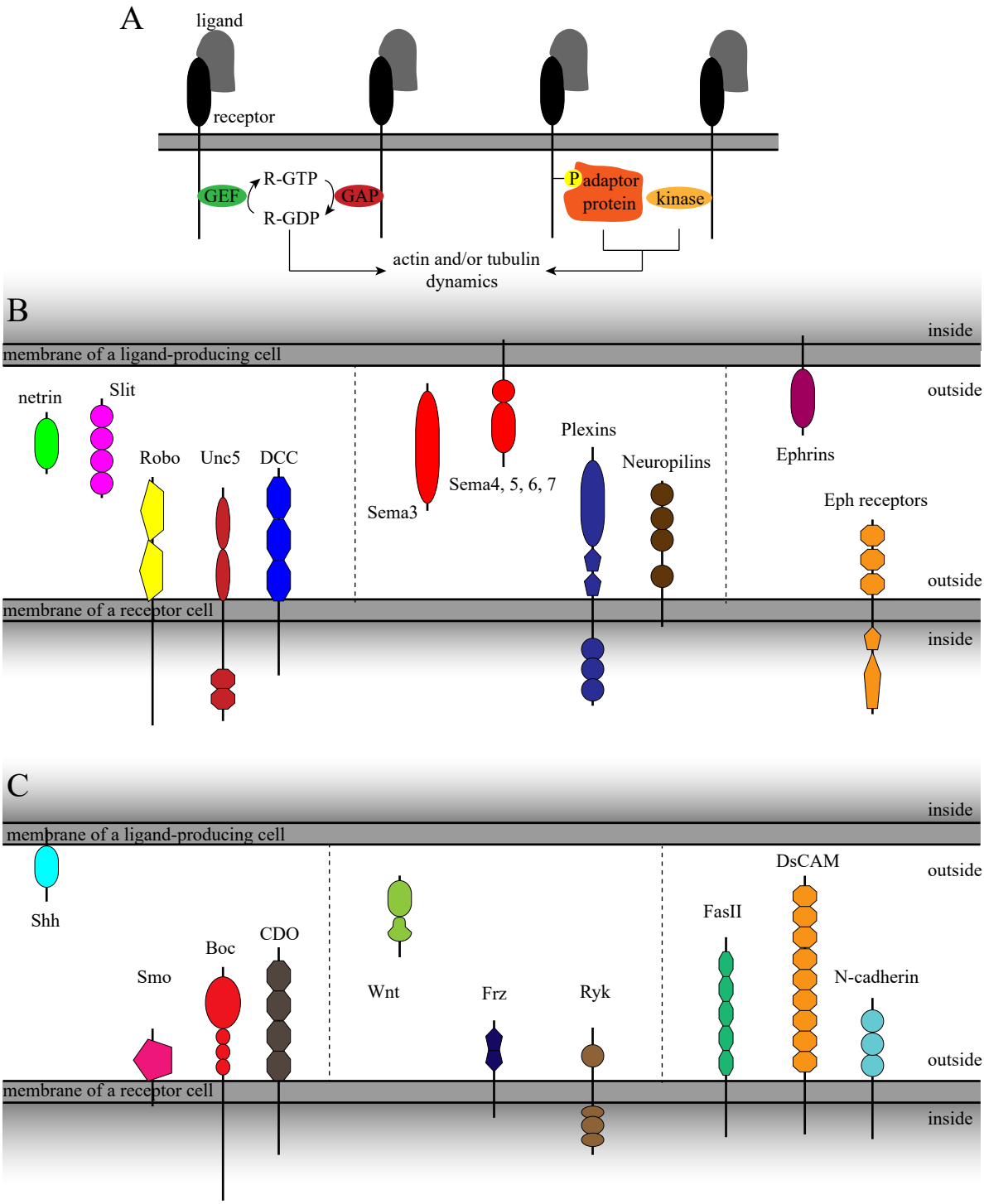

Figure 6. Axon guidance molecules. (A) Principle of signaling downstream from guidance receptors. Intracellular domains associate with small G proteins or may recruit kinases. (B and C) Schematic representation of secreted and membrane-anchored axon guidance molecules and their receptors. Morphogenes and adhesive molecules (C) may serve as guidance cues as well.

Semaphorins

Semaphorin (Sema) family of proteins comprises 5 classes in vertebrates (Sema3, 4, 5, 6, 7). Class 3 represents secreted molecules, whereas molecules from classes 4-7 are membrane-anchored (Pasterkamp, 2012). Plexins (Plxn) are the most common Sema receptors in neurons, they can be divided into four classes (PlxnA, B, C, D). The other receptors are integrins (for Sema7A) or immunoglobulin superfamily cell adhesion molecules (IgCAMs) (Pasterkamp et al., 2003). Secreted semaphorins require ligand-binding coreceptors as neuropilins (Neuropilin 1 or 2) (Takahashi et al., 1998). Semaphorins regulate multitude developmental processes in the nervous system (including neuronal migration, axon guidance and pruning, dendritic spine distribution and synapse formation), cardiovascular system and musculoskeletal system (Jongbloets and Pasterkamp, 2014).

The binding of semaphorins to their receptor complexes activates plexin GAP (GTPase-activating protein) domain (Nogi et al., 2010). Levels of active GTPases (Ras and Rap with GTP bound) are then reduced and lead to inhibition of PI3K-Akt signaling pathway, which further prevents inactivation of GSK3-β (Ito et al., 2006). Active GSK3-β then phosphorylates CRMP2 (Uchida et al., 2005). CRMP2 associates to microtubules in its dephosphorylated state and its phosphorylation decreases the binding (Sumi et al., 2018). Beside microtubules, signal from plexins also interferes with actin dynamic. In intervertebrates, proteins of the MICAL redox enzymes bind to cytosolic domain of plexins and oxidize actin subunits – therefore inducing F-actin disassembly (Terman et al., 2002, Hung et al., 2010). Interestingly, there is an antagonizing process promoting actin assembly – methionine sulfoxide reductase reduces oxidized actin (Manta and Gladyshev, 2017). In receptor complex for Sema3F that is composed from PlxnA3 and Nrp2, signal is also transmitted through Neuropilin intracellular domain. This small residue binds β2-chimaerin (a protein with GAP activity) in the absence of ligand. Upon Sema3F binding, β2-chimaerin is released and inactivates Rac1 by hydrolyzing its GTP. This cascade mediates stereotyped pruning of axons in hippocampus, but is redundant for axon growth or navigation (Riccomagno et al., 2012). Expression of constitutively active Rac1 into dentate gyrus during pruning period caused pruning failure, as well as knockout of β2-chimaerin (Riccomagno et al., 2012).

The very first member of large semaphorin family, Sema3A, is so far the most studied semaphorin. Originally named Fascilin IV (in grasshopper) or Collapsin (in chicks) (Kolodkin et al., 1992, Luo et al., 1993, Kolodkin et al., 1993), it belongs to a class 3 semaphorin. *Sema3a*$^{-/-}$ mice were generated 20 years ago and displayed significant overgrowth of selected peripheral nerves (n. V, n. VII, spinal nerves) demonstrating Sema3A's chemorepellant function (Taniguchi et al., 1997). This finding was further strengthened whilst mutant mice lacking various components of Sema3A receptor (*Nrp1*$^{-/-}$ or *PlxnA4*$^{-/-}$) show similar defects (Taniguchi et al., 1997). Later it was also shown that Sema3A signaling regulates development of axons in selected brain areas (including corpus callosum and

entorhinohippocampal projections) (Chedotal et al., 1998). Together with another secreted semaphorin, Sema3F, they also modulate development of dendrites and dendritic spines (Tran et al., 2009). Sema3F is a negative regulator of layer 5 cortical pyramidal neuron spine density in a segment of apical dendrites close to the cell body (Tran et al., 2009). While each cortical layer contains defined set of axons that arise from a specific brain region (layer 2 – callosal axons, layer 4 – thalamic axons etc.), inputs along the apical dendrite are clustered accordingly and their development is tightly regulated via distinct extracellular cues. On the other hand, Sema3A negatively regulates branching and spine formation in basal dendrites (Tran et al., 2009). Similar layer specificity for semaphorins can be seen in dentate gyrus – Sema3F decreases spine density in the inner and middle molecular layer. Secreted semaphorins also mediate stereotyped pruning of hippocampal and visual corticospinal axons (Bagri et al., 2003, Low et al., 2008).

Netrins

Netrins are extracellular proteins that act as a chemoattractants or chemorepellents, based on a cell type and receptor combination. In mammals, there are three secreted netrins (1, 3, 4) and two membrane-bound netrins (GPI-anchored G1 and G2) (Lai Wing Sun et al., 2011). Netrins are laminin-related proteins as their N-terminal sequences are homologous to N-terminal domains (V and VI) of laminins (Serafini et al., 1994). Receptors for secreted netrins include DCC, neogenin, UNC-5 homologues and DSCAM. GPI-anchored netrins bind to NGL-1 and NGL-2, transmembrane proteins distinct from secreted netrin receptors (Lai Wing Sun et al., 2011). They are enriched at synapses and participate at synaptogenesis. Chimeric receptor studies showed that intracellular domain of netrin receptors is central to mediate repellent or attractant responses (Hong et al., 1999). DCC alone promotes attraction but if it is expressed together with UNC5A, netrin1 will cause repulsion of such axon. Both netrin1 and DCC knockout mice die few hours within birth and present with disruption of multiple CNS commissures (Serafini et al., 1996, Fazeli et al., 1997).

Netrin 1 is the best characterized secreted netrin to date. It is expressed in the forebrain, cerebellum, spinal cord and the optic disc (Lai Wing Sun et al., 2011). In developing cerebellum, netrin1 is expressed by cells in the midline and DCC receptor by migrating progenitors from inferior olive (Ackerman et al., 1997, Goldowitz et al., 2000). Netrin binding causes activation of Cdk5 and GSK3-β which phosphorylates MAP1B (Del Rio et al., 2004). Netrin1 is also expressed at the spinal cord midline by the cells in the floor plate (FP) and ventricular zone (VZ) where it attracts commissural axons before crossing. Netrin deletion specifically in FP or VZ showed that VZ-derived netrin is the key for commissural axon attraction (Dominici et al., 2017). In contrast, trochlear motorneurons are repelled by netrins (Burgess et al., 2006), and netrin signaling also regulates axon branching – local application of netrin 1 induces polymerization of F-actin and formation of filopodial protrusions, thus promoting axon branch formation (Pascual et al., 2004).

Beside neurons, netrins also regulate development of oligodendrocytes (Lai Wing Sun et al., 2011). Precursors of oligodendrocytes express DCC and UNC-5A and are repelled by FP-derived gradient of netrin. In the white matter, netrin promotes elaboration of branched processes on maturating oligodendrocytes. RhoA and ROCK kinase mediate chemorepulsion, while inhibition of RhoA is required for process branching (Rajasekharan et al., 2009, Rajasekharan et al., 2010).

Ephrins

Ephrins are ligands of Eph tyrosine kinase receptors. They mediate signals that control various synaptic events, including synaptogenesis, synapse pruning and modulation of synaptic transmission. In addition, Ephrin-Eph pairs have been implicated in retinotectal mapping (Hruska and Dalva, 2012). There are two families of Ephrins: Ephrin As (1 – 5) and Ephrin Bs (1 – 3). Both families have their corresponding receptors, EphAs and EphBs. Class A Ephrins lack cytoplasmic domain, but are capable to recruit Src family kinases to trigger downstream signaling (Davy et al., 1999). Binding of EphBs to class B Ephrins trigger bidirectional signaling – forward (downstream from receptor, Eph, through activation of its kinase domain) and reverse (downstream from ligand, Ephrin, through phosphorylation of its intracellular domains) (Pasquale, 2008). Cytoplasmic tail of Ephrin-Bs contains multiple domains including Grb4 domain, PDZ binding domain and tyrosine residues for SH2/SH3 adaptor proteins (Hruska and Dalva, 2012).

Expression pattern of Eph/Ephrins in the brain is complex and diverse, it was studied mostly in the hippocampus. Complementary Eph/Ephrin pairs localize to different synaptic sites. In different brain regions, though, Ephrins may localize either in presynaptic or postsynaptic compartment (Kayser et al., 2011, McClelland et al., 2010, Hruska and Dalva, 2012). For example, in hippocampal mossy fibers, EphrinB3 and B1 are expressed presynaptically and EphB2 and EphB1 postsynaptically (in the CA3 region). Vice versa, in CA1, EphrinBs are found in spines closely to postsynaptic densities. Based on the localization pattern, both A- and B- Eph/Ephrins seem to play a prominent role in formation and modulation of excitatory synapses (Henderson et al., 2019). Indeed, mutant mice studies and *in vitro* co-culture assays described multitude dendritic spine defects and compromised synaptic functions. For example, EphA4 regulates dendritic spine morphogenesis in hippocampus (Murai et al., 2003), EphBs are important for formation of dendritic spines and synaptic plasticity (Henkemeyer et al., 2003). Recruitment and function of NMDA receptors is also regulated by EphBs. On the other hand, EphrinBs mediate EphB-dependent presynaptic differentiation through recruitment of syntenin-1 to the PDZ-binding domain (McClelland et al., 2009). Syntenin-1 promotes clustering of synaptic vesicles and maturation of synaptic active zone.

In addition to ephrin's role in synaptogenesis it has been also shown that in hippocampus, ephrins participate in stereotyped pruning via reverse signaling. Presynaptically expressed EphrinB3 activates Rac1 through Grb4 and Dock, which further leads to binding and activation of PAK1. Mice lacking

EphrinB3 present with aberrant mossy fiber axons (Xu and Henkemeyer, 2009). Together, Ephrin/Eph are complex regulators of synapse development and function, from their formation to their elimination.

Guidance of retinal ganglion cell axons is regulated by Ephrin expression gradients (Lim et al., 2008). After leaving the retina, axons have to pass optic chiasma and choose whether to cross to the contralateral site or not. In the optic tectum, axons are sorted along the anteroposterior and mediolateral axes. These features allow binocular vision. Contralateral axon targeting in the optic chiasma includes many regulatory molecules including EphrinB2, which is expressed by surrounding glial cells. Axons expressing EphB1 tend to grow ipsilaterally instead of crossing into the contralateral site.

Slits

Slits are large (~200 kDa) secreted proteins that bind to Robo receptors (shortcut for Roundabout, because of prominent phenotype observed originally in flies) (Hummel et al., 1999). The major function of Slit/Robo signaling is regulation of commissural axon guidance. This large group of axons is specific for organisms with bilateral symmetry and allows coordination of both sides of the body (Blockus and Chedotal, 2016). In the brain, commissural axons are located mainly in corpus callosum, anterior and posterior commissure, hippocampal commissure and fornix. In the spinal cord, commissural neuron are present thorough its entire length. Slit acts as a repellant cue that controls midline crossing through its binding to Robo (Kidd et al., 1999).

In most vertebrates, there are three Slit proteins (Slit 1 – 3). They bind to Robo through their LRR2 domain. Slits also bind to various extracellular matrix proteins (e.g. heparin sulfate, Neurexins, Collagen or Syndecan) that stabilize their interaction with receptor. Robo receptors are transmembrane proteins (Robo 1 – 4 in mammals) with no enzymatic activity, acting as scaffolds for other molecules (Blockus and Chedotal, 2016). Importantly, proteolytic cleavage of both Slits ad Robos appears to be important for signaling. There is a juxtamembrane conserved metalloproteinase cleavage site in the Robo receptor, which is exposed after Slit binding (Barak et al., 2014, Seki et al., 2010). Uncleavable form of Robo is inefficient to rescue the phenotype in Drosophila Robo mutants (Seki et al., 2010, Coleman et al., 2010). Slit is also fragmented into long N-terminal protein (Slit-N) and short C-terminal peptide (Slit-C). They differ in the strength of association with the cell membrane (Slit-N is stronger) and extracellular components (Slit-C). The function of Slit fragments is not yet clear. It is possible that in addition to Robos, Slit-N and Slit-C bind to another receptors or ECM components (Blockus and Chedotal, 2016). This was recently documented for both Slit-C (which binds to semaphoring receptor Plexin-A1) and Slit-N (which binds to Dscam1) (Delloye-Bourgeois et al., 2015, Dascenco et al., 2015).

It is important to note that in commissural axons, dynamic regulation of surface receptor expression is required. That means that receptor for repellant cue (e.g. Robo) should only be present in growth cone membrane after midline crossing to ensure that contralateral axons will grow away from the midline. In drosophila, protein named Comm ("commissureless") sorts Robo receptors to the endosomal pathway for degradation (Myat et al., 2002). After midline crossing, Comm is downregulated, allowing Robo to be expressed at the surface. In vertebrates, however, there is no Comm homolog known yet. Other mechanisms for Robo inactivation such as trans-interaction between different Robo members were suggested.

Mutant mice studies revealed several features of Slit/Robo pathway. Knockout of all three Slits in mice leads to midline re-crossing in the spinal cord and the stalling phenotype (Blockus and Chedotal, 2016). Robo1/2 double knockouts partially phenocopy Slit triple mutants suggesting another receptors/molecules downstream from Slit exist. Indeed, dystroglycan mutant mice also phenocopy the axon guidance midline defects (Wright et al., 2012). This is in line with observations which showed that dystroglycan promotes Slit/Robo interaction. Beyond nervous system, Slit/Robo signaling participate in stem cell regulation, angiogenesis and tumorigenesis (Blockus and Chedotal, 2016).

1.3 Signal transduction from the membrane to cytoskeleton

I have already mentioned various effectors downstream from guidance receptors, in this chapter I would like to concisely introduce the main principles of spreading the signal downstream from receptors. These involve endocytosis, receptor cleavage, activation of kinases and second messengers, and using small G protein switches.

Membrane-associated changes

Endocytosis of the ligand/receptor complex modulates receptor activation and signaling. For example, Ephrin-Eph complex (where both binding partners are membrane-bound) are internalized and create signaling endosomes which allow growth cone collapse. Bidirectional endocytosis is required for cell detachment (Egea and Klein, 2007, Gaitanos et al., 2016). In case of Sema3A signaling, low doses of Sema3A desensitize the growth cone because of rapid endocytosis of receptor-ligand complex (Piper et al., 2005). This adaptation mechanism resets sensitivity of the growth cone to a guidance cue and allows the growth in a gradient. Another example is the attraction/repulsion switch to Netrin1. If UNC5A receptors (repulsion mediators) are internalized, the remaining DCC receptors promote chemoattraction (Hong et al., 1999).

Next to endocytosis, proteolytic processing is used to modulate receptor activation on the membrane. ADAM10 family proteases have been show to participate in this process. For instance, Adam10 cleaves EphrinA2/EphA receptor complex (Janes et al., 2005). Binding of Eph changes conformation

of Ephrin and as a result recognition sequence for Adam10 is exposed. Functionally, the original adhesive interaction is converted to repulsion. Similarly, matrix metalloproteinases (MMPs) cleave EphB2 and change EphrinB/EphB adhesion into retraction. Homolog of ADAM in drosophila (Kuz) is also involved in neurogenesis. Kuz and y-secretase sequentially cleave Notch allowing its intracellular domain to be translocated into nucleus (Pan and Rubin, 1997). There are also hints that intracellular domains of the other receptors (e.g. DCC or Ephrin) may serve as transcription regulators as well.

Kinases

Examples of kinases associated with guidance receptors are Src family kinases (SFKs, e.g. Src or Fyn kinase), focal adhesion kinase (FAK), GSK3-β or Cyclin dependent kinase 5 (Cdk5). SFKs mediate repulsive signals downstream from EphA receptors in retinal ganglion cells and in cortical axons *in vitro*. Together with FAK, SFKs are involved in Netrin signaling (Lai Wing Sun et al., 2011). They are recruited do DCC receptor upon Netrin binding and phosphorylate its cytoplasmic P3 domain. Knockout of FAK reduces axon outgrowth and attraction induced by Netrin-1. Downstream from SFKs appears to be $p130^{CAS}$, Crk-associated substrate, inhibition of which also abolishes Netrin-induced neurite outgrowth (Ren et al., 2004).

Fyn and Cdk5 kinases mediate signal from Plexin A/Nrp1 receptor complex (Jongbloets and Pasterkamp, 2014). Tyrosin kinase inhibitors and Cdk inhibitors significantly decrease responses to Sema3A-induced growth cone collapse. Detailed analysis showed that Fyn kinase is recruited to the cytosolic domain of Plexin and phosphorylates Cdk5 (Sasaki et al., 2002). Cdk5 is an atypical cyclin dependent kinase because it is not involved in cell cycle regulation and it is also largely cyclin independent. Instead, Cdk5 requires coactivators p35 or p39, which are membrane-bound proteins, thus localizing Cdk5 in the close proximity to the cell membrane (Tsai et al., 1994). This prevents activation of Cdk5 inside the cytoplasm that have broad pathological consequences. There is also *in vivo* evidence of Sema3A/Fyn interaction since double $Sema3A^{+/-}$;$Fyn^{+/-}$ mutants exhibit defects in basal dendrite projections similar to $Sema3A^{-/-}$ or $Fyn^{-/-}$ mice (Morita et al., 2006). Cdk5 is further involved in neuron migration as it regulates multipolar-to-bipolar transition in migrating cells (Ohshima et al., 2007). $Cdk5^{-/-}$ mice display inverted cortical layering and die soon after birth. Cortex-specific Cdk5 knockouts display profound lamination defects in cortex and hippocampus and abnormal dendritic development in layer 5 neurons (Ye et al., 2014). Substrates of Cdk5 include doublecortin, ndel1, FAK and CRMP2.

Small GTPases

Rho and Ras GTPases (small G proteins consisting from one subunit) belong to the Ras superfamily and binds GTP/GDP. They are activated by guanine nucleotide exchange factors (GEFs) and

inactivated by GTPase-activating proteins (GAPs). GAPs increase intrinsic GTPase activity of Rho/Ras resulting in GTP hydrolysis whereas GEFs exchange GDP for GTP. In general, Rho GTPases are regulators of microtubule and actin dynamics in various processes including cell migration, axon growth and branching, dendritic spine development and others (Hall and Lalli, 2010). On the other hand, Ras GTPases are activated by adhesion receptors and promotes variety of signaling pathways (e.g. MAPK, PI3-kinase) that are important for protein translation and transport. I will mainly discuss the role of Rho GTPases in the context of guidance receptor signaling and cytoskeletal dynamics. There are three main Rho GTPases: Rho, Cdc42 and Rac. In a very simplistic way, Rho preferentially associates with repulsive cues and often acts antagonistically to Rac and Cdc42, which are downstream of attractants (Hall and Lalli, 2010). There is however far higher complexity in the system which relies on specific guidance receptor(s). As a whole, contribution of Rho GTPases to axon navigation is broad and depends on the spatiotemporal timing and neural type.

Sema3A-induced growth cone collapse depends on Rac and Rho (Jurney et al., 2002, Gallo, 2006). Rac-GTP interacts with cytoplasmic tail of the PlexinA1 receptor. It is likely that in this case the receptor is downstream of Rac since constitutively active version of PlexinA1 does not require Rac to mediate collapse. Rac may either induce conformational changes of the cytoplasmic tail or promotes receptor endocytosis (Jurney et al., 2002). On the other hand, Sema3F-induced stereotyped pruning is mediated by decreasing Rac1 activity. Nrp2 receptor associates with β2-chimaerin but Sema3F binding causes their dissociation. β2-chimaerin acts as a Rac1-GAP, decreases Rac-GTP levels and thus inactivates it (Riccomagno et al., 2012). Vice versa, reverse signaling from EphB receptors activates Rac1 and is also necessary for axon retraction (Xu and Henkemeyer, 2009). It remains question how these dynamic changes in Rac1 activity regulate cytoskeleton in a context of pruning. Alternatively, both Sema3F and EphrinB pathway may be specific for a given neuron type. Rho, and its downstream effector ROCK, are activated by Sema3A or Sema4D and promotes intraaxonal bundling of F-actin. Moreover, Sema3A induces local translation of RhoA in growth cones (Wu et al., 2005), further increasing the level of complexity of its regulation.

Axon repulsion through Ephrin/Eph partners is mediated by activation of Rho/ROCK and/or inhibition of Rac signaling (Wahl et al., 2000). For instance, EphrinB3/EphA4 contributes to the corticospinal tract formation. Here, RacGAP α-chimaerin is activated by tyrosine phophorylation and subsequently inhibits Rac. Mice lacking α-chimaerin (which results in hyperactive Rac) display corticospinal tract malformations (Iwasato et al., 2007). Activation of Rho involves its GEF called ephexin, however, mice lacking ephexin-1 have no prominent axon guidance defects which may reflect redundancy between different GEFs. Another example connects endocytosis of Ephrin/Eph complex – Eph triggers activation of VaV2 (which is a Cdc42/Rac1 GEF) that consequently leads to endocytosis of the complex and axon repulsion (Cowan et al., 2005).

Peptidyl-prolyl isomerases and protein folding

The peptidyl-prolyl isomerases (PPI) protein family contains enzymes that change cis/trans conformation of the X-Pro peptid bond (X represents any aminoacid) (Lu and Zhou, 2007). Among different X-Pro bonds, Ser/Thr-Pro motif is of special interest since it is targeted by a large group of kinases (Pro-directed protein kinases) which include e.g. Cdks, GSK3-β or JNKs. There are two modes of protein folding (and thus its function) regulation through this unique Ser/Thr-Pro motif – cis/trans isomerization and phosphorylation/dephosphorylation. Of the three distinct groups of PPIs (which include FK506-binding proteins (FKBPs), cyclophilins (Cyps) and Pin1), FKBPs and Cyps targets preferentially non-phosphorylated motif, while Pin1 is phospho-specific (Lavin and Mc Gee, 2015, Tong and Jiang, 2015, Lu et al., 1996).

PPIs have been implicated in protein synthesis, cell cycle regulation, cell growth and cancerogenesis (FKBPs are, for example, targets of anti-cancer and immunosupressive therapy). On top of that, Pin1 promotes neuron survival and protects against age-dependent neurodegeneration (Lu et al., 1999, Pastorino et al., 2006, Balastik et al., 2007). Mice lacking Pin1 develop hallmarks of Alzheimer's disease – neurofibrilary tangles containing hyperphosphorylated tau (Liou et al., 2003). Soluble Pin1 levels are decreased also in brains human subjects at late stages of Alzheimer's (Lu et al., 1999). However, there are still questions regarding the role of Pin1 under physiological conditions and particularly during development of the nervous system.

We have recently shown that Pin1-directed regulation of conformational changes tunes axon growth responses in Sema3A gradient (Balastik et al., 2015). Minimum levels of Sema3A are already capable to induce growth cone collapse in *Pin1*$^{-/-}$ neurons. Furthermore, *Pin1*$^{-/-}$ mouse embryos display aberrant axon growth in trigeminal nerve and entorhinnohippocampal pathway, previously showned to be regulated by Sema3A (Pozas et al., 2001, Taniguchi et al., 1997). CRMP2A, a long isoform of CRMP2 (see below), has been identified as a major target of Pin1 in axon development (Balastik et al., 2015).

1.4 The role of CRMP2 in nervous system patterning

The structure of CRMP2

CRMP2 was identified in 1995, originally as a molecule that mediates responsiveness to extracellular Sema3A in chick DRGs (Goshima et al., 1995). It's a 572 aminoacids long homolog of liver dihydropyrimidinase, but lacks its enzymatic activity. The molecule consists of several helices that are packed together and outside of this core, N terminus and C terminus are floating (Fig. 7A) (Niwa et al., 2017). Importantly, CRMP2 shares homology with other members of CRMP family, mainly with CRMP1, 3 and 4 (Yamashita and Goshima, 2012). Moreover, residues phosphorylated by Cdk5 or GSK3-β on the C teminus are identical in CRMP2 and CRMP4. CRMP2 alone exists as a homotetramer (Fig. 7B), but in combination with other CRMPs it may form heterotetramers. Structures of all five CRMPs have already been solved, however, very often without complete N- or C-termini (Fig. 8). This is particularly important because – as the last CRMP2 structure with the part of C-terminus (to aminoacid 525) suggests – these floating ends may serve as tetramer stabilizers. They are also well accesible on the surface of the molecule.

Two splice variants of *Crmp2* have been found differing at their N termini – CRMP2A (long isoform) and CRMP2B (Fig. 7C) (Yuasa-Kawada et al., 2003, Balastik et al., 2015). Various kinases target both N- and C- termini: CRMP2B is phosphorylated by Cdk5 at Ser522 (priming site for GSK3-β), by GSK3-β at Thr509, 514, Ser518, by SFKs kinases Fyn and Yes at Tyr32, 479 and by Rho kinase at Thr555 (Yoshimura et al., 2005, Uchida et al., 2005, Arimura et al., 2005). We have recently shown that CRMP2A is phosphorylated at N-terminal Ser27 by Cdk5, which promotes its interaction and stabilization by prolyl isomerase Pin1 (Balastik et al., 2015). This Ser27 also seems to be unique – other long isoforms of CRMPs (CRMP1A and CRMP4B, Fig. 8B) have another aminoacid in this position. Importantly, vast majority of CRMP research has been done on short isoforms – likely because they are more abundant in the brain – and it remains open question how do long isoforms differ functionally from the shorts.

Beside phosphorylation by various kinases, there are also other posttranslational modifications that modulate CRMP2 function – oxidation, sumoylation and glycosylation (Moutal et al., 2019). Oxidation of CRMP2 was observed *in vitro* in DRG neurons. Sema3A stimulation activates MICAL that produces hydrogen peroxide (Terman et al., 2002). Subsequently, CRMP2 is oxidized and may form complex with thioredoxin which further promotes its phosphorylation by GSK3-β (Morinaka et al., 2011). However, the relevance of this mechanism *in vivo* in vertebrates is questionable since recent analysis of *MICAL-1*$^{-/-}$ mice did not show any apparent defects in growth of PNS or CNS axons, as well as no alternation in growth cone collapse (Van Battum et al., 2014). Interestingly, MICAL-1 is strongly expressed in mossy fibers and regulates their lamination through membrane targeting of an

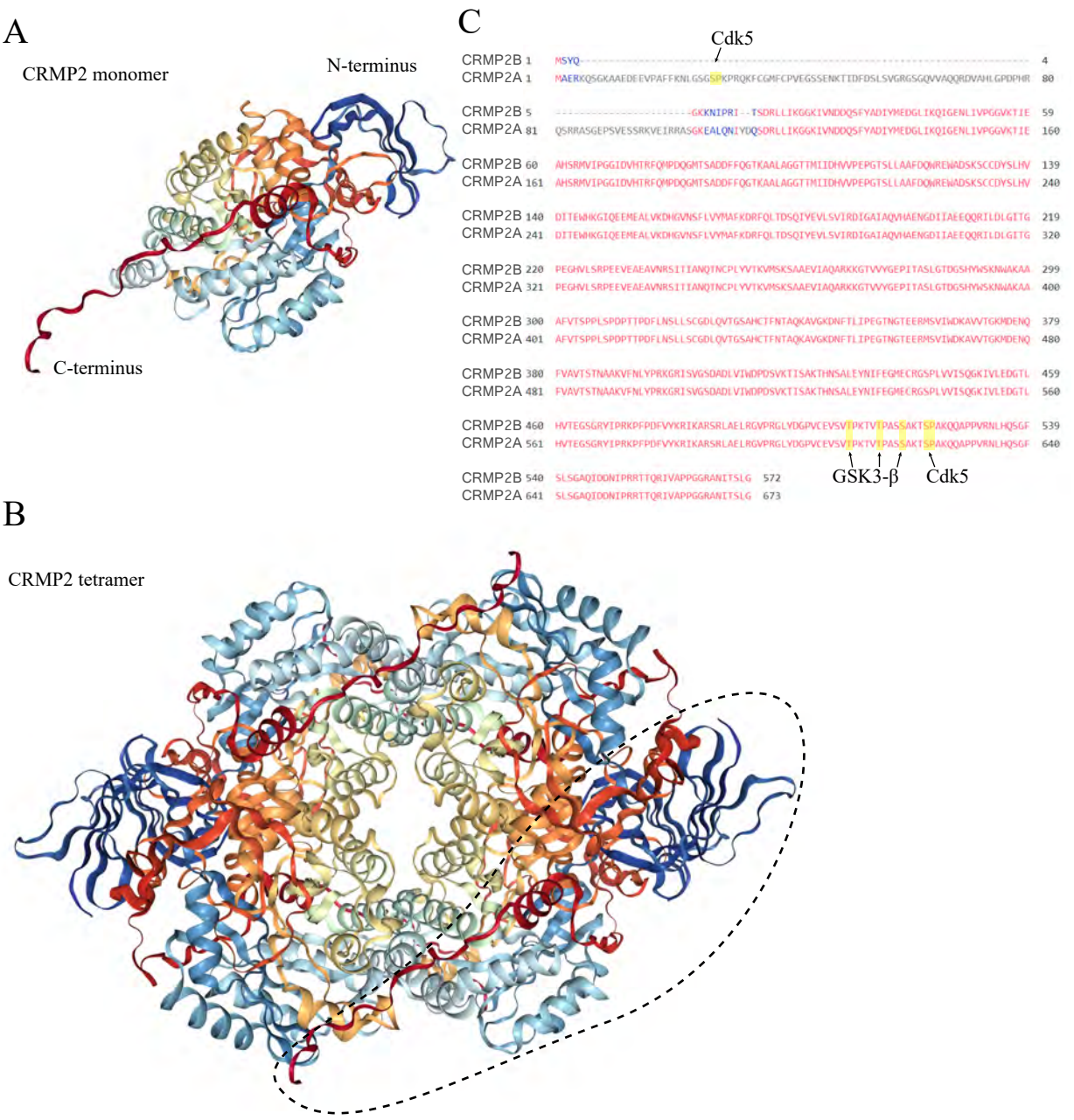

Figure 7. CRMP2 structure. (A) Crystal structure of CRMP2B (aminoacids 14 – 506). Structure of CRMP2A isoform is not known. (B) The structure of CRMP2 homotetramer. Dotted line depicts the monomer. Note the C-terminus extending to the nearby monomer. (C) Alignment of CRMP2 isoforms. Red letters represent the same aminoacids, blue letters are different residues. Yellow color highlights serins and threonins that are phosphorylated by Cdk5 or GSK3-β. Note that the main difference among CRMP2A and B is the N-teminus which is longer in CRMP2A. Importantly, at this N-terminus, CDK5 phospho-site is present.

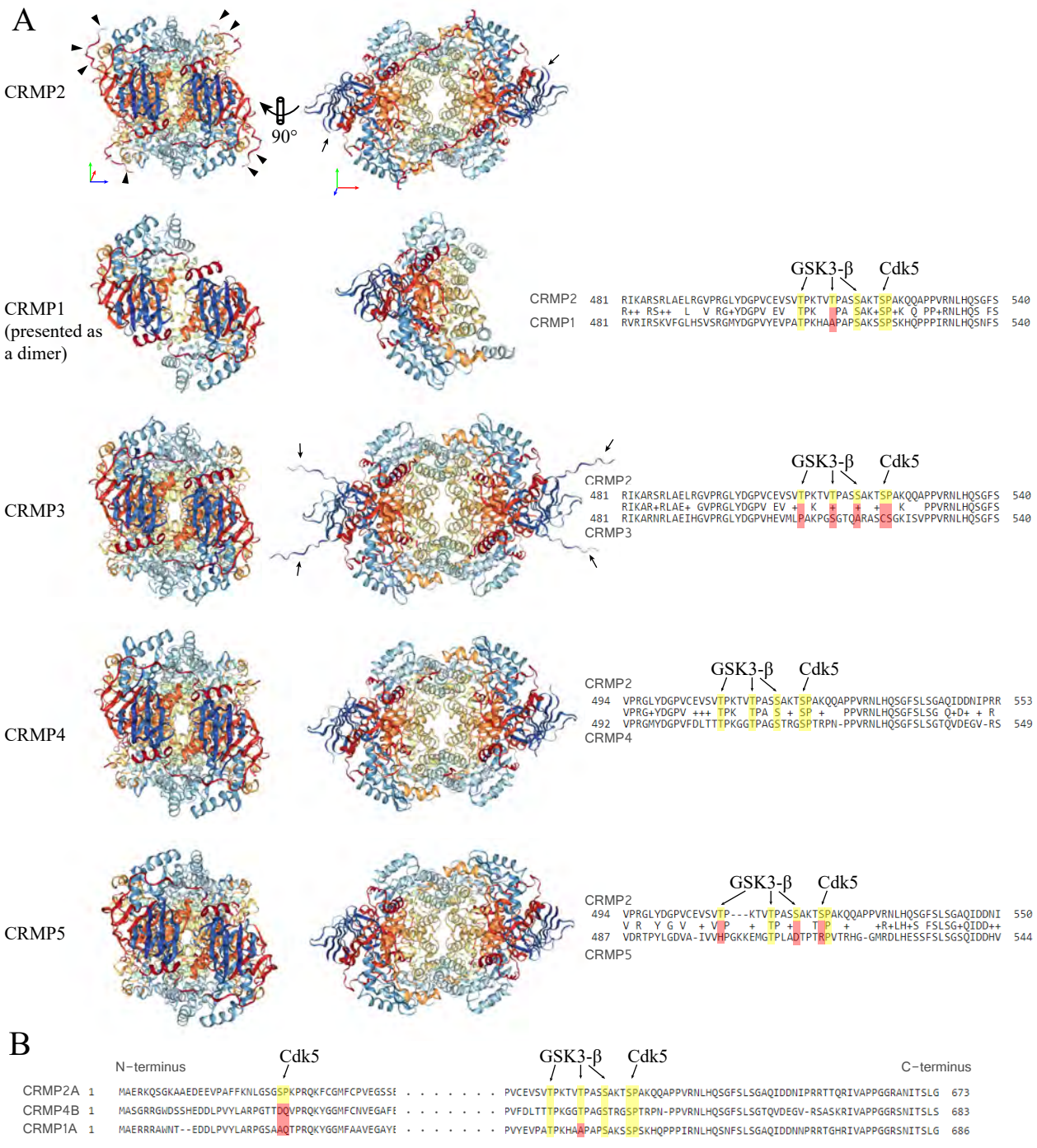

Figure 8. Comparison of CRMP family members. (A) All CRMPs (short isoforms) are presented as homotetramers but CRMP1 (only dimer was crystalized). On the right, C-termini are aligned whilst there is the highest variability among different CRMPs. Note that CRMP2 and CRMP4 have the same four residues that are recognized by kinases. (B) Alignment of N-termini and C-termini of all known long isoforms of CRMPs. C terminal tail is similar to short isoforms but Cdk5-phospho site at the N terminal tail of CRMP2A is unique. Structures: (Niwa et al., 2017, Deo et al., 2004, Ponnusamy and Lohkamp, 2013, http://www.rcsb.org/structure/4BKN, http://www.rcsb.org/structure/5NKS).

adhesion molecules. Sumoylation of CRMP2 (at Lys374) regulates surface expression of voltage-gated sodium channel NaV1.7 by preventing CRMP2-Numb binding which causes endocytosis of the channel (Dustrude et al., 2013). O-GlcNAcylation (by addition of N-acetylglucosamine to Ser517) is a modification that likely interferes with GSK3-β-induced phosphorylation of close residues (509, 514, 518) (Cole and Hart, 2001). Even if Ser522 is phosphorylated, glycosylation prevents phosphorylation at residues 509, 514 and 518. Interestingly, total phosphorylation of CRMP2 with both Cdk5 and GSK3-β prevents glycosylation.

CRMP2 binding partners

Since CRMP2 has little enzymatic activity (it may acts as a GAP for GTP-tubulin, but this finding remains controversial, (Chae et al., 2009)) it mainly serves as a structural protein which binds (and stabilizes) other protein or protein complexes depending on its phosphorylation status (Sumi et al., 2018, Moutal et al., 2019). First, CRMP2 monomer binds to other CRMP2 monomers and also to other CRMPs thus creating tetramers. The major interface for this interaction is arginine/lysine-rich helix H19 (aminoacids 466-487). The proportion of homo/heterotetramers in the brain is not known (Niwa et al., 2017). Next, CRMP2 binds to tubulin dimers and stabilizes them, allowing microtubules to grow (Fukata et al., 2002a, Niwa et al., 2017). Structural details of these interactions were puzzling because residues from a tubulin-binding fragment of CRMP2 are localized inside the globular domain once CRMP2 forms tetramers. Recently, CRMP2-tubulin complex structure was solved and showed that CRMP2 binds to tubulin plus ends via its H19 helix, forming a cap covering the GTP. CRMP2-tubulin heterotrimer is then incorporated into the growing microtubule and CRMP2 rapidly dissociates and forms tetramers again. Fitting the small angle X-ray scattering model with a crystal structure suggest that C-terminal tail extends along tubulin dimer and mediates tubulin binding to microtubules (Niwa et al., 2017).

Another CRMP2's binding partners are motor proteins kinesin and dynein (Kawano et al., 2005, Arimura et al., 2009a, Rahajeng et al., 2010). CRMP2 binds to dynein heavy chain through aminoacids 100-150 and 348-440 and interferes with its activity. Overexpression of CRMP2 disrupts dynein activity in COS-7 cells while its knockdown has no effect. Interestingly, while dynein binds to N-terminus of CRMP2, kinesin was found to bind to the above-mentioned helix H19 and C-terminal tail.

There is at least one protein that binds to the N-terminal region of CRMP2A – Pin1, phospho-specific prolyl isomerase (Balastik et al., 2015). Within CRMP2A, Pin1 changes the conformation (cis – trans) of peptide bond between Ser27 and Pro28, preferentially when Ser27 is phosphorylated. We directly visualized this binding by fluorescence lifetime imaging using fusion proteins GFP-Pin1 and mCherry-CRMP2A (Fig. 9). Lifetime of GFP decreases (indicating an interaction) when mCherry is within its FRET distance, e.g. when Pin1 is bound to CRMP2A. Binding was stronger after stimulation with

Sema3A that induces phosphorylation of CRMP2A. On the other hand, de-phosphomimetic mutation significantly decreases Pin1 binding. As a consequence of Pin1 deletion, phosphorylated CRMP2A is less stable and growth cone collapse can be induced by lower Sema3A concentrations. Mouse embryos lacking Pin1 display shorter trigeminal nerves at E11.5 (Balastik et al., 2015).

CRMP2 function

The original finding about CRMP2 and its role in Sema3A-induced growth cone collapse included injections of CRMP2 antibody into chick embryos or to cells (Goshima et al., 1995). Later it has been shown that CRMP2 promotes assembly of microtubules. Many *in vitro* experiments showed that CRMP2 is enriched in elongated axons (Arimura et al., 2000, Cole and Hart, 2001, Fukata et al., 2002a, Fukata et al., 2002b, Nishimura et al., 2003, Brittain et al., 2009). Its overexpression in WT neurons induces multiple Tau1-positive neurites, an observation that supports microtubule-stabilization function (Inagaki et al., 2001). Similarly, during neuronal polarization, CRMP2 is thought to stabilize microtubules as well (Ip et al., 2014).

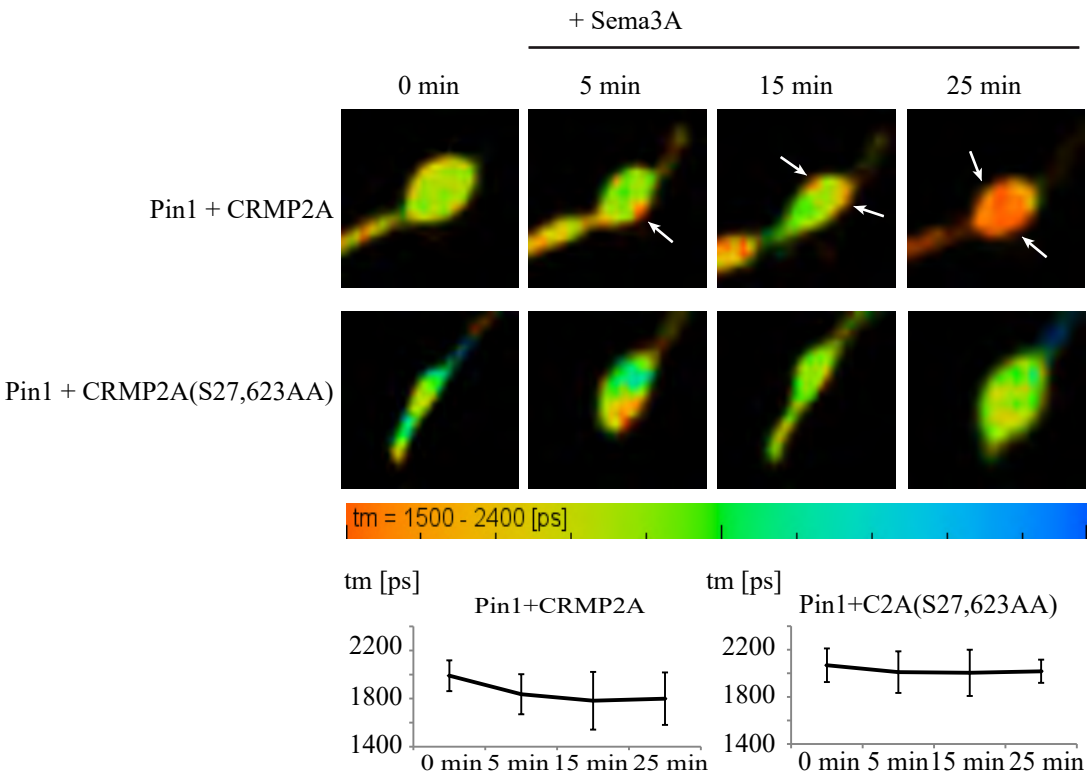

Figure 9. Interaction between CRMP2A and Pin1 visualized by FLIM. FLIM (fluorescence lifetime imaging) is a method for FRET (fluorescence resonance energy transfer) quantification. We measured lifetimes of GFP in cells transfected with fusion proteins – if mCherry is brought within the FRET distance of GFP, it decreases its fluorescence lifetime due to the interaction of the proteins. Hippocampal neurons were co-transfected with Pin1-GFP (Pin1) and CRMP2A-mCherry (CRMP2A), or CRMP2A(S27,623AA)-mCherry (CRMP2A(S27,623AA), de-phosphomimetic form of CRMP2A). Pin1 interacts preferentially with phosphorylated CRMP2A (note lifetime decrease after Sema3A treatment, which induces phosphorylation). Tm – mean lifetime.

Beside stabilizing microtubules, CRMP2 also regulates axonal transport. It can bind both kinesin and dynein and may serve as a scaffold that connects motor protein with its cargo(s). For example, CRMP2 regulates surface levels of TrkB via anterograde transport (Arimura et al., 2009b). CRMP2 interconnects motor protein kinesin-1 with Rab27, Slp1 and TrkB. Attenuation of TrkB anterograde transport by acute knockdown of CRMP2, Rab27 or Slp1 *in vitro* decreased BDNF-induced axonal outgrowth.

Recent studies suggested CRMP2 regulates neuronal migration in the cortex. In this case, CRMP2 is downstream from TrkB, mediating stabilization of the leading process of migrating neurons (Ip et al., 2011). Activation of TrkB (by its endogenous ligands BDNF and NT-3) induces inactivation of GSK3B (by phosphorylation of its Ser9) and dephosphorylation of CRMP2. Decreasing CRMP2 levels via shRNA-mediated knockdown caused accumulation of neurons in the IZ. These CRMP2-depleted cells failed to transit from multipolar to bipolar shape.

Finally, CRMP2 regulates voltage-gated sodium channel (NaV1.7). Loss of CRMP2 SUMOylation inhibits Na-channel activity (and counsequently reduces neuronal excitability), as well as the overexpression of non-phosphorylable CRMP2 (CRMP2 with S522A mutation) (Dustrude et al., 2013, Dustrude et al., 2017). Indeed, naïve non-phosphorylated, non-SUMOylated CRMP2 triggers NaV1.7 endocytosis via Numb adaptor protein.

Given that CRMP2 is involved in multiple intracellular processes that underlie proper neuronal functions, one might expect that aberrant CRMP2 activity will have severe consequences. Indeed, CRMP2 has been implicated in several neurological disorders. On the other hand, CRMP2 is also a possible therapeutic target for multiple sclerosis or chronic pain (Brittain et al., 2011, Petratos et al., 2012).

1.5 Clinical manifestation of defective nervous system development

Defects in neural migration and neurite growth

Human lissencephaly (smooth brain) is a congenital brain disorder that is underlie mainly by defects in neuronal migration . Microscopic findings in lissencephalic brains show impaired lamination with less elaborated gyri. Patients manifest with epilepsy, mental retardation and decreased motor functions. Genes implicated in migratory defects include PAFAH1B1 (LIS1), YWHAE (a member of 14-3-3 protein family), DCX (doublecortin) and RELN (reelin) (Dobyns et al., 1993, Reiner et al., 1993, Chong et al., 1997, Gleeson et al., 1998, Hong et al., 2000). Opposite to lissencephaly, polymicrogyria is a migration disorder characterized by excessive cerebral folding and malformations of cortical layering (Jaglin et al., 2009). Neuronally-expressed α- and β-tubulin genes, as well as motor proteins were implicated in this condition.

The most common cause of lissencephaly is mutation or deletion of human PAFAH1B1 gene (encoding protein LIS1) (Dobyns et al., 1993). LIS1 is evolutionary conserved and its deletion in mice causes severe lamination defects (cortical layers are not distinguishable, hippocampal regions are disorganized). It binds to tubulin, dynein and dynactin and regulates microtubule dynamics. As a result of decreased LIS1 protein levels, neuronal cell migration is affected due to defects in nucleus-centrosome coupling (Tsai and Gleeson, 2005). LIS1-dynein complex generates pulling force for movement of the nucleus. Migration of neurons is therefore slower. Additionally, LIS1 promotes polymerization of F-actin at distal ends of leading processes through regulation of small G proteins – it activates Cdc42/Rac1 ad inactivates RhoA. Smaller number of filopodia and less F-actin is found in LIS1-deficient neurons (Kholmanskikh et al., 2006).

Pathogenesis of polymicrogyria has been associated with mutation in tubulin genes (Jaglin and Chelly, 2009). Distinct neuronal abnormalities are connected with various mutations indicating a unique role of each of them in regulating cytoskeleton. For example, TUBB2B mutations affect basal ganglia, TUBA8 mutations cause callosal dysgenesis and optic nerve hypoplasia (Moon and Wynshaw-Boris, 2013). This extreme symptom variability is not surprising looking at the concept of a tubulin code (Magiera et al., 2018a, Magiera et al., 2018b). In fact, not only different α- and β- tubulin members, but also specific posttranslational modifications that occur on the C-terminus of the tubulin are all source of specificity of microtubules in various brain regions, neurons or their compartments.

One of the most common neurodevelopmental defects where axon growth is affected is agenesis of the corpus callosum (ACC). In this condition, hemispheres are not connected via corpus callosum (total agenesis) or only partially connected (hypoplasia, dysgenesis) (Fenlon and Richards, 2015, Nishikimi et al., 2013). ACA may be a part of various more complex syndromes (e.g. L1CAM syndrome, Aicardi syndrome or septo-optic dysplasia) (Kamnasaran, 2005). Although symptoms vary among individual patients, hypotonia, motor coordination defects or delayed developmental milestones are often present.

Various dendritic spine pathologies have been reported in subjects with certain neuropsychiatric disorders (Penzes et al., 2011). For example, in ASD patients, increased dendritic spine density was reported in frontal, temporal and parietal lobes (Tang et al., 2014). In fragile X syndrome, density of spines is also increased and further accompanied with their dysmorphology – spines are thin, long and tortuous (De Rubeis et al., 2012). Vice versa, in schizophrenia patients, there is less spines in prefrontal cortex and auditory cortex (Garey et al., 1998). Mouse studies revealed many candidate genes that could participate in pathogenesis of above-mentioned diseases and it is not surprising that they often localize in synapses. These include ProSAP/Shank scaffolding proteins, Neuroligins, FMRP, TSC, PTEN or DISC1 (Varghese et al., 2017). Numerous spine defects (changes in spine density, stability, motility or morphology) were observed *in vitro* and *in vivo* (Penzes et al., 2011).

CRMP2 involvement in pathogenesis of neurodevelopmental disorders

Deregulation of CRMP2 has been in humans associated with schizophrenia, autism spectrum disorder (ASD), mood disorders, epilepsy or Alzheimer's disease (Nakata et al., 2003, Liu et al., 2014, Clark et al., 2006, Quach et al., 2015, Braunschweig et al., 2013, De Rubeis et al., 2014) and Sfari Gene database). Among these, ASD and schizophrenia are of special interest since their symptomatic proximity but distinct pathogenesis. The exact role of CRMP2 in the development of these conditions has so far been elusive. CRMP2 deficiency in conditional knockout mice has been recently linked to schizophrenia due to changes in dendritic morphology (decreased spine number in CA1 neurons and layer 5 cortical neurons), behavioral changes (hyperactivity and social behavior impairment) and prepulse inhibition (PPI) deficit (Zhang et al., 2016, Makihara et al., 2016). Although schizophrenia and ASD share some behavioral characteristics (e.g. decreased cognitive functions, impaired social skills, repetitive behavior), they differ in the timing of their onset (early childhood for ASD, late adolescence for schizophrenia) and the nature of the underlying neuronal connectivity disorder (Lord et al., 2018, Gao and Penzes, 2015). Whereas hypoconnectivity (lower number of dendrites, dendritic spines, general decrease of white matter) is often present in schizophrenia, ASD has been associated with local hyperconectivity caused by either increased synapse formation or their incomplete pruning (Bourgeron, 2015). Because CRMP2 is downstream of Semaphorin signaling, which controls axonal pruning (Bagri et al., 2003), and it has been linked to both schizophrenia and ASD, it is one of the prime candidates to regulate this process. However, the *in vivo* analysis of both conditional and full CRMP2 knockout mice has to date mainly focused on the dendritic phenotype and associated behavioral aspects. In addition, the role of CRMP2 in class 3 semaphorin signaling (other than Sema3A), which has been previously linked to defects in pruning and ASD (particularly Sema3F) is so far not known.

2. Aim of the study

CRMP2 has been shown to regulate axon guidance by mediating Semaphorin 3A (Sema3A) signaling *in vitro*. On the other hand, CRMP2 is also a tubulin-binding molecule that promotes assembly of microtubules. Which of these two functions, if any, take precedence during physiological growth of axons is not known. It is also not clear how deletion of CRMP2 affects various aspects of neuronal development and function, since some results of recent CRMP2 mutant mice studies (Ip et al., 2011, Zhang et al., 2016, Makihara et al., 2016) were contradictory (e.g. role of CRMP2 in neuronal migration). Finally, despite the great amount of *in vitro* evidence supporting CRMP2's role in neuron polarization, axon initiation, growth or transport, no axon phenotype related to CRMP2 deficiency has so far been shown *in vivo* (Zhang et al., 2016, Makihara et al., 2016). This may indicate that either the *in vitro* CRMP2 deficiency phenotype is not in accord with the *crmp2*$^{-/-}$ mice phenotype or that the axon pathology is actually very specific.

The aim of this work is to characterize the function of CRMP2 in axon and dendrite development *in vivo* using newly generated *crmp2*$^{-/-}$ and *crmp2a*$^{-/-}$ mice. Next, we will explore the involvement of CRMP2 in a regulatory pathway of another class 3 semaphorin, Sema3F, which regulates limbic system development in mice and was implicated in neurodevelopmental disorders such as ASD (Sahay et al., 2003, Degano et al., 2009).

Furthermore, we will analyze possible involvement of CRMP2 in axon and dendritic spine pruning, while class 3 semaphorins participate in this process (Bagri et al., 2003) and only limited number of intracellular pruning mediators are known to date (Riccomagno and Kolodkin, 2015).

Finally, we will look for possible differences between two CRMP2 isoforms since the vast majority of previous studies focused only on the short one (CRMP2B). Although CRMP2B is more abundant in the brain compared to CRMP2A, the role of CRMP2A might be more specific as it has been so far found only in selected axons *in vivo* (Bretin et al., 2005). Moreover, CRMP2A is strongly expressed during embryonic development and its expression drops after birth. I will thus characterize specific CRMP2A contribution to axon development, and its regulation *in vitro* and *in vivo*.

3. Materials and methods

3.1. Resources

REAGENT or RESOURCE	SOURCE	IDENTIFIER
Antibodies		
CRMP2	WAKO	014-24821
CRMP2A, rabbit affinity purified	Balastik et al. 2015	N/A
CRMP2A, rabbit	Balastik et al. 2015	N/A
CRMP2A-S27, rabbit	Balastik laboratory	N/A
CRMP2-S522, sheep	Balastik laboratory	N/A
CRMP1	WAKO	017-24811
TUC4 (CRMP4)	Millipore	AB5454
neurofilaments	DSHB Iowa	AB_531793
MAP2	Abcam	ab70218
calbindin	Swant	CB-38a
VgluT2	Millipore	MAB5504
VgluT1	Millipore	AB5905
PSD95	Abcam	Ab12093
tau	Biotech	4019S
Olig2	Sigma	AB9610
βIII-Tubulin, conjugated to Alexa 488	Biolegend	801203
Secondary anti mouse conjugated to Alexa 488	Life Technologies	A-11029
Secondary anti rabbit conjugated to Alexa 594	Life Technologies	A-11037
Secondary anti mouse, conjugated to HRP	Life Technologies	31432
Secondary anti rabbit, conjugated to HRP	Life Technologies	31462
Bacterial and Virus Strains		
E. coli TOP10	Alberich-Jordà et al., 2012	
Chemicals, Peptides, and Recombinant Proteins		
S27-phospho-peptide CNLGSG(Sp)PKPRQK, for phospho-specific CRMP2A antibody generation	Balastik laboratory	N/A
Choleratoxin subunit B conjugated to Alexa 647	Thermo Fisher	C347777
DiI, DiO	Life Technologies	D282, D275
α-bungarotoxin conjugated to Alexa 594	Invitrogen	B13423
Antigen Unmasking Solution, Citric Acid Based	Vector	H-3300
Paraformaldehyde	Sigma Aldrich	P6148
Ethanol	VWR	20821.296
Bovine serum albumine	Sigma Aldrich	A3311
Tween20	Sigma Aldrich	274348
Mowiol	Sigma Aldrich	81381
Hoechst 33342	Sigma Aldrich	14533
Glycerol	Sigma Aldrich	G9012
Xylene	VWR	28975.291
Eukitt	Sigma Aldrich	3989
Laminin	Sigma Aldrich	L2020
Poly-D-lysine	Millipore	A-003-E
Poly-L-ornithine	Sigma Aldrich	P8638
Semaphorin 3A	R&D systems	5926-S3-025/CF
Semaphorin 3F	R&D systems	3237-S3-025/CF

Fc fragment, human	R&D systems	110-HG-100
DMSO	Sigma Aldrich	D8418
methanol	VWR	31985-047
Hydrogen peroxide	Sigma Aldrich	216763
Fetal bovine serum	Life Technologies	26140079
Neurobasal	Life Technologies	10888-022
HBSS 10x	Life Technologies	14065-049
Penicillin/Streptomycin	BioTech	SV30010
B-27	Life Technologies	17504044
OptiMEM	Life Technologies	31985
Lipofectamine 2000	Life Technologies	1662297
Diaminobenzidine	Sigma Aldrich	D8001
N-Propyl gallate	Sigma Aldrich	P3130
Polyvinylpyrollidone	Sigma Aldrich	PVP40
Tungsten microcarriers	Biorad	165-2269
Dichlormethan	P-Lab	D04101
Silica gel orange	Roth	P077.1
Sucrose	P-Lab	S01101
Sylgard 184 Silicone Elastomer kit	Dow Corning	101697
Critical Commercial Assays		
GenElute™ HP Endotoxin-Free Plasmid Maxiprep Kit	Sigma Aldrich	NA0410
Vectastain ABC kit	Vector	PK-6101/6102
Recombinant DNA		
Plasmid: CAGGS-EGFP	Balastik laboratory	N/A
Plasmid: CAGGS-mCherry	Balastik laboratory	N/A
Plasmid: pcDNA3.1-mCherry:CRMP2A (fusion protein)	Balastik laboratory	generated by Romana Weissova
Plasmid: pcDNA3.1-mGFP:CRMP2A (fusion protein)	Balastik laboratory	
Plasmid: pcDNA3.1-mCherry:CRMP2B (fusion protein)	Balastik laboratory	
Plasmid: pcDNA3.1-GFP:Pin1(fusion protein)	Balastik laboratory	N/A
Plasmid: CAGGS-CRMP2A	Balastik laboratory	generated by Barbora Pukajova
Plasmid: CAGGS-CRMP2B	Balastik laboratory	
Software and Algorithms		
Neurolucida 360	Neurolucida	N/A
Image J	NIH	N/A
Helicon focus	Helicon Soft	N/A
GraphPad Prism7	GraphPad	N/A
Adobe Photoshop	Adobe	N/A
Avisoft-SASLab Pro	Avisoft	N/A
Other		
Cell strainers, 40-µm	Biologix	N/A
Gene Gun helium-powered system	Biorad	N/A
Isopore Membrane filters 3.0 µm	Millipore	TSTP02500
Electroporator NEPA21	Nepa Gene	N/A
Stereomicroscope SMZ18	Nikon	N/A
CARV II/Nikon Ti-E spinning disc	Nikon	N/A (imaging core)
Leica TCS SP8 confocal microscope	Leica	N/A (imaging core)
Leica DMI6000 fluorescence microscope	Leica	N/A (imaging core)
FLIM module	Becker&Hickl	N/A (imaging core)

3.2. Animal housing, mouse lines, genotyping

All animal studies were ethically reviewed and performed in accordance with European directive 2010/63/EU and were approved by the Czech Central Commission for Animal Welfare. Mice, all in C57BL6/N background, were housed and handled according to the institutional committee guidelines with free access to food and water. Unless stated otherwise, adult mice used for experiments were 12 – 16 weeks old. For an experiments on mouse embryos, vaginal plugs were checked every morning during the mating period, day of positive plug is considered to be E0.5 (embryonic day 0.5) after conception.

Following mouse lines were used for experiment: *Pin1*$^{-/-}$ (Fujimori et al., 1999), *Crmp2*$^{-/-}$, *Crmp2a*$^{-/-}$,

DNA was isolated from a tail biopsy. Small piece of tissue was lysed at 55°C (lysis buffer: 100mM Tris pH 8.5, 5mM EDTA, 0.2% SDS, 200 mM NaCl, 100 µg/ml Proteinase K), DNA precipitated with sodium acetate and isopropanol, washed in 70% EtOH and dissolved in sterile water. 1µl was used for PCR. Plasmids for PCR are as follows:

CRMP2A:	
CR2A.WT.F	TCCCTCAACCCTCAGCTCT
CR2A.WT.R	GCTCGATTCAACAGATGGCT
22800.S2.R	TCCACCCCCAGGATGGAG
CRMP2:	
Ex2TAL5,6R	ACTTACCGTGATGCGTGGAA
C2.WT.F	TCACCCTCCCGGGACGAT
47090.S1.R	TCTACCAATGTTACAACACAGA
Pin1:	
MB-Pin1WT-R	GGATTAGAAGCAAGATTCGACT
MB-Pin1KO-R	CCACTTGTGTAGCGCCAAGTGC
MB-Pin1KO-F	CCGATCCTGTTCTGCAAACT

PCR protocols:

Protocol CRMP2/2A		
95°C	3 min	
95°C	50 s	
68°C	45 with TD -1°C	5x
72°C	2:30 min	
95°C	45 s	
60°C	45 s	35x
72°C	2:30 min	
72°C	3 min	
12°C	--	

Protocol Pin1		
95°C	3 min	
95°C	50 s	
68°C	40 with TD - 1°C	8x
72°C	2 min	
95°C	45 s	
60°C	30 s	35x
72°C	2 min	
72°C	3 min	
12°C	--	

PCR mixture	CRMP2/2A	
	V=	25 ul
PCR	samples	1
green buffer	2.5	2.5
dNTPs (10M)	0.5	0.5
PI (10uM)	1	1
PII	1	1
PIII	1	1
Betaine (5M)	5	5
water	12.9	12.9
Taq	0.1	0.1
DNA	1	

PCR mixture	Pin1	
	V=	25 ul
PCR	samples	1
green buffer	2.5	2.5
dNTPs (10M)	0.5	0.5
PI	1	1
PII	1	1
PIII	1	1
Betaine (5M)	0	0
water	17.9	17.9
Taq	0.1	0.1
DNA	1	

3.3. Brain isolation and preparation for analyses

Mice were anaesthetized by 30% zoletil/rometar (5:1) solution (i.m. injection, 100 – 150 µl). Animals were then perfused transcardially by 5 ml PBS and 50 ml of chilled 4% paraformaldehyde in PBS (4% PFA/PBS). Subsequently, the brain was removed from the skull, postfixed in 4% PFA/PBS overnight (4°C) and stored in PBS at 4°C.

In the case of sample preparation for histology, brains were washed in PBS overnight, trimmed and dehydrated in 50% ethanol (2 hours minimum). Then, brains were moved to 70% ethanol and processed in paraffin preparation station (histolab, Institute of Moleular Genetics). Subsequently, paraffin blocks were created and samples were sliced by microtome (7-µm sections). Slices were stored at room temperature until staining.

In all other cases, brains were washed in PBS and either traced by dyes or sliced by a vibratome. 150 µm – 250 µm-thick sections were created depending on age of the brain and purpose. Slices were stored in PBS at 4°C until imaging.

3.4. Immunohistochemistry, immunocytochemistry, whole-mount staining, western blotting

All these methods were performed as described (Balastik et al., 2015). Details are as follows:

For immunohistochemistry, paraffin sections were deparaffinated (2x 10 min. 100 % xylene, 2x 10 min. 100% ethanol, 3 min. 90% EtOH, 3min. 70% EtOH, 3 min. 50% EtOH) and washed in PBS. Antigen retrieval was performed in some cases using citrate-based antigen retrieval solution (Vector)

diluted 1:100 in water. Slices were blocked in 1% BSA/0.2% Tween/PBS (PBST) and incubated with primary antibodies overnight at 4°C. Next, slices were washed 3 x 5 min. in PBST and incubated with secondary antibodies (1:400) conjugated with Alexafluors, 2 hours at RT. Then, slices were washed 3 x 5 min. in PBST and mounted in Mowiol solution with Hoechst (1:1000). For bright field microscopy, slices were pretreated 15 min. in 3% H_2O_2 prior to blocking and ABC kit (secondary and tertiary antibodies with conjugated HRP, Vector) was used according manufactures instructions. HRP activity was detected with 0.05% DAB. Subsequently, slices were dehydrated in ethanol – xylene and embedded into Eukitt (Sigma).

Preparation of Mowiol solution: 9.6 g mowiol/9.6 ml Tris (1M, pH 8.5)/24 g glycerol/62.4 ml water, heat to 80°C, continuous stirring, takes ~ 3 – 4 hours to dissolve completely. Then centrifuge (5000g, 15 min) and aliquote. Store at -20°C.

Dissociated neurons that were analyzed by immunocytochemistry were fixed in 4% PFA/PBS, 10 min. at 4°C. After rapid washing with PBS, cells were permeabilized (0.1% tritonX-100 in PBS) for 15 min and blocked in 10% FBS/PBS for 30 minutes. Alternatively, for antigens that were not present at the cell membrane, 100% MetOH (-20°C, 5 min) was used for permeabilization. Cells were incubated with primary antibodies overnight (4°C), washed in PBS and incubated again with Alexafluor-conjugated secondary antibodies (1:1000). Coverslips were then mounted in Mowiol with Hoechst (1:1000).

Whole-mount immunohistochemistry was used for analysis of developing peripheral nervous system. This ancient method (Taniguchi et al., 1997) is still valuable for axon growth analysis *in vivo*. E10.5 – E12.5 embryos were isolated from time-pregnant mothers (heterocrosses, all embryos were genotyped) and processed as follows:

Whole mount immunohistochemistry.

1) embryo fixation – 4% PFA/PBS, 4°C, overnight
2) PBS washing, at least 8 hours (up to 48 hours), 4°C (change PBS 4 – 5x)
3) unmasking (4 – 10 min. 95 °C) – see below
4) washing – Dent‘s fix (20% DMSO/MetOH) – 30 min, 4°C
5) bleaching (5% H_2O_2 in Dent’s fix) – overnight, 4°C
6) washing – Dent‘s fix, 4°C (4 – 8 hours)
7) washing – PBS – 3x 30 min, 4°C
8) blocking – 5% FBS/20%DMSO/PBS (12 – 48 hours), 4°C
9) anti neurofilaments antibody, 1:100 – 4 days, room temperature (dilute in blocking solution)
10) washing – PBS (24 hours), 4°C

11) washing – 20%DMSO/PBS (overnight), 4°C
12) II anti mouse antibody, HRP-conjugated, 1:1000 (24 h, 4°C)
13) washing – 20% DMSO/PBS (2x 12 hours)
14) permeabilization – 0.6% Tween/PBS (overnight, 4°C)
15) washing – PBS (3x 10min), 4°C
16) DAB solution – in the dark, 4°C (0,05% DAB in PBS)
17) add 5 µl H_2O_2 (substrate for peroxidase reaction)
18) washing – PBS 10 min
19) clearing – glycerol 20% - 40% - 60% - 80% (dissolved in water)
20) store in 80% glycerol, 4°C.

Unmasking procedure – embryos were slowly heated in citrate buffer (1:100) from Vector (to reach 90 – 100°C in 6 minutes). Then, embryos were maintained at 90 – 100°C for 4 minutes, washed and cooled in PBS. Continue with cooling in Dent's fix (step 4).

Labeled embryos can be stored for months in 80% glycerol (at 4°C). To analyze axon growth, embryos were captured using Nikon SMZ18 stereomicroscope, processed with Helicon focus to create sharp 2D images and analyzed by Neurolucida.

Western blotting was performed as described (Balastik et al., 2015). Samples (either brains or their parts or dissociated cultured neurons) were dissociated in a lysis buffer (50 mM Hepes, 150 mM NaCl, 10% glycerol, 1% TritonX-100, 1.5 mM $MgCl_2$, 1 mM EGTA, 1 mM DTT, 1 mM Na_3VO_4, 100 mM NaF) with proteases inhibitors (cOmplete tablets, Roche), sonicated and spun down. Protein concentration in supernatant was determined by Bradford assay, samples were dissolved in a sample buffer at 0.5 – 2 µg/µl. Proteins were separated in 7.5% (mainly for CRMPs) or 15% (for Pin1 and similar smaller proteins) polyacrylamide gels and transferred to a PVDF membrane via wet transfer (4°C, overnight) or semidry transfer (room temperature, 2 hours). Proteins on membranes were then visualized by Coomasie staining, washed in 50%MetOH/10% Acetic acid/H_2O and 0.1% tween/TBS (TBST). Membranes were subsequently blocked in 5% milk/TBST and incubated with primary antibodies overnight. Membranes were then washed in TBST and incubated with HRP-conjugated secondary antibodies. Signal was detected by a chemiluminescence method. Briefly, membranes were washed in TBST and incubated with ECL solution (0.1M Tris, pH 8.8 with 1.25mM luminol, 0.2 mM p-coumaric acid and 0.006% H_2O_2) for 3 minutes. X-ray films were shortly (10 sec. – 5 min., depending on an antibody used) exposed to a membranes in a dark room and developed in a FUJI film developer. Films were scanned (DD scanner) and signal density was analyzed in ImageJ.

3.5. DiOlistics and DiI tracing

DiOlistics

We used diolistic approach using Gene Gun helium-powered system from Biorad to study neuron morphology in detail (Sherazee and Alvarez, 2013). Bullets were prepared as follows: tubing was coated with 10 mg/ml polyvinylpyrollidone (PVP). We mixed 100 mg Tungsten beads and 2.5 mg DiI or DiO (dissolved in CH_2Cl_2). After CH_2Cl_2 evaporation, resulted powder was transferred into alluminium-wrapped falcon tube and 3 ml H_20 were added. Solution was sonicated at 4°C until no clumps were visible (30 – 45 minutes at 4°C). Then, solution was sucked into tubing in prep station, beads settled down (2 – 5 min) and water was then removed. Tubing was rotated 1 hour during continuous drying with nitrogen (2-3 liters/min). Finally, 1.3 cm bullets were cut from tubing and stored in 4°C with silicagel beads to prevent rehydration.

Slices for diolistics were prepared as follows: mice were perfused with 20 ml 4% PFA/PBS, brains were isolated and postfixed 30 minutes in 4% PFA/PBS. Then, brains were washed 1 – 3 hours in PBS and 20 minutes in 15% sucrose/PBS following another 20 minutes in 30% sucrose/PBS at 4°C. 250 μm coronal or sagittal slices were prepared using vibratome. Prior to shooting, slices were treated 5 minutes in 15% sucrose and 5 minutes in 30% sucrose. Dye was carried using pressure 120 Psi and modified filter as described (Sherazee and Alvarez, 2013). After shooting, slices were washed 3x in PBS quickly and DiI was let to diffuse 40 min at 4°C. Slices were then mounted onto glass slice in 0.5% n-propylgallate/90% glycerol/PBS (NPG). Propylgallate was dissolved in DMSO (0.2 g/1 ml) and 100 μl of this solution was slowly added to a mixture containing 1 ml PBS10x and 9ml glycerol. Solution heated to 37°C, stirred few hours (2 hrs – overnight) and stored in a dark in 4°C.

Dendritic segments for analysis of spines were captured using Nikon spinning disc equipped with 100x oil-immersion objective. Serial z-stacks (0.3 μm steps) were analyzed by Neurolucida. In case of dendritic branching analysis, slices were scanned by Leica SP8 confocal microscope (25x oil-immersion objective). Dendritic trees of cortical pyramidal neurons and DG granule cells were manually reconstructed in 3D using Neurolucida.

DiI tracing.

For carbocyanine dye tracing mice were perfused transcardially with PBS and 4% PFA/PBS. Next, either small DiI crystal was placed or 0.1 μl of DiI solution was injected into target area (Balastik et al., 2015). We used 2.5 mg/100 μl concentration, DiI was dissolved in DMSO. After few weeks (see below), slices were prepared by vibratome and scanned by Leica TCS SP8 microscope. Details are as follows.

Corpus callosum tracing: DiI solution was injected into superficial layers of cortex. Brains were maintained in 4%PFA/PBS in 37°C for 3 – 4 weeks. Then, brains were cut in oblique (approx. +20° from a horizontal plane) direction, 150 µm-thick sections were prepared. Slices with traced axons were mounted onto glass slide in NPG mounting solution.

Hippocampo-septal axon tracing: After fixation, brains were trimmed to expose septum. DiI crystals were inserted into its medial part and brains were maintained in 4%PFA/PBS for 1-2 weeks. 100 µm (P0-1) or 150 µm (P8) coronal slices were prepared to screen for retrogradely labelled CA1 neurons in the hippocampus. We found a strong labeling of septohippocampal projections (e.g. axons arising from the septum entering the hippocampus) and also subicular neurons projecting to the medial septum in both WTs and knockouts. We screened for retrogradely labelled CA1 neurons in the hippocampus, whose presence at P8 indicates incomplete pruning (Bagri et al., 2003).

Visual cortical axon tracing: DiI solution was injected into primary visual area. After 2 – 3 weeks, brains (P9 n=3, adults n=5) were cut sagitally to 150 – 180 µm slices, that were mounted in NPG with Hoechst. The tracing pattern was compared with data from Allen brain atlas conectivity studies to ensure that we targeted correct area. We observed two axon branches in the diencephalon: first branch growing into pyramidal tract (corticospinal axons) and second to superior colliculus (collicular axons). To quantify the axonal growth into the pyramidal tract, we compared fluorescence intensity of corticospinal axons vs. intensity of axons before branching. We refer to this ratio as visual pruning index (VP index), with its lower values indicating presence of refinement.

3.6. In utero electroporations.

In utero electroporations were done as previously described (Haddad-Tovolli et al., 2013). E14.5 embryos (for analysis of migration) or E15.5 – E16.5 embryos (analysis of corpus callosum) were electroporated.

1. Setting up the surgery – electroporator, 37°C sterile PBS bath, heating lamp and heating pad were prepared, electrodes put in a sterile PBS, instruments sterilized. Prepare DNA (final concentration 3 µg/µl in PBS with 0.1% Fastgreen) and load it into a glass capillary.

2. Heating pad was covered by towels, mouse was placed into the anaesthasia induction box – isofluorane 2.5% + oxygen 1.5 ml/min.

3. Prepare an animal – after induction, mouse was placed on its back on the heating surgery pad. Limbs were fixed with lab tapes, ophtalmoseptonex was applied on the eyes (to prevent from drying) and fur on the abdomen was shaved.

4. Aimal's skin was cleaned with 70% EtOH, isofluorane decreased to 2%.

5. Laparotomy – 1.5 – 2 cm incision was made on the skin and on the muscles too, along the midline. Then place the sterile gauze (with a slit in its center) on the top of the incision and damp with preheated sterile PBS. Do not cut intestine or urine bladder.

6. Embryos (hidden in uterus) were slowly and carefully pulled out from the mother's abdomen. Damp all embryos immediately and repeat every 1 minute. Do not harm the uterus to prevent abortion. The most dangerous complications in this step are uterine rupture (sometimes possible to fix with single suture), or blooding from the uterine vessels (fatal).

7. Inject 1 – 3 µl of DNA solution into the brain ventricle.

8. Electric pulses delivery. Impedance should be checked before every electroporation, must be below 500 kΩ. Parameters for E14.5 embryos are: 33 V, 50 msec pulse + 950 msec pause, repeat 5x. Parameter for E15.5 embryos are the same, only voltage is higher (35 V minimum). Embryos should be damped before each electroporation, as well as electrodes should be quickly washed in sterile PBS.

9. After electroporation, abdominal cavity was filled with PBS and uterus was put back inside. Isofluorane was decreased to 1.5%. Muscles were sutured, subcutaneous injection of 1% Rimadyl was administered as a post-operative analgesia. Finally, skin was sutured and mouse was placed into the clean cage on a top of a heating pad. Food and water was available *ad libitum*.

10. After 2 hours, mouse was placed back to the animal house.

For most of the experiments, we used pCAGGS-EGFP or pCAGGS-mCherry plasmid. In case of rescue experiments, we injected mixture (3:2, 5 µg/µl total) of CRMP2A or CRMP2B together with EGFP, all again in pCAGGS plasmid. Embryos electroporated at E14.5 (migration assay) were analyzed at E17.5 after overnight fixation in 4% PFA/PBS. Embryonic brains were sliced (150 µm vibratome sections), counterstained with Hoechst and scanned by Leica TCS SP8. Embryos electroporated at E15.5 were analyzed at P6. Pups were nurtured by a foster mother. At P6, mice were sacrificed, brains were fixed in 4% PFA/PBS, sliced (150 µm vibratome sections) and scanned by Leica TCS SP8 or CARV II/Nikon Ti-E spinning disc.

3.7. Cell cultures, transfections, in vitro assays and imaging.

Primary neurons

Mouse E16.5 hippocampal neurons were prepared and cultured as described (Balastik et al., 2015). Briefly, pregnant mice were sacrifised, embryos isolated and decapitated in cold HBSS with 10 mM Hepes. Hippocampi and/or cortices were isolated, moved to Neurobasal medium (Neurobasal (Gibco) with 2.5% B27 supplement (Gibco), 2.5 mM glutamine and 1% Penicillin/Streptomycin solution) and triturated. Subsequently, solution was strained through a 40-µm strainer (Biologix) and spun down

(300g, 2 min., 4°C). Supernatant was removed, remaining cells resuspended in a fresh Neurobasal medium and counted. Neurons were plated into cultivation plates or cover slips coated previously with laminin (1 µg/ml) and poly-D-lysine (PDL, 50 µg/ml). Neurons were cultured in Neurobasal medium that was refreshed every two days.

Cultivation densities are as follows: 400.000/well in a 12-w plate, 100.000/well in a 24-w plate, 80.000/well in a glass-bottom 24-w plate and 4-well coverslip, 40.000/well in 8-well coverslip. Neurons for immunocytochemistry were cultured on glass coverslips in the 24-w plate. Coverslips were sterilized in 70% EtOH overnight, then washed extensively with sterile water and coated with PDL and laminine.

In selected cases, neurons were transfected using lipofectamine-2000 (Invitrogen), 24 hours after plating unless state otherwise. In brief, 2 µg DNA/well with 2 µl Lipofectamine/well were mixed in Optimem (Gibco) and incubated 30 minutes. Cells were washed in Optimem and incubated in DNA/Lipofectamine solution for 4 hours. In case of longitudinal experiments (more than 2 weeks), neurons were transfected at DIV14 with 2 µg DNA/well and 1 µl Lipofectamine/well.

In vitro assays for assessment of Sema3A/Sema3F regulation of axon growth and retraction were performed as follows. Mouse Sema3A and 3F (carrier free) or control Fc were purchased from R&D systems and were diluted to 1 mg/ml stock concentration in sterile PBS. At DIV 7 culture, medium volume was adjusted to 300 µl in each well. Neurons were photographed three times (with 20 minutes gaps), then 50 µl of fresh medium with semaphorins or control Fc was added. Subsequently, neurons were imaged every 20 minutes for 16 hours by Leica DMI6000 equipped with a heating box (37°C) and CO_2 atmosphere (5% CO_2).

In vitro analysis of dendritic spines was done on DIV21 – DIV25 neurons. Briefly, cultures were photographed (Leica SP8 microscope with a heating chamber and CO_2 atmosphere) at DIV21, positions were saved (LAS X software for Leica SP8 operation) and relocated again at DIV25 for the second photograph. Then, neurons were stimulated with semaphorins for 3 hours and photographed for the 3rd time.

Microfluidic culture experiments

Microfluidic chambers were prepared as described before (Ionescu et al., 2016) (Maimon et al., 2018). E11.5 – E12.5 spinal cord explants were dissected in cold HBSS and placed into Laminin (3 µg/ml) and Poly-L-Ornithine (1.5 µg/ml) coated proximal well. After 3 – 4 days, axons entered the distal compartment. Then, explants were labelled by Alexa 647-conjugated choleratoxin subunit B. 5 nM Sema3A of control Fc was applied distally and axons were photographed by Leica DMI6000 microscope every 10 minutes during 14 hours interval (n=7-8 chambers per condition, 3 experiments). Axons growing at least 50 µm were analyzed.

Microscopy

We used microscopes available in the microscopy facilities of both Institute of Physiology and Institute of Molecular Genetics. Details are as follows:

1) We used Leica SP8 confocal microscope for analysis of most of the DiI-traced brains, electroporated brains and for colocalization experiments. We created 3D stacks for further reconstructions.

2) We used Nikon Spinning disc microscope for routine immunohistochemistry and for analysis of dendritic spine details (using precise 100x oil-immersed objective).

3) For analysis of whole-mount immunolabeling of embryos, we captured samples by Nikon SMZ18 stereomicroscope.

4) FRET-FLIM analysis was performed by Leica SP8 equipped with Ti-Saphire laser (Chameleon Ultra I, Coherent) and time-correlated single photon counting (SPC) module from Becker&Hickl. Laser was tuned to 920 nm (simultaneous excitation of GFP and mCherry), emitted photons were segregated with a dichroic mirror (550 nm) and detected with two separate detectors (Leica HyD NDDs) placed downstream of two filters (green 525/50, red 610/75). Photons from a green (donor) channel were collected for 45 – 60 seconds. Images were analyzed in SPC image software.

5) Time-lapse imaging was performed by Leica Dmi6000 fluorescent microscope equipped with a 5% CO_2 atmosphere and 37°C chamber. Details of imaging are listed in respective experiments. Please find examples of time-lapse videos in the online supplement.

3.8 Image processing and statistics.

We used Neurolucida 360 software to reconstruct callosal axons from both in utero electroporation and DiI-tracing experiments. In case of horizontal sections, we picked only midline regions (approximatelly 100 μm from midline to each side) and traced axons semi-automatically using AutoNeuron algorhytm. To display overall axon growth direction, polar histograms and fan in diagrams were generated using Neurolucida explorer. Polar histograms show total axon length in a specific degree range. We counted lengths in each 20° of histogram. Fan in diagrams represents the same in another graphical view when all traced axons rise from a single point. Dendrites and dendritic spines were analyzed either with Neurolucida 360 or with NeuronJ plugin in ImageJ. Images from whole-mount preparations were processed in Helicon focus to create sharp projections. Growth of peripheral nerves and all data from time-lapse imaging series were analyzed in ImageJ. Neuron migration was analyzed in Image J using cell counter plugin. Measurements of axon pruning from immunohistochemistry and DiI-tracing experiments were done in ImageJ. In all figures, different

channels of image series were combined in pseudo-colour using the „screen" function in Adobe Photoshop, and adjusted to enhance low-intensity objects. For comparison of two independent groups, unpaired t-test was used unlike stated otherwise. Data from behavioural experiments were analyzed by ANOVA or Kruskal-Wallis test.

4. Results

4.1 The role of CRMP2 in axon guidance *in vivo*

Generation and overall characterization of *crmp2*$^{-/-}$ mice

Crmp2 gene possesses two mutually exclusive first exons, each of them with its own promotor, so two different mature mRNAs are then translated into two proteins: CRMP2A and CRMP2B. The vast majority of previous work in the field has focused on the most abundant isoform, the shorter one, CRMP2B. *Crmp2*$^{-/-}$ mice, which lack both isoform, were generated in Balastik's laboratory by TALEN mutagenesis (Fig. 10). Two TALEN pairs targeting sequences 185-150bp 5' of *crmp2* exon 2 and 183-218bp 3' of exon 3 (Fig 10A) were designed using TAL Effector Nucleotide Targeter 2.0 (https://tale-nt.cac.cornell.edu/) (Cermak et al., 2011, Doyle et al., 2012), assembled using the Golden Gate Cloning system (Cermak et al., 2011), and cloned into the ELD-KKR backbone plasmid. TALEN mRNAs (with total RNA concentration of 40 ng/μl) were microinjected into C57BL6/N-derived zygotes. Genomic DNA isolated from tail biopsies of newborn mice was screened by PCR for deletion of exon 2 and 3, deletion was confirmed by locus sequencing and mice used as founders of *crmp2*$^{-/-}$ line. Knockout of CRMP2 was confirmed by western blot analysis of brain lysates and by immunohistochemistry (Fig. 10B,C). CRMP2 functions as a phosphorylation-dependent switch – it binds and stabilizes microtubules in nonphosphorylated state and releases from them upon phosphorylation (Sumi et al., 2018). After years of experiments, there are multiple *in vitro* evidences of CRMP2's role in axon growth, cell polarity and dendrite development (reviewed in (Yamashita and Goshima, 2012, Ip et al., 2014, Moutal et al., 2019)). It was assumed that CRMP2 is vital for development of axons – even in 2015 some colleagues claimed (Quach et al., 2015) knockout of CRMP2 in mice is lethal (various attempt to generate *crmp2*$^{-/-}$ mice failed before). In order to test this hypothesis, we generated *crmp2*$^{-/-}$ mice to study functions of CRMP2 *in vivo*. Together, our CRMP2 knockout mice were viable and fertile and apparently more physically active in comparison with WT mice of the same strain (confirmed later in behavioral tests).

Previous *in vitro* and *in vivo* experiments using *in vivo* knockdown of CRMP2 suggested that CRMP2 regulates neuronal migration, neuronal polarity and axon and dendrite formation (Ip et al., 2014). We therefore investigated cytoarchitecture of areas where CRMP2 is highly expressed, that is, cerebral cortex, cerebellum and hippocampus. We performed *in utero* electroporation of GFP in E14.5 WT and CRMP2 knockout embryos and analyzed GFP-positive migrating neurons at E17.5 in brain slices after brain isolation and fixation. We found no defects in neuron distribution thorough the cortical plate at E17.5 (Fig. 11F) which could reflect different experimental paradigms. Similarly, we found unchanged cortical lamination in adult mice (Fig. 11E) further confirming our negative results from migration experiments (Fig. 11F).

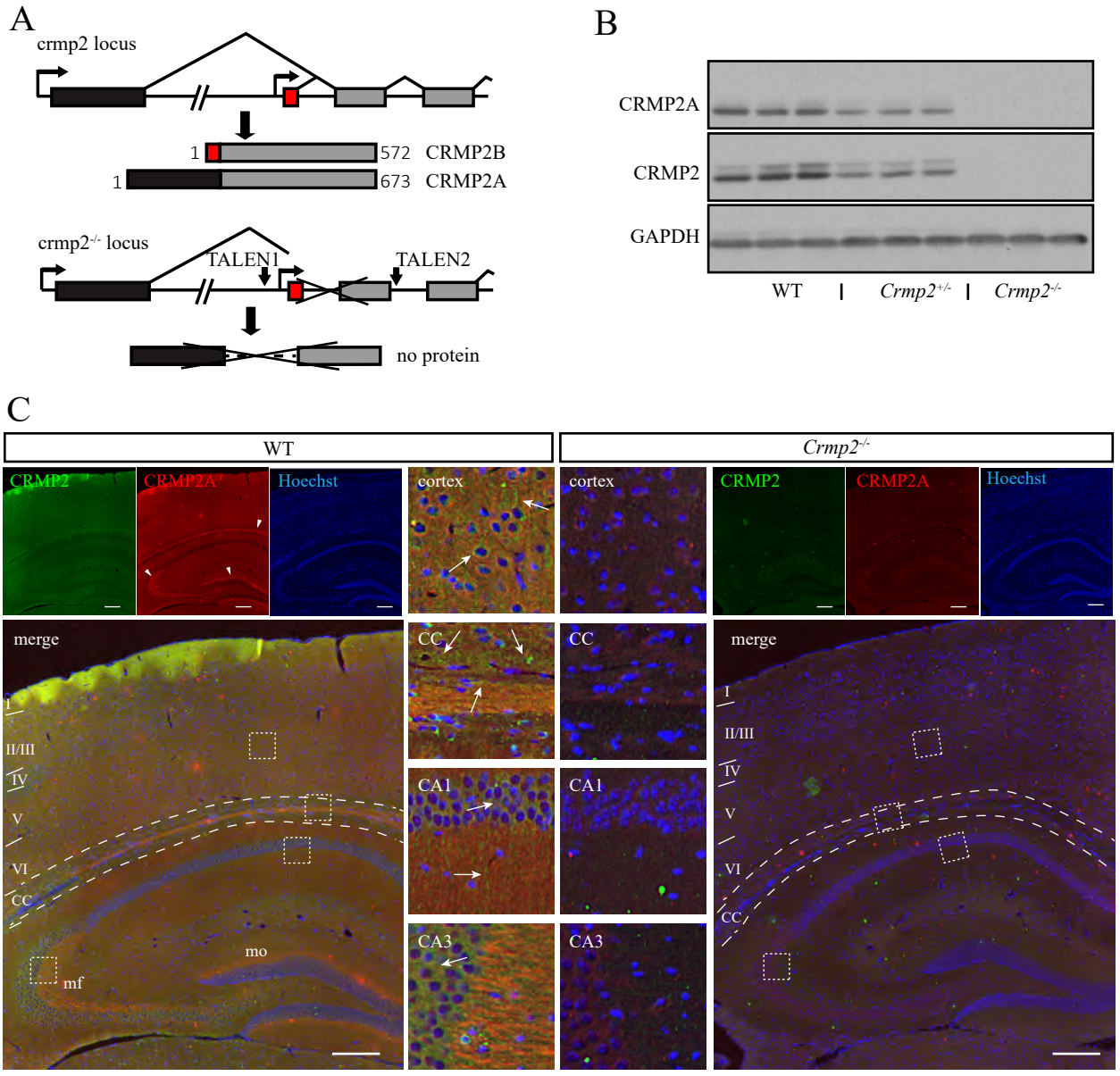

Figure 10. Generation of *crmp2*$^{-/-}$ mice. (A) Generation of CRMP2 knockout mice by TALEN mutagenesis. Alternative first exons are highlighted in black and red. (B) WB analysis of brain lysates of *crmp2*$^{+/+}$, $^{+/-}$ and $^{-/-}$ mice (left – one brain per genotype, right – 3 brains per genotype). (C) CRMP2 (A+B isoforms, arrows) and CRMP2A (arrowhead) isoform immunostaining of coronal brain sections from adult WT and *crmp2*$^{-/-}$ mice. Both isoforms are missing in *crmp2*$^{-/-}$ mice. CRMP2B is present throughout the cortex, and hippocampal CA1 and CA3 regions. CRMP2A is localized mostly in callosal axons (CC), mossy fibers (mf) and inner molecular layer (mo) of dentate gyrus. Scale bars: 100 μm.

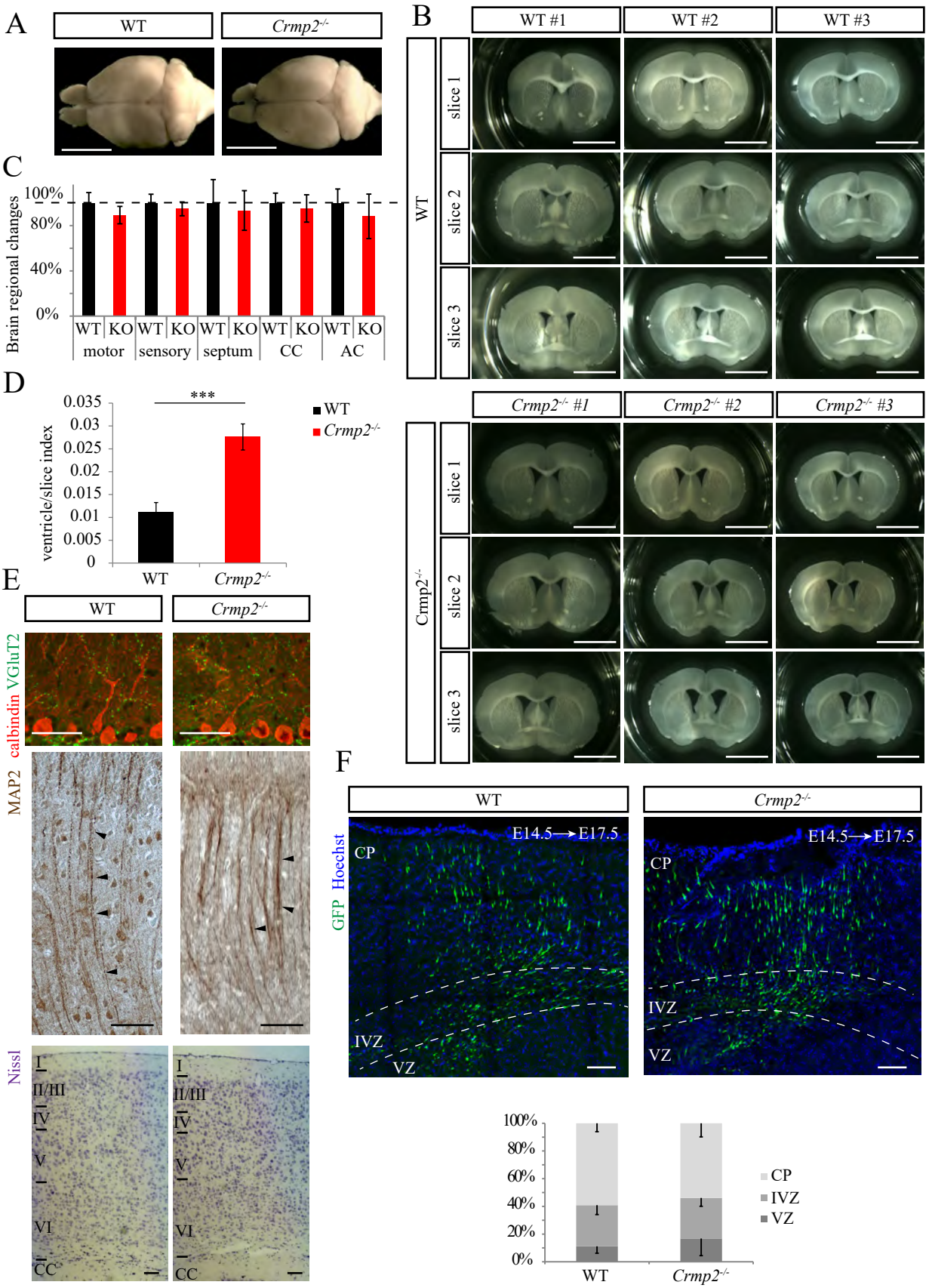
A
WT
Crmp2-/-
B
WT #1
WT #2
WT #3
WT
slice 1
slice 2
slice 3
Crmp2-/- #1
Crmp2-/- #2
Crmp2-/- #3
Crmp2-/-
C
Brain regional changes
100%
80%
40%
0%
WT KO WT KO WT KO WT KO WT KO
motor
sensory
septum
CC
AC
D
ventricle/slice index
0.035
0.03
0.025
0.02
0.015
0.01
0.005
0
***
WT
Crmp2-/-
E
calbindin VGluT2
MAP2
Nissl
I
II/III
IV
V
VI
CC
F
GFP Hoechst
E14.5→E17.5
CP
IVZ
VZ
100%
80%
60%
40%
20%
0%
CP
IVZ
VZ

Next, we studied cortical apical dendrites while Sema3A signaling is involved in regulation of their orientation and growth (Whitford et al., 2002) and CRMP2 is downstream from Sema3A (Goshima et al., 1995). We however found no differences between WT and *crmp2*$^{-/-}$ cortical apical dendrite orientation (Fig. 11E). Analysis of the brain size using both whole brains and serially-sectioned fixed brains showed no significance between WT and *crmp2*$^{-/-}$ mice (Fig. 11A, B), although there was a tendency for smaller cortical thickness in the knockouts (Fig. 11C). Cerebellar Purkynje cells (PC) also showed no major defects in their shape or distribution of excitatory synapses labeled by VGluT2 (Fig. 11E), although semaphorin signaling regulates development of PC's synapses (Uesaka et al., 2014). These negative results suggest that the role of CRMP2 in Sema3A signaling may be redundant. We however observed increased volume of lateral ventricles, similar as shown in the brain-specific knockouts, where authors suggest that as a sign of a neurodevelopmental defect (Fig. 11D, Zhang et al., 2016).

To conclude, it appears that CRMP2 is not vital for general brain development, unlike expected (Quach et al., 2015), as our *crmp2*$^{-/-}$ mice are not embryonically lethal and demonstrate only a mild neurodevelopmental defects.

Figure 11 (opposite). General appearance of *crmp2*$^{-/-}$ brains. (A) Upper view of WT and *crmp2*$^{-/-}$ brains showing similar brain size. Scale bars: 5 mm. (B) Three 250-μm coronal sections from n=3 WT and *crmp2*$^{-/-}$ mice demonstrate enlarged ventricles in *crmp2*$^{-/-}$ mice. Scale bars: 5mm. (C, D) Quantification of area (septum, ventricles) or width (motor and sensory cortex) or diameter (corpus callosum (CC) and anterior commissure (AC)) in brain slices from (B). The ventricle areas were normalized to total slice area (ventricle/slice index) WT 0.011±0.001, *crmp2*$^{-/-}$ 0.027±0.003, $p<0.001$). Mean ± SD, ***$p<0.001$, t-test. All other comparisons (C) were not significantly different and for clarity *crmp2*$^{-/-}$ values were normalized to WT values. (E) Comparison of synapses in Purkynje cells (stained with calbindin and VGluT2, scale bars: 50 μm), apical dendrites in the cortex (MAP2) and cortical lamination (Nissl) showed no differences between WTs and knockouts. Scale bars: 100 μm. (F) Analysis of cortical neuron migration (WT/*crmp2*$^{+/-}$ n=6, *crmp2*$^{-/-}$ n=4). Both WTs and heterozygous (Het) embryos were used as controls. Embryos were electroporated with GFP expressing plasmid at E14.5 and analyzed at E17.5. Quantification of percentages of GFP positive neurons in different layers is shown. CP – cortical plate, IVZ – interventricular zone, VZ – ventricular zone. Scale bars: 100 μm, mean ± SD, t-test.

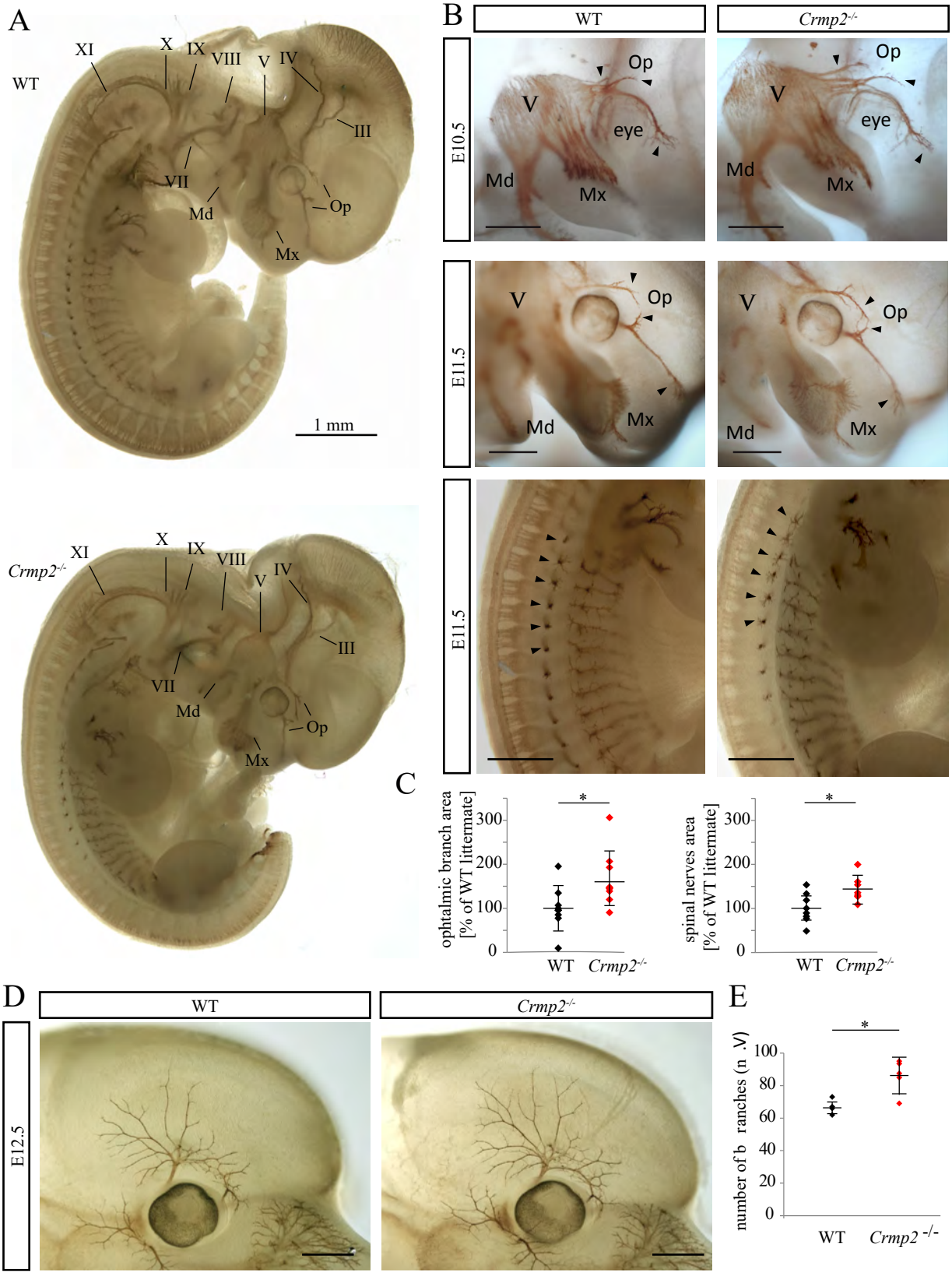
A
WT
XI
X
IX
VIII
V
IV
III
VII
Md
Op
Mx
1 mm
Crmp2-/-
B
WT
Crmp2-/-
E10.5
E11.5
E11.5
V
Op
eye
Md
Mx
C
ophtalmic branch area [% of WT littermate]
spinal nerves area [% of WT littermate]
300
200
100
0
*
WT
Crmp2-/-
D
E12.5
WT
Crmp2-/-
E
number of b ranches (n .V)
100
80
60
40
20
0
WT
Crmp2 -/-

Crmp2$^{-/-}$ mice display defects in the growth of cranial nerves.

CRMP2 has been shown to mediate Sema3A signaling and regulate axon growth guidance *in vitro* (Goshima et al., 1995). For example, in chick DRGs, Sema3A-induced growth cone collapse was reduced after anti-CRMP2 antibody treatment (Goshima et al., 1995). Overexpression of CRMP2 in hippocampal neurons induced growth of multiple axons from one cell (Inagaki et al., 2001). Similarly, in N1E-115 cells, CRMP2 overexpression increases number of neurites and promotes their elongation (Arimura et al., 2005).

To test whether CRMP2 deficiency leads to altered axon growth also *in vivo*, we first analyzed development of peripheral nerves in mouse embryos using whole-mount immunohistochemistry (Fig. 12A). At E10.5 – E12.5, axons are well distinguishable with anti-neurofilaments antibody which at this stage can still easily diffuse into the tissue. Peripheral nerves serve as a valid model of axon growth and guidance. For example, development of sensory cranial nerves is regulated by Sema3A and Slit (Kitsukawa et al., 1997, Taniguchi et al., 1997, Chen et al., 2000, Cheng et al., 2001). Both CRMP2 isoforms are present in cranial nerves during development (Fig. 13A).

Figure 12 (opposite). Whole-mount staining reveals axon guidance defects in peripheral nerves in *crmp2*$^{-/-}$

(A) Whole-mount immunohistochemistry with anti-neurofilaments antibody for visualization of peripheral nerves. All peripheral nerves are present in *crmp2*$^{-/-}$. III – occulomotor, IV – trochlear, V – trigeminal, VII – facial, VIII – vestibulocochlear, IX – glossoparyngeal. X – vagal, XI – accessory nerve. Op – ophthalmic branch, Mx – maxillar branch, Md – mandibular branch of the trigeminal nerve. (B) In *crmp2*$^{-/-}$ embryos, the growth of ophthalmic branch of the trigeminal nerve is increased and axons are defasciculated (first and second row, arrowheads). Similarly, we detected increased growth and branching of lateral branches of spinal nerves in *crmp2*$^{-/-}$ embryos (third row, arrowheads). Trigeminal nerve (V) and its branches (Op – ophthalmic, Mx – maxillar, Md – mandibular) as well as embryonic age (E10.5, E11.5) are indicated. Scale bars: 500 μm (C) Quantification of areas innervated by ophthalmic branches of trigeminal ganglions and spinal nerves, normalized to WT littermates (each dot depicts one embryo). Area of ophthalmic branch in *crmp2*$^{-/-}$ was increased by 66% ($p<0.05$, n=10, 3 litters). For spinal nerves, total area in knockouts was increased by 45% ($p<0.05$, WT n=8, *crmp2*$^{-/-}$ n=7, 3 litters). Mean ± SD, * $p<0.05$, t-test. (D) Whole-mount immunolabeling of embryos at E12.5 (WT n=4, *crmp2*$^{-/-}$ n=5, 2 litters), note the increased branching of the Op branch in *crmp2*$^{-/-}$. Scale bars: 500 μm. (E) Quantification of the number of the Op branches (WT 67±4.5, *crmp2*$^{-/-}$ 86±10.3, $p<0.05$), mean ± SD are shown, *$p<0.05$, t-test.

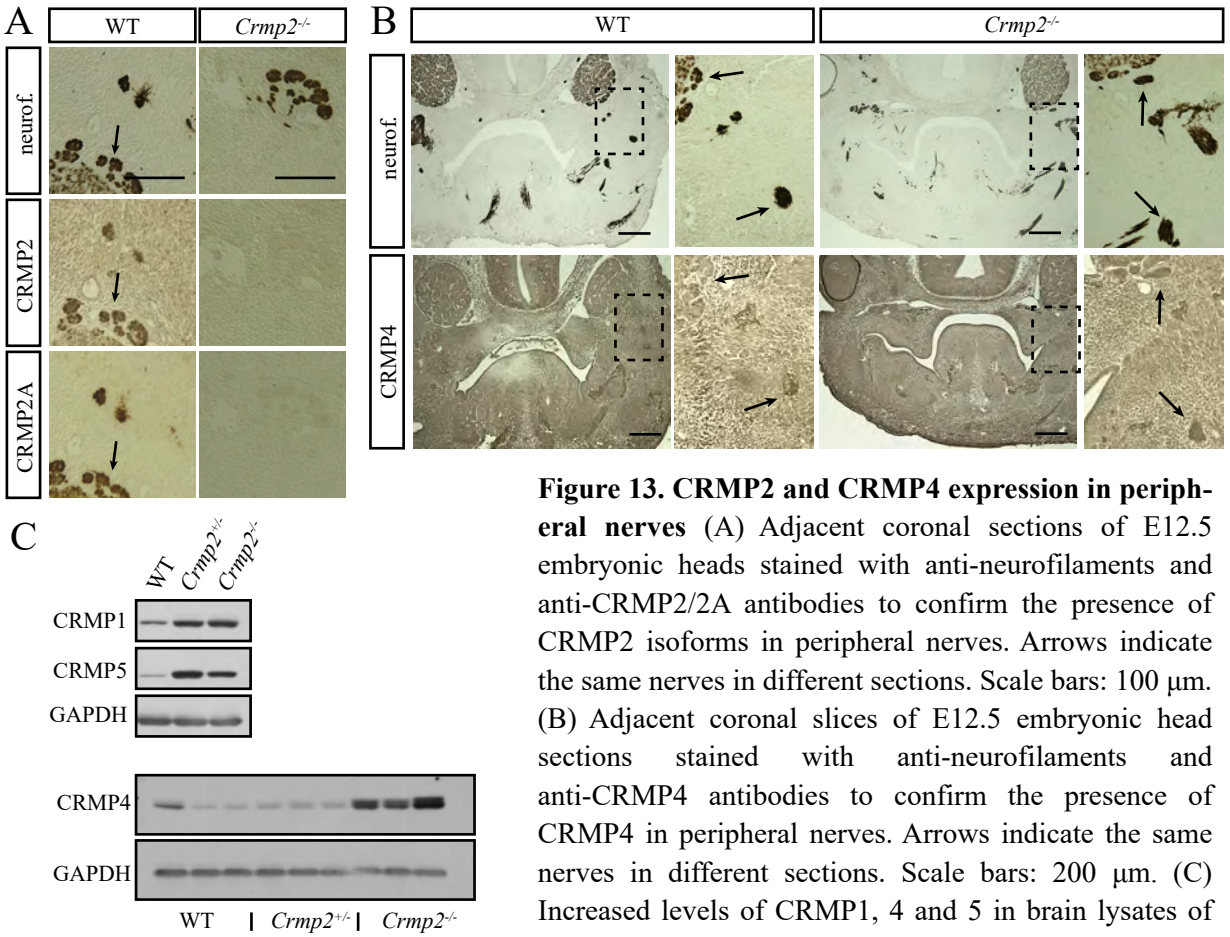

Figure 13. CRMP2 and CRMP4 expression in peripheral nerves (A) Adjacent coronal sections of E12.5 embryonic heads stained with anti-neurofilaments and anti-CRMP2/2A antibodies to confirm the presence of CRMP2 isoforms in peripheral nerves. Arrows indicate the same nerves in different sections. Scale bars: 100 µm. (B) Adjacent coronal slices of E12.5 embryonic head sections stained with anti-neurofilaments and anti-CRMP4 antibodies to confirm the presence of CRMP4 in peripheral nerves. Arrows indicate the same nerves in different sections. Scale bars: 200 µm. (C) Increased levels of CRMP1, 4 and 5 in brain lysates of homozygotes revealed by western blotting.

In our experiments, embryos from time-pregnant mothers were isolated, fixed in 4% PFA and stained with anti-neurofilaments antibody (Fig. 12A). Both WTs and knockouts from the same litter were analyzed. Embryos were cleared in ascending glycerol concentration (20% - 80%) and photographed with stereomicroscope. We quantified changes in neuron growth by measuring the area innervated by axons from each given nerve (E10.5 – E11.5, Fig. 12B) and branching by counting of the total number of branches (E12.5, Fig. 12D). The growth and branching of the ophthalmic branch of the trigeminal nerve was significantly increased in *crmp2*$^{-/-}$ mice at E10.5 – E12.5 (Fig. 12C, E) and similarly increased was the sprouting of the lateral branches of the spinal nerves (Fig. 12C). Axon projections from DRGs to the spinal cord were not changed in *crmp2*$^{-/-}$ mice, and neither was the growth of intercostal or upper/hind-limb nerves (Fig 12A, B).

We speculated that other CRMP family member(s) may promote axon growth in CRMP2-deficient neurons, since CRMP1 (Yamane et al., 2017) and CRMP4 (Fig. 13B) are also expressed in peripheral nerves. We indeed observed that CRMP1 and CRMP4 level is increased in the brain lysate of *crmp2*$^{-/-}$ mice (Fig. 13C). Since growth of both the ophthalmic branch as well as the lateral branches of the spinal nerves are negatively regulated by Sema3A (Taniguchi et al., 1997), our data support the function of CRMP2 as a mediator of Sema3A signaling. Moreover, our data thus indicate that the growth-promoting function of CRMP2 is redundant *in vivo* at least in the tested neurons, but that its function as a mediator of repulsive axon guidance signals is unique and cannot be fully rescued by other proteins.

Crmp2$^{-/-}$ neurons show decreased responses to Sema3A.

To directly demonstrate that CRMP2 deficiency interferes with Sema3A signaling in peripheral neurons isolated from *crmp2*$^{-/-}$ mice, we took an advantage of the microfluidic chamber approach for extraaxonal environment manipulation. In this chamber, cell bodies and axons are separated in proximal or distal compartment, respectively (Maimon et al., 2018). We prepared spinal cord explants from WT and *crmp2*$^{-/-}$ E11.5 – E12.5 embryos and cultured them for 4 – 5 days until motor neuron axons crossed to the distal compartment (Fig. 14A). Then, we stained axons with Alexa 647-conjugated choleratoxin subunit B and analyzed their growth by time-lapse imaging. Axons were imaged by fluorescence microscope equipped with an incubator chamber. At basal conditions the growth of WT and *crmp2*$^{-/-}$ explants and their axons was comparable indicating again that the axon growth-promoting function of CRMP2 is redundant, at least in the tested neurons. When we added Sema3A (5nM) to the distal (axonal) compartment, we observed decrease in the number of growing WT axons, as expected ($p<0.001$, Fig. 14B, C video 2). However, in *crmp2*$^{-/-}$ explants, Sema3A had no significant effect on the number of growing axons ($p=0,99$, Fig. 14B, C, video 2).

To test whether we detected a similar effect also in the CNS neurons, we next performed an *in vitro* axon outgrowth assay using isolated embryonic cortical neurons from E16.5 embryos. Neurons were plated at 24-well plate, transfected with EGFP at DIV1 and stimulated with Sema3A at DIV7-8. In WT, Sema3A decreased relative amount of long-growing (>100 μm) axons and, vice versa, increased number of axons growing less than 100 μm (Fig. 14D, E, video 3). Thus, similar to the previous experiment, CRMP2 deletion prevents Sema3A-induced axon growth responses. Together, in accord with the previously published data (Goshima et al., 1995, Brown et al., 2004), we demonstrate that CRMP2 mediates Sema3A signaling *in vitro* and participate in guidance of peripheral nerves in Sema3A-repelling regions *in vivo*.

CRMP2 regulates anatomy and axon guidance in Corpus Callosum.

In addition to the peripheral nerves, we analyzed the effect of CRMP2 deficiency on axonal growth also in the central nervous system. We detected anatomical changes in the largest axonal bundle of the brain, the Corpus callosum (CC), in *crmp2*$^{-/-}$ mice. The length of Corpus callosum (CC) was significantly reduced in juvenile (-19.2%, $p<0,05$) as well as adult (-19.5%, $p<0,05$) knockout mice as can be appreciated in both sagittal and coronal sections (Fig. 15A, B). More detailed labeling of the tract with anti-neurofilaments antibody showed that the posterior part of the CC (splenium) is markedly hypoplastic in *crmp2*$^{-/-}$ mice, ending rostrally to the habenular commissure, while the WT splenium is longer, located just above the habenular commissure (Fig. 15C). Callosal axons have been shown to be guided by various semaphorins including Sema3A (Zhou et al., 2013, Wu et al., 2014). Thus, we next asked whether dysgenesis of the CC we detected in *crmp2*$^{-/-}$ mice is also accompanied by defects in callosal axon guidance. We *in utero* electroporated WT and *crmp2*$^{-/-}$ embryonal cortices

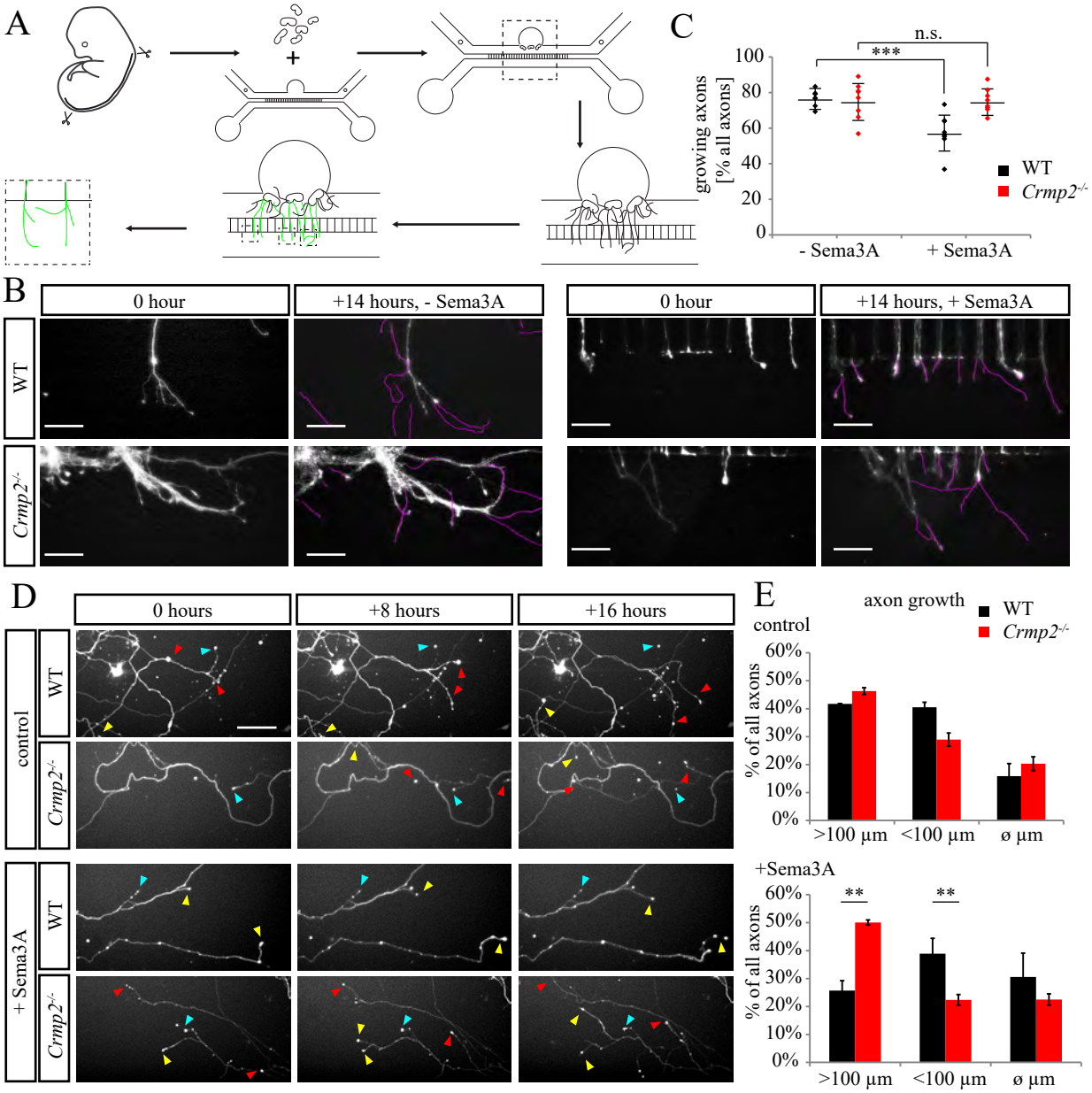

Figure 14. CRMP2 deletion abolishes effects of class 3 semaphorins (A) Experimental design of motor neuron cultures in microfluidic chambers using spinal cord explants. Dashed squares in the second row show areas that were scanned and analyzed. (B) Growth of motor neurons from E11.5 – E12.5 WT and *crmp2*$^{-/-}$ spinal cord explants in microfluidic chambers. Excerpts from 14 hour time-lapse imaging are shown. Upon application of Sema3A into distal compartment, WT axons tend to stop or slow down their growth unlike *crmp2*$^{-/-}$ axons. Purple lines highlight the growth path of individual axons in a distal chamber. Scale bars: 100 µm. See also video 2. (C) Quantification of the fraction of growing (>50 µm) axons in one imaging field (WT: control 76.8±5.7%, Sema3A 57.7±10.6%, p<0.001, *crmp2*$^{-/-}$: control 75.4±10.4%, Sema3A 75.4±6.7%, p=0.99), n=3 experiments per genotype, 7-8 explants per condition. Mean ± SD. *** p<0.001, 2-way ANOVA with Bonferroni's multiple comparisons test. (D) Time-lapse imaging of DIV7 cultured cortical neurons to assess axon growth after semaphorin stimulation. Upper panel: Axon behavior in medium without Semaphorins. Lower panel: stimulation with Sema3A decreases growth rate in WT but not *crmp2*$^{-/-}$ neurons. Red triangles show long (>100 µm) growing axons, yellow show short growing axons (<100 µm) and blue indicate steady non-growing axons (arrest). See also video 3. Scale bars: 100 µm. (E) Quantification of axon growth. After Sema3A stimulation, relative amount of long growing axons in *crmp2*$^{-/-}$ was significantly higher than in WTs (p=0.002), while number of short axons was lower (p=0.007). Mean ± SD. ** p<0.01, *** p<0.001, t-test.

with pCAGGS EGFP vector at E15.5, which results in labeling of cortical layer 2/3 (i.e. mainly callosal-projecting neurons). The brains were collected at postnatal day 6 (P6), fixed in 4% PFA and cut coronally to trace callosal axons in a hemisphere contralateral to the electroporation site (Fig. 15D, E). At this stage, axons from somatosensory cortex enter the contralateral cortex in WT (Wang et al., 2007). Most of the WT axons showed well organized, parallel growth. In contrast, *crmp2*$^{-/-}$ axons often failed to grow in an organized, parallel way upon leaving the main callosal tract, their distribution in the cortex seemed uneven. We tracked the electroporated axons after leaving callosal bundle at the contralateral site and quantified their tortuosity (i.e. the ratio of real length of the segment vs. distance of the first and last point of the segment, Fig. 15E). We found that tortuosity was significantly higher in *crmp2*$^{-/-}$ in comparison to WT ($p<0.001$, Fig. 15F).

Importantly, in some coronal sections of *crmp2*$^{-/-}$ mice we detected deregulated growth of callosal axons even in the midline. Together with the reduced length of corpus callosum in *crmp2*$^{-/-}$ mice in the rostro-caudal axis we detected (Fig. 15A – C) it was suggesting that CRMP2 deficiency may alter the rostro-caudal guidance of callosal axons in the midline. To test this hypothesis, we traced the callosal axons by injecting DiI into the fixed P9 and adult somatosensory cortices and analyzed organization and fasciculation of the traced axons in the midline (see Materials/Methods). We found that at P9, *crmp2*$^{-/-}$ axons were significantly more distorted as seen upon plotting to polar histograms or fan-in diagrams (interval (0°, ±20°): $p=0.05$, interval (±20°, ±40°): $p=0.02$, Fig. 16). However, no differences were present in adult brains indicating that the defects are corrected later in development. Together, our results show that CRMP2 is an important regulator of axon growth and guidance in both peripheral (PNS) as well as central nervous system (CNS) and that out of the two major functions of CRMP2 (promotion of axon growth and mediation of Sema3A-dependent axon guidance) the mediation of axon guidance takes precedence over the growth promotion *in vivo*.

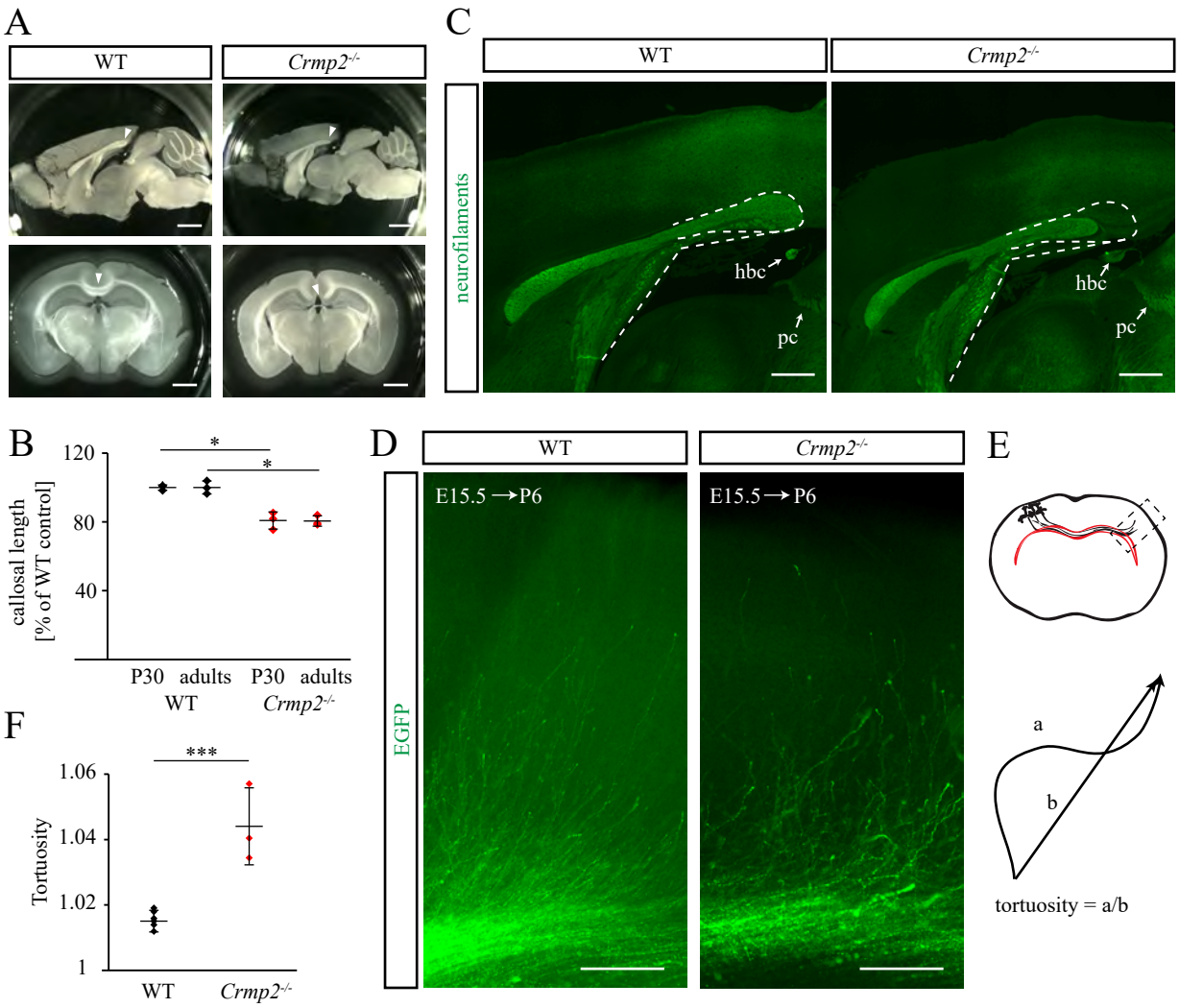

Figure 15. Defects in corpus callosum in *crmp2*$^{-/-}$ mice. (A) CRMP2 deficiency leads to callosal hypoplasia. Shortening of corpus callosum (arrowheads) is apparent in both sagittal (first row) and coronal sections (second row) of adult brains. Scale bars: 1 mm. (B) Quantification of callosal length in 30-days old mice (P30, n=3, *crmp2*$^{-/-}$ is 80.8±5% of WT, p=0.003) and adult mice (n=3, *crmp2*$^{-/-}$ is 80.5±3% of WT, p=0.002), mean ± SD, * p<0.05, t-test. (C) Labeling of adult corpus callosum with anti-neurofilaments antibody in sagittal sections. Outline depicts missing posterior part of the tract in *crmp2*$^{-/-}$ mice. Caudal part of the corpus callosum in WTs is located dorsally above the habenular commissure (hbc), while in *crmp2*$^{-/-}$ mice callosum terminates rostrally before reaching the hbc (arrows). PC indicates posterior commissure. Scale bars: 500 µm. (D) The growth of GFP-labeled callosal axons in the contralateral cortex at P6 (embryos were electroporated at E15.5, WT n=6, *crmp2*$^{-/-}$ n=3). Note the disorganized paths of *crmp2*$^{-/-}$ axons. Scale bars: 200 µm.(E) Schematic drawing of the callosal axon path. Pyramidal neurons in layer II/III projects their axons into the contralateral cortex (rectangle depicts the area displayed in (D)). Calculation of tortuosity: tortuosity=1 if a=b. (F) Quantification of tortuosity of axons upon their exit from the callosal tract (WT 1.016±0.003 vs. *crmp2*$^{-/-}$ 1.044±0.012, p<0.001), mean ± SD, ***<0.001, t-test.

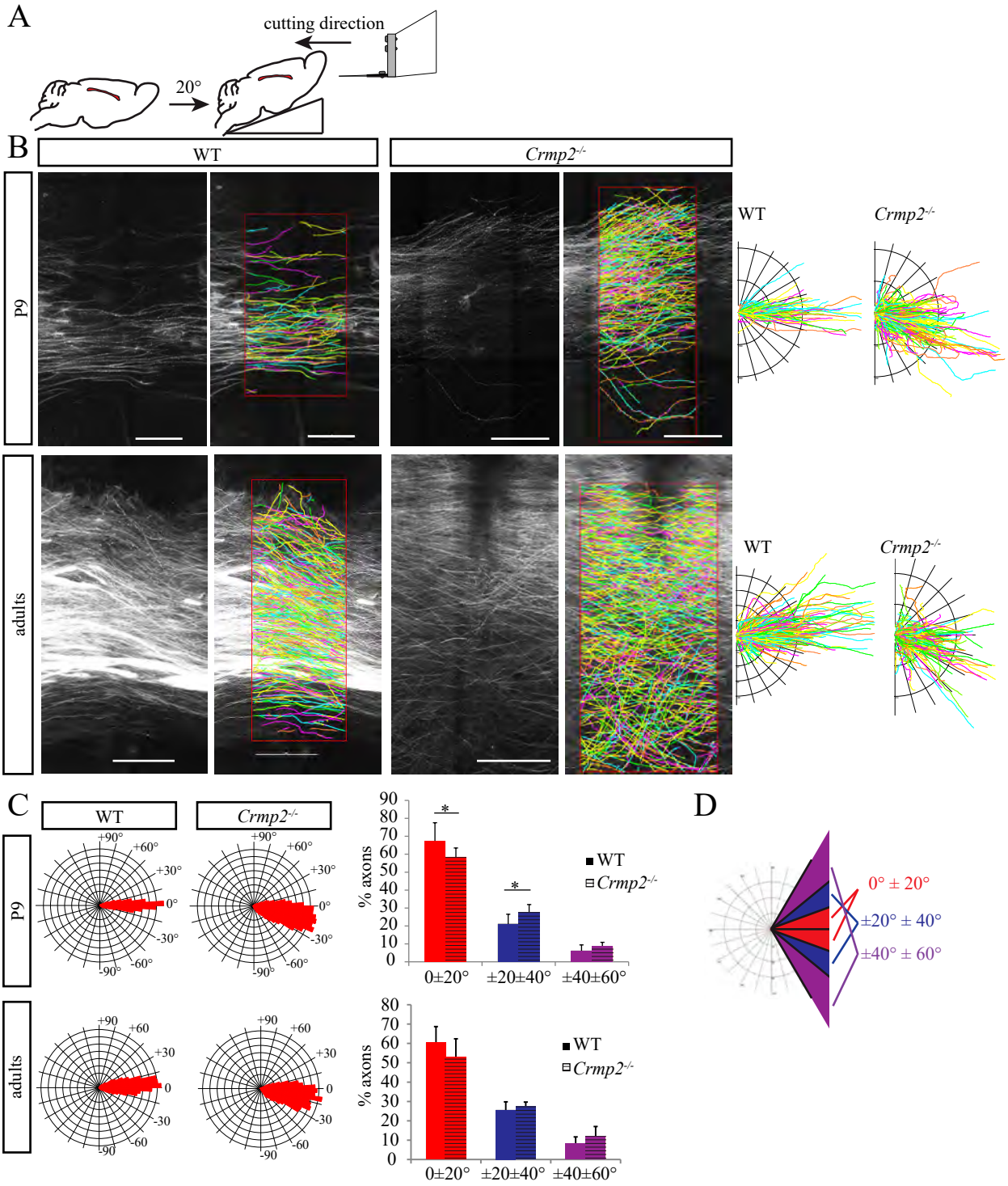

Figure 16. Callosal axon guidance analyzed in rostro-caudal plane. (A) Drawing of the experimental design used to prepare large sections of corpus callosum in one slice. (B) Left: DiI-labeled callosal axons from P9 and adult oblique brain sections and their reconstruction in Neurolucida 360 (P9: WT n=6, c*rmp2*$^{-/-}$ n=9, adults: WT n=9, *crmp2*$^{-/-}$ n=7). Right: fan in diagrams from tracings are presented as well. Scale bars: 200 µm. (C) Polar histograms of callosal axons reconstructed in (B). Note the broader range of axon growth angles in *crmp2*$^{-/-}$ mice. Proportion of axons growing in selected clusters in P9 (upper chart, WT, 0°-±20°: 67.3±10.3%; ±20°-±40°: 21.2±5.3%; ±40°-±60°: 6.22±3.2%; *crmp2*$^{-/-}$, 58.5±5%, p=0.05, 27.7±4.3%, p=0.02, 8.64±2.25%, p=0.1) and adults (bottom chart, WT, 0° -±20°: 60.5±8.23%; ±20°-±40°: 25.6±4.18%; ±40°-±60°: 8.24±3.47%; *crmp2*$^{-/-}$, 52.7±10%, p=0.1, 27.5±2.23%, p=0.3, 12.1±5%, p=0.09). mean ± SD, *p<0.05, t-test. (D) Schematic representation of polar histogram analysis by clustering the traced axons into 3 groups based on the growth angles

CRMP2 regulates development of Anterior Commissure

Analyzing the serial coronal section of *crmp2*$^{-/-}$ mice, we have noticed that temporal limbs of the anterior commissure (AC) appeared to be shorter, which we further confirmed by anti-neurofilaments staining (Fig. 17A). Development of AC is regulated by another class 3 semaphorin member, Sema3F (AC is missing or is extremely hypoplastic in *Sema3F*$^{-/-}$ and *Nrp2*$^{-/-}$ (Sema3F receptor) mice). We therefore carefully analyzed morphology of the AC in the horizontal sections (this plane is more appropriate for the analysis). In knockouts, the diameter of temporal limb was indeed significantly thinner and the olphactory limb defasciculated (Fig 17B, C). Our data thus suggest that CRMP2 may be involved in Sema3F signaling pathway as well.

In order to test this hypothesis, we next performed an *in vitro* axon outgrowth assay using isolated embryonic cortical neurons from E16.5 embryos. Neurons were transfected with EGFP at DIV1 and stimulated with Sema3F at DIV7. Similarly to our previous experiment with Sema3A (Fig. 14D), we observed that Sema3F significantly decreased axon growth responses in WT neurons, but its effect was abolished in *crmp2*$^{-/-}$ neurons indicating that CRMP2 mediates Sema3F signaling (Fig. 17D).

Beside AC, axon guidance in *Sema3F*$^{-/-}$ mice (Sahay et al. 2003) is affected also in the retroflex fascicle. Immunostaining of P6 brains with anti-neurofilaments antibody (marker of axon tracts) revealed that this structure is not affected in *crmp2*$^{-/-}$ mice (Fig. 17E).

Figure 17 (opposite). Growth of anterior commissure and retroflex fascicle in *crmp2*$^{-/-}$ mice. (A) At P14, anterior commissure (AC) is present in both WT and *crmp2*$^{-/-}$ mice. Coronal sections labeled with antibody against neurofilaments show reduced temporal limb extension. Scale bars: 1mm. (B) AC hypoplasia in *crmp2*$^{-/-}$ mice. Adult brains (n=3) were sliced horizontally (250 µm sections) to reveal both frontal and temporal limbs of an AC. Temporal limb in knockouts is thinner and frontal limb show various degree of defasciculation. Scale bars: 5 mm (left), 1 mm (details on the right). (C) Quantification of the diameter of AC in the temporal limb (*crmp2*$^{-/-}$ is 70±3% of WT, p=0.0056) and in the midline (*crmp2*$^{-/-}$ is 88±1% of WT, p=0.12). Mean ± SD, *p<0.05, t-test. (D) Time-lapse imaging of DIV7 cultured cortical neurons to assess axon growth after Sema3F stimulation. Quantification revealed that Sema3F decreases growth rate in WT but not *crmp2*$^{-/-}$ neurons (WT vs *crmp2*$^{-/-}$ long (>100 µm) p<0.001, short (<100 µm) p=0.009, arrest p<0.001). Scale bars: 100 µm. Mean ± SD, ** p<0.01, *** p<0.001, t-test. (E) Retroflex fascicle (fr), as well as mammilothalamic tract (mt) are normally formed in *crmp2*$^{-/-}$ mice. Coronal sections at the level of posterior commissure (pc) are shown. Scale bars: 1mm.

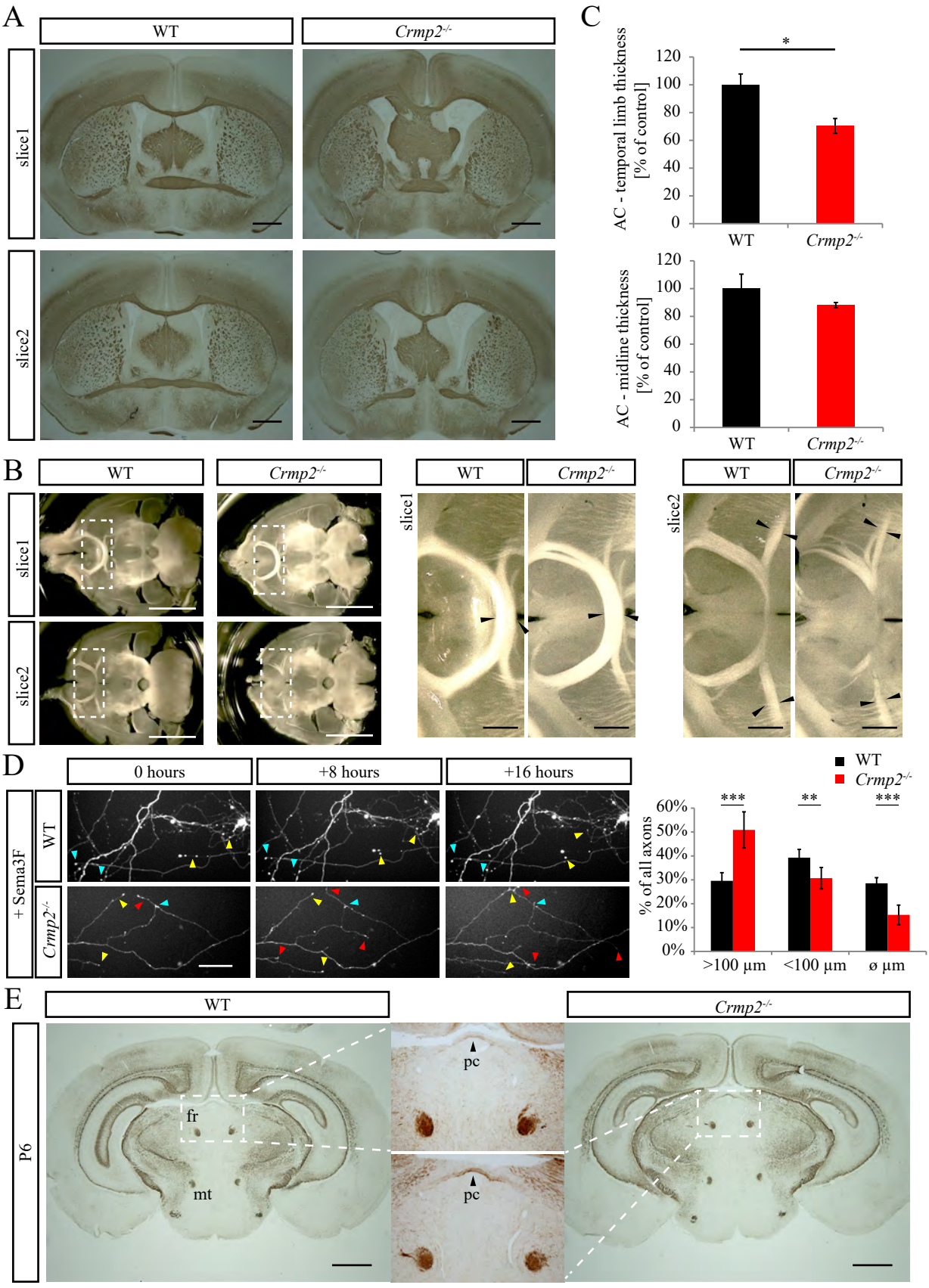
A
WT
Crmp2-/-
slice1
slice2
C
AC - temporal limb thickness [% of control]
AC - midline thickness [% of control]
*
120
100
80
60
40
20
0
WT
Crmp2-/-
B
WT
Crmp2-/-
slice1
slice2
D
0 hours
+8 hours
+16 hours
+ Sema3F
WT
Crmp2-/-
% of all axons
***
**
***
60%
50%
40%
30%
20%
10%
0%
>100 µm
<100 µm
ø µm
E
WT
Crmp2-/-
P6
fr
mt
pc
pc

4.2 Uncovering a novel role of CRMP2 in pruning

CRMP2 mediates Sema3F-, but not Sema3A-driven axon pruning in hippocampus

CRMP2 has been associated with neurodevelopmental disorders like schizophrenia (Zhang et al., 2016) and ASD characterized by altered brain connectivity (Penzes et al., 2011) and defects in postnatal synaptic refinement through axon and dendrite pruning (Garey, 2010, Bourgeron, 2015). Pruning is an important neurodevelopmental step that leads to elimination of exuberant or ineffective neuronal connections and is also regulated by axon guidance molecules, e.g. semaphorins (Riccomagno and Kolodkin, 2015). Importantly, in many regions Sema3F seems to play a more important role in pruning than Sema3A (Bagri et al., 2003, Low et al., 2008). As we found that CRMP2 mediates Sema3F signaling *in vitro*, we asked whether CRMP2 regulates axon pruning and if, in this function, it mediates Sema3A or rather Sema3F signaling. To address these questions, we analyzed two developing axonal tracts, regulated by either Sema3F-mediated pruning (the infrapyramidal bundle, IPB; (Bagri et al., 2003)) or Sema3A-mediated pruning (the hippocamposeptal bundle; (Bagri et al., 2003)).

First, we analyzed stereotyped pruning of infrapyramidal bundle (IPB) of hippocampal mossy fibers (i.e. axons of granule cells from dentate gyrus). These axons initially grow into both suprapyramidal and infrapyramidal regions of CA3, thus innervating CA3 apical or basal dendrites, respectively. Suprapyramidal tract persists until adulthood (the main bundle of mossy fibers) while IPB is eliminated (pruned) between P20 – P40. Pruning of IPB is regulated by Sema3F and its receptor complex (Nrp2/PlxnA3) (Bagri et al., 2003). At P14 (i.e. before pruning occurs) calbindin immunostaining revealed presence of IPB in both WT as well as *crmp2*$^{-/-}$ mice (Fig. 18A). Synapses were formed in both IPB and the main bundles as revealed by VGluT1 staining (Fig. 18A). In 7 weeks old animals, however, when pruning was complete in WT, the IPB remained present in *crmp2*$^{-/-}$ mice, and their IPB index (IPB length/main bundle length) was significantly higher than in WT ($p<0.001$, Fig. 18B – D). The same pattern of IPB pruning was detected also in sagittal sections (Fig. 18B, right). To determine the maturity of IPB synapses, we stained adult coronal sections with antibodies against VGluT2 or VGluT1, which are both expressed in developing mossy fibers, but in adult hippocampus only VgluT1 is present (Liu et al., 2005). We found VGluT1 in the main bundles of WTs and *crmp2*$^{-/-}$ mice, as well as in the unpruned IPBs of *crmp2*$^{-/-}$ (Fig. 18E). We did not detect the immature VgluT2 signal (Fig. 18D). Thus, the IPB axons formed during postnatal development persist in *crmp2*$^{-/-}$ mice into adulthood and form mature synapses. These results demonstrate that IPB pruning is defective in *crmp2*$^{-/-}$ mice (as is the case in *Sema3F*$^{-/-}$, *Nrp2*$^{-/-}$ and *PlxnA3*$^{-/-}$ mice) (Bagri et al., 2003).

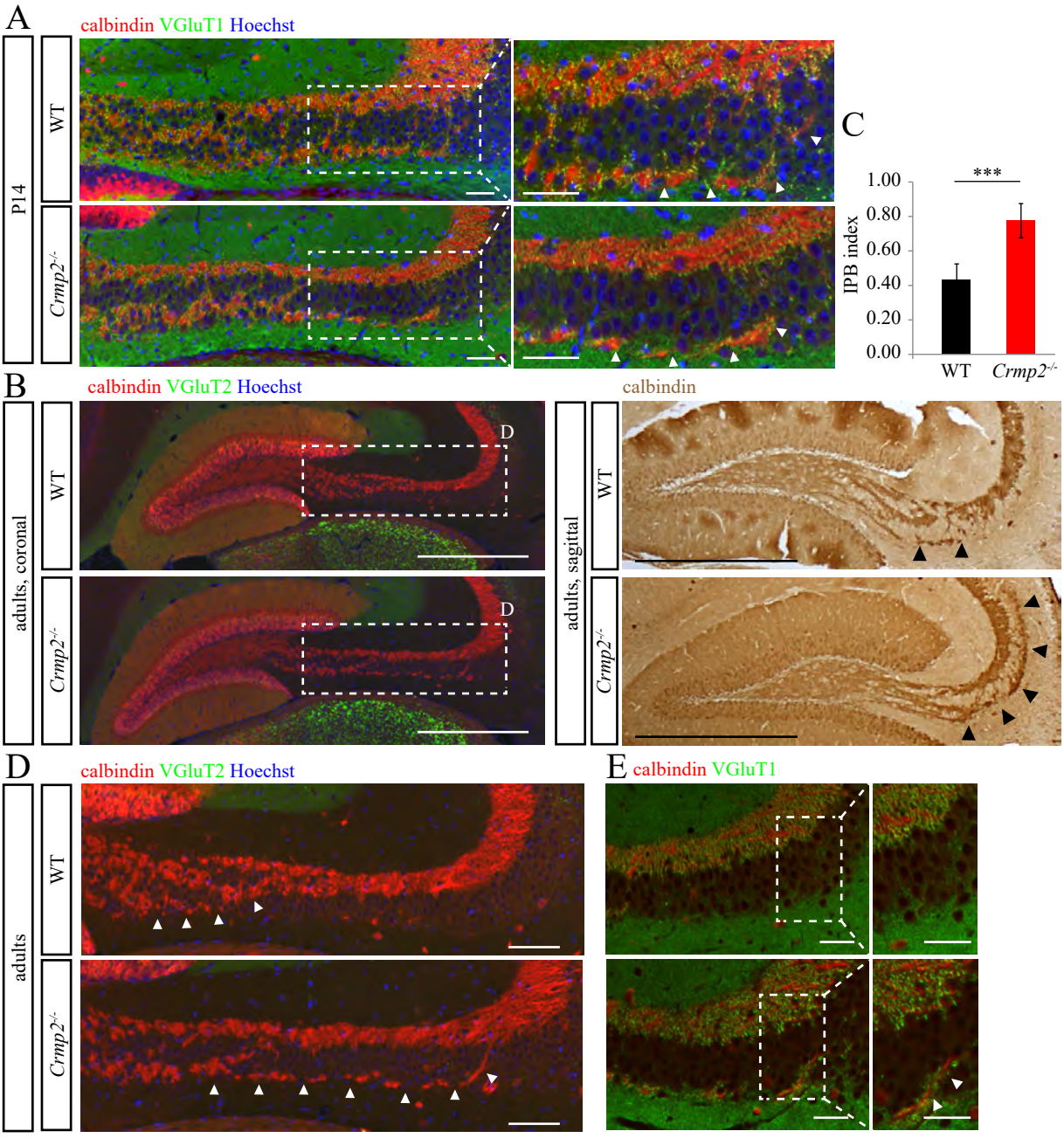

Figure 18. Infrapyramidal bundle fails to prune in *crmp2*$^{-/-}$ mice. (A) Coronal sections of P14 brains stained for calbindin and VgluT1. Infrapyramidal bundle (IPB) progresses into hippocampal CA3 region in both WT and *crmp2*$^{-/-}$ mice. Nuclei are counterstained with Hoechst 33342. Details from depicted regions (arrowheads) show the course of IPB. Scale bars: 100 µm. (B) Staining for calbindin (left: coronal plane, right: sagittal plane) shows unpruned infrapyramidal bundle in adult *crmp2*$^{-/-}$ mice. No VGluT2 signal in hippocampal CA3 region is present in WT and *crmp2*$^{-/-}$ indicating absence of immature synapses. Scale bars: 500 µm. (C) Quantification of IPB index (length of the IPB vs. main bundle, WT 0.43±0.05, *crmp2*$^{-/-}$ 0.78±0.05, $p<0.001$) counted from adult coronal sections (WT n=4, *crmp2*$^{-/-}$ n=5). Mean ± SD, ***$p<0.001$, t-test. (D) Details from depicted regions in (B), arrowheads show the course of IPB. Scale bars: 100 µm. (E) Staining for calbindin and VgluT1 shows mature synapses in the main bundle in both genotypes and in the IPB in *crmp2*$^{-/-}$ mice (arrowheads). Scale bars: 100 µm.

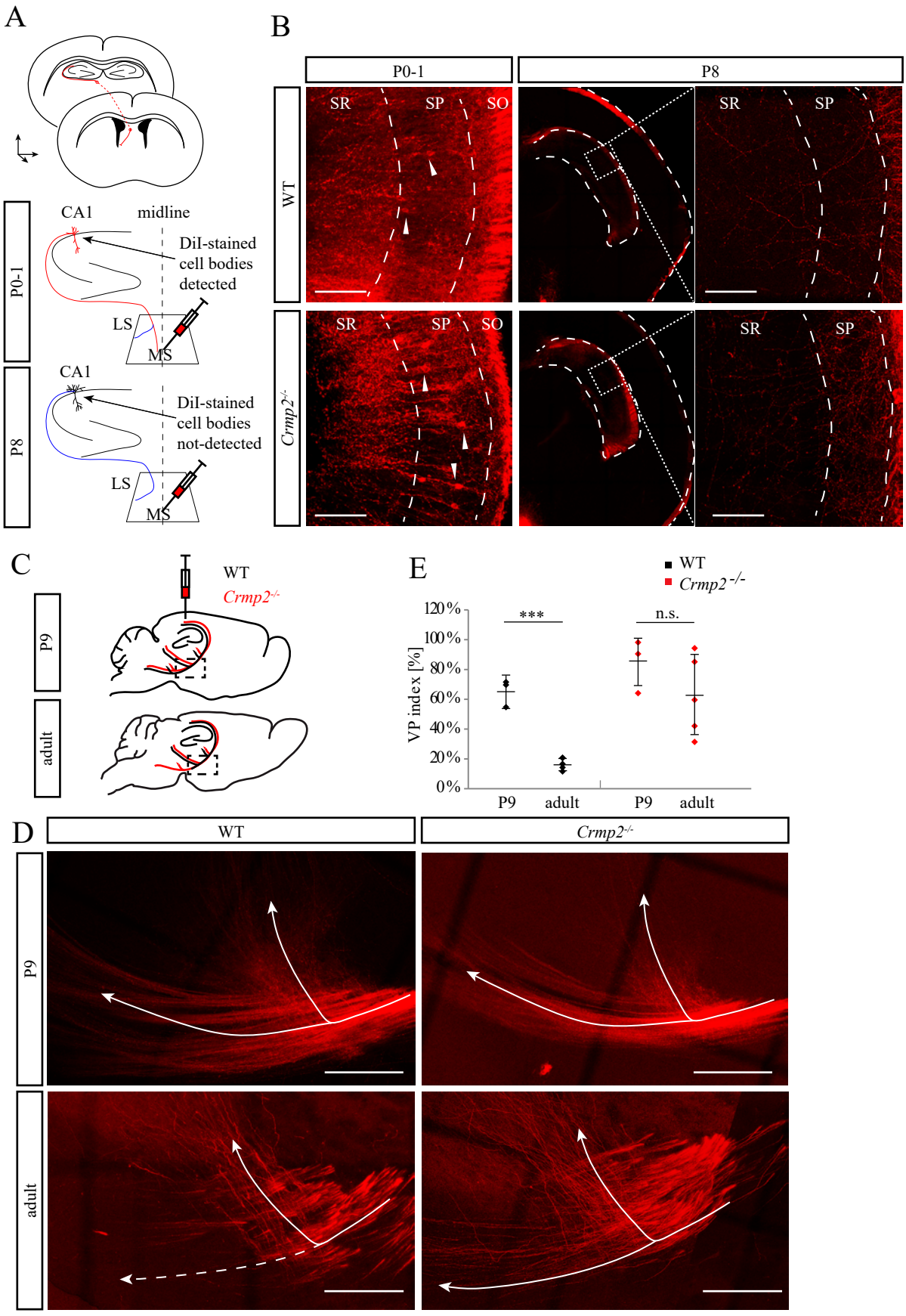
A
P0-1
CA1
midline
DiI-stained cell bodies detected
LS
MS
P8
CA1
DiI-stained cell bodies not-detected
LS
MS
B
P0-1
P8
WT
Crmp2-/-
SR
SP
SO
C
P9
adult
WT
Crmp2-/-
E
WT
Crmp2-/-
VP index [%]
120 %
100 %
80 %
60 %
40 %
20 %
0 %
***
n.s.
P9
adult
P9
adult
D
WT
Crmp2-/-
P9
adult

We next tested whether stereotyped pruning of a different group of axons arising from hippocampus – the hippocamposeptal axons – is also affected in *crmp2*$^{-/-}$ mice. CA1 neurons send their axons into medial and lateral septum at P0-1. However, at P8, only the axons to the lateral septum persist while the ones sent into the medial septum have disappeared (Linke et al., 1995). In this system, the pruning is mediated by Sema3A and not Sema3F (Bagri et al., 2003). Presence of hippocampal projections into the medial septum can be detected by retrograde labeling using DiI (Fig. 19A). We detected retrograde-stained CA1 neuron bodies at P0-1, but not at P8 in both WT and *crmp2*$^{-/-}$ (Fig. 19B). This indicates that the hippocamposeptal axon pruning is not affected by CRMP2 deficiency and that CRMP2 is a mediator of stereotyped axon pruning driven preferentially by Sema3F, but not Sema3A.

CRMP2 mediates stereotyped pruning of corticospinal projections of visual cortex

To further support the role of CRMP2 as a mediator of Sema3F-driven pruning, we analyzed pruning of corticospinal axons of visual cortex neurons that have previously been shown to be dependent on Sema3F signaling. Sema3F receptors, Nrp2 and PlxnA3, are expressed by pyramidal neurons in visual cortex. In the early developmental stages, these neurons send their projections not only to the superior colliculus but also to two inappropriate targets, i.e. the inferior colliculus (IC) and the spinal cord. During the third postnatal week, inappropriate axons are eliminated through a pruning process regulated by Sema3F (Low et al., 2008). We analyzed the development of the visual cortex projection by the means of DiI anterograde tracing (Fig. 19C, D). This approach allowed us to visualize the major branching point and axons located few hundred micrometers behind.

Figure 19 (opposite). Stereotyped pruning of hippocamposeptal and corticospinal visual axons. (A) Schematic drawing of the course of hippocamposeptal axons and DiI injections for retrograde tracing. Axons that initially enter medial septum (red axon colour at P0-1) are eliminated after few days, thus axons are not stained with DiI injected into the medial septum. LS and MS indicate lateral and medial septum, respectively. (B) Hippocamposeptal axons are pruned in both WT and *crmp2*$^{-/-}$ mice (n=3). At P0-1, regrogradely DiI-labeled CA1 pyramidal neurons showed strong signal in both WTs and *crmp2*$^{-/-}$ indicating presence of CA1 projections into the medial septum. Arrowheads in the left column show retrogradely labeled cell bodies. Conversely, at P8, no retrogradely labeled CA1 cell bodies were detected in CA1 granular layer in either WT or *crmp2*$^{-/-}$ mice. Squares in the second column are shown in a higher magnification in the third column. SR, SP and SO indicate stratum radiatum, stratum pyramidale and stratum oriens, respectively. Scale bars: 100 μm. (C) Schematic drawing of DiI injection and axon tracing. Axons that initially (P9) enter pyramidal tract fail to prune in *crmp2*$^{-/-}$ mice (red line). (D) Upper row: DiI tracing of the visual cortex axons at P9 (before pruning, n=3), sagittal sections. Branching point of the tract is shown. Lower row: visual cortex axons in adult mice (n=5) after pruning period. Note significantly reduced number of axons continuing into pyramidal tract in WT. (arrows – 2 branches of corticospinal visual axons). Maximum projections are shown. Scale bars: 200 μm. (E) Quantification of VP (visual pruning) index (fluorescence intensity of pyramidal axons after vs. before the branch point). Lower index thus indicates lower amount of axons in pyramidal tract. In WT animals after the pruning period, only a minor part of axons descends towards the pyramidal tract (WT: P9 0.65±0.09, adults 0.17±0.04, p=0.006). However, in *crmp2*$^{-/-}$ mice, corticospinal axons are still largely present, and their VP indexes are not significantly different between adult and P9 stages (c*rmp2*$^{-/-}$: P9 0.54±0.18, adults 0.62±0.27, p=0.24). Mean ± SD, **p<0.01, 2-way ANOVA with Bonferroni's multiple comparisons test.

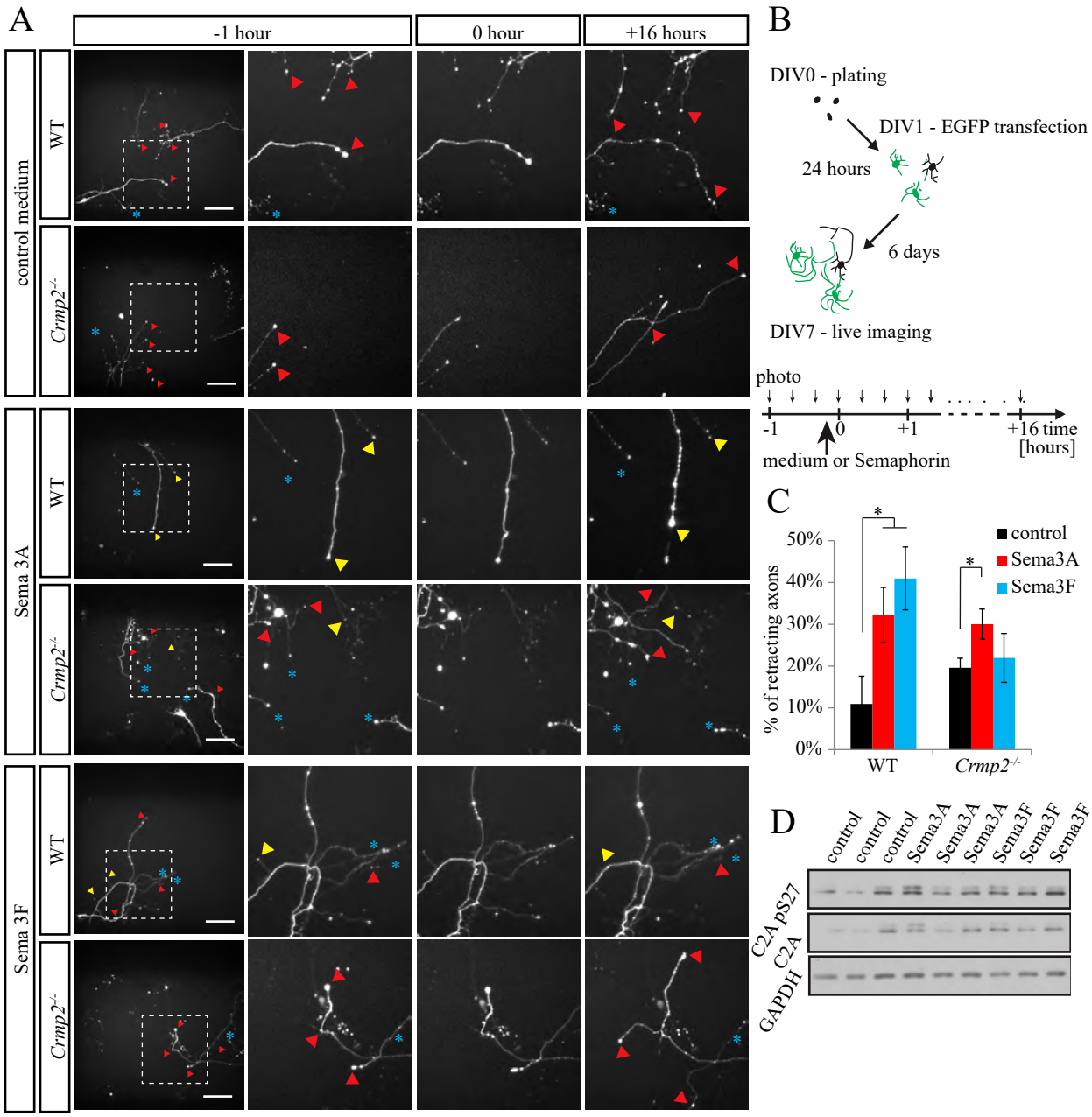

Figure 20. CRMP2 mediates Sema3F signaling in primary neurons. (A) Time-lapse imaging of DIV7 cultured hippocampal neurons to assess axon retraction/pruning after Semaphorin stimulation. Upper panel: Axon behavior in medium without Semaphorins. Middle panel: stimulation with Sema3A (1nM, n=669 axons for WT, 761 axons for knockout) causes retraction of both WT and *crmp2*$^{-/-}$ neurons. Lower panel: stimulation with Sema3F (5 nM, n=602 axons for WT, 955 axons for knockout) causes axon retraction in WT, but not in *crmp2*$^{-/-}$ neurons. Red triangles show growing axons, yellow show retracting axons and blue asterisks indicate steady non-growing axons. See also video 4. Scale bars: 100 µm. (B) Schematic drawing of the experimental setup. (C) Quantification of retracting axons (number of retracting vs. steady axons, 3 experiments). WT: control 13.4±5%, Sema3A 31.2±6% ($p<0.001$), Sema3F 36.9±8.7% ($p<0.001$); *crmp2*$^{-/-}$: control 19.8±1.8%, Sema3A 28.5±4.4% ($p<0.05$), Sema3F 22.4±4.1% ($p>0.99$), mean ± SD are shown. ***$p<0.001$, *$p<0.05$, 2-way ANOVA with Bonferroni's multiple comparisons test. (D) *In vitro* phosphorylation of CRMP2A by Sema3A and Sema3F.

In adult *crmp2*$^{-/-}$ mice, the inappropriate corticospinal axons were still largely present, and VP indexes (fluorescence intensity of corticospinal axons after vs. before the branch point) were not significantly different in *crmp2*$^{-/-}$ mice between adult and P9 stages ($p=0.27$, Fig. 19E), while they significantly dropped in WT ($p<0.05$, Fig. 19E). Our data demonstrate that CRMP2 indeed mediates postnatal refinement of corticospinal visual axons, which is consistent with its role as mediator of Sema3F signaling. In conclusion, we found significant differences between WT and *crmp2*$^{-/-}$ mice in stereotyped pruning in regions controlled by Sema3F (visual cortex axons, IPB). In contrast we found no differences in regions controlled by Sema3A (i.e. hippocamposeptal axons) suggesting CRMP2 mediates Sema3F-driven, but not Sema3A-driven axon pruning.

CRMP2 mediates Sema3F-dependent axon retraction in vitro.

In order to directly show that CRMP2 is necessary for Sema3F-triggered axon pruning, but dispensable for Sema3A-dependent pruning, we tested pruning *in vitro* in hippocampal neurons that are responsive to both Sema3A and Sema3F (Bagri et al., 2003). We prepared dissociated hippocampal cultures from WT and *crmp2*$^{-/-}$ E16.5 – E17.5 embryos and transfected them sparsely with EGFP at DIV1 to be able to follow single axon. At DIV7, we added Sema3A or Sema3F into the cultures and analyzed the axon behavior in fluorescence microscope by time-lapse imaging. DIV7, which is an early stage of synapse formation (Basarsky et al., 1994), was chosen to facilitate analysis of neurons in still less complex connectivity patterns. (Fig. 20A, B, video 4). We analyzed only stable axon terminals that did not show any movement in one hour period prior to addition of the guidance cues (45% of all labeled axon terminals). In control conditions in both wild-type and knockout, a small number of the stable axons were spontaneously retracting (WT 13%, KO 20%, $p=0.03$, Fig. 20C). After addition of either Sema3A or Sema3F into WT culture, we observed a 3-fold increase in axon retractions (32% for Sema3A, $p<0.001$, 41% for Sema3F, $p=0.0012$, Fig. 20C). However, in *crmp2*$^{-/-}$, this increase was detectable only after Sema3A (30%, $p=0.0026$) and not after Sema3F (22%, $p=0.23$). This data demonstrate, that in primary neuron cultures undergoing synaptogenesis, CRMP2 is essential to mediate Sema3F but not Sema3A signaling. This is in agreement with our *in vivo* findings that stereotyped pruning in *crmp2*$^{-/-}$ is affected in Sema3F-controled, but not in Sema3A-controled regions. Finally, we asked if Sema3F acts on CRMP2 by inducing changes in its phosphorylation status. We isolated hippocampal neurons from E18.5 rat embryos (to increase neuron yield), treated them at DIV4 with Sema3A or Sema3F for 3 hours and analyzed the levels of Ser27 phosphorylation in the cell lysates by western blotting (Ser27 is a Cdk5 phosphorylation site (Balastik et al., 2015) at CRMP2A isoform, which we found highly phosphorylated in hippocampus). Both semaphorins increased total levels of phosphorylated CRMP2A. (Fig. 20D), indicating that phosphorylation of Ser27 is downstream from both Sema3A and Sema3F.

4.3 The involvement of CRMP2 in dendrite development

CRMP2 regulates dendritic spine remodeling in hippocampal granule cells.

Besides triggering axon pruning, Sema3F regulates also the development of some classes of dendritic spines (e.g. spines of dentate gyrus (DG) granule cells) (Tran et al., 2009). In contrast, Sema3A/Nrp1 signaling seems to be dispensable for dendritic spine morphogenesis (Tran et al., 2009, Yamashita et al., 2007). In order to test whether CRMP2 participates also in spine development/morphogenesis, we DiOlistically (see methods) labeled DG neurons and analyzed their dendritic spines. We found significantly increased spine density in *crmp2*$^{-/-}$ adult DG granule cells compared to WTs (Fig. 21B, C, $p<0.001$). This phenotype was similar to that found in *Sema3F*$^{-/-}$ and *Nrp2*$^{-/-}$ (Tran et al., 2009). Next, we analyzed branching of the diolistically labeled DG granule cell dendrites. Sholl analysis (quantitative analysis of dendritic branching using numbers of interdissections of concentric circles with dendrites, see Fig. 25D) revealed no differences between WT and *crmp2*$^{-/-}$ mice (Fig. 21D, E, $p>0.99$), which is again in line with the phenotype of *Sema3F*$^{-/-}$ mice (Tran et al., 2009). Higher spine density could be a result of either increased generation of new spines, or defective pruning of spines, or both. Considering the axon pruning defects we found in Sema3F-regulated areas in *crmp2*$^{-/-}$ mice (see above), and considering Sema3F promotes loss of spines *in vitro* (Tran et al., 2009), we hypothesized that Sema3F regulates dendritic spine pruning through CRMP2. To test this hypothesis, we labeled and counted DG dendritic spine density in P30 (adolescent) mice when dendritic spines are virtually all formed and the pruning process starts (Petanjek et al., 2011, Bian et al., 2015). We found no differences in dendritic spine density between WTs and mutants at P30 (Fig. 21A, C, $p=0.47$), although knockout spines tended to be enlarged (Fig. 22A).

Figure 21 (opposite). CRMP2 regulates dendritic spine refinement in dentate gyrus granule cells.

(A, B) Dendritic spine density in DiOlistically labeled DG granule cells (n=3 animals, WT=61 dendrites, knockout=64 dendrites) is similar in WT and *crmp2*$^{-/-}$ mice at P30. In adults, however, spine density in *crmp2*$^{-/-}$ granule cells is increased comparing to WT (n=3 animals, WT=41 dendrites, knockout=37 dendrites). Scale bars: 5 μm. (C) Quantification of dendritic spine density in DG granule cells in the inner molecular layer (50 – 100 μm away from the soma). WT, P30: 12.5±2.2 spines/10 μm, adults: 9.95±2.3; *crmp2*$^{-/-}$, P30: 12.86±2.1 ($p>0.99$), adults: 12.88±2.9 ($p<0.001$), mean ± SD, ***$p<0.001$, 2-way ANOVA with Bonferroni correction. (D, E) Analysis of branching of DiOlistically labeled DG granule cell dendrites in adult WT and *crmp2*$^{-/-}$ mice (n=3 animals, ≥25 dendrites). Quantification of granule cell branching by Sholl analysis showed no significant differences ($p>0.99$). Scale bars: 50 μm, mean ± SEM, 2-way ANOVA with Bonferroni correction. (F) Defects in synapse elimination in the inner molecular layer revealed by double immunostaining with PSD95 (postsynaptic marker) and VGluT2 (presynaptic marker) antibodies. GL indicates granule cell layer, IML/OML indicate inner/outer molecular layer, respectively. Density of colocalized PSD95/VGLuT2 puncta was counted. IML: WT 109±21, *crmp2*$^{-/-}$ 156±15 ($p=0.004$). OML: WT 281±38, *crmp2*$^{-/-}$ 297±80 ($p=0.7$). Scale bars: 10 μm, mean ± SD, *$p<0.05$, t-test. (G, H) Spine density in DiOlistically labeled prefrontal cortex (PFC) pyramidal neurons is similar in WT and *crmp2*$^{-/-}$ mice in both juvenile (P25, n=3, ≥50 dendrites) and adult mice (n=3, ≥50 dendrites). WT, juvenile: 8.63±1.44 spines/10 μm, adults: 7.3±1.4; *crmp2*$^{-/-}$, P30: 9.05±1.73, $p=0.97$, adults: 6.98±1.53, $p>0.99$. Scale bars: 5 μm, mean ± SD, 2-way ANOVA with Bonferroni's multiple comparisons test.

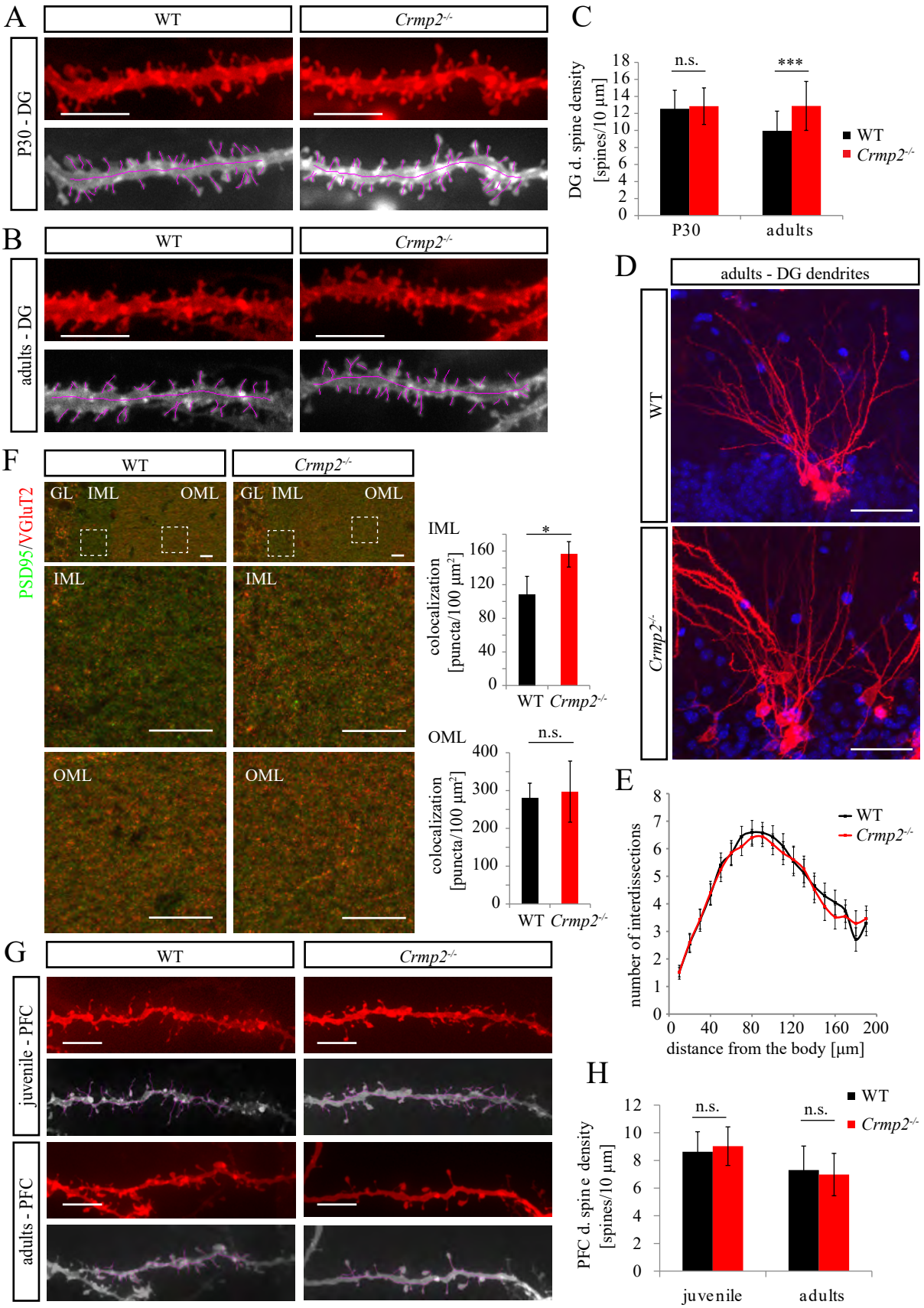
A
WT
Crmp2-/-
P30 - DG
B
adults - DG
C
DG d. spine density [spines/10 µm]
n.s.
***
P30
adults
WT
Crmp2-/-
D
adults - DG dendrites
E
number of interdissections
distance from the body [µm]
F
PSD95/VGluT2
GL IML OML
colocalization [puncta/100 µm2]
*
n.s.
G
juvenile - PFC
adults - PFC
H
PFC d. spine density [spines/10 µm]
juvenile

This indicates that the initial distribution of spines is unaltered in *crmp2*$^{-/-}$ mice and that it is the process of dendritic spine pruning that is defective in these mice. To further confirm the defect of synapse pruning in *crmp2*$^{-/-}$ mice, we labeled and counted excitatory synapses in DG. We found that the density of PSD95/VGluT2 – colocalized puncta was increased in the inner part of the molecular layer in knockouts, in line with our dendritic spine measurements ($p<0.05$, Fig. 21F). As DG spine morphogenesis is regulated through Sema3F (Tran et al., 2009), our findings indicate that CRMP2 mediates Sema3F-dependent pruning also in dendritic spines. We have next tested how CRMP2 modulates dendritic spine formation/elimination *in vitro* (Fig. 22B – E). We prepared hippocampal cultures and transfected neurons with GFP at DIV14. The same dendritic segments were scanned at DIV21 and DIV25. We found small decrease in spine density in WT ($p<0.05$) but not in *crmp2*$^{-/-}$ neurons (Fig. 22B, C). Knockout neurons presented with more spines in both DIV21 (n.s.) and DIV25 ($p<0.05$). Importantly, CRMP2 deletion prevented Sema3F-induced spine elimination at DIV25 (Fig. 22D, E). These observations are in accord with our *in vivo* and *in vitro* findings and further point to the role of CRMP2 in spine remodeling.

Defects in the distribution of dendritic spines due to aberrant synapse pruning are one of the key features of both ASD and schizophrenia. Generally, dendritic spine number in ASD patients is higher than in control subjects or variable in different regions, while in schizophrenia patients it is lower (Penzes et al., 2011). This applies particularly to some brain regions, e.g. prefrontal cortex (PFC), where excessive spine elimination has been associated with pathogenesis of schizophrenia (Garey et al., 1998). Since some phenotypical aspects of conditional *crmp2*$^{-/-}$ mice, like impaired sensorimotor gating, have been previously related to schizophrenia (Zhang et al., 2016), we asked whether CRMP2 deficiency in full CRMP2 knockout mice also leads to spine overpruning and reduced spine density in PFC. At P25, PFC spine density was similar in both WT and mutants (Fig. 21G, H $p=0.18$) and similar to our findings in the DG. Importantly, unlike in DG, we did not detect any significant difference in PFC spine density between adult WT and *crmp2*$^{-/-}$ mice (Fig. 21G, H $p=0.25$), which is not consistent with schizophrenia-like phenotype.

Figure 22 (opposite). Additional dendritic spine defects revealed *in vitro* and *in vivo*. (A) Analysis of 3D-reconstructed spine head diameters in DG revealed increased proportion of spines with enlarged heads at P30, but no changes in adults. Scale bars: 5 μm, ***$p<0.001$, Kolmogorov-Smirnov test. (B, C) Analysis of dendritic spine remodeling *in vitro*. E18.5 hippocampal neurons were transfected with GFP (at DIV 14) and the same dendrite segments were scanned at DIV 21 and DIV 25. Spine density decreased in WT neurons (DIV21 vs. DIV 25: 9.6±2.2 spines/10 μm vs. 8.4±2.4 spines/10 μm, $p=0.003$) but not in knockout neurons (DIV21 vs. DIV 25: 10.3±2.3 spines/10 μm vs. 9.9±2.6 spines/10 μm). Scale bars: 5 μm, mean ± SD, *$p<0.05$, paired t-test. (D, E) At DIV 25, neurons were photographed, treated with 5nM Sema3F or control Fc for 3 hours and photographed again. CRMP2 deficiency prevents Sema3F-induced spine elimination. WT neurons: Fc treatment (before vs. after) 7.8±2 vs. 8.6±1.8 spines/10 μm ($p=0.07$), Sema3F treatment (before vs. after) 9.2±3.2 vs. 8.4±2 spines/10 μm ($p=0.01$). *Crmp2*$^{-/-}$ neurons: Fc treatment (before vs. after) 9±2.5 vs. 9.4±2.9 spines/10 μm ($p=0.04$), Sema3F treatment (before vs. after) 10.9±2.2 vs. 11.2±2.4 spines/10 μm ($p=0.2$). Scale bars: 5 μm, mean ± SD, *$p<0.05$, paired t-test. (F, G) Analysis of DiOlistically labeled dendritic spine

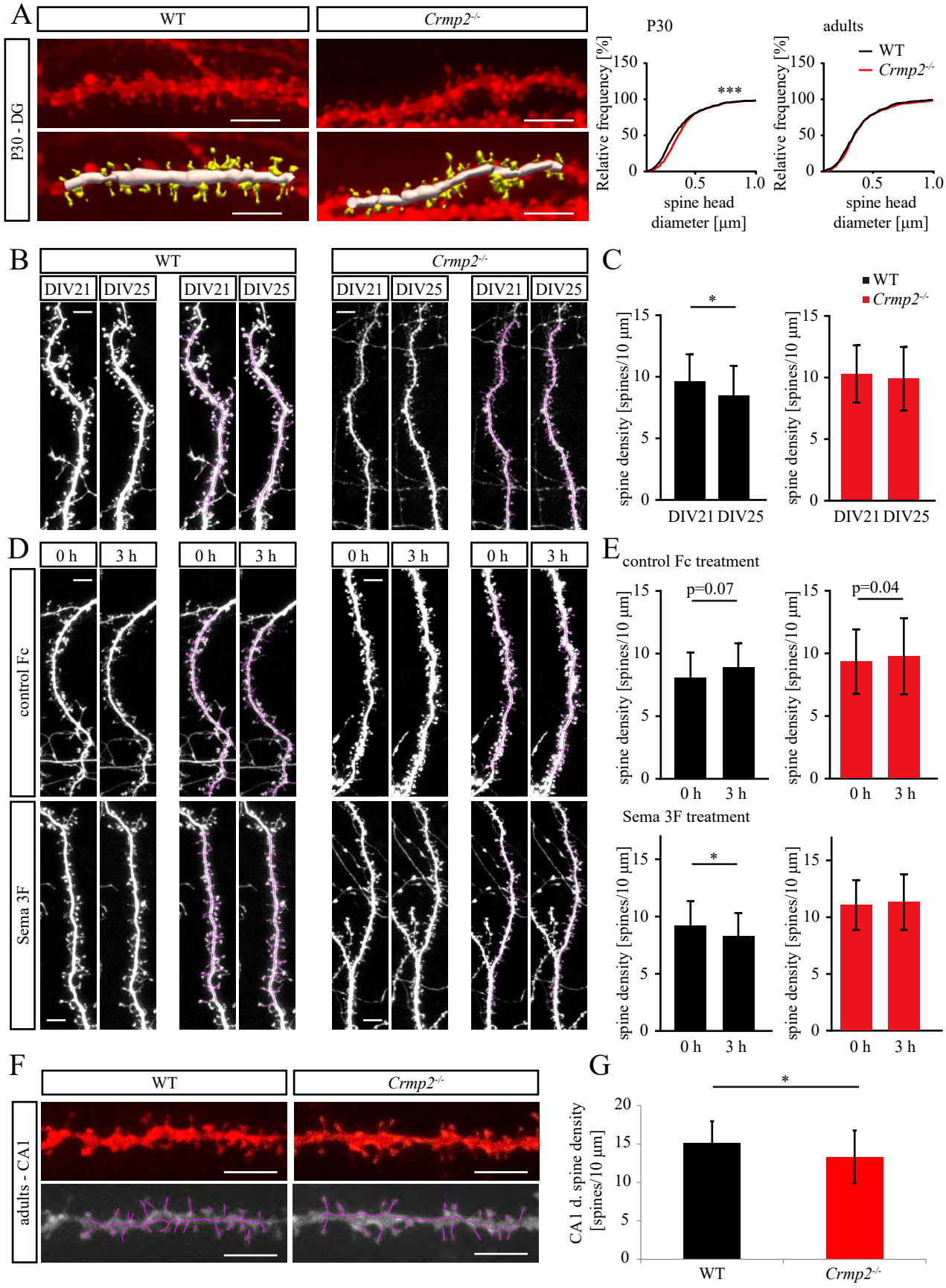

(contin. from previous page)

density in hippocampal CA1 region, secondary apical dendrites (n=3 mice per genotype, 36 dendrites). Density is significantly decreased in *crmp2*$^{-/-}$ mice (WT 15.2±2.8 spines/10 µm, *crmp2*$^{-/-}$ 13.3±3.4 spines/10 µm, p=0.02). Scale bars: 5 µm, *p<0.05, t-test.

4.4 Isoform-specific role of CRMP2A in axon guidance and pruning

CRMP2A mediates callosal axon guidance in a cell-autonomous manner.

In the next part of the project we aimed to investigate what is the role of CRMP2A isoform in axon development and refinement. Based on WB analysis, CRMP2B is much more abundant in the brain and its expression persists after birth. Expression of CRMP2A is relatively high during development and decreases rapidly in first postnatal weeks (Bretin et al., 2005). In fact, from ~P20, CRMP2A is detected mainly in the corpus callosum and dentate gyrus (Fig. 10C). Since we detected defects in the above-mentioned structures in full *crmp2*$^{-/-}$ mice, we asked how CRMP2A participates in their formation.

Crmp2a$^{-/-}$ mice were generated in Balastik's laboratory in parallel with the full knockouts. The first exon in crmp2 locus was deleted and as a result, transcription can only start from the second promotor (Fig. 23A). We confirmed selective CRMP2A deletion by both western blotting and immunohistochemistry (Fig. 23B, C) and, importantly, we did not observed upregulation of other CRMP2 members or CRMP2B isoform in these knockouts (Fig. 23C, G). General anatomy of the corpus callosum was not altered in *crmp2a*$^{-/-}$, unlike in full knockouts (Fig. 23D, F), but we detected ventriculomegaly ($p=0.053$, Fig. 23E, F), although less extensive in comparison with the full knockouts (*crmp2*$^{-/-}$ vs. *crmp2a*$^{-/-}$, $p=0.16$). However, development of callosal axons analyzed at P6 (after electroporation at E15.5) revealed defects comparable to those in *crmp2*$^{-/-}$ ($p<0.05$ for WT vs. *crmp2*$^{-/-}$ and *crmp2a*$^{-/-}$, Fig, 24A, B). Axons in the contralateral cortex were mostly not growing in parallel or straight but instead were twisted, changed growth directions more often and were less organized. These results suggest that the remaining CRMP2B isoform is not capable to mediate callosal axons guidance in *crmp2a*$^{-/-}$.

To further test this hypothesis, we performed CRMP2A or CRMP2B rescue experiments of *crmp2*$^{-/-}$ callosal phenotype. CRMP2A plus GFP (3:2 ratio) or CRMP2B plus GFP (3:2 ratio) were electroporated into E15.5 *crmp2*$^{-/-}$ embryos and brains were subsequently analyzed at P6. We observed nearly full rescue of CC axon guidance with CRMP2A ($p<0.05$) overexpression, but not with CRMP2B ($p=0.3$), which fits well with the observations from *crmp2a*$^{-/-}$ mice (Fig. 24A – C) and shows that CRMP2A regulates callosal axon guidance in a cell-autonomous manner. Together, our results strongly suggest CRMP2A is the major CRMP2 isoform responsible for CC targeting (Fig. 24A – C). However, CRMP2B is sufficient to maintain the entire callosum including the splenium that is missing in full *crmp2*$^{-/-}$ mice (Fig. 23D, Fig. 15C). This could be explained by involvement of glial

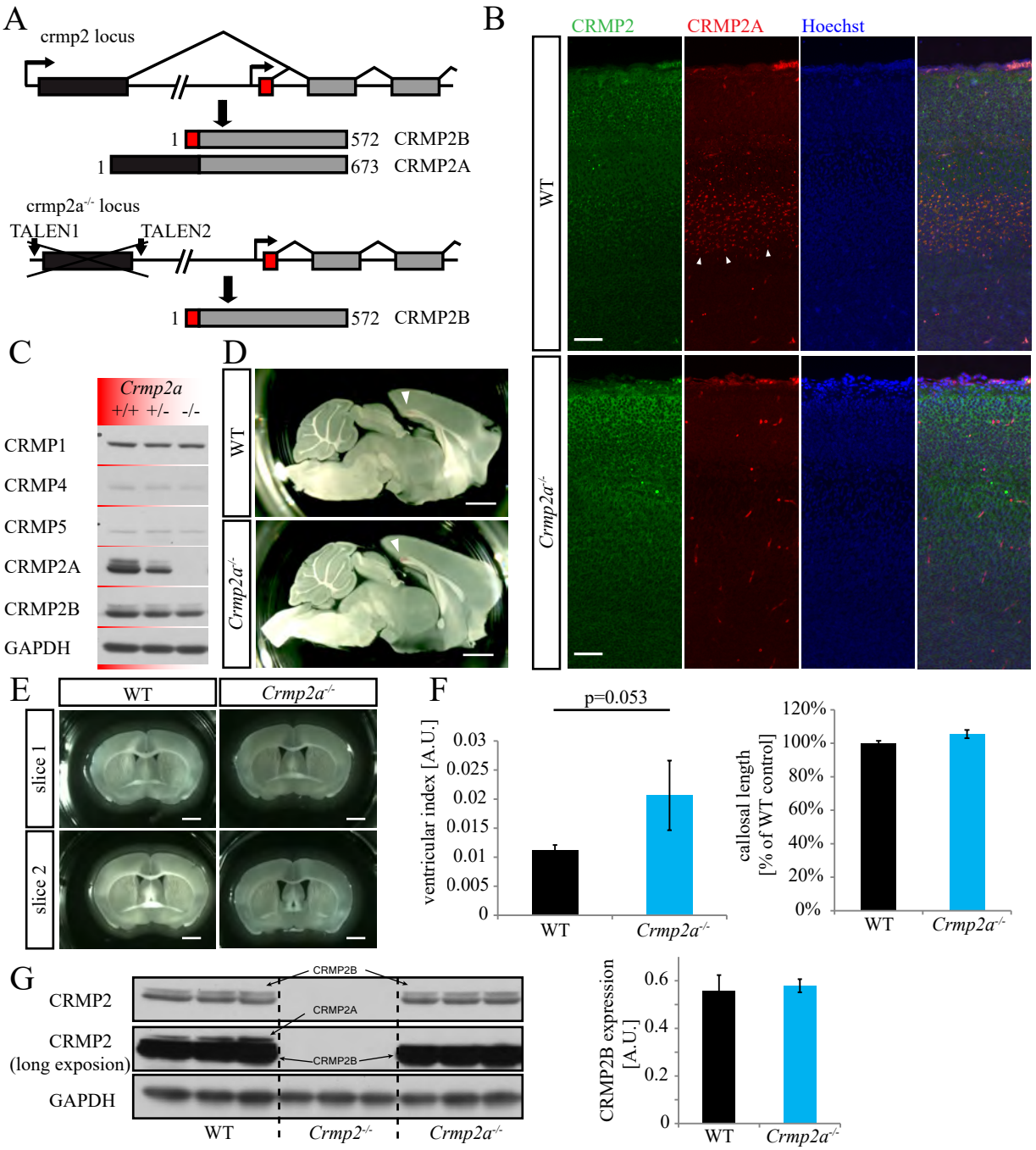

Figure 23. Isoform-specific *Crmp2a*$^{-/-}$ mice generation and characterization. (A) Generation of CRMP2A knockout mice by TALEN mutagenesis. Alternative first exons are highlighted in black and red. The second promotor is preserved thus CRMP2B is still expressed. (B) CRMP2 (A+B isoforms, green) and CRMP2A (red) isoform immunostaining of coronal brain sections from WT and *crmp2*$^{-/-}$ E17.5 embryos. Note specific CRMP2A deletion in *crmp2a*$^{-/-}$ mice. CRMP2B is present throughout the cortex, CRMP2A is localized mostly in developing axons (arrowhead). Nuclei were counterstained with Hoechst. Scale bars: 50 µm. (C) WB analysis of brain lysates of *crmp2a* $^{+/+}$, $^{+/-}$ and $^{-/-}$ mice (one brain per genotype). Note preserved short isoform and no compensatory effect of CRMP1, 4 and 5. (D) Unlike in full *crmp2*$^{-/-}$ mice, corpus callosum is fully formed in *crmp2a*$^{-/-}$. Scale bars: 1mm (E) Two consecutive coronal sections from WT and c*rmp2a*$^{-/-}$ demonstrate enlarged ventricles in knockouts. Scale bars: 1mm. (F) Quantification of ventricle area (left) from (E) and callosal length (right) from (D). The ventricle areas were normalized to total slice area (ventricular index, WT 0.0113±0.001, *crmp2*$^{-/-}$ 0.01±0.006, p=0.053). Mean ± SD, t-test. (G) WB showing CRMP2 isoforms with C-terminal CRMP2 antibody. Note that CRMP2A is detectable only after a long explosion time and its expression is much weaker than CRMP2B. Quantification show similar levels of CRMP2B in WTs and *crmp2a*$^{-/-}$. Mean ± SD, t-test.

cells on axon tract maintenance since CRMP2B is expressed in oligodendrocytes that create myelin sheets (Fig. 24D, (Bretin et al., 2005)). We counted oligodendrocyte density in splenium and found decreasing density trend in *crmp2*$^{-/-}$ mice suggesting CRMP2B may be important for oligodendrocyte development and/or function (Fig. 24D) and its absence in the oligodendrocytes could result in developmental defect of splenium in *crmp2*$^{-/-}$ mice.

CRMP2A mediates pruning of axons and spines of granule cells.

We next asked if selected CRMP2A deletion could affect pruning of DG's dendritic spines and mossy fibers. To test this hypothesis, we analyzed spine number by DiOlistic labeling of neurons. At P30 (before pruning), spine densities were comparable between WTs and knockouts. However, we observed significantly increased spine density in *crmp2a*$^{-/-}$ adult DG granule cells compared to WTs suggesting a pruning deficit in these mice (Fig. 25A, B). Comparison to our previous analysis of the full *crmp2*$^{-/-}$ mice showed no significant difference between both knockouts indicating that CRMP2A is a specific mediator of spine pruning in DG. In addition, we noticed decreased branching of DG granule cells in *crmp2a*$^{-/-}$ mice (Fig. 25C, D), which was not detected in full knockouts (Fig. 21D). Interestingly, decreased branching combined with increased spine density in the same neurons was observed also in newborn DG cells upon CRMP2 knockdown (Zhang et al., 2016). Since knockdown of CRMP2 targets both isoforms and we only detected comparable changes in *crmp2a*$^{-/-}$ mice, it is suggesting that CRMP2A isoform is required for development of DG dendrites. Absence of this phenotype in our full knockouts (Fig. 21D, E) is surprising, though, CRMP1 (which is upregulated in *crmp2*$^{-/-}$, Fig. 13C) may rescue dendritic phenotype while it has been previously shown that it is required for proper dendritic field organization (Makihara et al., 2016).

We next assessed pruning of IPB in hippocampus by immunohistochemistry using calbindin antibody. Unlike in spines, we observed only a partial defect of the IPB axons was partially sufficient (Fig. 25E). The length of *crmp2a*$^{-/-}$ IPB was half of the size of the adult *crmp2*$^{-/-}$ IPB (see Fig. 18). This could be explained by specific expression of CRMP2 isoforms in DG and CA3 – previous report suggested that CRMP2A localizes to mossy fiber axons, but not in CA3 dendrites (Bretin et al., 2005). We therefore investigated expression of CRMP2A/B in hippocampus in more detail in adult mice. We observed signal of total CRMP2 antibody in mossy fiber axons as well as in CA3 dendrites, however, CRMP2A antibody only stained axons (Fig. 25F, G). Since CRMP2 antibody recognizes both isoforms, we repeated this labeling in *crmp2a*$^{-/-}$ sections to label CRMP2B only. We found that total CRMP2 antibody stained dendrites, but not mossy fibers, in *crmp2a*$^{-/-}$ mice indicating CRMP2B is the main isoform in CA3 dendrites (Fig. 25F, G). Furthermore, double labeling of axonal (tau, synaptoporin) or dendritic (MAP2) markers together with phosphospecific antibodies revealed strong phosphorylation of CRMP2A (Ser27) in mossy fibers and CRMP2B (Ser522) in CA3 dendrites (Fig. 26A, B).

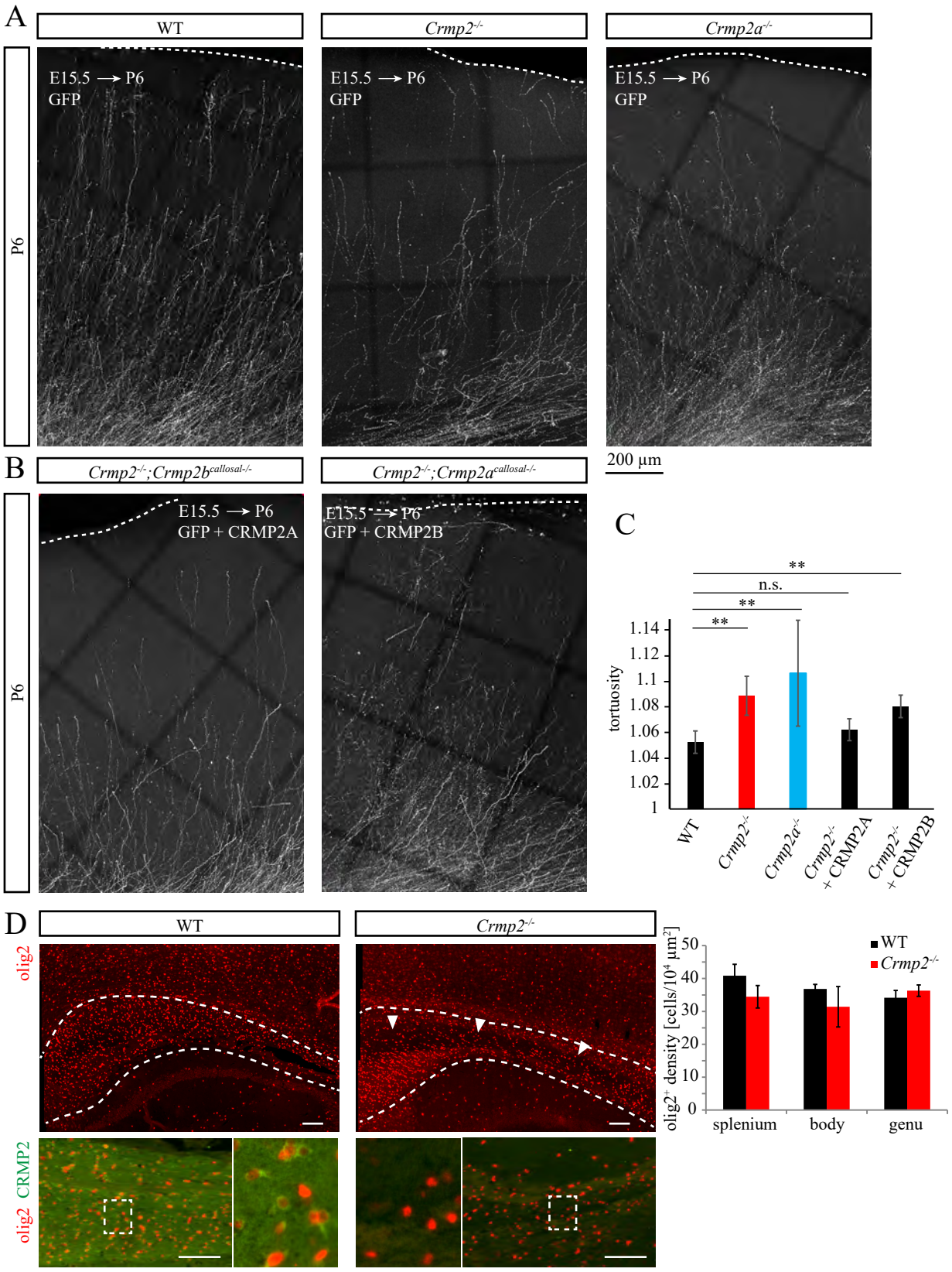

Figure 24. Cell-autonomous role of CRMP2A in guidance of callosal axons. (A) WT, *crmp2*$^{-/-}$ or *crmp2a*$^{-/-}$ E15.5 embryos were electroporated with GFP and axons in contralateral site to electroporation were analyzed at P6. Note twisted axons in both knockouts. (B) Rescue experiments were performed by co-electroporation of GFP with CRMP2A or CRMP2B into *crmp2*$^{-/-}$ embryos. CRMP2A rescues phenotype of CRMP2 knockout, while CRMP2B does not. Scale bars in A, B: 200 µm (C) Quantification of axon tortuosity from (A, B) in all genotypes. Mean ± SD, t-test. (C) Olig2 staining in sagittal brain sections in callosum (outline) reveals trend to decreased oligodendrocyte density in *crmp2*$^{-/-}$ (arrowheads). Co-labeling with CRMP2 revealed its expression in oligodendrocytes. Scale bars: 100 µm.

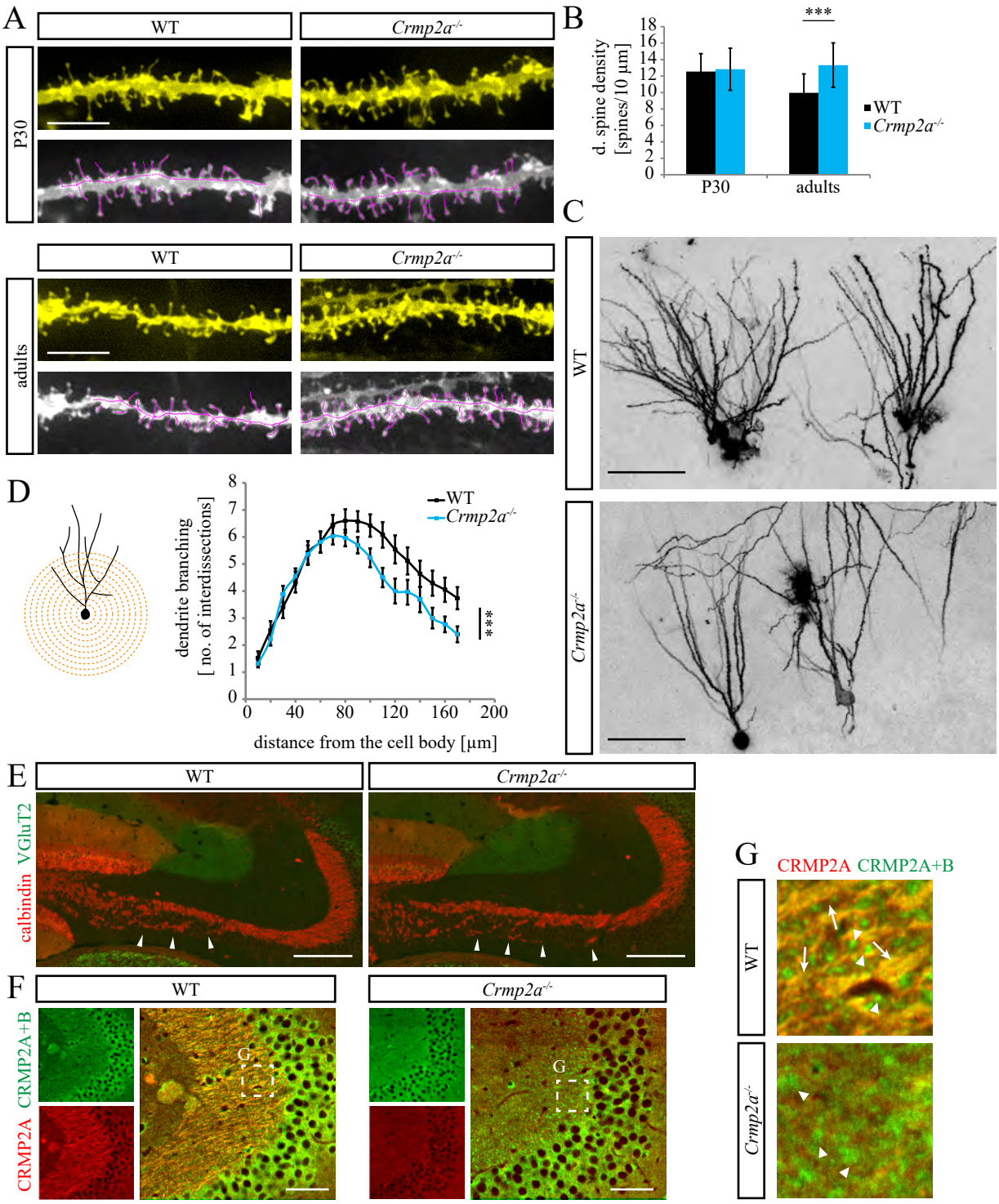

Figure 25. CRMP2A regulates DG dendrite development. (A, B) DiOlistically labeled dendritic spines in DG showed increased spine density in adult *crmp2a*$^{-/-}$ mice in comparison with age-matched WTs. P30 – WT: 12.55±2.2, *crmp2a*$^{-/-}$: 12.83±2.56 ($p=0.53$) adults – WT: 9.95±2.3, *crmp2a*$^{-/-}$: 13.32±2.7 ($p<0.001$), Mean±SD, t-test. Scale bars: 5 µm. (C) Decreased arborization of DG granule cells in *crmp2a*$^{-/-}$ mice. Neurons of adult mice were labeled DiOlistically, scanned in confocal microscope and reconstructed in Neurolucida. Scale bars: 100 µm. (D) Sholl analysis revealed decreased number of interdissections ($p<0.05$, principle of the analysis is shown on the left). Mean ± SEM, 2-way ANOVA with Bonferroni's multiple comparisons test. (E) Staining for calbindin shows some unpruned axons in infrapyramidal bundle of adult *crmp2a*$^{-/-}$ mice (arrowheads). No VGluT2 signal in hippocampal CA3 region is present in WT and *crmp2a*$^{-/-}$ suggesting mature synapses. Scale bars: 100 µm. (F, G) CRMP2A localizes predominantly to axons, while CRMP2 total antibody stains both axons (arrows) and dendrites (arrowheads). In *crmp2a*$^{-/-}$, CRMP2 total antibody signal is mainly detected in dendrites (arrowheads). Scale bars: 20 µm.

One possible explanation for these results could be that postsynaptic CRMP2B is responsible for pruning induction and CRMP2A is involved particularly in axon retraction. We have already shown that Sema3F induces pruning of axons that is prevented by CRMP2 deletion. To test an effect of CRMP2A deletion, we prepared hippocampal neuron culture from *crmp2a*$^{-/-}$ embryos, transfected neurons with GFP at DIV1 and tested Sema3A and Sema3F effect on pruning at DIV7 (Fig. 27A). Sema3A increased relative amount of retracted axons to about 40% ($p<0.05$, Fig. 27B) in *crmp2a*$^{-/-}$ neurons, similarly to WTs. Sema3F, though, induced only a moderate, statistically non-significant response (increase to 27%, $p=0.08$, Fig. 27B). These results are in accord with our *in vivo* data and together suggest that Sema3F signals preferentially via CRMP2A.

4.5 Pin1 regulates axon guidance by stabilizing CRMP2A

Pin1 is a phospho-specific peptidyl-prolyl isomerase catalyzing cis-trans isomerization of the Ser/Thr-Pro bond. Pin1 has a large number of substrates and regulates their stability, cell localization or enzymatic activity (Lu and Zhou, 2007). We have recently identified that Pin1 binds also to CRMP2A (Balastik et al., 2015). CRMP2A was pulled down from postnatal rodent brain with GST-Pin. Next, CRMP2A was similarly pulled down from lysates of transfected SH-SY5Y cells arrested in mitosis with nocodazole, suggesting that phosphorylation is crucial for the binding (Balastik et al., 2015). To further visualize this interaction *in vitro* in living cells, we performed FLIM-FRET analysis of CRMP2A-cherry (and its de-phosphomimetic mutants) and Pin1-GFP fusion proteins that were transfected into

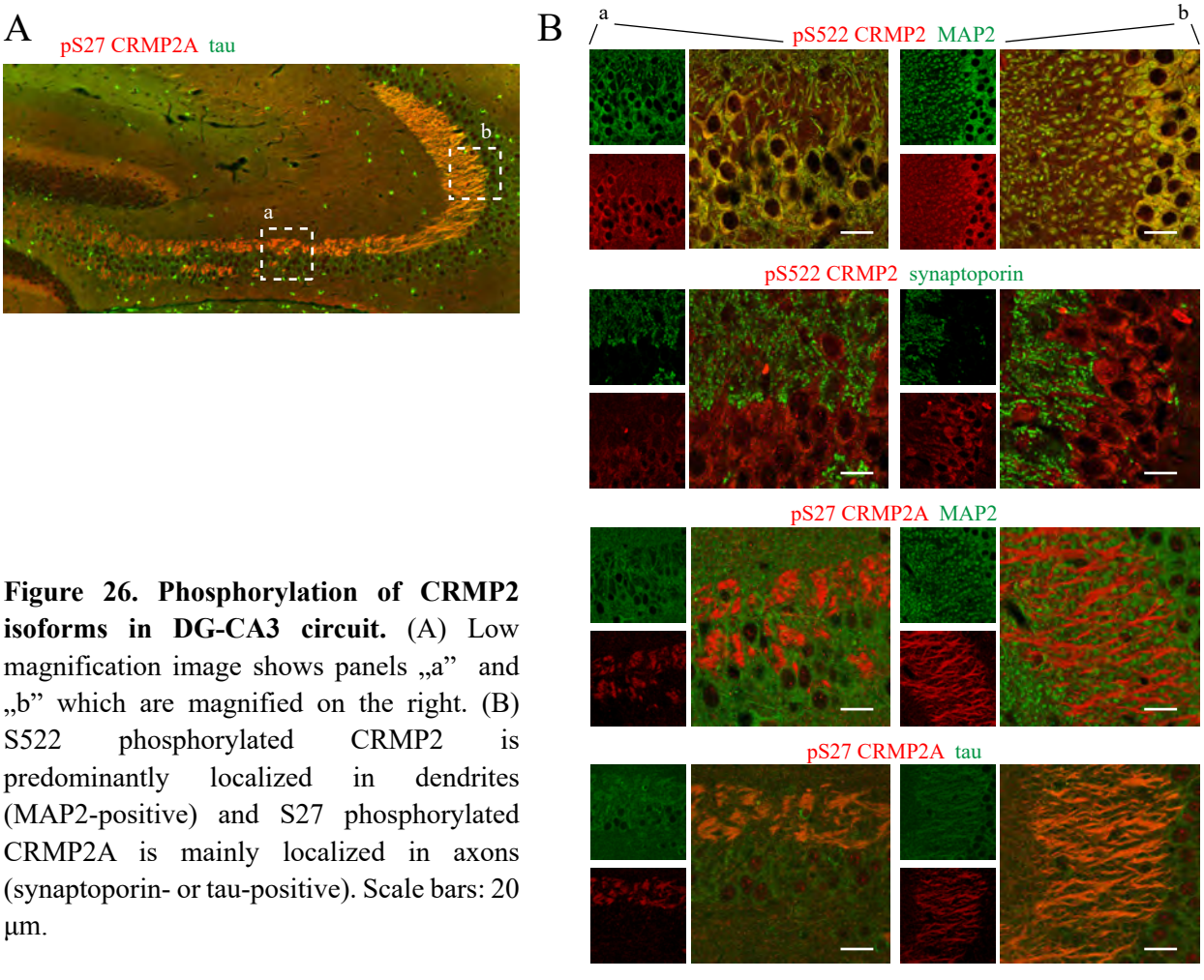

Figure 26. Phosphorylation of CRMP2 isoforms in DG-CA3 circuit. (A) Low magnification image shows panels „a" and „b" which are magnified on the right. (B) S522 phosphorylated CRMP2 is predominantly localized in dendrites (MAP2-positive) and S27 phosphorylated CRMP2A is mainly localized in axons (synaptoporin- or tau-positive). Scale bars: 20 µm.

dissociated hippocampal neurons (Fig. 28A). We indeed confirmed that Pin1 preferentially binds to phosphorylated CRMP2A – lifetime of Pin1-GFP was not changed when neurons were transfected with S27,623A-CRMP2A-mcherry (de-phosphomimetic form) – which is in line with our previous pulldowns. Moreover, stimulation with Sema3A (which induces S72 phosphorylation (Fig. 20D)) further decreased lifetime of Pin-GFP (Fig. 28A), thus supporting the phosphorylation-dependent CRMP2A-Pin1 interaction.

Since knockout of Pin1 enhanced growth cone responses to Sema3A (Balastik et al., 2015), we suggested that axon guidance errors in *Sema3a*$^{-/-}$ might be opposite to those in *Pin1*$^{-/-}$. We indeed observed e.g. decreased growth of trigeminal nerves in *Pin1*$^{-/-}$ E11.5 embryos (Balastik et al., 2015). Sema3A deficiency has been also recently shown to interfere with fasciculation of callosal axons of the somatosensory and motor cortex (Zhou et al., 2013). To further confirm that knockout of Pin1 potentiates Sema3A signaling, we studied fasciculation of callosal axons in *Pin1*$^{-/-}$ adult mice. DiI was injected into somatosensory cortex and brains were analyzed 3 weeks later. In line with the hypothesis, we found no significant changes between WTs and Pin1 knockouts when analyzing the diameter of DiI-positive axons in the CC midline (Fig. 28D). Interestingly, another recent study on *Pin1*$^{-/-}$ mice found that callosal axons of Pin1 mutants are even more fasciculated than in WTs (Sosa et al., 2016), which is also consistent with increased Sema3A signaling.

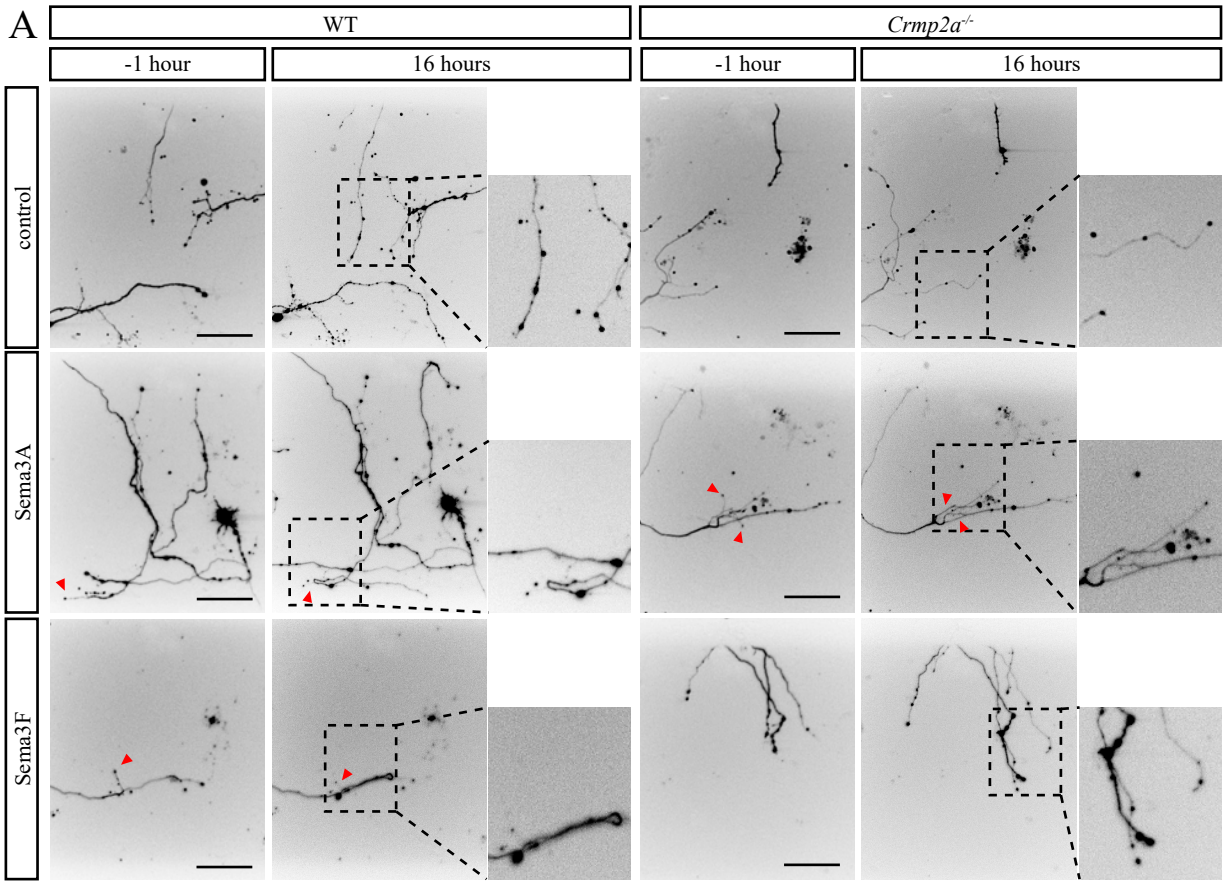

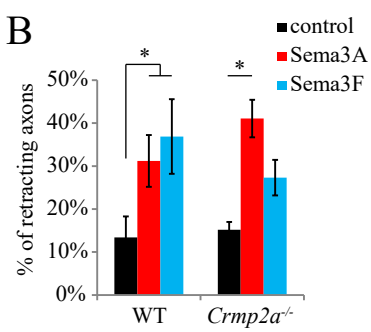

Figure 27. *In vitro* retraction assay in *crmp2a*$^{-/-}$ neurons. (A) DIV7 hippocampal neurons (transfected at DIV1 with GFP) were treated as indicated and time-lapsed for 16 hours. Sema3A induces axon retraction in both WT and *crmp2a*$^{-/-}$, while no significant Sema3F response was detected in *crmp2a*$^{-/-}$ neurons. Red arrowheads show retracting axons. Scale bars: 100 µm. (B) Quantification of retractions (WTs are the same as in figure 20) *crmp2a*$^{-/-}$ control: 15.2±3.8%, Sema3A: 41±5.2% ($p<0.05$), Sema3F: 27.3±6% ($p=0.08$), mean ± SD, t-test.

Next, having evidence that CRMP2A is highly phosphorylated in embryonic axons and in mossy fibers (Fig. 26), we hypothesized that Pin1 might participate in development of this axon tract, since it binds to phosphorylated CRMP2A (Fig. 28, (Balastik et al., 2015)). We first analyzed the level of pS27-CRMP2A in *Pin1*$^{-/-}$ brains to confirm our *in vitro* observations. Immunohistochemistry with antibody against S27-phosphorylated CRMP2A revealed that in developing axons, pS27 levels were indeed decreased, as expected (Fig. 28B). Next, we measured IPB length in *Pin1*$^{-/-}$ adult mice and found that it was very similar to c*rmp2a*$^{-/-}$, slightly but significantly longer than in WTs (Fig. 28C). These findings indicate that Pin1 and CRMP2A both participate in stereotyped pruning of mossy fibers.

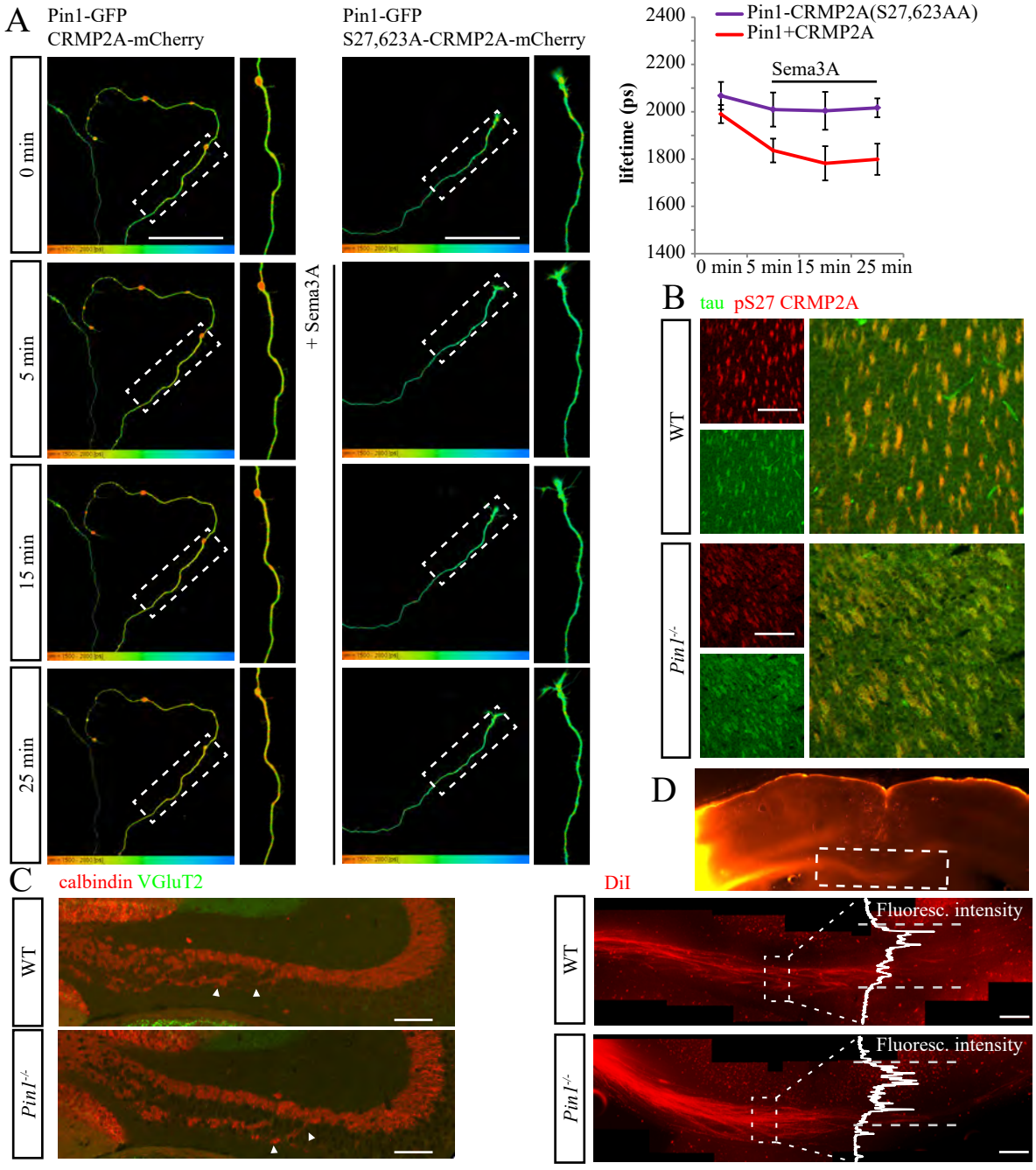

Figure 28. Regulation of CRMP2A through Pin1 binding. (A) Neurons were transfected with indicated plasmids and analyzed by FRET-FLIM. Lifetime of GFP is shown. Warmer colours indicate shorter lifetime, thus increased binding of Pin1 to CRMP2A. Sema3A stimulation further decreases lifetime of GFP. Scale bars: 50 µm. (B) CRMP2A phosphorylation in axons (stained by tau) is decreased in *Pin1*$^{-/-}$ embryos. Scale bars: 100 µm. (C) Staining for calbindin shows unpruned axons (arrowheads) in infrapyramidal bundle of adult *Pin1*$^{-/-}$ mice. Scale bars: 100 µm. (D) The fasciculation of S1 axons in CC midline is similar in WT and *Pin1*$^{-/-}$ mice. Scale bars: 100 µm.

5. Conclusion

In my PhD thesis work I successfully demonstrated that CRMP2 plays a central role in the postnatal refinement of the nervous system. I found that newly generated *crmp2*$^{-/-}$ mice display stereotyped axon pruning defects in multiple CNS regions. In addition, I uncovered that CRMP2 regulates development of the largest brain commissures – corpus callosum and anterior commissure. Importantly, CRMP2A, the longer CRMP2 isoform, is specifically involved in the regulation of contralateral callosal axon growth. Stability of CRMP2A is regulated by prolyl-isomerase Pin1, which binds specifically to Ser27-phosphorylated CRMP2A.

CRMP2 has been considered as a central part of the Sema3A signaling. The results of my PhD thesis project newly show that CRMP2 is downstream of Sema3F signaling as well. Finally, *crmp2*$^{-/-}$ mice display ASD-related changes in social behavior detectable already during first postnatal weeks. Since previously CRMP2 has been linked with pathogenesis of schizophrenia, it may serve as a molecular link linking class 3 Semaphorin signaling defects in both autism and schizophrenia.

Results related to CRMP2, pruning and Sema3F signaling are the part of our recent paper (Ziak et al., 2020). Results identifying CRMP2A as a Pin1-binding partner were published as well (Balastik et al., 2015). Data obtained from experiments related to *crmp2a*$^{-/-}$ are so far unpublished and were presented in several neurobiology meetings (CSHL meeting, 2018; EMBO workshop, 2018).

6. Discussion

CRMP2 has been long considered an important regulator of Semaphorin 3A-mediated axon guidance during embryonic development. Its expression, though, is high even in the early postnatal neurons, but its role in the postnatal development and adult neurons has so far been elusive. In my PhD thesis I successfully demonstrated that CRMP2 is not only mediator of Sema3A signaling regulating axon guidance in embryonic development, but importantly, that it plays a central role in the postnatal refinement of the nervous system. By analyzing the phenotype of newly generated *crmp2*$^{-/-}$ and *crmp2a*$^{-/-}$ mice we showed for the first time in an in vivo model, that CRMP2 deficiency indeed leads to axon guidance defects in CNS and PNS that could be attributed to changes of Sema3A signaling. Strikingly, we demonstrated that CRMP2 mediates also Sema3F signaling and that CRMP2 deficiency disrupts early postnatal Sema3F-mediated axon and dendritic spine refinement in multiple areas of the CNS. Changes in Sema3F signaling pathway have been considered a risk factor in the pathogenesis of ASD. In accord with that, we showed that *crmp2*$^{-/-}$ mice suffer from altered pruning and early postnatal social interaction defects previously linked to autism (see below). Together, our *in vivo* and *in vitro* data demonstrated a novel function of CRMP2 in postnatal fine-tuning of the nervous system by Sema3F, and showed that its deficiency in mice leads to neurodevelopmental defects associated with pathogenesis of the ASD in human. The function of CRMP2 in development is tightly regulated on multiple levels. We have demonstrated a novel, isoform specific regulatory mechanism controling CRMP2A stability in distal axons by conformational changes catalyzed by prolyl izomerase Pin1. Moreover, I have found that Pin1 deficiency leads to defects in stereotyped axon pruning similar as CRMP2A deficient mice further supporting the significance of the conformational regulation of CRMP2 in neural development.

CRMP2 deletion in mice as a model for neurodevelopmental disorders: comparison of brain-specific CRMP2 knockout mice with full CRMP2 knockouts

In the course of our study, conditional brain-specific *crmp2*$^{-/-}$ mice were generated (Zhang et al., 2016) and, soon after that, full CRMP2 knockout mice as well (Makihara et al., 2016, Nakamura et al., 2016). These studies focused particularly on behavioral aspects of CRMP2 deletion and defects in dendrite and dendritic spine development in various brain regions. Surprisingly, these studies revealed multiple behavioral discrepancies between these two mice lines.

First, analysis of conditional knockout mice revealed hyperactivity and prepulsed inhibition (PPI) deficit together with social behavior impairment. PPI is a test for evaluating sensorimotor gating – the phenomenon that is often altered in schizophrenia patients. In addition, clozapine (an antipsychotic drug) treatment was capable to reduce hyperactivity in conditional *crmp2*$^{-/-}$ mice. In contrast, in the full *crmp2*$^{-/-}$ mice PPI was not significantly different to WT (Zhang et al., 2016, Nakamura et al.,

2016). Another example of different behavior is the effect of CRMP2 deletion on anxiety – Nakamura et al. reported anxiolytic effect of total CRMP2 deletion, but there was no effect on anxiety-like behavior in conditional knockouts.

Second, morphological analysis showed increased volume of brain ventricles and impaired dendritic development in hippocampal CA1 and DG neurons, which is associated with schizophrenia, but also other neurodevelopmental disorders (Zhang et al., 2016). In full knockouts, dendritic branching was not attenuated, unlike in conditional model, but spine density was decreased in the layer 5 motor/sensory cortex.

Third, changes in the levels of other CRMP family members (CRMP1, 4) were reported in full CRMP2 knockout mice, but not in the conditional knockouts. The difference between these models is timing of CRMP2 deletion. Conditional, brain-specific knockouts express Cre recombinase, which is under the nestin promotor. Nestin is expressed in proliferating brain regions from embryonic day 11 in mice, later is expressed throughout the brain. This suggests that even a minor difference in the spatio-temporal inactivation of CRMP2 during development can have a major impact on the development and severity of the resulting neurodevelopmental defects.

In the full CRMP2 knockout mice we generated, we found several phenotypical defects present in the published conditional and full CRMP2 knockout mice (e.g. ventriculomegaly, spine density changes in DG, working memory defects, or hyperactivity) (Zhang et al., 2016, Tobe et al., 2017, Nakamura et al., 2016). We also found brain sizes comparable in both WTs and *crmp2*$^{-/-}$ mice, similar as reported in the conditional CRMP2 knockout mice, although we detected a non-significant tendency for a thinner cortex in the mutants. In addition, though, we demonstrate that CRMP2 deficiency leads to defects in axonal pruning and dendritic spine remodeling compatible with ASD rather than schizophrenia (Lord et al., 2018). As in other ASD mouse models (Schmeisser et al., 2012), the incomplete dendritic spine pruning is not present in all brain regions (e.g. we did not detect it in the prefrontal cortex or CA1 neurons). Interestingly, we detected DG spine pruning defect also in *crmp2a*$^{-/-}$ suggesting that CRMP2A plays a unique role in spine retraction.

To date, we further analyzed behavior of *crmp2*$^{-/-}$ animals (in collaboration with Prof. Ales Stuchlik, Mgr. Martina Janikova and Dr. Tomas Petrasek). Similar to (Nakamura et al., 2016), we did not detect schizophrenia-related behavioral changes in our mouse model (we performed AAPA task in a rotating carousel maze (Kristofikova et al., 2013)). Moreover, we have also tested social communication in 6 – 12 days old pups and revealed profound deficit in *crmp2*$^{-/-}$ mice. Importantly, we have measured defects in social interaction also in adult mice (knockouts do not show preference for mice to non-living objects, unlike WTs). Lack of sociability, observed already in first postnatal week, is again found in other ASD mouse models (Varghese et al., 2017). Following table (Tab. 1) summarizes results of the behavioral analysis of our and the other two CRMP2 deficient mouse lines:

Test	Description	Results		
		Xu (conditional knockout) (Zhang et al., 2016)	Goshima (Nakamura et al., 2016)	Balastik (Ziak et al., 2020)
Open field/home cage	(motor) activity/anxiety	increased total path	Hyperactivity	increased total path (in rotating arena)[a]
Y maze	working memory (short-term memory)	decreased alternation	not tested	decreased alternation
Object recognition	("short-term") memory	not tested	Decreased	not tested
Social tests[b]	social behavior	decreased sociability	decreased sociability	decreased sociability
Vocalization	Social behavior	Not tested	Not tested	decreased
Prepulse inhibition	gating (schizophrenia)	decreased	Normal	not tested
EPM[c]	Anxiety	no change	increased in open arm	increased in open arm
Morris WM[d]	spatial memory (long-term)	decreased	not tested	no change
AAPA[e]	cognitive flexibility (schizophrenia)	not tested	not tested	no change

Tab. 1: Comparison table for different CRMP2 deficient mouse lines. Green or red color indicates similar or different results, respectively.
a: we measured total path of the mice during AAPA task
b: Sociability was tested in a three-chamber test for social preference
c: EPM – Elevated plus maze with two closed and two opened arms
d: Morris water maze
e: AAPA – Active allothetic place avoidance task

In summary, there are multiple differences between conditional and full CRMP2 knockout mice in behavioral and biochemical level. Timing of CRMP2 inactivation therefore seems to influence the resulting phenotype. This phenomenon is actually interesting from clinical point of view – there is certain subgroup of ASD where mothers of autistic kids present with antibodies against proteins related to brain development (Braunschweig et al., 2013).

Functional redundancy of the CRMP family proteins.

As already mentioned, one of the differences between conditional and full CRMP2 knockout mice lies in the altered expression of other CRMP proteins. While in the conditional knockouts no differences in other CRMPs were detected, full CRMP2 knockout mice generated in our and other laboratories (Nakamura et al., 2016) showed both increased levels of CRMP1 and CRMP4 in the brain. CRMP1 and 4 are also sequentially and functionally close to CRMP2 and their expression pattern partially

overlaps (Bretin et al., 2005, Niisato et al., 2012). These changes may explain the surprisingly weak effect of CRMP2 deletion on axon growth, since it is known that both CRMP1 and CRMP4 also bind to tubulin dimers and may thus stabilize growing microtubules (Quach et al., 2015).

Based on the previous analysis of CRMP4 and CRMP1 knockout mice and our (and others) analysis of CRMP2 knockout mice, some unique functions of each of CRMP family members can be identified (Yamashita and Goshima, 2012). Namely, formation of CA1 dendrites and spines is affected in c*rmp1*$^{-/-}$, accompanied with impaired memory formation (Su et al., 2007, Yamashita et al., 2007). Dendritic abnormalities are further enhanced in double *crmp1*$^{-/-}$*;crmp2*$^{s522a\text{-}ki}$ mutants (S522A knock-in mutants express Cdk5-de-phosphomimetic form of CRMP2B) (Niisato et al., 2013). CRMP4, in contrast, negatively regulates dendritic branching (branch formation in CA1 dendrites is increased in *crmp4*$^{-/-}$ (Niisato et al., 2012)).

Contrary to *crmp2*$^{-/-}$ mice, CRMP2A knockouts showed no compensatory changes in expression of other CRMPs and the remaining short CRMP2B isoform is capable to support axon growth. Immunohistochemistry also revealed that CRMP2A is usually located along the axon to its very distal end, while CRMP2B localizes to both dendrites and axons (we supported this with overexpression of fusion CRMP2B-cherry of CRMP2A-cherry in neurons *in vitro* and *in vivo*, not shown*)*. Nevertheless, in one of analyzed region, the corpus callosum, it seems that CRMP2A is indispensable for regulation of axon growth. Our rescue experiments revealed that CRMP2A has significantly greater effect on axonal guidance than CRMP2B (Fig. 24). The explanation of this effect is yet unclear although electroporation experiments with fluorescently-tagged CRMP2A and CRMP2B suggested CRMP2A localizes in distal axons more often than CRMP2B (not shown) and thus may be the better regulator of the axonal growth cone guidance.

The role of CRMP2 in axon pruning.

Initial growth of axons and dendrites during embryonic and early postnatal period results in an embryonic template that must be later refined to generate a functional healthy nervous system. (Luo and O'Leary, 2005). Stereotyped refinement of nervous system was uncovered in several regions: Infrapyramidal bundle (IPB) axons in hippocampus are retracted between P14 – P30 in mice (Riccomagno et al., 2012), or corticospinal axons from layer 5 visual cortex are eliminated between P9 – P25 (Low et al., 2008). In addition, density of dendritic spines and synapses in various brain regions in mice and humans peaks between childhood and adolescence (Bian et al., 2015, Petanjek et al., 2011) and then a subpopulation of the synapses is eliminated before adulthood. Pruning also occurs in peripheral nervous system (e.g. initial polyneuronal innervation of muscle fibers is later refined – so that each muscle fiber is innervated by one motor axon (Tapia et al., 2012, Brill et al., 2016)).

Knockout mice studies identified extracellular cues and receptors that mediates pruning in rodents. These include Sema3A and its receptor complex (Nrp1/PlxnA4), and Sema3F and its receptors (Nrp2/PlxnA3), EphrinB3-EphB2 reverse signaling and C4 component of complement (Bagri et al., 2003, Xu and Henkemeyer, 2009, Cocchi et al., 2016). Intracellular pathways that translate extracellular signal to cytoskeleton are however poorly understood. In our study, we identified CRMP2 as a novel mediator of pruning in rodent brain triggered preferentially by Sema3F.

Sema3F binds preferentially to Nrp2/PlxnA3 receptor complex and is important regulator of neural development. Deficiency of Sema3F, Nrp2 or PlxnA3 results in defects in stereotyped pruning of hippocampal infrapyramidal bundle (IPB), distribution of DG dendritic spines, or anterior commissures, (Riccomagno et al., 2012, Tran et al., 2009, Chen et al., 2000). Moreover, *PlxnA3/A4*$^{-/-}$ mice display defects in pruning of visual axons (Low et al., 2008). Similarly, in our *crmp2*$^{-/-}$ mice, we found all: IPB pruning defect, alteration of DG spine density (Figs 18, 21) as well as defects in pruning of visual cortex axons (Fig 19). Moreover, our *in vitro* assays (Figs 20, 22) showed Sema3F is unable to induce axon and dendritic spine retraction in hippocampal neurons isolated from *crmp2*$^{-/-}$ embryos. In addition to Sema3F, IPB is also regulated by Ephrin-B3 reverse signaling. It is possible to speculate that CRMP2, and in particular CRMP2A isoform, which is expressed in mossy fibers, conveys signaling of both Sema3F and Ephrin-B3. Further studies will assess this hypothesis in more detail.

Sema3A has been shown to orchestrate pruning of e.g. CA1 hippocamposeptal or callosal axons (Vanderhaeghen and Cheng, 2010, Zhou et al., 2013). As CRMP2 has originally been identified as a mediator of Sema3A (Goshima et al., 1995), we hypothesized that CRMP2 is involved also in Sema3A-triggered pruning. However, we were not able to confirm this hypothesis, as we did not detect CA1 axons in medial septum by retrograde tracing after the pruning period in *crmp2*$^{-/-}$ pups (Bagri et al., 2003) (Fig 19). In callosal axons, we found significant differences in axon guidance between WT and *crmp2*$^{-/-}$ mice in P6 – P9 mice (Fig 15, 16), but the significance was lost in adult mice (Fig 16), which could be due to presence of effective Sema3A-dependent axon pruning. It is possible that other members of CRMP family (CRMP4, CRMP1) partially rescue CRMP2 deficiency in Sema3A signaling. This would be in agreement with the only mild defects we detected in the developing *crmp2*$^{-/-}$ peripheral nerves. In line with these *in vivo* data, we found that Sema3A (but not Sema3F) was able to partially induce axon retraction of the stalling *crmp2*$^{-/-}$, and particularly *crmp2a*$^{-/-}$ axons in 1-week-old hippocampal neuron cultures (Figs 20, 27). Relatively high variability in these experiments could be due to different sensitivity of individual synapses to semaphorin stimulation.

Importantly, we also did not find any defect in the pruning of neuromuscular junctions (NMJs) in *crmp2*$^{-/-}$ mice (not shown). At the end of the embryonic development each synapse is innervated by up to ten axon branches of different motor units (Tapia et al., 2012). During the first two postnatal weeks,

all except one terminal branch are pruned back establishing singly innervated NMJs (Sanes and Lichtman, 1999). While the exact molecular cascade regulating motor axon pruning is not known, Sema3A seems to play a role in the process as its receptor, Nrp1, is expressed in presynaptic axon terminals (Venkova et al., 2014). Moreover, Sema3A secreted from Schwann cells participates in NMJ remodeling (De Winter et al., 2006). Sema3F signaling has so far not been linked to motor axon pruning.

Dendritic spine density changes dynamically during childhood and adolescence. In mice, spine density peaks around 1 month and then decreases to reach stable levels around 2 months (Bian et al., 2015). It has been shown that distribution of dendritic spines is regulated by class 3 Semaphorins (Tran et al., 2009). Previous *in vitro* experiments showed that Sema3F, but not Sema3A, decreases PSD-95 positive puncta in dissociated DG neurons (Tran et al., 2009). Accordingly, Sema3F-treated cortical neurons displayed decrease in apical dendrite spine density (Tran et al., 2009). Our in vitro assay in hippocampal neurons also confirmed this finding (Fig. 22). Adult *Sema3F*$^{-/-}$, *Nrp2*$^{-/-}$ and *PlxnA3*$^{-/-}$ mice show increased spine density in several brain regions, in particular DG dendrites (Tran et al., 2009, Demyanenko et al., 2014). Both c*rmp2*$^{-/-}$ and c*rmp2a*$^{-/-}$ mice partially mimic this phenotype as we also found increased spine density in adult, but not in P30 DG granule cells (Figs 21, 25). Interestingly, in *Sema3F*$^{-/-}$ mice, increased DG spine density is detectable already during spine generation (P21) and is largely retained into adulthood, while in WT they are subsequently pruned (Tran et al., 2009). In our mutants, we did not find increased DG spine density in the pre-pruning period (P30), but similar to *Sema3F*$^{-/-}$ mice, we did find defects in DG spine pruning. Before pruning, spines also tended to be relatively enlarged in *crmp2*$^{-/-}$ mice (Fig 22). Similar observations were found in Sema3F- and Nrp2-deficient mice using electron microscopy. Aberrant spine size could reflect disruption in actin dynamic. *In vitro* analysis of dendritic spine remodeling further supports our *in vivo* findings. Together, this data suggest that while Sema3F signaling regulates both spine generation and pruning, CRMP2, and especially CRMP2A isoform contributes mainly to spine pruning.

CRMP2 in axonal growth *in vivo*.

As demonstrated in knockout lines of Sema3A and its downstream targets (*Sema3A*$^{-/-}$, *Nrp1*$^{-/-}$, *PlxnA4*$^{-/-}$ mice), Sema3A signaling is an essential regulator of development of rodent trigeminal nerve, facial nerve, DRGs projection, olphactory bulb, hippocampal formation and corpus callosum (Kitsukawa et al., 1997, Taniguchi et al., 1997, Schwarting et al., 2000, Friedel et al., 2005, Pozas et al., 2001, Schwarz et al., 2008, Zhou et al., 2013, Wu et al., 2014). Surprisingly, although Sema3A or Nrp1 deletion causes strong overgrowth of some peripheral nerves (e.g. trigeminal and spinal axons) (Kitsukawa et al., 1997, Taniguchi et al., 1997), we found only a mild overgrowth and increased branching of these axons upon deletion of its downstream mediator CRMP2 in *crmp2*$^{-/-}$ mice (Fig 12). This could be due to a partial rescue of Sema3A signaling in these neurons by other CRMP family

members as mentioned before. Moreover, CRMP4 (Fig 13) and CRMP1 (Yamane et al., 2017) are expressed in peripheral nerves suggesting that their elevation could rescue the reduced axon growth caused by full CRMP2 deficiency.

Similarly, previous *in vitro* studies demonstrated axon growth-promoting effect of CRMP2, while we did not detect any axon growth reduction in *crmp*$^{-/-}$ mice. This may be because the role of CRMP2 in regulation of axon growth, neuron polarization and migration has so far been studied *in vitro* using an acute knockdown of CRMP2 rather than *in vivo* in full knockout mice, which we used in our experiments and where the CRMP2 deficiency may be compensated by other genes (e.g. CRMP1 or CRMP4).

Electroporation studies of *Sema3A*$^{-/-}$ or *Nrp1*$^{floxed/floxed}$ brains demonstrated their role in the development of corpus callosum, with mispositioned axons in callosal midline and axonal mistargeting in contralateral cortex at P8 (Zhou et al., 2013). Defects in axon pruning of this region were also suggested (Zhou et al., 2013). Using the in utero electroporation and DiI tracing in *crmp2*$^{-/-}$ mice we also found defective guidance of callosal axons in the contralateral cortex and their altered orientation in the midline in the rostrocaudal axis (Fig 15). Strikingly, electroporation of *crmp2a*$^{-/-}$ mutants revealed similar pattern and re-expression of CRMP2A rescued the phenotype (Fig. 24), indicating the key role of CRMP2A in these processes.

Notably, Sema3F signaling is essential also for guidance of specific cranial nerves and was related to development of limbic system and anterior commissure (Sahay et al., 2003, Giger et al., 2000). From these, we only detected partial malformation of AC in *crmp2*$^{-/-}$ mice (AC is missing in *Sema3F*$^{-/-}$ or *Nrp2*$^{-/-}$ mice) suggesting CRMP2 may participate also in Sema3F-mediated axon guidance (Fig 17). Indeed, bath application of Sema3F into cultured cortical neurons significantly decreased growth rate in WTs, but not in CRMP2-deficient axons (Fig. 14).

Previous *in vitro* and *in vivo* experiments suggested that CRMP2 also regulates neuronal migration and multipolar-to-bipolar transition (Ip et al., 2014). However, using the *in utero* electroporation to GFP-label and trace a subpopulation of developing cortical neurons, we found no significant changes in neuron distribution in the developing WT and mutant cortical plates at E17.5 (Fig 11). This likely reflects different experimental paradigms used in the studies (somatic knockdown vs. full knockout) (Ip et al., 2014). Moreover, CRMP1 has previously been associated with neuronal migration as *crmp1*$^{-/-}$ mice display lamination defects (Yamashita et al., 2006), therefore it is plausible that CRMP1 could compensate function of CRMP2 in this process.

Regulation of CRMP2A through Pin1.

We uncovered the role of Pin1 in axon guidance under physiological conditions. We found that Pin1 binds to and stabilizes CRMP2A phosphorylated by Cdk5 on the Ser27-Pro28 motif. Knockout of Pin1

caused S27-CRMP2A decrease (Fig. 27), as well as axon outgrowth decrease (Balastik et al., 2015). *Pin1*$^{-/-}$ neurons are more sensitive to Sema3A stimulation. However, changes of axonal growth in *Pin1*$^{-/-}$ embryos were detected only in selected areas (e.g. ophthalmic branch of the trigeminal nerve), thus pointing to specificity of this mode of axon growth regulation that might be caused by variable levels of Pin1 in the growth cones. For example, in callosal axons, Pin1 was not detected in the growth cones, unlike CRMPs (Poulopoulos et al., 2019). In line with these recent data, we also did not observed any changes in callosal axon fasciculation (Balastik et al., 2015).

We tested genetic interaction between Sema3A signaling and Pin1in zebrafish embryos. We knocked down Sema3A receptor (Nrp1) to silence Sema3A signaling. As a result, we observed motor neuron growth defects (Balastik et al., 2015), similarly as published before (Feldner et al., 2005). Importantly, simultaneous knockdown of Nrp1 and Pin1 partially rescued this phenotype thus supporting Pin1 role in Sema3A signaling.

CRMP2 involvement in pathogenesis of neurodevelopmental disorders.

Deregulation of CRMP2 has been linked to several neurodevelopmental disorders (Sfari Gene database, https://gene.sfari.org/database/human-gene/DPYSL2). Recently published analysis of conditional brain-specific (Zhang et al., 2016) and full *crmp2* knockout mice (Nakamura et al., 2016) showed multiple behavioral defects associated with CRMP2 deficiency. Notably, conditional knockout mice revealed hyperactivity and prepulsed inhibition (PPI) deficit together with social behavior impairment. PPI is a test for evaluating sensorimotor gating – the phenomenon that is often altered in schizophrenia patients. In addition, clozapine (an antipsychotic drug) treatment was capable to reduce hyperactivity in conditional *crmp2*$^{-/-}$ mice. Furthermore, morphological analysis showed increased volume of brain ventricles and impaired dendritic development in hippocampal CA1 and DG neurons, which is associated with schizophrenia, but also other neurodevelopmental disorders (Zhang et al., 2016). Importantly, the analysis of the full and conditional CRMP2 knockout mice revealed also their significant differences. In particular, while PPI was reduced in the conditional mice, in the full *crmp2*$^{-/-}$ mice it was not significantly different to WT (Zhang et al., 2016, Nakamura et al., 2016). This suggests that even a minor difference in the spatio-temporal inactivation of CRMP2 during development can have a major impact on the development and severity of the resulting neurodevelopmental defects. In the full CRMP2 knockout mice we generated, we found several phenotypical defects present in the published conditional and full CRMP2 knockout mice (e.g. ventriculomegaly, spine density changes in DG, working memory defects, or hyperactivity) (Zhang et al., 2016, Tobe et al., 2017). We also found brain sizes comparable to both WTs and the full *crmp2*$^{-/-}$ mice, similar as reported in the conditional CRMP2 knockout mice (Zhang et al., 2016, Tobe et al., 2017), although we detected a non-significant tendency for a thinner cortex in the knockout mice (Fig. 11). In addition, though, we demonstrate that CRMP2 knockout leads to defects in axonal pruning and dendritic spine remodeling compatible with

ASD rather than schizophrenia (Lord et al., 2018). As in other ASD mouse models (Schmeisser et al., 2012), the dendritic spine pruning deficiency is not present in all brain regions (e.g. we did not detect it in the prefrontal cortex (Fig 21) or CA1 neurons (Fig 22)). This may reflect different spatio-temporal combinations of expression of CRMP2 (and its isoforms) and Semaphorins in specific brain regions (of note, there is a strong expression of CRMP2A isoform specifically in molecular layer of DG (Fig 10), that shows the pruning deficiency). The detail role of CRMP2 isoforms in axon pruning will be analyzed in future studies.

Morphological changes were accompanied by altered social communication in early postnatal (P8 and P12) mutants and decreased sociability in adults (not shown). Defects in the early postnatal ultrasonic vocalizations followed by dendritic spine pathology have been previously observed in several mouse models of ASD (Reynolds et al., 2016, Binder and Lugo, 2017, Schmeisser et al., 2012) further corroborating the role of CRMP2 in the pathogenesis of ASD. The connection between altered sociability and impairment of stereotyped axon pruning is much less clear. Nevertheless, functional variants of Otx-1 gene associated with social interaction deficit and ASD in humans (Liu et al., 2011) and mice lacking Otx-1 have defects in stereotyped axon pruning (Weimann et al., 1999).

Importantly, Sema3F signaling has been also implicated in the pathogenesis of ASD. Sema3F or NRP2 deficient mice show both behavioral and neuropathological aspects of ASD (Li et al., 2019) and Sema3F interacts with multiple ASD-related genes e.g. fragile X mental retardation protein or MECP2 (Degano et al., 2009). Thus, by linking Sema3F and CRMP2 signaling and comparing the histological as well as behavioral effects of their deficiency, our data strongly implicate that the Sema3F-CRMP2 signaling plays an important role in ASD pathogenesis.

7. References

ACKERMAN, S. L., KOZAK, L. P., PRZYBORSKI, S. A., RUND, L. A., BOYER, B. B. & KNOWLES, B. B. 1997. The mouse rostral cerebellar malformation gene encodes an UNC-5-like protein. *Nature,* 386**,** 838-42.

ARIMURA, N., HATTORI, A., KIMURA, T., NAKAMUTA, S., FUNAHASHI, Y., HIROTSUNE, S., FURUTA, K., URANO, T., TOYOSHIMA, Y. Y. & KAIBUCHI, K. 2009a. CRMP-2 directly binds to cytoplasmic dynein and interferes with its activity. *J Neurochem,* 111**,** 380-90.

ARIMURA, N., INAGAKI, N., CHIHARA, K., MENAGER, C., NAKAMURA, N., AMANO, M., IWAMATSU, A., GOSHIMA, Y. & KAIBUCHI, K. 2000. Phosphorylation of collapsin response mediator protein-2 by Rho-kinase. Evidence for two separate signaling pathways for growth cone collapse. *J Biol Chem,* 275**,** 23973-80.

ARIMURA, N. & KAIBUCHI, K. 2007. Neuronal polarity: from extracellular signals to intracellular mechanisms. *Nat Rev Neurosci,* 8**,** 194-205.

ARIMURA, N., KIMURA, T., NAKAMUTA, S., TAYA, S., FUNAHASHI, Y., HATTORI, A., SHIMADA, A., MENAGER, C., KAWABATA, S., FUJII, K., IWAMATSU, A., SEGAL, R. A., FUKUDA, M. & KAIBUCHI, K. 2009b. Anterograde transport of TrkB in axons is mediated by direct interaction with Slp1 and Rab27. *Dev Cell,* 16**,** 675-86.

ARIMURA, N., MENAGER, C., KAWANO, Y., YOSHIMURA, T., KAWABATA, S., HATTORI, A., FUKATA, Y., AMANO, M., GOSHIMA, Y., INAGAKI, M., MORONE, N., USUKURA, J. & KAIBUCHI, K. 2005. Phosphorylation by Rho kinase regulates CRMP-2 activity in growth cones. *Mol Cell Biol,* 25**,** 9973-84.

ARLOTTA, P. & PASCA, S. P. 2019. Cell diversity in the human cerebral cortex: from the embryo to brain organoids. *Curr Opin Neurobiol,* 56**,** 194-198.

AZEVEDO, F. A., CARVALHO, L. R., GRINBERG, L. T., FARFEL, J. M., FERRETTI, R. E., LEITE, R. E., JACOB FILHO, W., LENT, R. & HERCULANO-HOUZEL, S. 2009. Equal numbers of neuronal and nonneuronal cells make the human brain an isometrically scaled-up primate brain. *J Comp Neurol,* 513**,** 532-41.

BAAS, P. W., DEITCH, J. S., BLACK, M. M. & BANKER, G. A. 1988. Polarity orientation of microtubules in hippocampal neurons: uniformity in the axon and nonuniformity in the dendrite. *Proc Natl Acad Sci U S A,* 85**,** 8335-9.

BAGRI, A., CHENG, H. J., YARON, A., PLEASURE, S. J. & TESSIER-LAVIGNE, M. 2003. Stereotyped pruning of long hippocampal axon branches triggered by retraction inducers of the semaphorin family. *Cell,* 113**,** 285-99.

BALASTIK, M., LIM, J., PASTORINO, L. & LU, K. P. 2007. Pin1 in Alzheimer's disease: multiple substrates, one regulatory mechanism? *Biochim Biophys Acta,* 1772**,** 422-9.

BALASTIK, M., ZHOU, X. Z., ALBERICH-JORDA, M., WEISSOVA, R., ZIAK, J., PAZYRA-MURPHY, M. F., COSKER, K. E., MACHONOVA, O., KOZMIKOVA, I., CHEN, C. H., PASTORINO, L., ASARA, J. M., COLE, A., SUTHERLAND, C., SEGAL, R. A. & LU, K. P. 2015. Prolyl Isomerase Pin1 Regulates Axon Guidance by Stabilizing CRMP2A Selectively in Distal Axons. *Cell Rep,* 13**,** 812-28.

BARAK, R., LAHMI, R., GEVORKYAN-AIRAPETOV, L., LEVY, E., TZUR, A. & OPATOWSKY, Y. 2014. Crystal structure of the extracellular juxtamembrane region of Robo1. *J Struct Biol,* 186**,** 283-91.

BASARSKY, T. A., PARPURA, V. & HAYDON, P. G. 1994. Hippocampal synaptogenesis in cell culture: developmental time course of synapse formation, calcium influx, and synaptic protein distribution. *J Neurosci,* 14**,** 6402-11.

BAUDOIN, J. P., VIOU, L., LAUNAY, P. S., LUCCARDINI, C., ESPESO GIL, S., KIYASOVA, V., IRINOPOULOU, T., ALVAREZ, C., RIO, J. P., BOUDIER, T., LECHAIRE, J. P., KESSARIS, N., SPASSKY, N. & METIN, C. 2012. Tangentially migrating neurons assemble a primary cilium that promotes their reorientation to the cortical plate. *Neuron,* 76**,** 1108-22.

BIAN, W. J., MIAO, W. Y., HE, S. J., QIU, Z. & YU, X. 2015. Coordinated Spine Pruning and Maturation Mediated by Inter-Spine Competition for Cadherin/Catenin Complexes. *Cell,* 162**,** 808-22.

BINDER, M. S. & LUGO, J. N. 2017. NS-Pten knockout mice show sex- and age-specific differences in ultrasonic vocalizations. *Brain Behav,* 7**,** e00857.

BLOCKUS, H. & CHEDOTAL, A. 2016. Slit-Robo signaling. *Development,* 143**,** 3037-44.

BOURGERON, T. 2015. From the genetic architecture to synaptic plasticity in autism spectrum disorder. *Nat Rev Neurosci,* 16**,** 551-63.

BRADKE, F. & DOTTI, C. G. 1997. Neuronal polarity: vectorial cytoplasmic flow precedes axon formation. *Neuron,* 19**,** 1175-86.

BRADKE, F. & DOTTI, C. G. 1999. The role of local actin instability in axon formation. *Science,* 283**,** 1931-4.

BRADKE, F. & DOTTI, C. G. 2000. Establishment of neuronal polarity: lessons from cultured hippocampal neurons. *Curr Opin Neurobiol,* 10**,** 574-81.

BRAUNSCHWEIG, D., KRAKOWIAK, P., DUNCANSON, P., BOYCE, R., HANSEN, R. L., ASHWOOD, P., HERTZ-PICCIOTTO, I., PESSAH, I. N. & VAN DE WATER, J. 2013. Autism-specific maternal autoantibodies recognize critical proteins in developing brain. *Transl Psychiatry,* 3**,** e277.

BRETIN, S., REIBEL, S., CHARRIER, E., MAUS-MOATTI, M., AUVERGNON, N., THEVENOUX, A., GLOWINSKI, J., ROGEMOND, V., PREMONT, J., HONNORAT, J. & GAUCHY, C. 2005. Differential expression of CRMP1, CRMP2A, CRMP2B, and CRMP5 in axons or dendrites of distinct neurons in the mouse brain. *J Comp Neurol,* 486**,** 1-17.

BRILL, M. S., KLEELE, T., RUSCHKIES, L., WANG, M., MARAHORI, N. A., REUTER, M. S., HAUSRAT, T. J., WEIGAND, E., FISHER, M., AHLES, A., ENGELHARDT, S., BISHOP, D. L., KNEUSSEL, M. & MISGELD, T. 2016. Branch-Specific Microtubule Destabilization Mediates Axon Branch Loss during Neuromuscular Synapse Elimination. *Neuron,* 92**,** 845-856.

BRITTAIN, J. M., DUARTE, D. B., WILSON, S. M., ZHU, W., BALLARD, C., JOHNSON, P. L., LIU, N., XIONG, W., RIPSCH, M. S., WANG, Y., FEHRENBACHER, J. C., FITZ, S. D., KHANNA, M., PARK, C. K., SCHMUTZLER, B. S., CHEON, B. M., DUE, M. R., BRUSTOVETSKY, T., ASHPOLE, N. M., HUDMON, A., MEROUEH, S. O., HINGTGEN, C. M., BRUSTOVETSKY, N., JI, R. R., HURLEY, J. H., JIN, X., SHEKHAR, A., XU, X. M., OXFORD, G. S., VASKO, M. R., WHITE, F. A. & KHANNA, R. 2011. Suppression of inflammatory and neuropathic pain by uncoupling CRMP-2 from the presynaptic Ca(2)(+) channel complex. *Nat Med,* 17**,** 822-9.

BRITTAIN, J. M., PIEKARZ, A. D., WANG, Y., KONDO, T., CUMMINS, T. R. & KHANNA, R. 2009. An atypical role for collapsin response mediator protein 2 (CRMP-2) in neurotransmitter release via interaction with presynaptic voltage-gated calcium channels. *J Biol Chem,* 284**,** 31375-90.

BROWN, M., JACOBS, T., EICKHOLT, B., FERRARI, G., TEO, M., MONFRIES, C., QI, R. Z., LEUNG, T., LIM, L. & HALL, C. 2004. Alpha2-chimaerin, cyclin-dependent Kinase 5/p35, and its target collapsin response mediator protein-2 are essential components in semaphorin 3A-induced growth-cone collapse. *J Neurosci,* 24**,** 8994-9004.

BURGESS, R. W., JUCIUS, T. J. & ACKERMAN, S. L. 2006. Motor axon guidance of the mammalian trochlear and phrenic nerves: dependence on the netrin receptor Unc5c and modifier loci. *J Neurosci,* 26**,** 5756-66.

CAMPBELL, K. & GOTZ, M. 2002. Radial glia: multi-purpose cells for vertebrate brain development. *Trends Neurosci,* 25**,** 235-8.

CERMAK, T., DOYLE, E. L., CHRISTIAN, M., WANG, L., ZHANG, Y., SCHMIDT, C., BALLER, J. A., SOMIA, N. V., BOGDANOVE, A. J. & VOYTAS, D. F. 2011. Efficient design and assembly of custom TALEN and other TAL effector-based constructs for DNA targeting. *Nucleic Acids Res,* 39**,** e82.

CLARK, D., DEDOVA, I., CORDWELL, S. & MATSUMOTO, I. 2006. A proteome analysis of the anterior cingulate cortex gray matter in schizophrenia. *Mol Psychiatry,* 11**,** 459-70, 423.

COCCHI, E., DRAGO, A. & SERRETTI, A. 2016. Hippocampal Pruning as a New Theory of Schizophrenia Etiopathogenesis. *Mol Neurobiol,* 53**,** 2065-81.

COLE, R. N. & HART, G. W. 2001. Cytosolic O-glycosylation is abundant in nerve terminals. *J Neurochem,* 79**,** 1080-9.

COLEMAN, H. A., LABRADOR, J. P., CHANCE, R. K. & BASHAW, G. J. 2010. The Adam family metalloprotease Kuzbanian regulates the cleavage of the roundabout receptor to control axon repulsion at the midline. *Development,* 137**,** 2417-26.

COURCHET, J., LEWIS, T. L., JR., LEE, S., COURCHET, V., LIOU, D. Y., AIZAWA, S. & POLLEUX, F. 2013. Terminal axon branching is regulated by the LKB1-NUAK1 kinase pathway via presynaptic mitochondrial capture. *Cell,* 153**,** 1510-25.

COWAN, C. W., SHAO, Y. R., SAHIN, M., SHAMAH, S. M., LIN, M. Z., GREER, P. L., GAO, S., GRIFFITH, E. C., BRUGGE, J. S. & GREENBERG, M. E. 2005. Vav family GEFs link activated Ephs to endocytosis and axon guidance. *Neuron,* 46**,** 205-17.

DASCENCO, D., ERFURTH, M. L., IZADIFAR, A., SONG, M., SACHSE, S., BORTNICK, R., URWYLER, O., PETROVIC, M., AYAZ, D., HE, H., KISE, Y., THOMAS, F., KIDD, T. & SCHMUCKER, D. 2015. Slit and Receptor Tyrosine Phosphatase 69D Confer Spatial Specificity to Axon Branching via Dscam1. *Cell,* 162**,** 1140-54.

DAVY, A., GALE, N. W., MURRAY, E. W., KLINGHOFFER, R. A., SORIANO, P., FEUERSTEIN, C. & ROBBINS, S. M. 1999. Compartmentalized signaling by GPI-anchored ephrin-A5 requires the Fyn tyrosine kinase to regulate cellular adhesion. *Genes Dev,* 13**,** 3125-35.

DAWSON, H. N., FERREIRA, A., EYSTER, M. V., GHOSHAL, N., BINDER, L. I. & VITEK, M. P. 2001. Inhibition of neuronal maturation in primary hippocampal neurons from tau deficient mice. *J Cell Sci,* 114**,** 1179-87.

DE RUBEIS, S., FERNANDEZ, E., BUZZI, A., DI MARINO, D. & BAGNI, C. 2012. Molecular and cellular aspects of mental retardation in the Fragile X syndrome: from gene mutation/s to spine dysmorphogenesis. *Adv Exp Med Biol,* 970**,** 517-51.

DE RUBEIS, S., HE, X., GOLDBERG, A. P., POULTNEY, C. S., SAMOCHA, K., CICEK, A. E., KOU, Y., LIU, L., FROMER, M., WALKER, S., SINGH, T., KLEI, L., KOSMICKI, J., SHIH-CHEN, F., ALEKSIC, B., BISCALDI, M., BOLTON, P. F., BROWNFELD, J. M., CAI, J., CAMPBELL, N. G., CARRACEDO, A., CHAHROUR, M. H., CHIOCCHETTI, A. G., COON, H., CRAWFORD, E. L., CURRAN, S. R., DAWSON, G., DUKETIS, E., FERNANDEZ, B. A., GALLAGHER, L., GELLER, E., GUTER, S. J., HILL, R. S., IONITA-LAZA, J., JIMENZ GONZALEZ, P., KILPINEN, H., KLAUCK, S. M., KOLEVZON, A., LEE, I., LEI, I., LEI, J., LEHTIMAKI, T., LIN, C. F., MA'AYAN, A., MARSHALL, C. R., MCINNES, A. L., NEALE, B., OWEN, M. J., OZAKI, N., PARELLADA, M., PARR, J. R., PURCELL, S., PUURA, K., RAJAGOPALAN, D., REHNSTROM, K., REICHENBERG, A., SABO, A., SACHSE, M., SANDERS, S. J., SCHAFER, C., SCHULTE-RUTHER, M., SKUSE, D., STEVENS, C., SZATMARI, P., TAMMIMIES, K., VALLADARES, O., VORAN, A., LI-SAN, W., WEISS, L. A., WILLSEY, A. J., YU, T. W., YUEN, R. K., STUDY, D. D. D., HOMOZYGOSITY MAPPING COLLABORATIVE FOR, A., CONSORTIUM, U. K., COOK, E. H., FREITAG, C. M., GILL, M., HULTMAN, C. M., LEHNER, T., PALOTIE, A., SCHELLENBERG, G. D., SKLAR, P., STATE, M. W., SUTCLIFFE, J. S., WALSH, C. A., SCHERER, S. W., ZWICK, M. E., BARETT, J. C., CUTLER, D. J., ROEDER, K., DEVLIN, B., DALY, M. J. & BUXBAUM, J. D. 2014. Synaptic, transcriptional and chromatin genes disrupted in autism. *Nature,* 515**,** 209-15.

DE WINTER, F., VO, T., STAM, F. J., WISMAN, L. A., BAR, P. R., NICLOU, S. P., VAN MUISWINKEL, F. L. & VERHAAGEN, J. 2006. The expression of the chemorepellent Semaphorin 3A is selectively induced in terminal Schwann cells of a subset of neuromuscular synapses that display limited anatomical plasticity and enhanced vulnerability in motor neuron disease. *Mol Cell Neurosci,* 32**,** 102-17.

DEGANO, A. L., PASTERKAMP, R. J. & RONNETT, G. V. 2009. MeCP2 deficiency disrupts axonal guidance, fasciculation, and targeting by altering Semaphorin 3F function. *Mol Cell Neurosci,* 42**,** 243-54.

DEHAY, C. & KENNEDY, H. 2007. Cell-cycle control and cortical development. *Nat Rev Neurosci,* 8**,** 438-50.

DEL RIO, J. A., GONZALEZ-BILLAULT, C., URENA, J. M., JIMENEZ, E. M., BARALLOBRE, M. J., PASCUAL, M., PUJADAS, L., SIMO, S., LA TORRE, A., WANDOSELL, F., AVILA, J. & SORIANO, E. 2004.

MAP1B is required for Netrin 1 signaling in neuronal migration and axonal guidance. *Curr Biol,* 14**,** 840-50.

DELLOYE-BOURGEOIS, C., JACQUIER, A., CHAROY, C., REYNAUD, F., NAWABI, H., THOINET, K., KINDBEITER, K., YOSHIDA, Y., ZAGAR, Y., KONG, Y., JONES, Y. E., FALK, J., CHEDOTAL, A. & CASTELLANI, V. 2015. PlexinA1 is a new Slit receptor and mediates axon guidance function of Slit C-terminal fragments. *Nat Neurosci,* 18**,** 36-45.

DEMYANENKO, G. P., MOHAN, V., ZHANG, X., BRENNAMAN, L. H., DHARBAL, K. E., TRAN, T. S., MANIS, P. B. & MANESS, P. F. 2014. Neural cell adhesion molecule NrCAM regulates Semaphorin 3F-induced dendritic spine remodeling. *J Neurosci,* 34**,** 11274-87.

DOBYNS, W. B., REINER, O., CARROZZO, R. & LEDBETTER, D. H. 1993. Lissencephaly. A human brain malformation associated with deletion of the LIS1 gene located at chromosome 17p13. *JAMA,* 270**,** 2838-42.

DOMINICI, C., MORENO-BRAVO, J. A., PUIGGROS, S. R., RAPPENEAU, Q., RAMA, N., VIEUGUE, P., BERNET, A., MEHLEN, P. & CHEDOTAL, A. 2017. Floor-plate-derived netrin-1 is dispensable for commissural axon guidance. *Nature,* 545**,** 350-354.

DOTTI, C. G. & BANKER, G. A. 1987. Experimentally induced alteration in the polarity of developing neurons. *Nature,* 330**,** 254-6.

DOTTI, C. G., SULLIVAN, C. A. & BANKER, G. A. 1988. The establishment of polarity by hippocampal neurons in culture. *J Neurosci,* 8**,** 1454-68.

DOYLE, E. L., BOOHER, N. J., STANDAGE, D. S., VOYTAS, D. F., BRENDEL, V. P., VANDYK, J. K. & BOGDANOVE, A. J. 2012. TAL Effector-Nucleotide Targeter (TALE-NT) 2.0: tools for TAL effector design and target prediction. *Nucleic Acids Res,* 40**,** W117-22.

DUSTRUDE, E. T., PEREZ-MILLER, S., FRANCOIS-MOUTAL, L., MOUTAL, A., KHANNA, M. & KHANNA, R. 2017. A single structurally conserved SUMOylation site in CRMP2 controls NaV1.7 function. *Channels (Austin),* 11**,** 316-328.

DUSTRUDE, E. T., WILSON, S. M., JU, W., XIAO, Y. & KHANNA, R. 2013. CRMP2 protein SUMOylation modulates NaV1.7 channel trafficking. *J Biol Chem,* 288**,** 24316-31.

EGEA, J. & KLEIN, R. 2007. Bidirectional Eph-ephrin signaling during axon guidance. *Trends Cell Biol,* 17**,** 230-8.

FAZELI, A., DICKINSON, S. L., HERMISTON, M. L., TIGHE, R. V., STEEN, R. G., SMALL, C. G., STOECKLI, E. T., KEINO-MASU, K., MASU, M., RAYBURN, H., SIMONS, J., BRONSON, R. T., GORDON, J. I., TESSIER-LAVIGNE, M. & WEINBERG, R. A. 1997. Phenotype of mice lacking functional Deleted in colorectal cancer (Dcc) gene. *Nature,* 386**,** 796-804.

FELDNER, J., BECKER, T., GOISHI, K., SCHWEITZER, J., LEE, P., SCHACHNER, M., KLAGSBRUN, M. & BECKER, C. G. 2005. Neuropilin-1a is involved in trunk motor axon outgrowth in embryonic zebrafish. *Dev Dyn,* 234**,** 535-49.

FENLON, L. R. & RICHARDS, L. J. 2015. Contralateral targeting of the corpus callosum in normal and pathological brain function. *Trends Neurosci,* 38**,** 264-72.

FRIEDEL, R. H., PLUMP, A., LU, X., SPILKER, K., JOLICOEUR, C., WONG, K., VENKATESH, T. R., YARON, A., HYNES, M., CHEN, B., OKADA, A., MCCONNELL, S. K., RAYBURN, H. & TESSIER-LAVIGNE, M. 2005. Gene targeting using a promoterless gene trap vector ("targeted trapping") is an efficient method to mutate a large fraction of genes. *Proc Natl Acad Sci U S A,* 102**,** 13188-93.

FUJIMORI, F., TAKAHASHI, K., UCHIDA, C. & UCHIDA, T. 1999. Mice lacking Pin1 develop normally, but are defective in entering cell cycle from G(0) arrest. *Biochem Biophys Res Commun,* 265**,** 658-63.

FUKATA, Y., ITOH, T. J., KIMURA, T., MENAGER, C., NISHIMURA, T., SHIROMIZU, T., WATANABE, H., INAGAKI, N., IWAMATSU, A., HOTANI, H. & KAIBUCHI, K. 2002a. CRMP-2 binds to tubulin heterodimers to promote microtubule assembly. *Nat Cell Biol,* 4**,** 583-91.

FUKATA, Y., KIMURA, T. & KAIBUCHI, K. 2002b. Axon specification in hippocampal neurons. *Neurosci Res,* 43**,** 305-15.

GAITANOS, T. N., KOERNER, J. & KLEIN, R. 2016. Tiam-Rac signaling mediates trans-endocytosis of ephrin receptor EphB2 and is important for cell repulsion. *J Cell Biol,* 214**,** 735-52.

GALLO, G. 2006. RhoA-kinase coordinates F-actin organization and myosin II activity during semaphorin-3A-induced axon retraction. *J Cell Sci,* 119**,** 3413-23.

GALLO, G. 2011. The cytoskeletal and signaling mechanisms of axon collateral branching. *Dev Neurobiol,* 71**,** 201-20.

GAO, R. & PENZES, P. 2015. Common mechanisms of excitatory and inhibitory imbalance in schizophrenia and autism spectrum disorders. *Curr Mol Med,* 15**,** 146-67.

GAREY, L. 2010. When cortical development goes wrong: schizophrenia as a neurodevelopmental disease of microcircuits. *J Anat,* 217**,** 324-33.

GAREY, L. J., ONG, W. Y., PATEL, T. S., KANANI, M., DAVIS, A., MORTIMER, A. M., BARNES, T. R. & HIRSCH, S. R. 1998. Reduced dendritic spine density on cerebral cortical pyramidal neurons in schizophrenia. *J Neurol Neurosurg Psychiatry,* 65**,** 446-53.

GIGER, R. J., CLOUTIER, J. F., SAHAY, A., PRINJHA, R. K., LEVENGOOD, D. V., MOORE, S. E., PICKERING, S., SIMMONS, D., RASTAN, S., WALSH, F. S., KOLODKIN, A. L., GINTY, D. D. & GEPPERT, M. 2000. Neuropilin-2 is required in vivo for selective axon guidance responses to secreted semaphorins. *Neuron,* 25**,** 29-41.

GIL-SANZ, C., FRANCO, S. J., MARTINEZ-GARAY, I., ESPINOSA, A., HARKINS-PERRY, S. & MULLER, U. 2013. Cajal-Retzius cells instruct neuronal migration by coincidence signaling between secreted and contact-dependent guidance cues. *Neuron,* 79**,** 461-77.

GIL, V., NOCENTINI, S. & DEL RIO, J. A. 2014. Historical first descriptions of Cajal-Retzius cells: from pioneer studies to current knowledge. *Front Neuroanat,* 8**,** 32.

GLEESON, J. G., ALLEN, K. M., FOX, J. W., LAMPERTI, E. D., BERKOVIC, S., SCHEFFER, I., COOPER, E. C., DOBYNS, W. B., MINNERATH, S. R., ROSS, M. E. & WALSH, C. A. 1998. Doublecortin, a brain-specific gene mutated in human X-linked lissencephaly and double cortex syndrome, encodes a putative signaling protein. *Cell,* 92**,** 63-72.

GOFFINET, A. M. 1984. Events governing organization of postmigratory neurons: studies on brain development in normal and reeler mice. *Brain Res,* 319**,** 261-96.

GOLDOWITZ, D., HAMRE, K. M., PRZYBORSKI, S. A. & ACKERMAN, S. L. 2000. Granule cells and cerebellar boundaries: analysis of Unc5h3 mutant chimeras. *J Neurosci,* 20**,** 4129-37.

GONCALVES, J. T., BLOYD, C. W., SHTRAHMAN, M., JOHNSTON, S. T., SCHAFER, S. T., PARYLAK, S. L., TRAN, T., CHANG, T. & GAGE, F. H. 2016. In vivo imaging of dendritic pruning in dentate granule cells. *Nat Neurosci,* 19**,** 788-91.

GOSHIMA, Y., NAKAMURA, F., STRITTMATTER, P. & STRITTMATTER, S. M. 1995. Collapsin-induced growth cone collapse mediated by an intracellular protein related to UNC-33. *Nature,* 376**,** 509-14.

GRANDBARBE, L., BOUISSAC, J., RAND, M., HRABE DE ANGELIS, M., ARTAVANIS-TSAKONAS, S. & MOHIER, E. 2003. Delta-Notch signaling controls the generation of neurons/glia from neural stem cells in a stepwise process. *Development,* 130**,** 1391-402.

HADDAD-TOVOLLI, R., SZABO, N. E., ZHOU, X. & ALVAREZ-BOLADO, G. 2013. Genetic manipulation of the mouse developing hypothalamus through in utero electroporation. *J Vis Exp*.

HALL, A. & LALLI, G. 2010. Rho and Ras GTPases in axon growth, guidance, and branching. *Cold Spring Harb Perspect Biol,* 2**,** a001818.

HARADA, A., OGUCHI, K., OKABE, S., KUNO, J., TERADA, S., OHSHIMA, T., SATO-YOSHITAKE, R., TAKEI, Y., NODA, T. & HIROKAWA, N. 1994. Altered microtubule organization in small-calibre axons of mice lacking tau protein. *Nature,* 369**,** 488-91.

HENDERSON, N. T., LE MARCHAND, S. J., HRUSKA, M., HIPPENMEYER, S., LUO, L. & DALVA, M. B. 2019. Ephrin-B3 controls excitatory synapse density through cell-cell competition for EphBs. *Elife,* 8.

HENKEMEYER, M., ITKIS, O. S., NGO, M., HICKMOTT, P. W. & ETHELL, I. M. 2003. Multiple EphB receptor tyrosine kinases shape dendritic spines in the hippocampus. *J Cell Biol,* 163**,** 1313-26.

HOERDER-SUABEDISSEN, A. & MOLNAR, Z. 2015. Development, evolution and pathology of neocortical subplate neurons. *Nat Rev Neurosci,* 16**,** 133-46.

HONG, K., HINCK, L., NISHIYAMA, M., POO, M. M., TESSIER-LAVIGNE, M. & STEIN, E. 1999. A ligand-gated association between cytoplasmic domains of UNC5 and DCC family receptors converts netrin-induced growth cone attraction to repulsion. *Cell,* 97**,** 927-41.

HONG, S. E., SHUGART, Y. Y., HUANG, D. T., SHAHWAN, S. A., GRANT, P. E., HOURIHANE, J. O., MARTIN, N. D. & WALSH, C. A. 2000. Autosomal recessive lissencephaly with cerebellar hypoplasia is associated with human RELN mutations. *Nat Genet,* 26**,** 93-6.

HRUSKA, M. & DALVA, M. B. 2012. Ephrin regulation of synapse formation, function and plasticity. *Mol Cell Neurosci,* 50**,** 35-44.

HUMMEL, T., SCHIMMELPFENG, K. & KLAMBT, C. 1999. Commissure formation in the embryonic CNS of Drosophila. *Dev Biol,* 209**,** 381-98.

HUNG, R. J., YAZDANI, U., YOON, J., WU, H., YANG, T., GUPTA, N., HUANG, Z., VAN BERKEL, W. J. & TERMAN, J. R. 2010. Mical links semaphorins to F-actin disassembly. *Nature,* 463**,** 823-7.

CHAE, Y. C., LEE, S., HEO, K., HA, S. H., JUNG, Y., KIM, J. H., IHARA, Y., SUH, P. G. & RYU, S. H. 2009. Collapsin response mediator protein-2 regulates neurite formation by modulating tubulin GTPase activity. *Cell Signal,* 21**,** 1818-26.

CHEDOTAL, A., DEL RIO, J. A., RUIZ, M., HE, Z., BORRELL, V., DE CASTRO, F., EZAN, F., GOODMAN, C. S., TESSIER-LAVIGNE, M., SOTELO, C. & SORIANO, E. 1998. Semaphorins III and IV repel hippocampal axons via two distinct receptors. *Development,* 125**,** 4313-23.

CHEN, H., BAGRI, A., ZUPICICH, J. A., ZOU, Y., STOECKLI, E., PLEASURE, S. J., LOWENSTEIN, D. H., SKARNES, W. C., CHEDOTAL, A. & TESSIER-LAVIGNE, M. 2000. Neuropilin-2 regulates the development of selective cranial and sensory nerves and hippocampal mossy fiber projections. *Neuron,* 25**,** 43-56.

CHENG, H. J., BAGRI, A., YARON, A., STEIN, E., PLEASURE, S. J. & TESSIER-LAVIGNE, M. 2001. Plexin-A3 mediates semaphorin signaling and regulates the development of hippocampal axonal projections. *Neuron,* 32**,** 249-63.

CHONG, S. S., PACK, S. D., ROSCHKE, A. V., TANIGAMI, A., CARROZZO, R., SMITH, A. C., DOBYNS, W. B. & LEDBETTER, D. H. 1997. A revision of the lissencephaly and Miller-Dieker syndrome critical regions in chromosome 17p13.3. *Hum Mol Genet,* 6**,** 147-55.

INAGAKI, N., CHIHARA, K., ARIMURA, N., MENAGER, C., KAWANO, Y., MATSUO, N., NISHIMURA, T., AMANO, M. & KAIBUCHI, K. 2001. CRMP-2 induces axons in cultured hippocampal neurons. *Nat Neurosci,* 4**,** 781-2.

IONESCU, A., ZAHAVI, E. E., GRADUS, T., BEN-YAAKOV, K. & PERLSON, E. 2016. Compartmental microfluidic system for studying muscle-neuron communication and neuromuscular junction maintenance. *Eur J Cell Biol,* 95**,** 69-88.

IP, J. P., FU, A. K. & IP, N. Y. 2014. CRMP2: functional roles in neural development and therapeutic potential in neurological diseases. *Neuroscientist,* 20**,** 589-98.

IP, J. P., SHI, L., CHEN, Y., ITOH, Y., FU, W. Y., BETZ, A., YUNG, W. H., GOTOH, Y., FU, A. K. & IP, N. Y. 2011. alpha2-chimaerin controls neuronal migration and functioning of the cerebral cortex through CRMP-2. *Nat Neurosci,* 15**,** 39-47.

ITO, Y., OINUMA, I., KATOH, H., KAIBUCHI, K. & NEGISHI, M. 2006. Sema4D/plexin-B1 activates GSK-3beta through R-Ras GAP activity, inducing growth cone collapse. *EMBO Rep,* 7**,** 704-9.

IWASATO, T., KATOH, H., NISHIMARU, H., ISHIKAWA, Y., INOUE, H., SAITO, Y. M., ANDO, R., IWAMA, M., TAKAHASHI, R., NEGISHI, M. & ITOHARA, S. 2007. Rac-GAP alpha-chimerin regulates motor-circuit formation as a key mediator of EphrinB3/EphA4 forward signaling. *Cell,* 130**,** 742-53.

JAGLIN, X. H. & CHELLY, J. 2009. Tubulin-related cortical dysgeneses: microtubule dysfunction underlying neuronal migration defects. *Trends Genet,* 25**,** 555-66.

JAGLIN, X. H., POIRIER, K., SAILLOUR, Y., BUHLER, E., TIAN, G., BAHI-BUISSON, N., FALLET-BIANCO, C., PHAN-DINH-TUY, F., KONG, X. P., BOMONT, P., CASTELNAU-PTAKHINE, L., ODENT, S., LOGET, P., KOSSOROTOFF, M., SNOECK, I., PLESSIS, G., PARENT, P., BELDJORD, C., CARDOSO, C., REPRESA, A., FLINT, J., KEAYS, D. A., COWAN, N. J. & CHELLY, J. 2009. Mutations in the beta-tubulin gene TUBB2B result in asymmetrical polymicrogyria. *Nat Genet,* 41**,** 746-52.

JANES, P. W., SAHA, N., BARTON, W. A., KOLEV, M. V., WIMMER-KLEIKAMP, S. H., NIEVERGALL, E., BLOBEL, C. P., HIMANEN, J. P., LACKMANN, M. & NIKOLOV, D. B. 2005. Adam meets Eph: an ADAM substrate recognition module acts as a molecular switch for ephrin cleavage in trans. *Cell,* 123**,** 291-304.

JIN, L. W., MASLIAH, E., IIMOTO, D., DETERESA, R., MALLORY, M., SUNDSMO, M., MORI, N., SOBEL, A. & SAITOH, T. 1996. Neurofibrillary tangle-associated alteration of stathmin in Alzheimer's disease. *Neurobiol Aging,* 17**,** 331-41.

JONGBLOETS, B. C. & PASTERKAMP, R. J. 2014. Semaphorin signalling during development. *Development,* 141**,** 3292-7.

JURNEY, W. M., GALLO, G., LETOURNEAU, P. C. & MCLOON, S. C. 2002. Rac1-mediated endocytosis during ephrin-A2- and semaphorin 3A-induced growth cone collapse. *J Neurosci,* 22**,** 6019-28.

KAMNASARAN, D. 2005. Agenesis of the corpus callosum: lessons from humans and mice. *Clin Invest Med,* 28**,** 267-82.

KAWANO, Y., YOSHIMURA, T., TSUBOI, D., KAWABATA, S., KANEKO-KAWANO, T., SHIRATAKI, H., TAKENAWA, T. & KAIBUCHI, K. 2005. CRMP-2 is involved in kinesin-1-dependent transport of the Sra-1/WAVE1 complex and axon formation. *Mol Cell Biol,* 25**,** 9920-35.

KAYSER, M. S., LEE, A. C., HRUSKA, M. & DALVA, M. B. 2011. Preferential control of basal dendritic protrusions by EphB2. *PLoS One,* 6**,** e17417.

KHOLMANSKIKH, S. S., KOELLER, H. B., WYNSHAW-BORIS, A., GOMEZ, T., LETOURNEAU, P. C. & ROSS, M. E. 2006. Calcium-dependent interaction of Lis1 with IQGAP1 and Cdc42 promotes neuronal motility. *Nat Neurosci,* 9**,** 50-7.

KIDD, T., BLAND, K. S. & GOODMAN, C. S. 1999. Slit is the midline repellent for the robo receptor in Drosophila. *Cell,* 96**,** 785-94.

KITSUKAWA, T., SHIMIZU, M., SANBO, M., HIRATA, T., TANIGUCHI, M., BEKKU, Y., YAGI, T. & FUJISAWA, H. 1997. Neuropilin-semaphorin III/D-mediated chemorepulsive signals play a crucial role in peripheral nerve projection in mice. *Neuron,* 19**,** 995-1005.

KOLODKIN, A. L., MATTHES, D. J. & GOODMAN, C. S. 1993. The semaphorin genes encode a family of transmembrane and secreted growth cone guidance molecules. *Cell,* 75**,** 1389-99.

KOLODKIN, A. L., MATTHES, D. J., O'CONNOR, T. P., PATEL, N. H., ADMON, A., BENTLEY, D. & GOODMAN, C. S. 1992. Fasciclin IV: sequence, expression, and function during growth cone guidance in the grasshopper embryo. *Neuron,* 9**,** 831-45.

KOLODKIN, A. L. & TESSIER-LAVIGNE, M. 2011. Mechanisms and molecules of neuronal wiring: a primer. *Cold Spring Harb Perspect Biol,* 3.

KRISTOFIKOVA, Z., VRAJOVA, M., SIROVA, J., VALES, K., PETRASEK, T., SCHONIG, K., TEWS, B., SCHWAB, M., BARTSCH, D., STUCHLIK, A. & RIPOVA, D. 2013. N-Methyl-d-Aspartate Receptor - Nitric Oxide Synthase Pathway in the Cortex of Nogo-A-Deficient Rats in Relation to Brain Laterality and Schizophrenia. *Front Behav Neurosci,* 7**,** 90.

KUNDA, P., PAGLINI, G., QUIROGA, S., KOSIK, K. & CACERES, A. 2001. Evidence for the involvement of Tiam1 in axon formation. *J Neurosci,* 21**,** 2361-72.

LAI WING SUN, K., CORREIA, J. P. & KENNEDY, T. E. 2011. Netrins: versatile extracellular cues with diverse functions. *Development,* 138**,** 2153-69.

LAVIN, P. T. & MC GEE, M. M. 2015. Cyclophilin function in Cancer; lessons from virus replication. *Curr Mol Pharmacol,* 9**,** 148-64.

LETOURNEAU, P. C., SHATTUCK, T. A. & RESSLER, A. H. 1987. "Pull" and "push" in neurite elongation: observations on the effects of different concentrations of cytochalasin B and taxol. *Cell Motil Cytoskeleton,* 8**,** 193-209.

LEWIS, T. L., JR., COURCHET, J. & POLLEUX, F. 2013. Cell biology in neuroscience: Cellular and molecular mechanisms underlying axon formation, growth, and branching. *J Cell Biol,* 202**,** 837-48.

LI, Z., JAGADAPILLAI, R., GOZAL, E. & BARNES, G. 2019. Deletion of Semaphorin 3F in Interneurons Is Associated with Decreased GABAergic Neurons, Autism-like Behavior, and Increased Oxidative Stress Cascades. *Mol Neurobiol*.

LIM, B. K., MATSUDA, N. & POO, M. M. 2008. Ephrin-B reverse signaling promotes structural and functional synaptic maturation in vivo. *Nat Neurosci,* 11**,** 160-9.

LINKE, R., PABST, T. & FROTSCHER, M. 1995. Development of the hippocamposeptal projection in the rat. *J Comp Neurol,* 351**,** 602-16.

LIOU, Y. C., SUN, A., RYO, A., ZHOU, X. Z., YU, Z. X., HUANG, H. K., UCHIDA, T., BRONSON, R., BING, G., LI, X., HUNTER, T. & LU, K. P. 2003. Role of the prolyl isomerase Pin1 in protecting against age-dependent neurodegeneration. *Nature,* 424**,** 556-61.

LIU, X., MALENFANT, P., REESOR, C., LEE, A., HUDSON, M. L., HARVARD, C., QIAO, Y., PERSICO, A. M., COHEN, I. L., CHUDLEY, A. E., FORSTER-GIBSON, C., RAJCAN-SEPAROVIC, E., LEWIS, M. E. & HOLDEN, J. J. 2011. 2p15-p16.1 microdeletion syndrome: molecular characterization and association of the OTX1 and XPO1 genes with autism spectrum disorders. *Eur J Hum Genet,* 19**,** 1264-70.

LIU, X. B., LOW, L. K., JONES, E. G. & CHENG, H. J. 2005. Stereotyped axon pruning via plexin signaling is associated with synaptic complex elimination in the hippocampus. *J Neurosci,* 25**,** 9124-34.

LIU, Y., PHAM, X., ZHANG, L., CHEN, P. L., BURZYNSKI, G., MCGAUGHEY, D. M., HE, S., MCGRATH, J. A., WOLYNIEC, P., FALLIN, M. D., PIERCE, M. S., MCCALLION, A. S., PULVER, A. E., AVRAMOPOULOS, D. & VALLE, D. 2014. Functional variants in DPYSL2 sequence increase risk of schizophrenia and suggest a link to mTOR signaling. *G3 (Bethesda),* 5**,** 61-72.

LORD, C., ELSABBAGH, M., BAIRD, G. & VEENSTRA-VANDERWEELE, J. 2018. Autism spectrum disorder. *Lancet,* 392**,** 508-520.

LOW, L. K., LIU, X. B., FAULKNER, R. L., COBLE, J. & CHENG, H. J. 2008. Plexin signaling selectively regulates the stereotyped pruning of corticospinal axons from visual cortex. *Proc Natl Acad Sci U S A,* 105**,** 8136-41.

LU, K. P., HANES, S. D. & HUNTER, T. 1996. A human peptidyl-prolyl isomerase essential for regulation of mitosis. *Nature,* 380**,** 544-7.

LU, K. P. & ZHOU, X. Z. 2007. The prolyl isomerase PIN1: a pivotal new twist in phosphorylation signalling and disease. *Nat Rev Mol Cell Biol,* 8**,** 904-16.

LU, P. J., WULF, G., ZHOU, X. Z., DAVIES, P. & LU, K. P. 1999. The prolyl isomerase Pin1 restores the function of Alzheimer-associated phosphorylated tau protein. *Nature,* 399**,** 784-8.

LUO, L. & O'LEARY, D. D. 2005. Axon retraction and degeneration in development and disease. *Annu Rev Neurosci,* 28**,** 127-56.

LUO, Y., RAIBLE, D. & RAPER, J. A. 1993. Collapsin: a protein in brain that induces the collapse and paralysis of neuronal growth cones. *Cell,* 75**,** 217-27.

MAGIERA, M. M., BODAKUNTLA, S., ZIAK, J., LACOMME, S., MARQUES SOUSA, P., LEBOUCHER, S., HAUSRAT, T. J., BOSC, C., ANDRIEUX, A., KNEUSSEL, M., LANDRY, M., CALAS, A., BALASTIK, M. & JANKE, C. 2018a. Excessive tubulin polyglutamylation causes neurodegeneration and perturbs neuronal transport. *EMBO J,* 37.

MAGIERA, M. M., SINGH, P., GADADHAR, S. & JANKE, C. 2018b. Tubulin Posttranslational Modifications and Emerging Links to Human Disease. *Cell,* 173**,** 1323-1327.

MAIMON, R., IONESCU, A., BONNIE, A., SWEETAT, S., WALD-ALTMAN, S., INBAR, S., GRADUS, T., TROTTI, D., WEIL, M., BEHAR, O. & PERLSON, E. 2018. miR126-5p Downregulation Facilitates Axon Degeneration and NMJ Disruption via a Non-Cell-Autonomous Mechanism in ALS. *J Neurosci,* 38**,** 5478-5494.

MAKIHARA, H., NAKAI, S., OHKUBO, W., YAMASHITA, N., NAKAMURA, F., KIYONARI, H., SHIOI, G., JITSUKI-TAKAHASHI, A., NAKAMURA, H., TANAKA, F., AKASE, T., KOLATTUKUDY, P. & GOSHIMA, Y. 2016. CRMP1 and CRMP2 have synergistic but distinct roles in dendritic development. *Genes Cells,* 21**,** 994-1005.

MANTA, B. & GLADYSHEV, V. N. 2017. Regulated methionine oxidation by monooxygenases. *Free Radic Biol Med,* 109**,** 141-155.

MCCLELLAND, A. C., HRUSKA, M., COENEN, A. J., HENKEMEYER, M. & DALVA, M. B. 2010. Trans-synaptic EphB2-ephrin-B3 interaction regulates excitatory synapse density by inhibition of postsynaptic MAPK signaling. *Proc Natl Acad Sci U S A,* 107**,** 8830-5.

MCCLELLAND, A. C., SHEFFLER-COLLINS, S. I., KAYSER, M. S. & DALVA, M. B. 2009. Ephrin-B1 and ephrin-B2 mediate EphB-dependent presynaptic development via syntenin-1. *Proc Natl Acad Sci U S A,* 106**,** 20487-92.

MOLYNEAUX, B. J., ARLOTTA, P. & MACKLIS, J. D. 2007a. Molecular development of corticospinal motor neuron circuitry. *Novartis Found Symp,* 288**,** 3-15; discussion 15-20, 96-8.

MOLYNEAUX, B. J., ARLOTTA, P., MENEZES, J. R. & MACKLIS, J. D. 2007b. Neuronal subtype specification in the cerebral cortex. *Nat Rev Neurosci,* 8**,** 427-37.

MOON, H. M. & WYNSHAW-BORIS, A. 2013. Cytoskeleton in action: lissencephaly, a neuronal migration disorder. *Wiley Interdiscip Rev Dev Biol,* 2**,** 229-45.

MORINAKA, A., YAMADA, M., ITOFUSA, R., FUNATO, Y., YOSHIMURA, Y., NAKAMURA, F., YOSHIMURA, T., KAIBUCHI, K., GOSHIMA, Y., HOSHINO, M., KAMIGUCHI, H. & MIKI, H. 2011. Thioredoxin mediates oxidation-dependent phosphorylation of CRMP2 and growth cone collapse. *Sci Signal,* 4**,** ra26.

MORITA, A., YAMASHITA, N., SASAKI, Y., UCHIDA, Y., NAKAJIMA, O., NAKAMURA, F., YAGI, T., TANIGUCHI, M., USUI, H., KATOH-SEMBA, R., TAKEI, K. & GOSHIMA, Y. 2006. Regulation of dendritic branching and spine maturation by semaphorin3A-Fyn signaling. *J Neurosci,* 26**,** 2971-80.

MOUTAL, A., WHITE, K. A., CHEFDEVILLE, A., LAUFMANN, R. N., VITIELLO, P. F., FEINSTEIN, D., WEIMER, J. M. & KHANNA, R. 2019. Dysregulation of CRMP2 Post-Translational Modifications Drive Its Pathological Functions. *Mol Neurobiol,* 56**,** 6736-6755.

MURAI, K. K., NGUYEN, L. N., IRIE, F., YAMAGUCHI, Y. & PASQUALE, E. B. 2003. Control of hippocampal dendritic spine morphology through ephrin-A3/EphA4 signaling. *Nat Neurosci,* 6**,** 153-60.

MYAT, A., HENRY, P., MCCABE, V., FLINTOFT, L., ROTIN, D. & TEAR, G. 2002. Drosophila Nedd4, a ubiquitin ligase, is recruited by Commissureless to control cell surface levels of the roundabout receptor. *Neuron,* 35**,** 447-59.

NAKAMURA, H., YAMASHITA, N., KIMURA, A., KIMURA, Y., HIRANO, H., MAKIHARA, H., KAWAMOTO, Y., JITSUKI-TAKAHASHI, A., YONEZAKI, K., TAKASE, K., MIYAZAKI, T., NAKAMURA, F., TANAKA, F. & GOSHIMA, Y. 2016. Comprehensive behavioral study and proteomic analyses of CRMP2-deficient mice. *Genes Cells,* 21**,** 1059-1079.

NAKAMUTA, S., FUNAHASHI, Y., NAMBA, T., ARIMURA, N., PICCIOTTO, M. R., TOKUMITSU, H., SODERLING, T. R., SAKAKIBARA, A., MIYATA, T., KAMIGUCHI, H. & KAIBUCHI, K. 2011. Local application of neurotrophins specifies axons through inositol 1,4,5-trisphosphate, calcium, and Ca2+/calmodulin-dependent protein kinases. *Sci Signal,* 4**,** ra76.

NAKATA, K., UJIKE, H., SAKAI, A., TAKAKI, M., IMAMURA, T., TANAKA, Y. & KURODA, S. 2003. The human dihydropyrimidinase-related protein 2 gene on chromosome 8p21 is associated with paranoid-type schizophrenia. *Biol Psychiatry,* 53**,** 571-6.

NAMBA, T., FUNAHASHI, Y., NAKAMUTA, S., XU, C., TAKANO, T. & KAIBUCHI, K. 2015. Extracellular and Intracellular Signaling for Neuronal Polarity. *Physiol Rev,* 95**,** 995-1024.

NAMBA, T., NAKAMUTA, S., FUNAHASHI, Y. & KAIBUCHI, K. 2011. The role of selective transport in neuronal polarization. *Dev Neurobiol,* 71**,** 445-57.

NIISATO, E., NAGAI, J., YAMASHITA, N., ABE, T., KIYONARI, H., GOSHIMA, Y. & OHSHIMA, T. 2012. CRMP4 suppresses apical dendrite bifurcation of CA1 pyramidal neurons in the mouse hippocampus. *Dev Neurobiol,* 72**,** 1447-57.

NIISATO, E., NAGAI, J., YAMASHITA, N., NAKAMURA, F., GOSHIMA, Y. & OHSHIMA, T. 2013. Phosphorylation of CRMP2 is involved in proper bifurcation of the apical dendrite of hippocampal CA1 pyramidal neurons. *Dev Neurobiol,* 73**,** 142-51.

NISHIKIMI, M., OISHI, K. & NAKAJIMA, K. 2013. Axon guidance mechanisms for establishment of callosal connections. *Neural Plast,* 2013**,** 149060.

NISHIMURA, T., FUKATA, Y., KATO, K., YAMAGUCHI, T., MATSUURA, Y., KAMIGUCHI, H. & KAIBUCHI, K. 2003. CRMP-2 regulates polarized Numb-mediated endocytosis for axon growth. *Nat Cell Biol,* 5**,** 819-26.

NISHIMURA, T., YAMAGUCHI, T., KATO, K., YOSHIZAWA, M., NABESHIMA, Y., OHNO, S., HOSHINO, M. & KAIBUCHI, K. 2005. PAR-6-PAR-3 mediates Cdc42-induced Rac activation through the Rac GEFs STEF/Tiam1. *Nat Cell Biol,* 7**,** 270-7.

NIWA, S., NAKAMURA, F., TOMABECHI, Y., AOKI, M., SHIGEMATSU, H., MATSUMOTO, T., YAMAGATA, A., FUKAI, S., HIROKAWA, N., GOSHIMA, Y., SHIROUZU, M. & NITTA, R. 2017. Structural basis for CRMP2-induced axonal microtubule formation. *Sci Rep,* 7**,** 10681.

NOGI, T., YASUI, N., MIHARA, E., MATSUNAGA, Y., NODA, M., YAMASHITA, N., TOYOFUKU, T., UCHIYAMA, S., GOSHIMA, Y., KUMANOGOH, A. & TAKAGI, J. 2010. Structural basis for semaphorin signalling through the plexin receptor. *Nature,* 467**,** 1123-7.

OHSHIMA, T., HIRASAWA, M., TABATA, H., MUTOH, T., ADACHI, T., SUZUKI, H., SARUTA, K., IWASATO, T., ITOHARA, S., HASHIMOTO, M., NAKAJIMA, K., OGAWA, M., KULKARNI, A. B. & MIKOSHIBA, K. 2007. Cdk5 is required for multipolar-to-bipolar transition during radial neuronal migration and proper dendrite development of pyramidal neurons in the cerebral cortex. *Development,* 134**,** 2273-82.

PAN, D. & RUBIN, G. M. 1997. Kuzbanian controls proteolytic processing of Notch and mediates lateral inhibition during Drosophila and vertebrate neurogenesis. *Cell,* 90**,** 271-80.

PASCUAL, M., POZAS, E., BARALLOBRE, M. J., TESSIER-LAVIGNE, M. & SORIANO, E. 2004. Coordinated functions of Netrin-1 and Class 3 secreted Semaphorins in the guidance of reciprocal septohippocampal connections. *Mol Cell Neurosci,* 26**,** 24-33.

PASQUALE, E. B. 2008. Eph-ephrin bidirectional signaling in physiology and disease. *Cell,* 133**,** 38-52.

PASTERKAMP, R. J. 2012. Getting neural circuits into shape with semaphorins. *Nat Rev Neurosci,* 13**,** 605-18.

PASTERKAMP, R. J., PESCHON, J. J., SPRIGGS, M. K. & KOLODKIN, A. L. 2003. Semaphorin 7A promotes axon outgrowth through integrins and MAPKs. *Nature,* 424**,** 398-405.

PASTORINO, L., SUN, A., LU, P. J., ZHOU, X. Z., BALASTIK, M., FINN, G., WULF, G., LIM, J., LI, S. H., LI, X., XIA, W., NICHOLSON, L. K. & LU, K. P. 2006. The prolyl isomerase Pin1 regulates amyloid precursor protein processing and amyloid-beta production. *Nature,* 440**,** 528-34.

PENZES, P., CAHILL, M. E., JONES, K. A., VANLEEUWEN, J. E. & WOOLFREY, K. M. 2011. Dendritic spine pathology in neuropsychiatric disorders. *Nat Neurosci,* 14**,** 285-93.

PETANJEK, Z., JUDAS, M., SIMIC, G., RASIN, M. R., UYLINGS, H. B., RAKIC, P. & KOSTOVIC, I. 2011. Extraordinary neoteny of synaptic spines in the human prefrontal cortex. *Proc Natl Acad Sci U S A,* 108**,** 13281-6.

PETRATOS, S., OZTURK, E., AZARI, M. F., KENNY, R., LEE, J. Y., MAGEE, K. A., HARVEY, A. R., MCDONALD, C., TAGHIAN, K., MOUSSA, L., MUN AUI, P., SIATSKAS, C., LITWAK, S., FEHLINGS, M. G., STRITTMATTER, S. M. & BERNARD, C. C. 2012. Limiting multiple sclerosis related axonopathy by blocking Nogo receptor and CRMP-2 phosphorylation. *Brain,* 135**,** 1794-818.

PIPER, M., SALIH, S., WEINL, C., HOLT, C. E. & HARRIS, W. A. 2005. Endocytosis-dependent desensitization and protein synthesis-dependent resensitization in retinal growth cone adaptation. *Nat Neurosci,* 8**,** 179-86.

POLLEUX, F., WHITFORD, K. L., DIJKHUIZEN, P. A., VITALIS, T. & GHOSH, A. 2002. Control of cortical interneuron migration by neurotrophins and PI3-kinase signaling. *Development,* 129**,** 3147-60.

PORTERA-CAILLIAU, C., WEIMER, R. M., DE PAOLA, V., CARONI, P. & SVOBODA, K. 2005. Diverse modes of axon elaboration in the developing neocortex. *PLoS Biol,* 3**,** e272.

POULOPOULOS, A., MURPHY, A. J., OZKAN, A., DAVIS, P., HATCH, J., KIRCHNER, R. & MACKLIS, J. D. 2019. Subcellular transcriptomes and proteomes of developing axon projections in the cerebral cortex. *Nature,* 565**,** 356-360.

POZAS, E., PASCUAL, M., NGUYEN BA-CHARVET, K. T., GUIJARRO, P., SOTELO, C., CHEDOTAL, A., DEL RIO, J. A. & SORIANO, E. 2001. Age-dependent effects of secreted Semaphorins 3A, 3F, and 3E on developing hippocampal axons: in vitro effects and phenotype of Semaphorin 3A (-/-) mice. *Mol Cell Neurosci,* 18**,** 26-43.

QUACH, T. T., HONNORAT, J., KOLATTUKUDY, P. E., KHANNA, R. & DUCHEMIN, A. M. 2015. CRMPs: critical molecules for neurite morphogenesis and neuropsychiatric diseases. *Mol Psychiatry,* 20**,** 1037-45.

RAHAJENG, J., GIRIDHARAN, S. S., NASLAVSKY, N. & CAPLAN, S. 2010. Collapsin response mediator protein-2 (Crmp2) regulates trafficking by linking endocytic regulatory proteins to dynein motors. *J Biol Chem,* 285**,** 31918-22.

RAJASEKHARAN, S., BAKER, K. A., HORN, K. E., JARJOUR, A. A., ANTEL, J. P. & KENNEDY, T. E. 2009. Netrin 1 and Dcc regulate oligodendrocyte process branching and membrane extension via Fyn and RhoA. *Development,* 136**,** 415-26.

RAJASEKHARAN, S., BIN, J. M., ANTEL, J. P. & KENNEDY, T. E. 2010. A central role for RhoA during oligodendroglial maturation in the switch from netrin-1-mediated chemorepulsion to process elaboration. *J Neurochem,* 113**,** 1589-97.

REINER, O., CARROZZO, R., SHEN, Y., WEHNERT, M., FAUSTINELLA, F., DOBYNS, W. B., CASKEY, C. T. & LEDBETTER, D. H. 1993. Isolation of a Miller-Dieker lissencephaly gene containing G protein beta-subunit-like repeats. *Nature,* 364**,** 717-21.

REN, X. R., MING, G. L., XIE, Y., HONG, Y., SUN, D. M., ZHAO, Z. Q., FENG, Z., WANG, Q., SHIM, S., CHEN, Z. F., SONG, H. J., MEI, L. & XIONG, W. C. 2004. Focal adhesion kinase in netrin-1 signaling. *Nat Neurosci,* 7**,** 1204-12.

REYNOLDS, C. D., NOLAN, S. O., JEFFERSON, T. & LUGO, J. N. 2016. Sex-specific and genotype-specific differences in vocalization development in FMR1 knockout mice. *Neuroreport,* 27**,** 1331-1335.

RICCOMAGNO, M. M., HURTADO, A., WANG, H., MACOPSON, J. G., GRINER, E. M., BETZ, A., BROSE, N., KAZANIETZ, M. G. & KOLODKIN, A. L. 2012. The RacGAP beta2-Chimaerin selectively mediates axonal pruning in the hippocampus. *Cell,* 149**,** 1594-606.

RICCOMAGNO, M. M. & KOLODKIN, A. L. 2015. Sculpting neural circuits by axon and dendrite pruning. *Annu Rev Cell Dev Biol,* 31**,** 779-805.

RUGARLI, E. I. & BALLABIO, A. 1995. Reelin: a novel extracellular matrix protein involved in brain lamination. *Bioessays,* 17**,** 832-4.

SAHAY, A., MOLLIVER, M. E., GINTY, D. D. & KOLODKIN, A. L. 2003. Semaphorin 3F is critical for development of limbic system circuitry and is required in neurons for selective CNS axon guidance events. *J Neurosci,* 23**,** 6671-80.

SANES, J. R. & LICHTMAN, J. W. 1999. Development of the vertebrate neuromuscular junction. *Annu Rev Neurosci,* 22**,** 389-442.

SASAKI, Y., CHENG, C., UCHIDA, Y., NAKAJIMA, O., OHSHIMA, T., YAGI, T., TANIGUCHI, M., NAKAYAMA, T., KISHIDA, R., KUDO, Y., OHNO, S., NAKAMURA, F. & GOSHIMA, Y. 2002. Fyn and Cdk5 mediate semaphorin-3A signaling, which is involved in regulation of dendrite orientation in cerebral cortex. *Neuron,* 35**,** 907-20.

SEKI, M., WATANABE, A., ENOMOTO, S., KAWAMURA, T., ITO, H., KODAMA, T., HAMAKUBO, T. & ABURATANI, H. 2010. Human ROBO1 is cleaved by metalloproteinases and gamma-secretase and migrates to the nucleus in cancer cells. *FEBS Lett,* 584**,** 2909-15.

SERAFINI, T., COLAMARINO, S. A., LEONARDO, E. D., WANG, H., BEDDINGTON, R., SKARNES, W. C. & TESSIER-LAVIGNE, M. 1996. Netrin-1 is required for commissural axon guidance in the developing vertebrate nervous system. *Cell,* 87**,** 1001-14.

SERAFINI, T., KENNEDY, T. E., GALKO, M. J., MIRZAYAN, C., JESSELL, T. M. & TESSIER-LAVIGNE, M. 1994. The netrins define a family of axon outgrowth-promoting proteins homologous to C. elegans UNC-6. *Cell,* 78**,** 409-24.

SHERAZEE, N. & ALVAREZ, V. A. 2013. DiOlistics: delivery of fluorescent dyes into cells. *Methods Mol Biol,* 940**,** 391-400.

SHU, T., AYALA, R., NGUYEN, M. D., XIE, Z., GLEESON, J. G. & TSAI, L. H. 2004. Ndel1 operates in a common pathway with LIS1 and cytoplasmic dynein to regulate cortical neuronal positioning. *Neuron,* 44**,** 263-77.

SCHMEISSER, M. J., EY, E., WEGENER, S., BOCKMANN, J., STEMPEL, A. V., KUEBLER, A., JANSSEN, A. L., UDVARDI, P. T., SHIBAN, E., SPILKER, C., BALSCHUN, D., SKRYABIN, B. V., DIECK, S., SMALLA, K. H., MONTAG, D., LEBLOND, C. S., FAURE, P., TORQUET, N., LE SOURD, A. M., TORO, R., GRABRUCKER, A. M., SHOICHET, S. A., SCHMITZ, D., KREUTZ, M. R., BOURGERON, T., GUNDELFINGER, E. D. & BOECKERS, T. M. 2012. Autistic-like behaviours and hyperactivity in mice lacking ProSAP1/Shank2. *Nature,* 486**,** 256-60.

SCHWARTING, G. A., KOSTEK, C., AHMAD, N., DIBBLE, C., PAYS, L. & PUSCHEL, A. W. 2000. Semaphorin 3A is required for guidance of olfactory axons in mice. *J Neurosci,* 20**,** 7691-7.

SCHWARZ, Q., WAIMEY, K. E., GOLDING, M., TAKAMATSU, H., KUMANOGOH, A., FUJISAWA, H., CHENG, H. J. & RUHRBERG, C. 2008. Plexin A3 and plexin A4 convey semaphorin signals during facial nerve development. *Dev Biol,* 324**,** 1-9.

SONG, A. H., WANG, D., CHEN, G., LI, Y., LUO, J., DUAN, S. & POO, M. M. 2009. A selective filter for cytoplasmic transport at the axon initial segment. *Cell,* 136**,** 1148-60.

SOSA, L. J., MALTER, J. S., HU, J., BUSTOS PLONKA, F., OKSDATH, M., NIETO GUIL, A. F., QUIROGA, S. & PFENNINGER, K. H. 2016. Protein interacting with NIMA (never in mitosis A)-1 regulates axonal growth cone adhesion and spreading through myristoylated alanine-rich C kinase substrate isomerization. *J Neurochem,* 137**,** 744-55.

SPERRY, R. W. 1963. Chemoaffinity in the Orderly Growth of Nerve Fiber Patterns and Connections. *Proc Natl Acad Sci U S A,* 50**,** 703-10.

STANCO, A., SZEKERES, C., PATEL, N., RAO, S., CAMPBELL, K., KREIDBERG, J. A., POLLEUX, F. & ANTON, E. S. 2009. Netrin-1-alpha3beta1 integrin interactions regulate the migration of interneurons through the cortical marginal zone. *Proc Natl Acad Sci U S A,* 106**,** 7595-600.

SU, K. Y., CHIEN, W. L., FU, W. M., YU, I. S., HUANG, H. P., HUANG, P. H., LIN, S. R., SHIH, J. Y., LIN, Y. L., HSUEH, Y. P., YANG, P. C. & LIN, S. W. 2007. Mice deficient in collapsin response mediator protein-1 exhibit impaired long-term potentiation and impaired spatial learning and memory. *J Neurosci,* 27**,** 2513-24.

SUMI, T., IMASAKI, T., AOKI, M., SAKAI, N., NITTA, E., SHIROUZU, M. & NITTA, R. 2018. Structural Insights into the Altering Function of CRMP2 by Phosphorylation. *Cell Struct Funct,* 43**,** 15-23.

SUTER, D. M. & MILLER, K. E. 2011. The emerging role of forces in axonal elongation. *Prog Neurobiol,* 94**,** 91-101.

TAKAHASHI, T., NAKAMURA, F., JIN, Z., KALB, R. G. & STRITTMATTER, S. M. 1998. Semaphorins A and E act as antagonists of neuropilin-1 and agonists of neuropilin-2 receptors. *Nat Neurosci,* 1**,** 487-93.

TAKANO, T., XU, C., FUNAHASHI, Y., NAMBA, T. & KAIBUCHI, K. 2015. Neuronal polarization. *Development,* 142**,** 2088-93.

TAKEI, Y., TENG, J., HARADA, A. & HIROKAWA, N. 2000. Defects in axonal elongation and neuronal migration in mice with disrupted tau and map1b genes. *J Cell Biol,* 150**,** 989-1000.

TANG, G., GUDSNUK, K., KUO, S. H., COTRINA, M. L., ROSOKLIJA, G., SOSUNOV, A., SONDERS, M. S., KANTER, E., CASTAGNA, C., YAMAMOTO, A., YUE, Z., ARANCIO, O., PETERSON, B. S., CHAMPAGNE, F., DWORK, A. J., GOLDMAN, J. & SULZER, D. 2014. Loss of mTOR-dependent macroautophagy causes autistic-like synaptic pruning deficits. *Neuron,* 83**,** 1131-43.

TANIGUCHI, M., YUASA, S., FUJISAWA, H., NARUSE, I., SAGA, S., MISHINA, M. & YAGI, T. 1997. Disruption of semaphorin III/D gene causes severe abnormality in peripheral nerve projection. *Neuron,* 19**,** 519-30.

TAPIA, J. C., WYLIE, J. D., KASTHURI, N., HAYWORTH, K. J., SCHALEK, R., BERGER, D. R., GUATIMOSIM, C., SEUNG, H. S. & LICHTMAN, J. W. 2012. Pervasive synaptic branch removal in the mammalian neuromuscular system at birth. *Neuron,* 74**,** 816-29.

TERMAN, J. R., MAO, T., PASTERKAMP, R. J., YU, H. H. & KOLODKIN, A. L. 2002. MICALs, a family of conserved flavoprotein oxidoreductases, function in plexin-mediated axonal repulsion. *Cell,* 109**,** 887-900.

TESSIER-LAVIGNE, M. & GOODMAN, C. S. 1996. The molecular biology of axon guidance. *Science,* 274**,** 1123-33.

TOBE, B. T. D., CRAIN, A. M., WINQUIST, A. M., CALABRESE, B., MAKIHARA, H., ZHAO, W. N., LALONDE, J., NAKAMURA, H., KONOPASKE, G., SIDOR, M., PERNIA, C. D., YAMASHITA, N., WADA, M., INOUE, Y., NAKAMURA, F., SHERIDAN, S. D., LOGAN, R. W., BRANDEL, M., WU, D., HUNSBERGER, J., DORSETT, L., DUERR, C., BASA, R. C. B., MCCARTHY, M. J., UDESHI, N. D., MERTINS, P., CARR, S. A., ROULEAU, G. A., MASTRANGELO, L., LI, J., GUTIERREZ, G. J., BRILL, L. M., VENIZELOS, N., CHEN, G., NYE, J. S., MANJI, H., PRICE, J. H., MCCLUNG, C. A., AKISKAL, H. S., ALDA, M., CHUANG, D. M., COYLE, J. T., LIU, Y., TENG, Y. D., OHSHIMA, T., MIKOSHIBA, K., SIDMAN, R. L., HALPAIN, S., HAGGARTY, S. J., GOSHIMA, Y. & SNYDER, E. Y. 2017. Probing the lithium-response pathway in hiPSCs implicates the phosphoregulatory set-point for a cytoskeletal modulator in bipolar pathogenesis. *Proc Natl Acad Sci U S A,* 114**,** E4462-E4471.

TONG, M. & JIANG, Y. 2015. FK506-Binding Proteins and Their Diverse Functions. *Curr Mol Pharmacol,* 9**,** 48-65.

TRAN, T. S., RUBIO, M. E., CLEM, R. L., JOHNSON, D., CASE, L., TESSIER-LAVIGNE, M., HUGANIR, R. L., GINTY, D. D. & KOLODKIN, A. L. 2009. Secreted semaphorins control spine distribution and morphogenesis in the postnatal CNS. *Nature,* 462**,** 1065-9.

TSAI, L. H., DELALLE, I., CAVINESS, V. S., JR., CHAE, T. & HARLOW, E. 1994. p35 is a neural-specific regulatory subunit of cyclin-dependent kinase 5. *Nature,* 371**,** 419-23.

TSAI, L. H. & GLEESON, J. G. 2005. Nucleokinesis in neuronal migration. *Neuron,* 46**,** 383-8.

UESAKA, N., UCHIGASHIMA, M., MIKUNI, T., NAKAZAWA, T., NAKAO, H., HIRAI, H., AIBA, A., WATANABE, M. & KANO, M. 2014. Retrograde semaphorin signaling regulates synapse elimination in the developing mouse brain. *Science,* 344**,** 1020-3.

UCHIDA, Y., OHSHIMA, T., SASAKI, Y., SUZUKI, H., YANAI, S., YAMASHITA, N., NAKAMURA, F., TAKEI, K., IHARA, Y., MIKOSHIBA, K., KOLATTUKUDY, P., HONNORAT, J. & GOSHIMA, Y. 2005. Semaphorin3A signalling is mediated via sequential Cdk5 and GSK3beta phosphorylation of CRMP2: implication of common phosphorylating mechanism underlying axon guidance and Alzheimer's disease. *Genes Cells,* 10**,** 165-79.

VAN BATTUM, E. Y., GUNPUT, R. A., LEMSTRA, S., GROEN, E. J., YU, K. L., ADOLFS, Y., ZHOU, Y., HOOGENRAAD, C. C., YOSHIDA, Y., SCHACHNER, M., AKHMANOVA, A. & PASTERKAMP, R. J. 2014. The intracellular redox protein MICAL-1 regulates the development of hippocampal mossy fibre connections. *Nat Commun,* 5**,** 4317.

VANDERHAEGHEN, P. & CHENG, H. J. 2010. Guidance molecules in axon pruning and cell death. *Cold Spring Harb Perspect Biol,* 2**,** a001859.

VARGHESE, M., KESHAV, N., JACOT-DESCOMBES, S., WARDA, T., WICINSKI, B., DICKSTEIN, D. L., HARONY-NICOLAS, H., DE RUBEIS, S., DRAPEAU, E., BUXBAUM, J. D. & HOF, P. R. 2017. Autism spectrum disorder: neuropathology and animal models. *Acta Neuropathol,* 134**,** 537-566.

VENKOVA, K., CHRISTOV, A., KAMALUDDIN, Z., KOBALKA, P., SIDDIQUI, S. & HENSLEY, K. 2014. Semaphorin 3A signaling through neuropilin-1 is an early trigger for distal axonopathy in the SOD1G93A mouse model of amyotrophic lateral sclerosis. *J Neuropathol Exp Neurol,* 73**,** 702-13.

WAHL, S., BARTH, H., CIOSSEK, T., AKTORIES, K. & MUELLER, B. K. 2000. Ephrin-A5 induces collapse of growth cones by activating Rho and Rho kinase. *J Cell Biol,* 149**,** 263-70.

WANG, C. L., ZHANG, L., ZHOU, Y., ZHOU, J., YANG, X. J., DUAN, S. M., XIONG, Z. Q. & DING, Y. Q. 2007. Activity-dependent development of callosal projections in the somatosensory cortex. *J Neurosci,* 27**,** 11334-42.

WEIMANN, J. M., ZHANG, Y. A., LEVIN, M. E., DEVINE, W. P., BRULET, P. & MCCONNELL, S. K. 1999. Cortical neurons require Otx1 for the refinement of exuberant axonal projections to subcortical targets. *Neuron,* 24**,** 819-31.

WHITFORD, K. L., DIJKHUIZEN, P., POLLEUX, F. & GHOSH, A. 2002. Molecular control of cortical dendrite development. *Annu Rev Neurosci,* 25**,** 127-49.

WRIGHT, K. M., LYON, K. A., LEUNG, H., LEAHY, D. J., MA, L. & GINTY, D. D. 2012. Dystroglycan organizes axon guidance cue localization and axonal pathfinding. *Neuron,* 76**,** 931-44.

WU, K. Y., HE, M., HOU, Q. Q., SHENG, A. L., YUAN, L., LIU, F., LIU, W. W., LI, G., JIANG, X. Y. & LUO, Z. G. 2014. Semaphorin 3A activates the guanosine triphosphatase Rab5 to promote growth cone collapse and organize callosal axon projections. *Sci Signal,* 7**,** ra81.

WU, K. Y., HENGST, U., COX, L. J., MACOSKO, E. Z., JEROMIN, A., URQUHART, E. R. & JAFFREY, S. R. 2005. Local translation of RhoA regulates growth cone collapse. *Nature,* 436**,** 1020-1024.

XU, N. J. & HENKEMEYER, M. 2009. Ephrin-B3 reverse signaling through Grb4 and cytoskeletal regulators mediates axon pruning. *Nat Neurosci,* 12**,** 268-76.

YAMANE, M., YAMASHITA, N., HIDA, T., KAMIYA, Y., NAKAMURA, F., KOLATTUKUDY, P. & GOSHIMA, Y. 2017. A functional coupling between CRMP1 and Nav1.7 for retrograde propagation of Semaphorin3A signaling. *J Cell Sci,* 130**,** 1393-1403.

YAMASHITA, N. & GOSHIMA, Y. 2012. Collapsin response mediator proteins regulate neuronal development and plasticity by switching their phosphorylation status. *Mol Neurobiol,* 45**,** 234-46.

YAMASHITA, N., MORITA, A., UCHIDA, Y., NAKAMURA, F., USUI, H., OHSHIMA, T., TANIGUCHI, M., HONNORAT, J., THOMASSET, N., TAKEI, K., TAKAHASHI, T., KOLATTUKUDY, P. & GOSHIMA, Y. 2007. Regulation of spine development by semaphorin3A through cyclin-dependent kinase 5 phosphorylation of collapsin response mediator protein 1. *J Neurosci,* 27**,** 12546-54.

YAMASHITA, N., UCHIDA, Y., OHSHIMA, T., HIRAI, S., NAKAMURA, F., TANIGUCHI, M., MIKOSHIBA, K., HONNORAT, J., KOLATTUKUDY, P., THOMASSET, N., TAKEI, K., TAKAHASHI, T. & GOSHIMA, Y. 2006. Collapsin response mediator protein 1 mediates reelin signaling in cortical neuronal migration. *J Neurosci,* 26**,** 13357-62.

YE, T., IP, J. P., FU, A. K. & IP, N. Y. 2014. Cdk5-mediated phosphorylation of RapGEF2 controls neuronal migration in the developing cerebral cortex. *Nat Commun,* 5**,** 4826.

YI, J. J., BARNES, A. P., HAND, R., POLLEUX, F. & EHLERS, M. D. 2010. TGF-beta signaling specifies axons during brain development. *Cell,* 142**,** 144-57.

YOSHIMURA, T., KAWANO, Y., ARIMURA, N., KAWABATA, S., KIKUCHI, A. & KAIBUCHI, K. 2005. GSK-3beta regulates phosphorylation of CRMP-2 and neuronal polarity. *Cell,* 120**,** 137-49.

YU, F. & SCHULDINER, O. 2014. Axon and dendrite pruning in Drosophila. *Curr Opin Neurobiol,* 27**,** 192-8.

YU, W., QIANG, L., SOLOWSKA, J. M., KARABAY, A., KORULU, S. & BAAS, P. W. 2008. The microtubule-severing proteins spastin and katanin participate differently in the formation of axonal branches. *Mol Biol Cell,* 19**,** 1485-98.

YUASA-KAWADA, J., SUZUKI, R., KANO, F., OHKAWARA, T., MURATA, M. & NODA, M. 2003. Axonal morphogenesis controlled by antagonistic roles of two CRMP subtypes in microtubule organization. *Eur J Neurosci,* 17**,** 2329-43.

ZHANG, H., KANG, E., WANG, Y., YANG, C., YU, H., WANG, Q., CHEN, Z., ZHANG, C., CHRISTIAN, K. M., SONG, H., MING, G. L. & XU, Z. 2016. Brain-specific Crmp2 deletion leads to neuronal development deficits and behavioural impairments in mice. *Nat Commun,* 7.

ZHOU, F. Q., ZHOU, J., DEDHAR, S., WU, Y. H. & SNIDER, W. D. 2004. NGF-induced axon growth is mediated by localized inactivation of GSK-3beta and functions of the microtubule plus end binding protein APC. *Neuron,* 42**,** 897-912.

ZHOU, J., WEN, Y., SHE, L., SUI, Y. N., LIU, L., RICHARDS, L. J. & POO, M. M. 2013. Axon position within the corpus callosum determines contralateral cortical projection. *Proc Natl Acad Sci U S A,* 110**,** E2714-23.

ZIAK, J., WEISSOVA, R., JERABKOVA, K., JANIKOVA, M., MAIMON, R., PETRASEK, T., PUKAJOVA, B., KLEISNEROVA, M., WANG, M., BRILL, M. S., KASPAREK, P., ZHOU, X., ALVAREZ-BOLADO, G., SEDLACEK, R., MISGELD, T., STUCHLIK, A., PERLSON, E. & BALASTIK, M. 2020. CRMP2 mediates Sema3F-dependent axon pruning and dendritic spine remodeling. *EMBO Rep***,** e48512.

8. Supplement

Original papers related to the PhD thesis work:

Jakub Ziak, Romana Weissova, Kateřina Jeřábková, Martina Janikova, Roy Maimon, Tomas Petrasek, Barbora Pukajova, Mengzhe Wang, Monika S. Brill, Marie Kleisnerova, Petr Kasparek, Xunlei Zhou, Gonzalo Alvarez-Bolado, Radislav Sedlacek, Thomas Misgeld, Ales Stuchlik, Eran Perlson, Martin Balastik. *CRMP2 mediates Sema3F-dependent axon pruning and dendritic spine remodeling.* **EMBO R.**, 2020 Jan 9:e48512. doi: 10.15252/embr.201948512.

The paper is available in the supplement of the print version of the thesis (p. 105). The paper is also available online: https://www.embopress.org/doi/10.15252/embr.201948512

Balastik M, Zhou XZ, Alberich-Jorda M, Weissova R, **Žiak J**, Pazyra-Murphy MF, Cosker KE, Machonova O, Kozmikova I, Chen CH, Pastorino L, Asara JM, Cole A, Sutherland C, Segal RA, Lu KP. *Prolyl Isomerase Pin1 Regulates Axon Guidance by Stabilizing CRMP2A Selectively in Distal Axons.* **Cell Rep.** 2015 Oct 27;13(4):812-828.

The paper is available in the supplement of the print version of the thesis (p. 128). Free version of this paper is also available online:
https://www.cell.com/cell-reports/fulltext/S2211-1247(15)01037-2?innerTabgraphical_S2211124715010372=

Videos related to figures 4, 14 and 20, together with video legends, are available in the online version of the thesis.

Original papers unrelated to the thesis and CV are present in the thesis annotation.

Paper 1: *CRMP2 mediates Sema3F-dependent axon pruning and dendritic spine remodeling.*

In this paper, we generated *crmp2*$^{-/-}$ mice and demonstrated that CRMP2 is involved in both Sema3A and Sema3F signaling pathways and mediates pruning of axons and dendritic spines. We found that CRMP2 has a moderate effect on Sema3A-dependent axon guidance *in vivo*, and its deficiency leads to a mild defect in axon guidance in peripheral nerves and corpus callosum. We also showed that *crmp2*$^{-/-}$ mice display prominent defects in stereotyped axon pruning in hippocampus and visual cortex and altered dendritic spine remodeling, which are consistent with impaired Sema3F signaling and with models of autism spectrum disorder (ASD). Indeed, we demonstrated that CRMP2 mediates Sema3F signaling in primary neurons and that *crmp2*$^{-/-}$ mice display ASD-related social behavior changes in early postnatal period as well as in adults. Together, we uncovered Sema3F – CRMP2 axis that is important for synapse pruning and confirmed that its dysfunction shares histological and behavioral features of ASD.

I contributed to all experiments in this paper, except for the generation of the knockout mice, which was done before I joined the laboratory. I performed the immunohistochemistry, gene gun, axon/dendritic spine tracing and the *in utero* electroporation experiments, as well as the analysis of all data, I prepared the figures and contributed on the writing of the manuscript. I also developed an *in vitro* assay for studying axon and dendritic spine retraction. Finally, I was responsible for related mouse colonies. Behavior of mice was tested in collaboration with Dpt. Of Neurophysiology of the Memory (Institute of Physiology) and I contributed to data analysis. Pruning of NMJs was analyzed in colaboration with the laboratory of prof. T. Misgeld in Munich (Institute of Neuronal Cell Biology) and I participated on the sample preparation.

Article

TRANSPARENT PROCESS

EMBO reports

CRMP2 mediates Sema3F-dependent axon pruning and dendritic spine remodeling

Jakub Ziak[1,2], Romana Weissova[1,2,†], Kateřina Jeřábková[3,†], Martina Janikova[4], Roy Maimon[5], Tomas Petrasek[4], Barbora Pukajova[1,2], Marie Kleisnerova[1], Mengzhe Wang[6], Monika S Brill[6], Petr Kasparek[3], Xunlei Zhou[7], Gonzalo Alvarez-Bolado[7], Radislav Sedlacek[3], Thomas Misgeld[6,8], Ales Stuchlik[4], Eran Perlson[5] & Martin Balastik[1,*]

Abstract

Regulation of axon guidance and pruning of inappropriate synapses by class 3 semaphorins are key to the development of neural circuits. Collapsin response mediator protein 2 (CRMP2) has been shown to regulate axon guidance by mediating semaphorin 3A (Sema3A) signaling; however, nothing is known about its role in synapse pruning. Here, using newly generated *crmp2*$^{-/-}$ mice we demonstrate that CRMP2 has a moderate effect on Sema3A-dependent axon guidance *in vivo*, and its deficiency leads to a mild defect in axon guidance in peripheral nerves and the corpus callosum. Surprisingly, *crmp2*$^{-/-}$ mice display prominent defects in stereotyped axon pruning in hippocampus and visual cortex and altered dendritic spine remodeling, which is consistent with impaired Sema3F signaling and with models of autism spectrum disorder (ASD). We demonstrate that CRMP2 mediates Sema3F signaling in primary neurons and that *crmp2*$^{-/-}$ mice display ASD-related social behavior changes in the early postnatal period as well as in adults. Together, we demonstrate that CRMP2 mediates Sema3F-dependent synapse pruning and its dysfunction shares histological and behavioral features of ASD.

Keywords axon guidance; collapsin response mediator protein 2; dendritic spines; semaphorins; synapse pruning

Subject Categories Cell Adhesion, Polarity & Cytoskeleton; Neuroscience

DOI 10.15252/embr.201948512 | Received 17 May 2019 | Revised 11 December 2019 | Accepted 12 December 2019

EMBO Reports (2020) e48512

Introduction

The pattern of axonal connections is established during pre- and postnatal development by a cascade of multiple events. In embryogenesis, axonal growth cones are guided to their targets and multiple axon branches are formed. Since both correct and incorrect projections are formed, the embryonic brain connectome is only transient and the inaccurate connections are eliminated (pruned) in the early postnatal development [1]. Defects in development and maturation of brain circuits have been linked to several neurodevelopmental disorders including autism spectrum disorder (ASD), schizophrenia, or epilepsy [2–4].

Generally, two types of pruning are recognized: (i) small-scale axon pruning, regulated by neural activity or trophic support and (ii) large-scale stereotyped axon pruning, which is genetically predetermined [1,3]. Stereotyped pruning can be further histologically divided into degeneration-like [5] and retraction-like [6], which has been linked to secreted semaphorins and their coreceptors, e.g., plexin-A4 and plexin-A3 [6,7]. Intracellular mediators that transmit signals from plexins in axon pruning are not completely understood. One of the key molecule downstream of semaphorin 3A (Sema3A) signaling that directly interacts with cytoskeleton components is collapsin response mediator protein 2 (CRMP2) [8–10]. In its non-phosphorylated state, CRMP2 binds to tubulin dimers and promotes their polymerization [11]. However, upon phosphorylation, it dissociates from microtubules promoting growth cone collapse [12]. Two splice variants of Crmp2 have been found that differ at the N-terminus—CRMP2A and CRMP2B [13,14]. CRMP2B is phosphorylated by cyclin-dependent kinase 5 (CDK5) at Ser522, by GSK-3β at Thr509, Thr514, and Ser518, and by Rho kinase at Thr555 [12,15,16]. We have recently shown that CRMP2A is phosphorylated at N-terminal Ser27 by Cdk5,

1 Department of Molecular Neurobiology, Institute of Physiology of the Czech Academy of Sciences, Prague, Czech Republic
2 Faculty of Science, Charles University in Prague, Prague, Czech Republic
3 Department of Transgenic Models of Diseases and Czech Centre for Phenogenomics, Institute of Molecular Genetics of the Czech Academy of Sciences, Prague, Czech Republic
4 Department of Neurophysiology of the Memory, Institute of Physiology of the Czech Academy of Sciences, Prague, Czech Republic
5 Department of Physiology and Pharmacology, Sackler Faculty of Medicine, Tel-Aviv University, Tel-Aviv, Israel
6 Institute of Neuronal Cell Biology, Technical University Munich, Munich, Germany
7 Institute of Anatomy and Cell Biology, Heidelberg University, Heidelberg, Germany
8 German Center for Neurodegenerative Diseases and Munich Cluster for Systems Neurology, Munich, Germany
*Corresponding author. Tel: +420 241 062 822; E-mail: martin.balastik@fgu.cas.cz
†These authors contributed equally to this work

which promotes its interaction and stabilization by prolyl isomerase Pin1 [14]. Recently, CRMP2 deficiency in conditional knockout mice has been linked to schizophrenia due to changes in dendritic morphology (decreased spine number in CA1 neurons and layer 5 cortical neurons), behavioral changes (hyperactivity and social behavior impairment), and prepulse inhibition (PPI) deficit [17,18]. In addition to schizophrenia, deregulation of CRMP2 has been in humans associated with autism spectrum disorder (ASD), mood disorders, epilepsy, or Alzheimer's disease [19–24], (*SFARI* Gene database). Among these, ASD and schizophrenia are of special interest since their symptomatic proximity but distinct pathogenesis. The exact role of CRMP2 in the development of these conditions has so far been elusive. Although schizophrenia and ASD share some behavioral characteristics (e.g., decreased cognitive functions, impaired social skills, repetitive behavior), they differ in the timing of their onset (early childhood for ASD, late adolescence for schizophrenia) [25] and the nature of the underlying neuronal connectivity disorder. Whereas hypoconnectivity (lower number of dendrites, dendritic spines, general decrease of white matter) is often present in schizophrenia, ASD has been associated with local hyperconnectivity caused by either increased synapse formation or their incomplete pruning [26]. Because CRMP2 is downstream of semaphorin signaling, which controls axonal pruning [6], and it has been linked to both schizophrenia and ASD, it is one of the prime candidates to regulate this process. However, the *in vivo* analysis of both conditional and full CRMP2 knockout mice has to date mainly focused on the dendritic phenotype and associated behavioral aspects. In addition, the role of CRMP2 in class 3 semaphorin signaling (other than Sema3A), which has been previously linked to defects in pruning and ASD (particularly Sema3F), is so far not known.

In order to characterize the function of CRMP2 in axon growth, guidance, and pruning and its role in class 3 semaphorin signaling *in vivo*, we generated CRMP2 full knockout mice ($crmp2^{-/-}$). We show that CRMP2 participates in regulation of axon guidance in both central and peripheral nervous systems. In peripheral nervous system, deficiency of CRMP2 leads to mild overgrowth and increased branching of ophthalmic branch of trigeminal nerve and other selected peripheral nerves. In the central nervous system, we detected defects in postnatal callosal axon growth and guidance. Both of these systems are regulated by Sema3A, which was previously shown to induce CRMP2 phosphorylation and signaling *in vitro*. Indeed, we confirm that primary motor and DRG neurons isolated from $crmp2^{-/-}$ mice have defects mediating Sema3A signaling.

Importantly, we show that CRMP2 is essential also for synaptic refinement as $crmp2^{-/-}$ mice demonstrate defective stereotyped pruning of axons arising from hippocampus and visual cortex and inadequate elimination of dendritic spines in dentate gyrus (DG). Pruning in both of these systems is dependent on Sema3F rather than Sema3A, and its defect is in accord with ASD rather than schizophrenia-like phenotype. In agreement with this hypothesis, we show that CRMP2 is essential for Sema3F-induced axon retraction and dendritic spine remodeling in primary hippocampal cultures and that $crmp2^{-/-}$ mice suffer from ultrasonic vocalizations defect in early postnatal stages as well as social behavioral changes in adults linked to ASD.

In summary, we provide evidence that in addition to its role in Sema3A-dependent axon guidance, CRMP2 is a key mediator of Sema3F-dependent axon pruning and dendritic spine remodeling. Our data highlight the importance of CRMP2 in neural circuit formation and refinement *in vivo* and demonstrate that its deficiency leads to defects in neural development associated with neurodevelopmental disorders, in particular ASD and schizophrenia.

Results

Crmp2 deficiency leads to axonal growth defects in peripheral nerves

We used TALEN (transcription activator-like effector nucleases) mutagenesis to delete the second and third exons of the *Crmp2* locus leading to a knockout of both CRMP2 protein isoforms CRMP2A and CRMP2B (Figs 1A and B, and EV1A and B). The knockout mice were viable and fertile, and the size of their brains was similar to the WT littermates (Fig EV1C). In agreement with Ref. [17], we observed ventriculomegaly in the homozygous mice (Fig EV1D and E).

CRMP2 has been shown to mediate Sema3A signaling and regulate axon guidance *in vitro* [8]. To test whether CRMP2 deficiency leads to altered axon growth also *in vivo*, we first analyzed the development of peripheral nerves in E10.5–E12.5 embryos using whole-mount immunohistochemistry (Fig EV2A) as their development is regulated by Sema3A [27–30]. We quantified changes in neuron growth by measuring the area innervated by axons from each given nerve and branching by counting of the total number of branches. The growth and branching of ophthalmic branch of the trigeminal nerve were significantly increased in $crmp2^{-/-}$ mice at E10.5–E12.5 and similarly increased was the sprouting of the lateral branches of the spinal nerves. (Axon projections from dorsal root ganglions (DRGs) to the spinal cord were not changed in $crmp2^{-/-}$ mice) (Figs 1C–E, and EV2B and C). Since CRMP2 deficiency *in vivo* led to increased, rather than reduced axon growth, our data indicate that the growth-promoting function of CRMP2 can be compensated *in vivo* at least in the tested neurons, but that its function as a mediator of repulsive axon guidance signals is unique and cannot be fully rescued by other proteins. Since the growth of both ophthalmic branch and the lateral branches of the spinal nerves is negatively regulated by Sema3A [28], our data support the function of CRMP2 as a mediator of Sema3A signaling.

To directly demonstrate that CRMP2 deficiency interferes with Sema3A signaling in peripheral neurons isolated from $crmp2^{-/-}$ mice, we took an advantage of microfluidic chamber approach for extraaxonal environment manipulation. In this chamber, cell bodies and axons are separated in proximal or distal compartment, respectively [31]. We prepared spinal cord explants from WT and $crmp2^{-/-}$ E11.5–E12.5 embryos and cultured them for 4–5 days until motor neuron axons crossed to the distal compartment (Fig EV2H). Then, we stained axons with Alexa 647-conjugated cholera toxin subunit B and analyzed their growth by live imaging. Without Sema3A addition, the growth of WT and $crmp2^{-/-}$ explants and their axons were comparable indicating again that the axon growth-promoting function of CRMP2 is redundant, at least in the tested neurons. When we added Sema3A (5 nM) to the distal (axonal) compartment, we observed decrease in the number of growing WT axons, as expected ($P < 0.001$, Fig 1F and G, Movie EV1). However, in $crmp2^{-/-}$ explants, Sema3A had no significant effect on the number of growing axons ($P = 0.99$, Fig 2F and G, Movie EV1). In addition, we

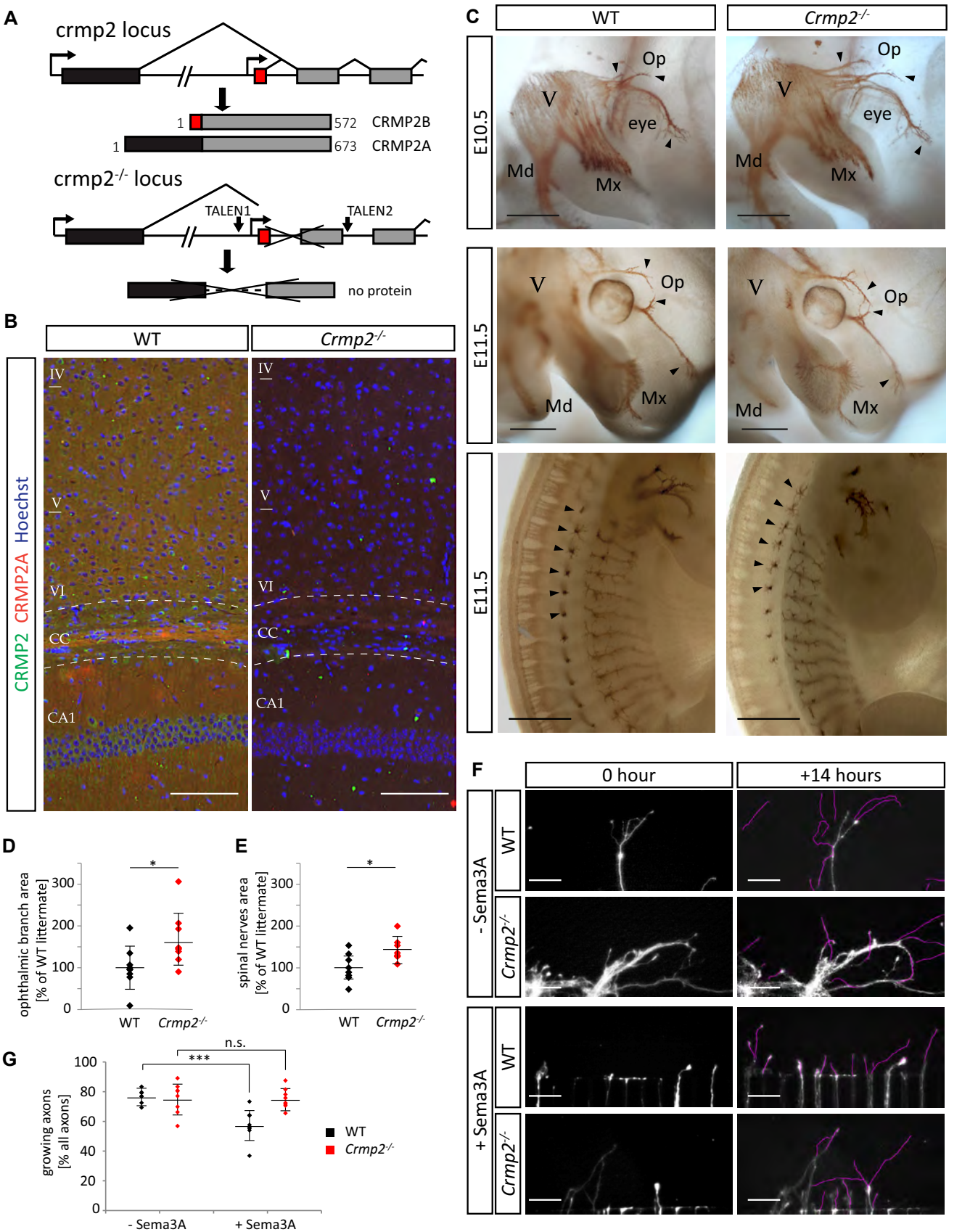
A
crmp2 locus
1
572
CRMP2B
1
673
CRMP2A
crmp2-/- locus
TALEN1
TALEN2
no protein
B
WT
Crmp2-/-
CRMP2 CRMP2A Hoechst
IV
V
VI
CC
CA1
C
WT
Crmp2-/-
E10.5
E11.5
E11.5
Op
V
eye
Md
Mx
D
ophthalmic branch area [% of WT littermate]
300
200
100
0
*
WT
Crmp2-/-
E
spinal nerves area [% of WT littermate]
300
200
100
0
*
WT
Crmp2-/-
G
growing axons [% all axons]
100
80
60
40
20
0
n.s.
***
- Sema3A
+ Sema3A
WT
Crmp2-/-
F
0 hour
+14 hours
- Sema3A
+ Sema3A
WT
Crmp2-/-

Figure 1.

Figure 1. CRMP2 deficiency leads to axonal growth defects in peripheral nerves.

A Generation of crmp2 knockout mice by TALEN mutagenesis. Alternative first exons are highlighted in black and red.

B CRMP2 expression in adult cortex (layers VI–IV), corpus callosum (CC), and hippocampal area CA1. CRMP2 (green) is expressed throughout the cortex and hippocampus, and CRMP2A (red) is particularly strongly expressed in a subset of callosal axons. Nuclei are counterstained with Hoechst 33342. Scale bars: 50 μm.

C Whole-mount immunohistochemistry with anti-neurofilaments antibody for visualization of peripheral nerves. In $crmp2^{-/-}$ embryos, the growth of ophthalmic branch of the trigeminal nerve is increased and axons are defasciculated (first and second rows, arrowheads). Similarly, we detected increased growth and branching of lateral branches of spinal nerves in $crmp2^{-/-}$ embryos (third row, arrowheads). Trigeminal nerve (V) and its branches (Op—ophthalmic, Mx—maxillar, Md—mandibular) are indicated. Scale bars: 500 μm.

D, E Quantification of areas innervated by ophthalmic branches of trigeminal ganglion and spinal nerve, normalized to WT littermates (each dot depicts one embryo). Area of ophthalmic branch in $crmp2^{-/-}$ was increased by 66% ($P < 0.05$, $n = 10$, 3 litters). For spinal nerves, total area in knockouts was increased by 45% ($P < 0.05$, WT $n = 8$, $crmp2^{-/-}$ $n = 7$, 3 litters). Mean ± SD, *$P < 0.05$, t-test.

F Growth of motor neurons from E11.5–E12.5 WT and $crmp2^{-/-}$ spinal cord explants in microfluidic chambers. Excerpts from 14-h time-lapse imaging are shown. Upon application of Sema3A into distal compartment, WT axons tend to stop or slow down their growth unlike $crmp2^{-/-}$ axons. Purple lines highlight the growth path of individual axons in a distal chamber. Scale bars: 100 μm. See also Movie EV1.

G Quantification of the fraction of growing (> 50 μm) axons in one imaging field (WT: control 76.8 ± 5.7%, Sema3A 57.7 ± 10.6%, $P < 0.001$, $crmp2^{-/-}$: control 75.4 ± 10.4%, Sema3A 75.4 ± 6.7%, $P = 0.99$), $n = 3$ experiments per genotype, 7–8 explants per condition. Mean ± SD. ***$P < 0.001$, 2-way ANOVA with Bonferroni's multiple comparison test.

analyzed Sema3A-induced growth cone collapse in E11.5–E12.5 isolated DRGs. Neurons were treated with Sema3A for 30 min, then fixed, and stained for actin and β3-tubulin. In $crmp2^{-/-}$ neurons, responsiveness to Sema3A was significantly decreased (Fig EV2G) which is in accord with the previously published data [8,32]. Thus, our data demonstrate that CRMP2 mediates Sema3A signaling *in vitro* and participates in guidance of multiple peripheral nerves in Sema3A-regulated regions *in vivo*.

CRMP2 regulates anatomy and axon guidance in corpus callosum

In addition to the peripheral nerves, we analyzed the effect of CRMP2 deficiency on axonal growth also in the central nervous system. We detected anatomical changes in the largest axonal bundle of the brain, the corpus callosum, in $crmp2^{-/-}$ mice. The length of corpus callosum was significantly reduced in juvenile (−19.2%, $P < 0.05$) as well as adult (−19.5%, $P < 0.05$) knockout mice as can be appreciated in both sagittal and coronal sections (Fig 2A and B). More detailed labeling of the tract with anti-neurofilaments antibody showed that the posterior part of the corpus callosum (splenium) is markedly hypoplastic in $crmp2^{-/-}$ mice, ending rostrally to the habenular commissure, while the WT splenium is longer, located just above the habenular commissure (Fig 2C).

Callosal axons have been shown to be guided by Sema3A [33,34]. Thus, we analyzed whether dysgenesis of the corpus callosum we detected in $crmp2^{-/-}$ mice is also accompanied by defects in callosal axon guidance. We *in utero* electroporated WT and $crmp2^{-/-}$ embryonal cortices with pCAGGS-EGFP vector at E15.5, which results in labeling of cortical layer 2/3 (i.e., mainly callosal-projecting neurons). The brains were collected at postnatal day 6 (P6), fixed in 4% PFA, and cut coronally to trace callosal axons in a hemisphere contralateral to the electroporation site (Fig 2D and E). At this stage, axons from somatosensory cortex enter the contralateral cortex in WT [35]. Most of the WT axons showed well organized, parallel growth. In contrast, $crmp2^{-/-}$ axons often failed to grow in an organized, parallel way upon leaving the main callosal tract, their distribution in the cortex seemed uneven. We tracked the electroporated axons after leaving callosal bundle at the contralateral site and quantified their tortuosity (i.e., the ratio of real length of the segment vs. distance of the first and last point of the segment, Fig 2E). We found that tortuosity was significantly higher in $crmp2^{-/-}$ in comparison with WT ($P < 0.001$, Fig 2F).

Importantly, in some coronal sections of $crmp2^{-/-}$ mice we detected deregulated growth of callosal axons even in the midline. Together with the reduced length of corpus callosum in $crmp2^{-/-}$ mice in the rostro-caudal axis we detected (Fig 2A–C), it was suggested that CRMP2 deficiency may alter the rostro-caudal guidance of callosal axons in the midline. To test this hypothesis, we traced the callosal axons by injecting DiI into the fixed P9 and adult somatosensory cortices and analyzed organization and fasciculation of the traced axons in the midline (see Materials and Methods). We found that at P9, $crmp2^{-/-}$ axons were significantly more distorted as seen upon plotting to polar histograms or fan-in diagrams (interval (0°, ±20°): $P < 0.05$, interval (±20°, ±40°): $P = 0.02$, Fig 2H–I, Appendix Fig S1A and B).

Together, our results show that CRMP2 regulates growth and guidance of selected axons in both peripheral (PNS) and central nervous system (CNS). In addition, since CRMP2 deficiency in $crmp2^{-/-}$ mice leads to enhanced, rather than reduced axon growth, our results suggest that in the analyzed PNS and CNS regions, the mediation of the repulsive axon guidance signals by CRMP2 takes precedence over its axon growth-promoting function.

CRMP2 mediates Sema3F-driven, but not Sema3A-driven axon pruning

CRMP2 has been associated with neurodevelopmental disorders like schizophrenia and ASD characterized by altered brain connectivity [36] and defects in postnatal synaptic refinement through axon and dendrite pruning [26,37]. Importantly, in many regions Sema3F seems to play a more important role in pruning than Sema3A [6,7]. Therefore, we asked whether CRMP2 regulates axon pruning and if, in this function, it mediates Sema3A or rather Sema3F signaling. For this, we analyzed two developing axonal systems showing either Sema3F-mediated pruning (the infrapyramidal bundle, IPB; [6]) or Sema3A-mediated pruning (the hippocamposeptal bundle; [6]). First, we analyzed stereotyped pruning of infrapyramidal bundle (IPB) of hippocampal mossy fibers taking place between P20 and P40 and regulated by Sema3F and its receptor complex (Nrp2/PlxnA3) [6]. At P14 (i.e., before pruning), calbindin immunostaining revealed the presence of IPB in both WT and $crmp2^{-/-}$ mice (Fig 3A and B). Synapses were formed in both IPB and the main bundles as revealed by VGluT1 staining (Fig 3A and B). In 7-week-old animals, however, when pruning was complete in WT, the IPB remained

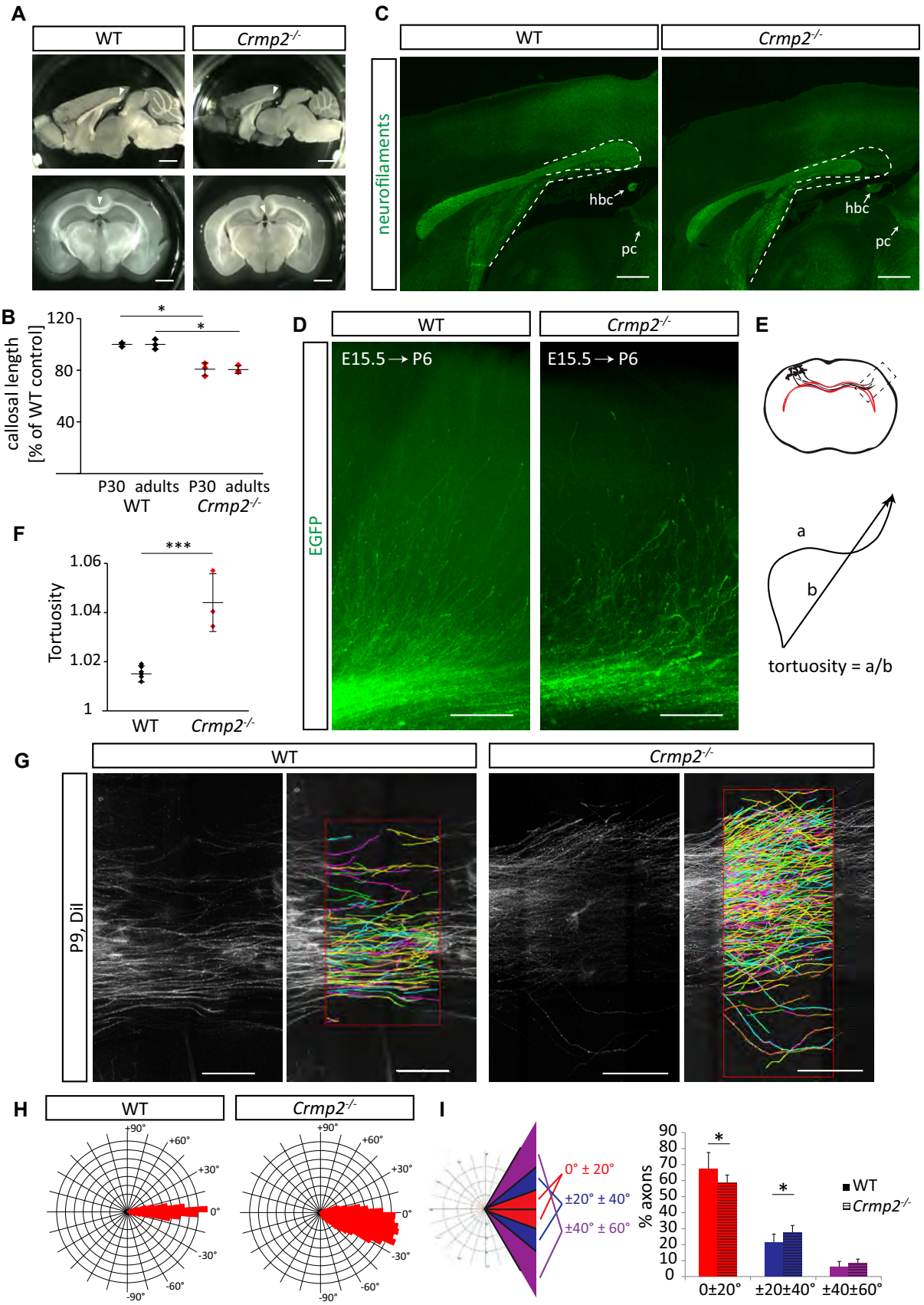
A
WT
Crmp2-/-
C
WT
Crmp2-/-
neurofilaments
hbc
pc
B
callosal length [% of WT control]
120
80
40
*
*
P30 adults P30 adults
WT Crmp2-/-
D
WT
Crmp2-/-
EGFP
E15.5 → P6
E15.5 → P6
E
a
b
tortuosity = a/b
F
***
Tortuosity
1.06
1.04
1.02
1
WT
Crmp2-/-
G
WT
Crmp2-/-
P9, DiI
H
WT
Crmp2-/-
+90°
+60°
+30°
0°
-30°
-60°
-90°
I
0° ± 20°
±20° ± 40°
±40° ± 60°
% axons
90
80
70
60
50
40
30
20
10
0
*
*
WT
Crmp2-/-
0±20°
±20±40°
±40±60°

Figure 2.

Figure 2. CRMP2 regulates postnatal development of corpus callosum.

A CRMP2 deficiency leads to callosal hypoplasia. Shortening of corpus callosum (arrowheads) is apparent in both sagittal (first row) and coronal sections (second row) of adult brains. Scale bars: 1 mm.

B Quantification of callosal length in 30-day-old mice (P30, $n = 3$, $crmp2^{-/-}$ is 80.8 ± 5% of WT, $P = 0.003$) and adult mice ($n = 3$, $crmp2^{-/-}$ is 80.5 ± 3% of WT, $P = 0.002$), mean ± SD, $^{*}P < 0.05$, *t*-test.

C Labeling of adult corpus callosum with anti-neurofilaments antibody in sagittal sections. Outline depicts missing posterior part of the tract in $crmp2^{-/-}$ mice. Caudal part of the corpus callosum in WTs is located dorsally above the habenular commissure (hbc), while in $crmp2^{-/-}$ mice, callosum terminates rostrally before reaching the hbc (arrows). PC indicates posterior commissure. Scale bars: 500 μm.

D The growth of GFP-labeled callosal axons in the contralateral cortex at P6 (embryos were electroporated at E15.5). Note the disorganized paths of $crmp2^{-/-}$ axons. Scale bars: 200 μm.

E Schematic drawing of the callosal axon path and axonal tortuosity calculation. Pyramidal neurons in layer II/III project their axons into the contralateral cortex [rectangle depicts the area displayed in (D)]. Axonal tortuosity quantification as shown in (F), tortuosity = 1 if a = b.

F Quantification of tortuosity of axons (WT $n = 6$ pups, $crmp2^{-/-}$ $n = 3$ pups) upon their exit from the callosal tract (WT 1.016 ± 0.003 vs. $crmp2^{-/-}$ 1.044 ± 0.012, $P < 0.001$), mean ± SD, $^{***}P < 0.001$, *t*-test.

G DiI-labeled callosal axons from P9 oblique brain sections (see the Appendix Fig S1) and their reconstruction in Neurolucida 360 (WT $n = 6$, $crmp2^{-/-}$ $n = 9$). Scale bars: 200 μm.

H Polar histograms of callosal axons reconstructed in (G). Note the broader range of axon growth angles in $crmp2^{-/-}$ mice.

I Left: schematic representation of polar histogram analysis by clustering the traced axons (WT $n = 6$ pups, $crmp2^{-/-}$ $n = 9$ pups) into three groups based on the growth angles. Right: proportion of axons growing in selected clusters (WT, 0° to ±20°: 67.3 ± 10.3%; ±20° to ±40°: 21.2 ± 5.3%; ±40° to ±60°: 6.22 ± 3.2%; $crmp2^{-/-}$, 58.5 ± 5%, $P = 0.047$, 27.7 ± 4.3%, $P = 0.022$, 8.64 ± 2.25%, $P = 0.11$), mean ± SD, $^{*}P < 0.05$, *t*-test.

present in $crmp2^{-/-}$ mice, and their IPB index (IPB length/main bundle length) was significantly higher than in WT ($P < 0.001$, Fig 3C–G). The same pattern of IPB pruning was detected also in sagittal sections (Fig EV3A). To determine the maturity of IPB synapses, we stained adult coronal sections with antibodies against VgluT2 or VgluT1, which are both expressed in developing mossy fibers, but in adult hippocampus only VgluT1 is present [38]. We found VgluT1 in the main bundles of WTs and $crmp2^{-/-}$ mice, as well as in the unpruned IPBs of $crmp2^{-/-}$ (Fig 3E and F). We did not detect the immature VgluT2 signal (Fig 3C and D). Thus, the IPB axons formed during postnatal development persist in $crmp2^{-/-}$ mice into adulthood and form mature synapses. These results demonstrate that IPB pruning is defective in $crmp2^{-/-}$ mice (as is the case in $Sema3F^{-/-}$, $Nrp2^{-/-}$, and $PlxnA3^{-/-}$ mice) [6].

We next tested whether stereotyped pruning of a different group of axons arising from hippocampus—the hippocamposeptal axons of CA1 pyramidal neurons—is also affected in $crmp2^{-/-}$ mice. CA1 neurons send their axons into medial and lateral septum at P0–1. However, at P8, only the axons projecting to the lateral septum persist, while the ones projecting into the medial septum are pruned [39]. In this system, the pruning is mediated by Sema3A and not Sema3F [6]. Our analysis of the development of the CA1 hippocamposeptal axons in $crmp2^{-/-}$ mouse brains by retrograde DiI tracing (Fig EV3B) showed no change in these brains as compared to WT brains at P0 or P8, indicating that the Sema3A-mediated pruning of hippocamposeptal axons is not affected in $crmp2^{-/-}$ mice.

To further support the role of CRMP2 as a mediator of Sema3F-driven pruning, we analyzed pruning of corticospinal axons of visual cortex neurons that have been previously shown to be dependent on Sema3F signaling. In the early developmental stages, these neurons send their projections not only to the superior colliculus but also to two inappropriate targets, i.e., the inferior colliculus (IC) and the spinal cord. During the third postnatal week, inappropriate axons are eliminated through a pruning process regulated by Sema3F [7]. We analyzed the development of the visual cortex projection by the means of DiI anterograde tracing (Fig 4A and B). At P9, before the pruning period, there was no significant difference between WT and $crmp2^{-/-}$ in the VP index (fluorescence intensity of corticospinal axons after vs. before the branch point). In adult WT mice, though, the inappropriate corticospinal axons were largely pruned [VP index significantly dropped ($P < 0.01$, Fig 4C)], while in $crmp2^{-/-}$ mice, they were still largely present [the VP indexes were not significantly different between P9 and adult ($P = 0.24$); Fig 4C]. These data demonstrate that CRMP2 participates in postnatal refinement of corticospinal visual axons and is consistent with its role in mediating Sema3F signaling.

While, in development, both CNS and PNS projections are refined by pruning, we did not detect changes in the pruning of the peripheral neuromuscular junctions (NMJs) in $crmp2^{-/-}$ mice using trigonum sterni muscle [the number of double-innervated NMJs was similar in WT and mutant mice at P11 ($P > 0.99$, Fig EV3C and D)].

Finally, we asked whether Sema3F-dependent axonal guidance is also mediated by CRMP2. Axon guidance is affected in two specific axonal bundles in $Sema3F^{-/-}$ mice [40]—namely the anterior commissure (AC) and the retroflex fascicle. Immunostaining of P6 and P14 brains with anti-neurofilaments antibody revealed that both structures are present in $crmp2^{-/-}$ mice (Fig EV4A and D). However, temporal limb of the AC appeared to be hypoplastic. We therefore analyzed morphology of AC in the horizontal sections (Fig EV4B). In knockouts, the diameter of temporal limb was indeed significantly thinner and the olfactory limb defasciculated (Fig EV4B and C). The data thus indicate that CRMP2 also contributes to Sema3F-driven axon guidance.

In conclusion, we found significant differences between WT and $crmp2^{-/-}$ mice in stereotyped pruning in regions controlled by Sema3F (visual cortex axons, IPB). In contrast, we found no differences in regions controlled by Sema3A (i.e., hippocamposeptal axons) suggesting that CRMP2 mediates Sema3F-driven, but not Sema3A-driven axon pruning.

CRMP2 mediates Sema3F-dependent axon retraction *in vitro*

In order to directly show that CRMP2 is necessary for Sema3F-triggered axon pruning, but dispensable for Sema3A-dependent pruning, we tested pruning in an *in vitro* system. We prepared dissociated hippocampal cultures from WT and $crmp2^{-/-}$ E16.5 embryos and transfected them with EGFP at DIV1 (1 day *in vitro*). At DIV7, we added Sema3A or Sema3F into the cultures and analyzed the axon behavior in fluorescence microscope by time-lapse imaging. DIV7,

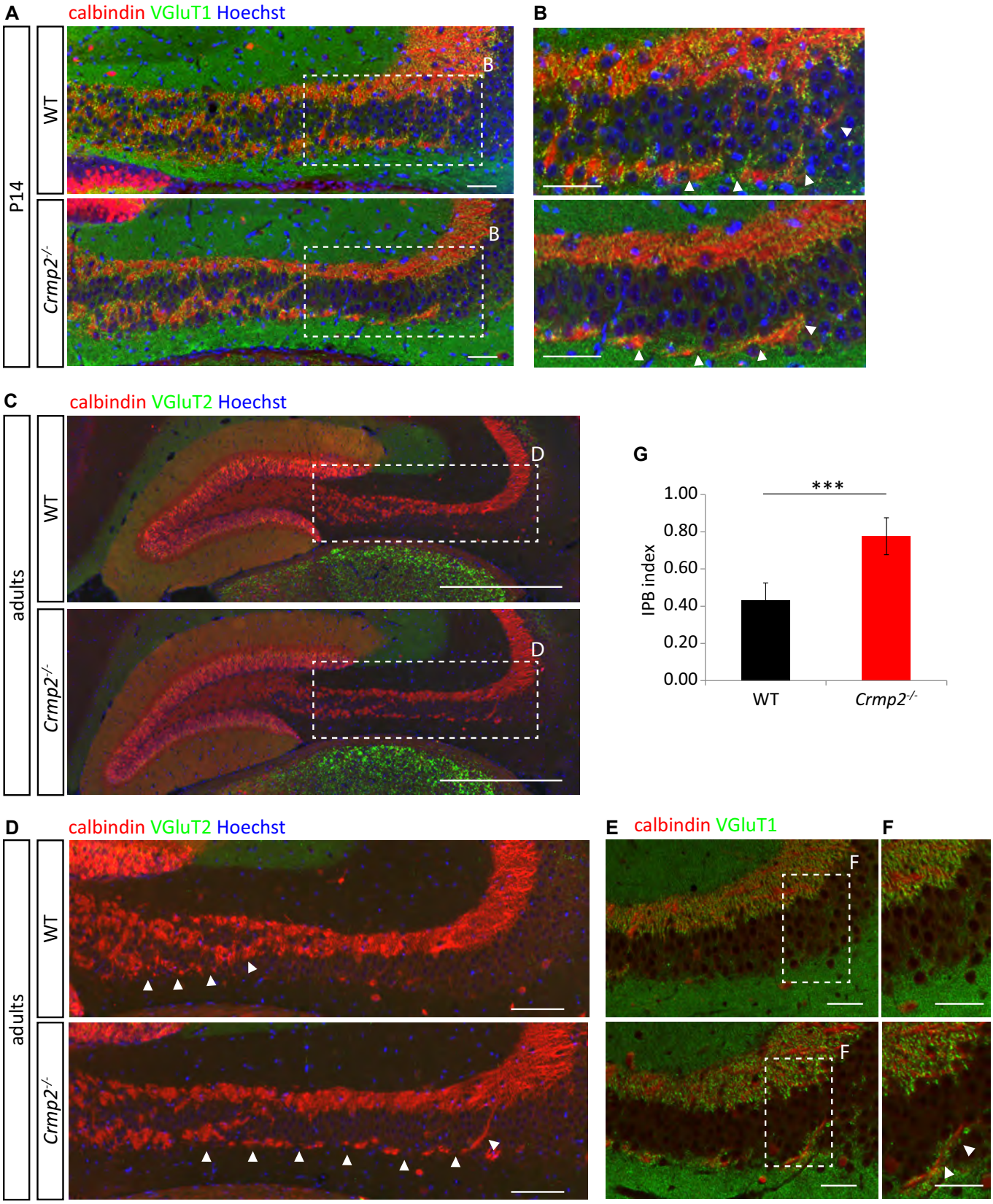
A
calbindin VGluT1 Hoechst
P14
WT
Crmp2-/-
B
B
B
C
calbindin VGluT2 Hoechst
adults
WT
Crmp2-/-
D
D
G
***
IPB index
1.00
0.80
0.60
0.40
0.20
0.00
WT
Crmp2-/-
D
calbindin VGluT2 Hoechst
adults
WT
Crmp2-/-
E
calbindin VGluT1
F
F
F

Figure 3.

Figure 3. Infrapyramidal bundle fails to prune in *crmp2*$^{-/-}$ mice.

A, B (A) Coronal sections of P14 brains stained for calbindin and VgluT1. Infrapyramidal bundle (IPB) progresses into hippocampal CA3 region in both WT and *crmp2*$^{-/-}$ mice. Nuclei are counterstained with Hoechst 33342. (B) Details from depicted regions in (A), arrowheads show the course of IPB. Scale bars: 100 μm.

C, D (C) Staining for calbindin shows unpruned infrapyramidal bundle in adult *crmp2*$^{-/-}$ mice. No VGluT2 signal in hippocampal CA3 region is present in WT and *crmp2*$^{-/-}$ suggesting mature synapses. Scale bars: 500 μm. (D) Details from depicted regions in (C), arrowheads show the course of IPB. Scale bars: 100 μm.

E, F Staining for calbindin and VgluT1 shows mature synapses in the main bundle in both genotypes and in the IPB in *crmp2*$^{-/-}$ mice (arrowheads). Scale bars: 100 μm.

G Quantification of IPB index (length of the IPB vs. main bundle, WT 0.43 ± 0.05, *crmp2*$^{-/-}$ 0.78 ± 0.05, $P < 0.001$) counted from adult coronal sections (WT $n = 4$ mice, *crmp2*$^{-/-}$ $n = 5$ mice). Mean ± SD, ***$P < 0.001$, *t*-test.

which is an early stage of synapse formation [41], was chosen to facilitate analysis of neurons in still less complex connectivity patterns (Fig 5A and B, Movies EV2 and EV3). We analyzed only stable axon terminals that did not show any movement in 1-h period prior to addition of the guidance cues (45% of all labeled axon terminals). In control conditions in both wild-type and knockout, a small number of the stable axons were spontaneously retracting (WT 13%, KO 20%, $P = 0.03$, Fig 5C). After addition of either Sema3A or Sema3F into WT culture, we observed a three-fold increase in axon retractions (32% for Sema3A, $P < 0.001$, 41% for Sema3F, $P < 0.001$, Fig 5C). However, in *crmp2*$^{-/-}$, this increase was detectable only after Sema3A (30%, $P < 0.05$) and not after Sema3F (22%, $P > 0.99$). These data demonstrate, that in primary neuron cultures undergoing synaptogenesis, CRMP2 is essential to mediate Sema3F but not Sema3A signaling. This is in agreement with our *in vivo* findings that stereotyped pruning in *crmp2*$^{-/-}$ is affected in Sema3F-controlled, but not in Sema3A-controled regions.

CRMP2 regulates dendritic spine remodeling in hippocampal granule cells

Besides triggering axon pruning, Sema3F regulates also the development of some classes of dendritic spines (e.g., spines of dentate gyrus (DG) granule cells) [42]. In contrast, Sema3A/Nrp1 signaling seems to be dispensable for dendritic spine morphogenesis [42,43]. In order to test whether CRMP2 participates also in spine development/morphogenesis, we DiOlistically labeled DG neurons and analyzed their dendritic spines. Surprisingly, we found significantly increased spine density in *crmp2*$^{-/-}$ adult DG granule cells compared to WTs (Fig 6B and C, $P < 0.001$). This phenotype was similar to that found in *Sema3F*$^{-/-}$ and *Nrp2*$^{-/-}$ [42]. Next, we analyzed branching of DG granule cell dendrites. Sholl analysis revealed no differences between WT and *crmp2*$^{-/-}$ mice (Fig 6D and E, $P > 0.99$), which is again in line with the phenotype of *Sema3F*$^{-/-}$ mice [42].

Higher spine density could be a result of either increased generation of new spines or defective pruning of spines or both. Considering the axon pruning defects we found in Sema3F-regulated areas in *crmp2*$^{-/-}$ mice (see above), and considering that Sema3F promotes loss of spines *in vitro* [42], we hypothesized that Sema3F regulates dendritic spine pruning through CRMP2. To test this hypothesis, we labeled and counted DG dendritic spine density in P30 (adolescent) mice when dendritic spines are virtually all formed and the pruning process starts [44,45]. We found no differences in dendritic spine density between WTs and mutants at P30 (Fig 6A and C, $P > 0.99$). This indicates that the formation of spines is unaltered in *crmp2*$^{-/-}$ mice and that it is the process of dendritic spine pruning that is defective in these mice. To support this hypothesis, we tested whether the number of excitatory synapses is also increased in DG of adult *crmp2*$^{-/-}$ mice using PSD95 and VGluT2 post- and pre-synaptic markers, respectively. We found that in *crmp2*$^{-/-}$ mice, the density of colocalized PSD95/VGluT2 puncta was indeed increased in the inner part of the molecular layer (Fig 6F), which is in agreement with DG synaptic pruning deficit. As DG spine morphogenesis is regulated through Sema3F [42], our findings indicate that CRMP2 mediates Sema3F-dependent synapse pruning.

Finally, we analyzed the role of CRMP2 in Sema3F-induced dendritic spine remodeling *in vitro*. We prepared hippocampal cultures, transfected neurons with GFP at DIV14, and analyzed the same dendritic segments at DIV21 and DIV25 (Fig EV5B). We detected significantly decreased spine density at DIV25 in WT neurons consistent with ongoing spine remodeling, but not in *crmp2*$^{-/-}$ neurons (Fig EV5C). Importantly, treatment of WT DIV25 neurons with Sema3F induced elimination of their spines, but no significant effect was detected in CRMP2-deficient neurons (Fig EV5D and E). These observations are in accord with our *in vivo* findings and further support the role of CRMP2 as mediator of Sema3F-driven spine remodeling.

Defects in the distribution of dendritic spines due to aberrant synapse refinement are one of the key features of both ASD and schizophrenia. Generally, dendritic spine number in ASD patients is higher than in control subjects or variable in different regions, while in schizophrenia patients, it is lower [36]. This applies particularly to some brain regions, e.g., prefrontal cortex (PFC), where excessive spine elimination has been associated with pathogenesis of schizophrenia [46]. Since some phenotypical aspects of conditional *crmp2*$^{-/-}$ mice like impaired sensorimotor gating have been related to schizophrenia [17], we asked whether CRMP2 deficiency also leads to spine overpruning and reduced spine density in PFC. At P25, PFC spine density was similar in both WT and mutants (Fig 6F and G, $P = 0.97$) and similar to our findings in the DG. Importantly, unlike in DG, we did not detect any significant difference in PFC spine density between adult WT and *crmp2*$^{-/-}$ mice (Fig 6G and H, $P > 0.99$), which is not consistent with schizophrenia-like phenotype.

Crmp2$^{-/-}$ mice display juvenile sociability defects, memory impairment, and decreased anxiety

While schizophrenia shares some behavioral symptoms with autism (e.g., cognitive and social deficits), it differs in the onset of the disease, as ASD manifests typically in 3-year-old children while schizophrenia in the adolescence at the earliest [25,37]. This suggests that any changes underlying ASD must be present already

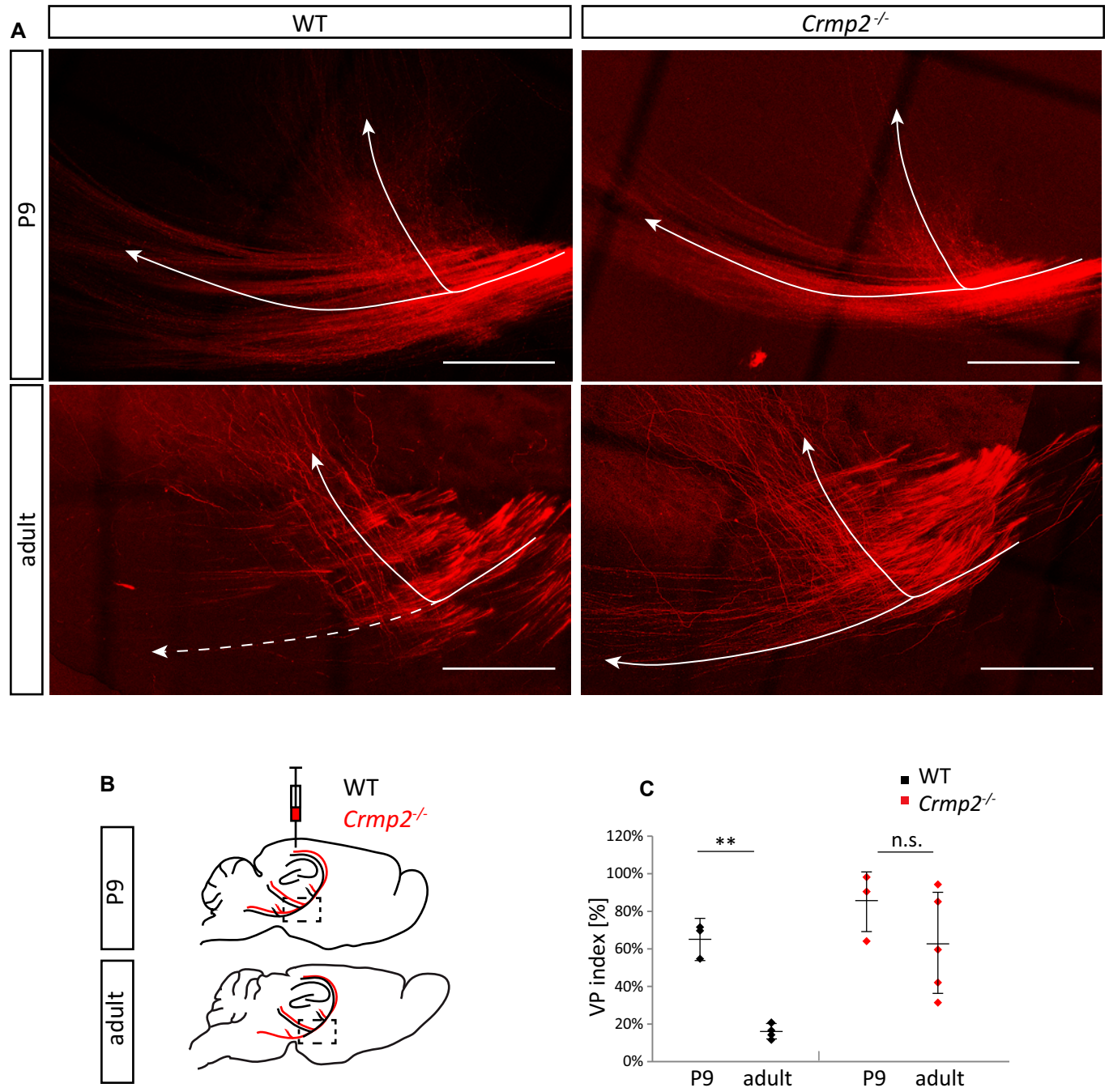

Figure 4. Defective pruning of corticospinal visual axons in *crmp2*$^{-/-}$ mice.

A Upper row: DiI tracing of the visual cortex axons at P9 (before pruning), sagittal sections. Branching point of the tract is shown. Lower row: visual cortex axons in adult mice after pruning period. Note significantly reduced number of axons continuing into pyramidal tract in WT (dashed arrow) (arrows—2 branches of corticospinal visual axons). Maximum projections are shown. Scale bars: 200 μm.

B Schematic drawing of DiI injection and axon tracing. Axons that initially enter pyramidal tract fail to prune in *crmp2*$^{-/-}$ mice (red line).

C Quantification of VP (visual pruning) index (fluorescence intensity of pyramidal axons after vs. before the branch point). In WT animals after the pruning period, only a minor part of axons descends toward the pyramidal tract (WT: P9 0.65 ± 0.09, adults 0.17 ± 0.04, $P = 0.006$). However, in *crmp2*$^{-/-}$ mice, corticospinal axons are still largely present, and their VP indexes are not significantly different between adult and P9 stages (*crmp2*$^{-/-}$: P9 0.54 ± 0.18, adults 0.62 ± 0.27, $P = 0.24$). Mean ± SD, $^{**}P < 0.01$, 2-way ANOVA with Bonferroni's multiple comparison test. P9: $n = 3$ pups/genotype, adults: $n = 5$ mice/genotype.

very early in postnatal development. To assess this hypothesis, we wanted to see whether CRMP2 deficiency results in juvenile behavioral changes. To this effect, we analyzed ultrasonic vocalization (USV) in P6, P8, and P12 WT and *crmp2*$^{-/-}$ pups as a measure of their sociability [47]. We recorded USVs of WT and mutant pups in 5-min intervals after isolation from their mothers

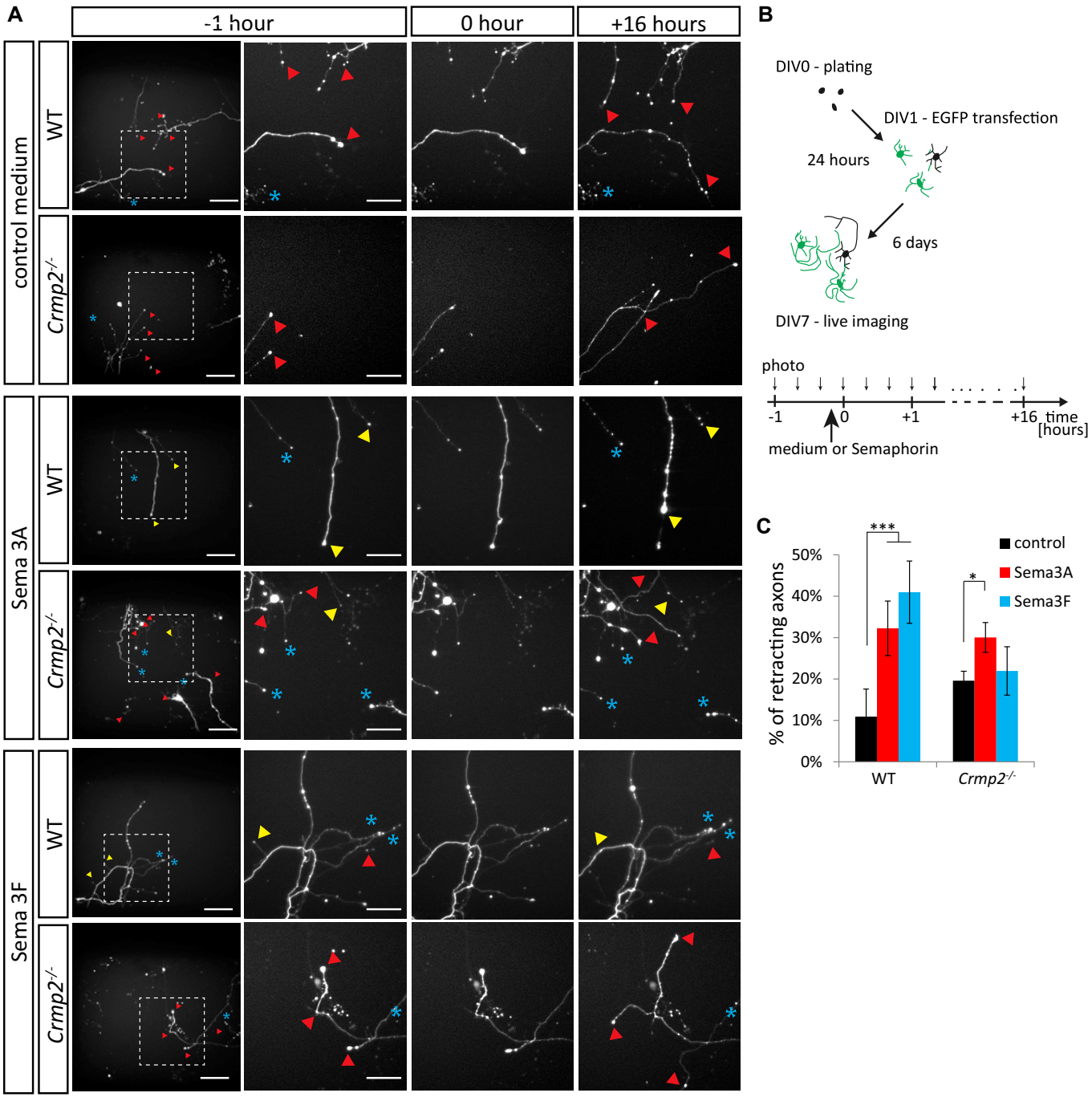

Figure 5. CRMP2 mediates Sema3F signaling in primary neurons.

A Time-lapse imaging of DIV7 cultured hippocampal neurons before and after semaphorin stimulation. Upper panel: axon growth without semaphorin stimulation. Middle panel: stimulation with Sema3A (0 h) (1 nM, n = 669 axons for WT, 761 axons for knockout) causes retraction of both WT and *crmp2*$^{-/-}$ neurons. Lower panel: stimulation with Sema3F (5 nM, n = 602 axons for WT, 955 axons for knockout) causes axon retraction in WT, but not in *crmp2*$^{-/-}$ neurons. Red triangles depict growing axons, yellow retracting axons, and blue asterisks indicate steady non-growing axons. See also Movies EV2 and EV3. Scale bars: 100 μm (whole image field) and 50 μm (magnified).

B Schematic drawing of the experimental setup.

C Quantification of retracting axons (number of retracting vs. steady axons, three experiments). WT: control 13.4 ± 5%, Sema3A 31.2 ± 6% ($P < 0.001$), Sema3F 36.9 ± 8.7% ($P < 0.001$); *crmp2*$^{-/-}$: control 19.8 ± 1.8%, Sema3A 28.5 ± 4.4% ($P < 0.05$), Sema3F 22.4 ± 4.1% ($P > 0.99$), mean ± SD are shown. ***$P < 0.001$, *$P < 0.05$, 2-way ANOVA with Bonferroni's multiple comparison test.

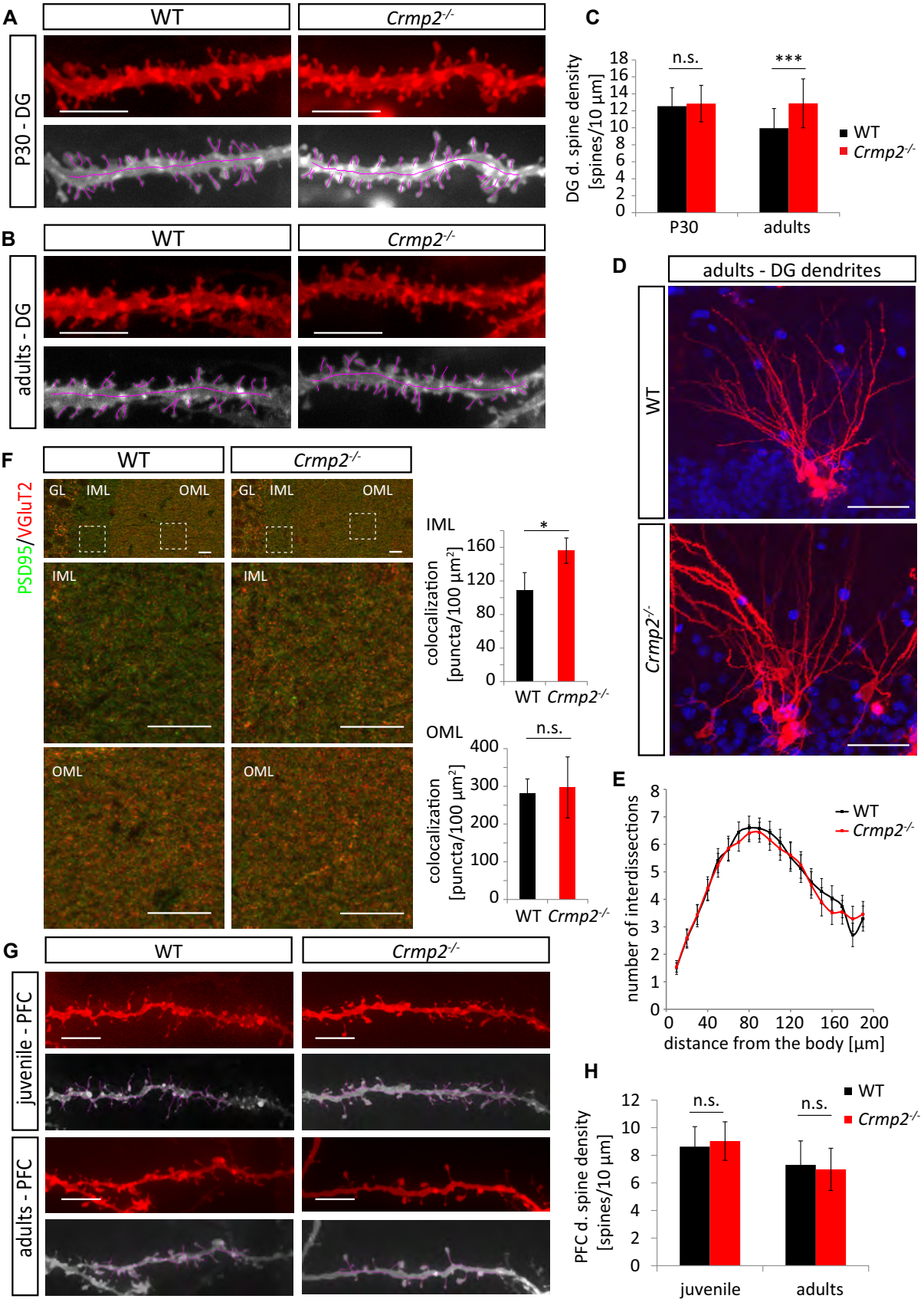
A
WT
Crmp2-/-
P30 - DG
B
adults - DG
C
DG d. spine density [spines/10 µm]
n.s.
***
P30
adults
WT
Crmp2-/-
D
adults - DG dendrites
E
number of interdissections
distance from the body [µm]
F
PSD95/VGluT2
GL IML OML
colocalization [puncta/100 µm2]
*
n.s.
G
juvenile - PFC
adults - PFC
H
PFC d. spine density [spines/10 µm]
juvenile
adults

Figure 6.

Figure 6. CRMP2 regulates dendritic spine refinement in dentate gyrus granule cells.

A, B Dendritic spine density in DiOlistically labeled DG granule cells is similar in WT and *crmp2*$^{-/-}$ mice at P30. In adults, however, spine density in *crmp2*$^{-/-}$ granule cells is increased comparing to WT. Scale bars: 5 μm.

C Quantification of dendritic spine density in DG granule cells in the inner molecular layer (50–100 μm away from the soma). WT, P30: 12.5 ± 2.2 spines/10 μm, adults: 9.95 ± 2.3; *crmp2*$^{-/-}$, P30: 12.86 ± 2.1 ($P > 0.99$), adults: 12.88 ± 2.9 ($P < 0.001$), mean ± SD, ***$P < 0.001$, 2-way ANOVA with Bonferroni correction. P30: 3 animals/genotype, WT = 61 dendrites, knockout = 64 dendrites; adults: 3 animals/genotype, WT = 41 dendrites, knockout = 37 dendrites.

D, E Analysis of branching of DiOlistically labeled DG granule cell dendrites in adult WT and *crmp2*$^{-/-}$ mice ($n = 3$ animals, ≥ 25 dendrites). Quantification of granule cell branching by Sholl analysis showed no significant differences ($P > 0.99$). Scale bars: 50 μm, mean ± SEM, 2-way ANOVA with Bonferroni correction.

F Defects in synapse elimination in the inner molecular layer revealed by double immunostaining with PSD95 and VGluT2 antibodies ($n = 5$ mice/genotype). GL indicates granule cell layer, and IML/OML indicate inner/outer molecular layer, respectively. Density of colocalized PSD95/VGLuT2 puncta was counted. IML: WT 109 ± 21, *crmp2*$^{-/-}$ 156 ± 15 ($P = 0.004$). OML: WT 281 ± 38, *crmp2*$^{-/-}$ 297 ± 80 ($P = 0.7$). Scale bars: 10 μm, mean ± SD, *$P < 0.05$, *t*-test.

G Spine density in DiOlistically labeled prefrontal cortex (PFC) is similar in WT and *crmp2*$^{-/-}$ mice in both juvenile and adult mice. Scale bars: 5 μm.

H Quantification of dendritic spine density of PFC pyramidal neurons, basal dendrites (WT, juvenile: 8.63 ± 1.44 spines/10 μm, adults: 7.3 ± 1.4; *crmp2*$^{-/-}$, juvenile: 9.05 ± 1.73, $P = 0.97$, adults: 6.98 ± 1.53, $P > 0.99$), mean ± SD, 2-way ANOVA with Bonferroni's multiple comparison test. P25: $n = 3$, ≥ 50 dendrites; adults: $n = 3$, ≥ 50 dendrites.

and found that at P6 the number of calls was similar between both groups ($P = 0.73$), but decreased significantly in the mutants at P8 ($P = 0.015$; Fig 7A–C). At P12, the mutants were almost completely silent ($P = 0.002$); in fact, only two mutant pups from 13 vocalized at all (10/14 in WT). The duration of the individual calls was also significantly shorter in *crmp2*$^{-/-}$ pups in both P8 ($P = 0.011$) and P12 ($P = 0.003$) (Fig 7B). This early onset social behavior defects have been described in numerous mouse models of ASD with dendritic spine pathology [26], some of which also showed dendritic spine pathology later in adults [48–51]. To broaden the analysis of *crmp2*$^{-/-}$ social abnormalities also to the adult animals, we performed a three-chamber sociability test. We found disruption of social preference in knockouts since they spent similar time exploring both stranger mice and neutral object, unlike WT, that preferred the mice (WT $P < 0.001$, *crmp2*$^{-/-}$ $P = 0.07$, Fig 7D, Appendix Fig S2A). On the other hand, social novelty seems to be preserved in *crmp2*$^{-/-}$ mice, although less expressed than in WT animals (WT $P < 0.001$, *crmp2*$^{-/-}$ $P < 0.05$, Fig 7D, Appendix Fig S2B).

We next asked whether hippocampus-dependent memory functions are affected in *crmp2*$^{-/-}$ mice as they exhibit aberrant inputs from DG into CA3 (unpruned mossy fibers) and increased spine density in DG granule cells (input from entorhinal cortex). We tested working memory using Y-maze (a three-arm maze) where WT and mutants showed comparable level of exploratory activity (Fig 7H). However, the ratio of spontaneous arm alternation was significantly lower in *crmp2*$^{-/-}$ mice (Fig 7I, $P = 0.0058$) indicating a working memory impairment [17]. In contrast, long-term memory and general behavioral flexibility seem not to be affected in *crmp2*$^{-/-}$ mice as revealed by active place avoidance on a rotating arena test (Appendix Fig S2C).

Similar to other CRMP2-deficient mouse models [17,52], we detected anxiety impairment in *crmp2*$^{-/-}$ mice using elevated plus maze. In the task, the knockouts also demonstrated increased activity during exploration of the maze (Fig 7E), spent more time in the open arms of the maze ($P < 0.001$), and visited them more often ($P = 0.0016$) than their WT counterparts (Fig 7F and G) suggesting decreased anxiety, or perhaps a more general lack of adequate response to potentially dangerous situations. This phenotype may reflect the hippocampal phenotype of *crmp2*$^{-/-}$ mice as lesions in particularly ventral hippocampus have been shown to result in similar decreased anxiety in mouse models [53].

Discussion

CRMP2 has been long considered an important regulator of semaphorin 3A-mediated axon guidance during embryonic development. Its expression, though, is high even in the early postnatal neurons, but its role in the postnatal development and adult neurons has so far been elusive. In the present study, we demonstrated that CRMP2 is not only mediator of Sema3A signaling regulating axon guidance in embryonic development, but importantly, that it plays a central role in the postnatal refinement of the nervous system. By generating new *crmp2*$^{-/-}$ mice and analyzing their phenotype, we first showed that CRMP2 deficiency *in vivo* leads to axon guidance defects in CNS and PNS that could be attributed to changes of Sema3A signaling. Strikingly, we demonstrated that CRMP2 mediates also Sema3F signaling and that CRMP2 deficiency disrupts early postnatal Sema3F-mediated axon and dendritic spine refinement in multiple areas of the CNS and in hippocampal neuron cultures. Changes in Sema3F signaling pathway have been considered a risk factor in the pathogenesis of ASD. In accord with that, we showed that *crmp2*$^{-/-}$ mice suffer from altered pruning and both early postnatal and adult social interaction defects previously linked to autism. Together, our *in vivo* and *in vitro* data demonstrated a novel function of CRMP2 in postnatal fine-tuning of the nervous system by Sema3F and showed that its deficiency in mice leads to neurodevelopmental defects associated with pathogenesis of the ASD in human.

Regulation of axon and dendritic pruning by Sema3F and CRMP2

Initial growth of axons and dendrites during embryonic and early postnatal period results in an embryonic template that must be later refined to generate a functional healthy nervous system [54]. Stereotyped refinement of nervous system was uncovered in several regions: (i) Infrapyramidal bundle (IPB) axons of hippocampal mossy fibers are retracted between P14 and P30 in mice [55]; (ii) excess of layer 2/3 callosal axons of motor, sensory, and visual cortex is refined until P30 [33]; and (iii) corticospinal axons from layer 5 visual cortex are eliminated between P9 and P25 [7]. In addition, density of dendritic spines in various brain regions in mice and humans peaks between childhood and adolescence [44,45] and its significant portion is eliminated until adulthood. Finally, pruning also occurs in peripheral nervous system—originally polyneuronal innervation of muscle fibers is later in

development refined so that each muscle fiber is innervated by only one motor axon [56,57].

Knockout mouse studies identified extracellular cues and receptors that mediates pruning in rodents. These include Sema3A and its receptor complex (Nrp1/PlxnA4), and Sema3F and its receptors (Nrp2/PlxnA3), ephrin-B3–EphB2 reverse signaling, and C4 component of complement [6,58,59]. Intracellular pathways that translate extracellular signal to cytoskeleton are however poorly understood. Here, we identified CRMP2 as a novel mediator of pruning in rodent brain triggered by Sema3F.

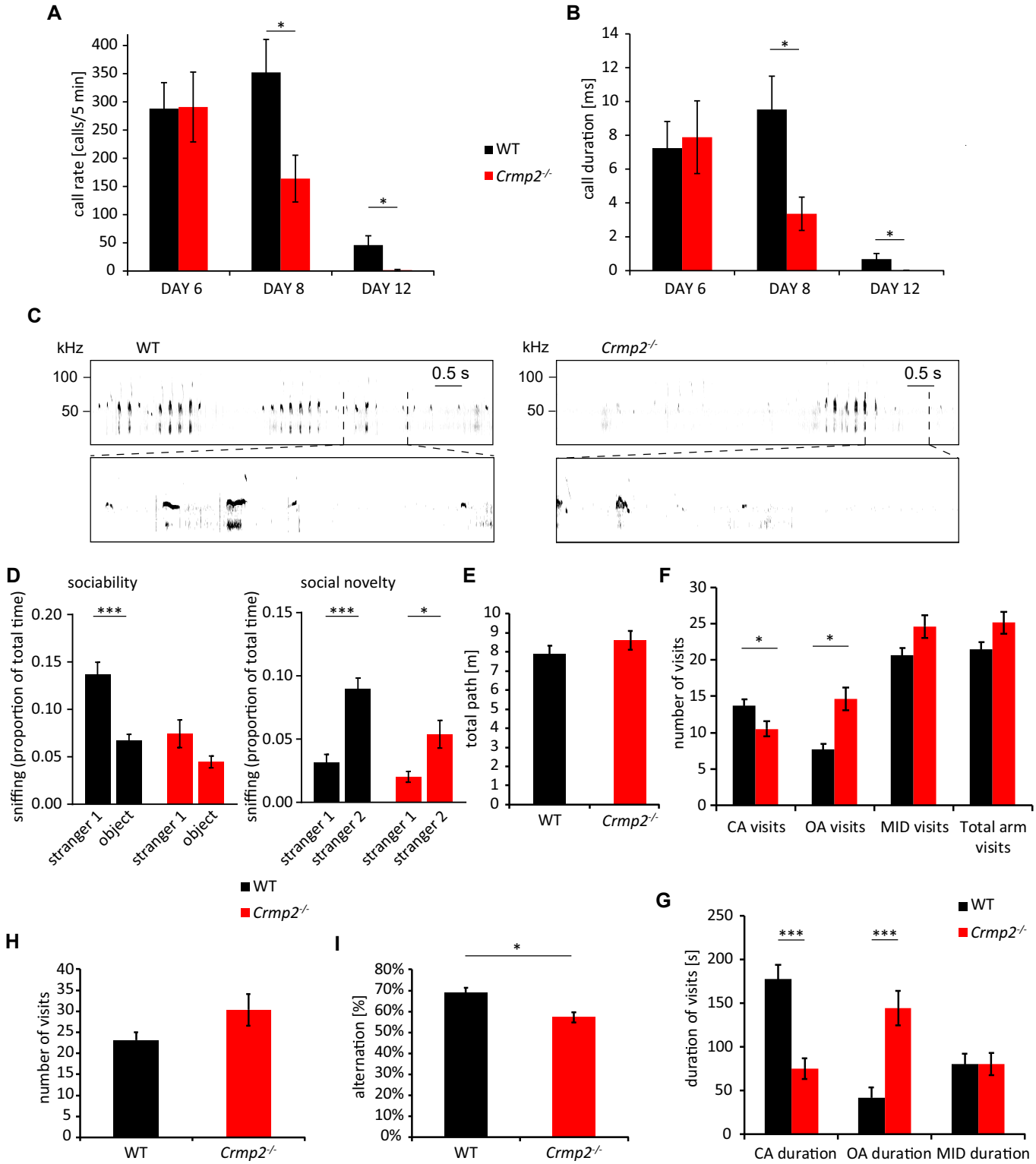

Figure 7.

Figure 7. Behavioral analysis of *crmp2*$^{-/-}$ mice.

A, B Ultrasonic vocalization was measured at P6, P8, and P12 (WT n = 14 pups, *crmp2*$^{-/-}$ n = 13 pups). In *crmp2*$^{-/-}$ mice, there is a significant decrease in the rate and duration of calls at P8 (call rate, WT 352 ± 58/5 min, *crmp2*$^{-/-}$ 164 ± 41/5 min, P = 0.015; call duration, WT 9.52 ± 2 ms, *crmp2*$^{-/-}$ 3.36 ± 1 ms, P = 0.011) and P12 (call rate, WT 46 ± 16/5 min *crmp2*$^{-/-}$ 1.54 ± 1.24/5 min, P = 0.002; call duration, WT 0.68 ± 0.35 ms, *crmp2*$^{-/-}$ 0.007 ± 0.006 ms, P = 0.002). Mean ± SEM, *P < 0.05, t-test (P6, P8), Mann–Whitney test (P12).

C Representative sonograms of the P8 mice.

D 3-chamber test (WT n = 11 mice, *crmp2*$^{-/-}$ n = 13 mice). In sociability phase, WT mice spent significantly more time with a social partner (stranger 1), unlike knockouts [WT—stranger 1: 0.14 ± 0.01, object: 0.07 ± 0.007 (P = 0.0001); *crmp2*$^{-/-}$—stranger 1: 0.07 ± 0.01, object: 0.04 ± 0.006 (P = 0.07)]. In social novelty phase, when an object was substituted with a second social partner (stranger 2), both WTs and knockouts preferred novel mice to known mice [WT—stranger 1: 0.03 ± 0.006, stranger 2: 0.09 ± 0.008 (P < 0.0001); *crmp2*$^{-/-}$—stranger 1: 0.02 ± 0.004, stranger 2: 0.05 ± 0.01 (P = 0.02)]. Mean ± SEM, *P < 0.05, ***P < 0.001, t-test.

E–G Elevated plus maze test (n = 10 mice/genotype). (E) Total distance walked is similar in WT and *crmp2*$^{-/-}$ (WT 7.9 ± 0.45 m, *crmp2*$^{-/-}$ 8.6 ± 0.5 m, P = 0.3). (F) Frequency and (G) duration of open arm (OA) visits are increased in *crmp2*$^{-/-}$ mice suggesting decreased anxiety. CA denotes closed arms, MID denotes the transition zone between arms, and total arm visits represent a sum of visits in all four arms. (CA frequency: WT 13.7 ± 0.9/5 min, *crmp2*$^{-/-}$ 10.5 ± 1.1/5 min, P = 0.04; OA frequency: WT 7.7 ± 0.8/5 min, *crmp2*$^{-/-}$ 14.6 ± 1.7/5 min, P = 0.002; MID frequency: WT 20.6 ± 1/5 min, *crmp2*$^{-/-}$ 24.6 ± 1.6/5 min, P = 0.06; total arm visits: WT 21.4 ± 1/5 min, *crmp2*$^{-/-}$ 25.1 ± 1.5/5 min, P = 0.07; CA duration: WT 177 ± 17 s, *crmp2*$^{-/-}$ 75.3 ± 12.6 s, P < 0.001; OA duration: WT 42 ± 12.6 s, *crmp2*$^{-/-}$ 144.4 ± 21 s, P < 0.001; MID duration: WT 80.26 ± 11.5 s, *crmp2*$^{-/-}$ 80.17 ± 12.6 s, P = 0.99), mean ± SEM, *P < 0.05, ***P < 0.001, t-test.

H, I Y-maze test (WT n = 9 mice, *crmp2*$^{-/-}$ n = 8 mice). Decreased alternations between arms of the maze indicate impaired working memory (number of visits, WT: 23.1 ± 1.9, *crmp2*$^{-/-}$ 30.4 ± 3.8, P = 0.12; alternations, WT 68.8 ± 2.5%, *crmp2*$^{-/-}$ 57.3 ± 2.5%, P = 0.006), mean ± SEM, *P < 0.05, t-test.

Sema3F binds preferentially to Nrp2/PlxnA3 receptor complex and is important regulator of neural development. Deficiency of Sema3F, Nrp2, or PlxnA3 results in defects in stereotyped pruning of hippocampal infrapyramidal bundle, distribution of DG dendritic spines, or anterior commissures, [42,55]. Moreover, *PlxnA3/A4*$^{-/-}$ mice display defects in pruning of visual axons. Similarly, in our *crmp2*$^{-/-}$ mice, we found all: IPB pruning defect, alteration of DG spine density (Figs 3 and 6), and defects in pruning of visual cortex axons (Fig 4). Moreover, our *in vitro* assays (Figs 5 and EV5) showed Sema3F is unable to induce axon and dendritic spine retraction in hippocampal neurons isolated from *crmp2*$^{-/-}$ embryos. In addition to Sema3F, IPB is also regulated by ephrin-B3 reverse signaling. It is possible to speculate that CRMP2, and in particular CRMP2A isoform, which is expressed in mossy fibers, conveys signaling of both Sema3F and ephrin-B3. Further studies will assess this hypothesis in more detail.

Sema3A has been shown to orchestrate pruning of, e.g., CA1 hippocamposeptal or callosal axons [3,33]. As CRMP2 has originally been identified as a mediator of Sema3A [8], we hypothesized that CRMP2 is involved also in Sema3A-triggered pruning. However, we did not find any evidence that would support this hypothesis. We did not detect DiI-positive CA1 neuron bodies by retrograde tracing from medial septum after the pruning period in *crmp2*$^{-/-}$ pups [6] (Fig EV3B). In callosal axons, we found significant differences in axon guidance between WT and *crmp2*$^{-/-}$ mice in P6–P9 mice (Fig 2), but the significance was lost in adult mice (Appendix Fig S1C–E), which could be due to the presence of effective Sema3A-dependent axon pruning. In line with these *in vivo* data, we found that Sema3A (but not Sema3F) was able to partially induce axon retraction of the stalling *crmp2*$^{-/-}$ axons in 1-week-old hippocampal neuron cultures (Fig 6). Relatively high variability in this experiment could be due to different sensitivity of individual synapses to semaphorin stimulation.

Importantly, we also did not find any defect in the pruning of neuromuscular junctions (NMJs) in *crmp2*$^{-/-}$ mice (Fig EV3C and D). At the end of the embryonic development, each synapse is innervated by up to 10 axon branches of different motor units [56]. During the first two postnatal weeks, all except one terminal branch are pruned back establishing singly innervated NMJs [60]. While the exact molecular cascade regulating motor axon pruning is not known, Sema3A seems to play a role in the process as its receptor, Nrp1, is expressed in pre-synaptic axon terminals [61]. Moreover, Sema3A secreted from Schwann cells participates in NMJ remodeling [62]. Sema3F signaling has so far not been linked to motor axon pruning.

Dendritic spine density changes dynamically during childhood and adolescence. In mice, spine density peaks around 1 month and then decreases to reach stable levels around 2 months [45]. It has been shown that distribution of dendritic spines is regulated by class 3 semaphorins [42]. Previous *in vitro* experiments showed that Sema3F, but not Sema3A, decreases PSD-95-positive puncta in dissociated DG neurons [42]. Accordingly, Sema3F-treated cortical neurons displayed decrease in apical dendrite spine density [42]. Adult *Sema3F*$^{-/-}$, *Nrp2*$^{-/-}$, and *PlxnA3*$^{-/-}$ mice show increased spine density in several brain regions, in particular DG dendrites [42,63]. *Crmp2*$^{-/-}$ mice partially mimic this phenotype as we also found increased spine density in adult, but not in P30 DG granule cells (Fig 6). Interestingly, in *Sema3F*$^{-/-}$ mice, increased DG spine density is detectable already during spine generation (P21) and is largely retained into adulthood, while in WT, they are subsequently pruned [42]. In *crmp2*$^{-/-}$ *mice*, we did not find increased DG spine density in the pre-pruning period (P30, Fig 6A), but similar to *Sema3F*$^{-/-}$ mice, we did find defects in DG spine pruning. Before pruning, spines also tended to be relatively enlarged in *crmp2*$^{-/-}$ mice (Fig EV5A). Similar observations were found in Sema3F- and Nrp2-deficient mice using electron microscopy [42]. Aberrant spine size could reflect disruption in actin dynamic. *In vitro* analysis of dendritic spine remodeling further supports our *in vivo* findings (Fig EV5). Together, these data suggest that while Sema3F signaling regulates both spine generation and pruning, CRMP2 contributes mainly to spine pruning.

CRMP2 in axonal growth *in vivo*

As demonstrated in knockout lines of Sema3A and its downstream targets (*Sema3A*$^{-/-}$, *Nrp1*$^{-/-}$, and *PlxnA4*$^{-/-}$ mice), Sema3A signaling is an essential regulator of the development of rodent trigeminal nerve, facial nerve, DRGs projection, olfactory bulb, hippocampal formation, and corpus callosum [27,28,33,34,64–67]. Surprisingly, although Sema3A or Nrp1 deletion causes strong

overgrowth of some peripheral nerves (e.g., trigeminal and spinal axons) [27,28], we found only a mild overgrowth and increased branching of these axons upon deletion of its downstream mediator CRMP2 in *crmp2*$^{-/-}$ mice (Figs 1 and EV2). This could be due to a partial rescue of Sema3A signaling in these neurons by other CRMP family members as mentioned before. Indeed, we and others [52] found that full CRMP2 deficiency *in vivo* is associated with increase of CRMP1 and CRMP4 levels (Fig EV2). CRMP1 and CRMP4 are sequentially and functionally close to CRMP2, and their expression pattern partially overlaps [68,69]. Moreover, CRMP4 (Fig EV2) and CRMP1 [70] are expressed in peripheral nerves suggesting that their elevation could rescue the reduced axon growth caused by acute CRMP2 deficiency. Increased expression of CRMP1 or CRMP4 could partially compensate for CRMP2 deficiency not only in Sema3A-dependent axon guidance but also in pruning, as we did not detect significant defects in Sema3A-dependent axon pruning in *crmp2*$^{-/-}$ neurons *in vivo* or *in vitro* (Figs 5 and EV3).

Previous *in vitro* studies demonstrated axon growth-promoting effect of CRMP2, while we did not detect any axon growth reduction in *crmp2*$^{-/-}$ mice. This may be because the role of CRMP2 in regulation of axon growth, neuron polarization, and migration has so far been studied *in vitro* using an acute knockdown of CRMP2 rather than *in vivo* in full knockout mice, which we used in our experiments and where the CRMP2 deficiency may be better compensated by other genes (e.g., CRMP1 or CRMP4).

Electroporation studies of *Sema3A*$^{-/-}$ or *Nrp1*$^{floxed/floxed}$ brains demonstrated their role in the development of corpus callosum, with mispositioned axons in callosal midline and axonal mistargeting in contralateral cortex at P8 [33]. Defects in axon pruning of this region were also suggested [33]. Using the *in utero* electroporation and DiI tracing in *crmp2*$^{-/-}$ mice, we also found defective guidance of callosal axons in the contralateral cortex and their altered orientation in the midline in the rostro-caudal axis (Fig 2).

Notably, Sema3F signaling is essential also for guidance of specific cranial nerves and was related to the development of limbic system and anterior commissure [40,71]. From these, we only detected partial malformation of AC in *crmp2*$^{-/-}$ mice (AC is missing in *Sema3F*$^{-/-}$ or *Nrp2*$^{-/-}$ mice) suggesting CRMP2 may participate also in Sema3F-mediated axon guidance (Fig EV4).

Previous *in vitro* and *in vivo* experiments suggested that CRMP2 also regulates neuronal migration [72]. However, using the *in utero* electroporation, we found no significant changes in neuron distribution in the developing WT and mutant cortical plates at E17.5 (Fig EV1F). This likely reflects different experimental paradigms used in the studies (somatic knockdown vs. full knockout) [72].

CRMP2 involvement in pathogenesis of neurodevelopmental disorders

Deregulation of CRMP2 has been linked to several neurodevelopmental disorders (*SFARI* Gene database, https://gene.sfari.org/database/human-gene/DPYSL2). Recently published analysis of conditional brain-specific [17] and full *crmp2* knockout mice [52] showed multiple behavioral defects associated with CRMP2 deficiency. Notably, conditional knockout mice revealed hyperactivity and prepulsed inhibition (PPI) deficit together with social behavior impairment. PPI is a test for evaluating sensorimotor gating—the phenomenon that is often altered in schizophrenia patients. In addition, clozapine (an antipsychotic drug) treatment was capable to reduce hyperactivity in conditional *crmp2*$^{-/-}$ mice. Furthermore, morphological analysis showed increased volume of brain ventricles and impaired dendritic development in hippocampal CA1 and DG neurons, which is associated with schizophrenia, but also other neurodevelopmental disorders [17]. Importantly, the analysis of the full and conditional CRMP2 knockout mice revealed also their significant differences. In particular, while PPI was reduced in the conditional mice and in the full *crmp2*$^{-/-}$ mice, it was not significantly different to WT [17,52]. This suggests that even a minor difference in the spatio-temporal inactivation of CRMP2 during development can have a major impact on the development and severity of the resulting neurodevelopmental defects. In the full CRMP2 knockout mice, we generated, we found several phenotypical defects present in the published conditional and full CRMP2 knockout mice (e.g., ventriculomegaly, spine density changes in DG, working memory defects, or hyperactivity) [17,73]. We also found brain sizes comparable in both WTs and *crmp2*$^{-/-}$ mice, similar as reported in the CRMP2 knockout mice [17,73], although we detected a non-significant tendency for a thinner cortex in the knockout mice (not shown) in agreement with the hypoplastic corpus callosum and anterior commissure. Changes in interhemispheric connectivity have recently been linked to ASD and schizophrenia through CYFIP1, a CRMP2 binding partner [74,75]. Importantly, we demonstrate that CRMP2 knockout leads to defects in axonal pruning and dendritic spine remodeling compatible with ASD rather than schizophrenia [25] (Figs 3, 4 and 6). Similar to other ASD mouse models [49], also in *crmp2*$^{-/-}$ mice the dendritic spine pruning deficiency is not present in all brain regions [e.g., we did not detect it in the prefrontal cortex (Fig 6F and G) or CA1 neurons (Fig EV5F and G)]. This may reflect specific spatio-temporal combinations of expression of CRMP2 (and its isoforms) and semaphorins in different brain regions (of note, there is a strong expression of CRMP2A isoform specifically in the inner molecular layer of DG (Fig EV1A), where we detected the pruning deficiency). The detail role of CRMP2 isoforms in axon pruning will be analyzed in future studies.

Morphological changes were accompanied by altered social communication in early postnatal (P8 and P12) mutants and decreased sociability in adults (Fig 7) further corroborating the role of CRMP2 in the pathogenesis of ASD. Defects in early postnatal USVs followed by dendritic spine pathology have been previously observed in several mouse models of ASD [49–51]. The connection between early postnatal altered sociability and impairment of stereotyped axon pruning is much less clear. Nevertheless, defects in stereotyped axon pruning have been associated with social interaction deficit and ASD in humans and mice, e.g., through functional variants and knockouts of Otx-1 gene [76,77].

Importantly, Sema3F signaling has been also implicated in the pathogenesis of ASD. Sema3F- or NRP2-deficient mice show both behavioral and neuropathological aspects of ASD [78], and Sema3F interacts with multiple ASD-related genes, e.g., fragile X mental retardation protein or MECP2 [79]. Thus, by linking Sema3F and CRMP2 signaling and comparing the histological as well as behavioral effects of their deficiency, our data strongly implicate that the Sema3F-CRMP2 signaling plays an important role in ASD pathogenesis. Since previously CRMP2 has been linked with pathogenesis of schizophrenia, it may serve as a

molecular link connecting class 3 semaphorin signaling defects to both ASD and schizophrenia.

Materials and Methods

Animals

All animal studies were ethically reviewed and performed in accordance with European directive 2010/63/EU and were approved by the Czech Central Commission for Animal Welfare. Mice, all in C57BL6/N background, were housed and handled according to the institutional committee guidelines with free access to food and water. Unless stated otherwise, adult mice used for experiments were 12–16 weeks old. See Appendix Table S1 for number of animals used in experiments.

Crmp2$^{-/-}$ mice generation

We used TALEN mutagenesis (transcription activator-like effector nucleases) to generate *crmp2*$^{-/-}$ mice. Two TALEN pairs targeting sequences 185–150 bp 5′ of *crmp2* exon 2 and 183–218 bp 3′ of exon 3 (Fig 1A) were designed using TAL Effector Nucleotide Targeter 2.0 (https://tale-nt.cac.cornell.edu/) [80,81], assembled using the Golden Gate Cloning system [80], and cloned into the ELD-KKR backbone plasmid. DNA-binding domains of TALENs specific for the desired target sites within the crmp2 locus consisted of following repeats: HD-HD-NN-HD-HD-HD-NG-NI-NN-HD-NG-NN-NN-NI-NG-HD-NG (5′ TALEN-crmp2-ex1), NN-HD-NI NI-NG-HD-HD-NG-HD-NG-NN-NG-HD-NG-HD-NG-NG (3′ TALEN-crmp2-ex1), HD-HD-NI-NI-NN-NI-NN-NG-HD-NI-HD-NG-NN-NI-NN-HD-NG-NG (5′ TALEN-crmp2-ex2), and NN-HD-NI-HD-NI-NG-NG-HD-NG-NI-HD-HD-NI-NI-NG-NN-NG (3′ TALEN-crmp2-ex2). All TALEN plasmids were used for production of TALEN encoding mRNA as described previously [82]. TALEN mRNAs (with total RNA concentration of 40 ng/μl) were microinjected into C57BL6/N-derived zygotes. Genomic DNA isolated from tail biopsies of newborn mice was screened by PCR for deletion of exons 1 and 2 (3,673 bp) (primers F1: 5′-ATATCCCACGATTCTGACCAATCA-3′ and R1: 5′-CCAAATAACTGCAGTGTAGCCTAT-3′), and deletion was confirmed by locus sequencing and mice used as founders of *crmp2*$^{-/-}$ line. The mouse line was genotyped by PCR using locus-specific primers: R1: ACTTACCGTGATGCGTGGAA, F1: TCACCCTCCCGGGACGAT, and R2: TCTACCAATGTTACAACACAGA.

Antibodies, cell dyes, and plasmids

Primary antibodies used in this study are as follows: mouse anti-CRMP2 and hamster anti-CRMP1 (WAKO, IHC 1:200, WB 1:5,000), rabbit anti-TUC4 (CRMP4, Millipore, IHC 1:400, WB 1:5,000), rabbit affinity purified anti-CRMP2A (IHC 1:75) [14], rabbit anti-CRMP2A (WB, 1:30,000) [14], mouse anti-neurofilaments (2H3 antigen, DSHB Iowa, 1:150), rabbit anti-MAP2 (Abcam, 1:300), rabbit anti-calbindin (Swant, 1:600), mouse anti-VgluT2 and anti-VGluT1 (Millipore, 1:400), goat anti-PSD95 (Millipore, 1:200), mouse anti-tau (Abcam, 1:500), mouse anti-βIII-Tubulin conjugated to Alexa 488 (BioLegend, 1:200), mouse anti-actin (Sigma, 1:500), and rabbit anti-βIII-Tubulin (Sigma, 1:500). Secondary fluorescent antibodies were conjugated with various Alexa Fluor dyes: anti-mouse (Alexa 488 or 594), anti-rabbit (Alexa 594), and anti-goat (Alexa 488), diluted 1:400. Hoechst 33342 (1 μg/ml) was used to counterstain cell nuclei. In some cases, ABC kit (Vector Laboratories) was used for detection. For whole-mount immunostaining, secondary anti-mouse antibody conjugated with HRP was used (1:1,000). For Western blots, secondary anti-mouse, anti-rabbit, or anti-hamster conjugated with HRP was used (1:10,000). Cholera toxin subunit B conjugated to Alexa 647, DiI, and DiO was purchased from Thermo Fisher. α-Bungarotoxin conjugated to Alexa 594 was purchased from Invitrogen (50 μg/ml; 1:50). EGFP was cloned into pCAGGS vector.

Histology, immunohistochemistry, and biochemistry

Mice were perfused transcardially with PBS and ice-cold 4% paraformaldehyde (PFA) in PBS. Brains were isolated and postfixed overnight at 4°C in 4% PFA/PBS. Subsequently, brains were washed in PBS and processed as described previously [14,83]. Seven-μm-thick paraffin sections were created. Immunohistochemistry was done as described previously [14]. Sections were deparaffinated as follows: 2 × 10 min 100% xylene, 2 × 10 min 100% ethanol, 3 min 90% EtOH, 3 min 70% EtOH, 3 min 50% EtOH, and PBS. Antigen retrieval was performed in some cases using citrate-based antigen retrieval solution (Vector) diluted 1:100 in water. Slices were blocked in 1% BSA/0.2% Tween/PBS (PBST) and incubated with primary antibodies overnight at 4°C. Next, slices were washed 3 × 5 min in PBST and incubated with secondary antibodies conjugated with Alexa Fluors, 2 h at RT. Then, slices were washed 3 × 5 min in PBST and mounted in Mowiol with Hoechst (1:1,000). For bright-field microscopy, slices were pretreated 15 min in 3% H_2O_2 prior to blocking and ABC kit (Vector) was used according to the manufacturer's instructions. HRP activity was detected with 0.05% DAB. Subsequently, slices were dehydrated in ethanol–xylene and embedded into Eukitt. Brain protein isolation, SDS–PAGE, and Western blotting were done as described previously [14].

Whole-mount immunohistochemistry

Whole-mount immunohistochemistry was performed as described previously [14] with some modifications. E10.5–E12.5 embryos were isolated from time-pregnant mothers. WTs and knockouts from the same litter were compared. Embryos were fixed in 4% PFA/PBS overnight, 4°C. Next day, they were washed with PBS and unmasked in 1:100 diluted antigen retrieval solution (Vector). Embryos were then washed again in PBS for 10 min (RT) followed 30 min in Dent fixative (20% DMSO/methanol) at 4°C. Subsequently, all samples were bleached overnight at 4°C in 5% H_2O_2/20% DMSO/methanol. Next, embryos were blocked overnight in 10% FBS/20% DMSO/PBS at 4°C and then incubated in anti-neurofilaments antibody clone 2H3 for 4 days (dilution 1:100 in blocking solution) followed by secondary HRP-conjugated antibody (1:1,000) for 24 h. Then, embryos were washed in 20% DMSO/PBS and incubated in 0.6% Tween/PBS overnight. Finally, samples were washed in PBS and incubated in 0.05% DAB for 2 h. H_2O_2 was then used as a substrate. Labeled embryos were washed in PBS and cleared in ascending glycerol concentration (20, 40, 60, and 80%). They were stored in 80% glycerol at 4°C. Images were captured using Nikon

SMZ18 stereomicroscope and post-processed in Helicon focus to create sharp images. Surface area occupied by a given nerve was measured in ImageJ. Axons were traced in Neurolucida 360.

DiOlistics and DiI tracing

We used DiOlistic approach using Gene Gun helium-powered system from Bio-Rad. Bullets were prepared as described [84], and tubing was coated with 10 mg/ml polyvinylpyrollidone (PVP). We mixed 100 mg Tungsten beads and 2.5 mg DiI or DiO (dissolved in CH_2Cl_2). After CH_2Cl_2 evaporation, resulted powder was transferred into aluminum-wrapped falcon tube and 3 ml H_2O was added. Solution was sonicated at 4°C until no clumps were visible (30–45 min). Then, solution was sucked into tubing in prep station, beads were able to settle down, and water was removed. Tubing was rotated 1 h during continuous drying with nitrogen (2–3 l/min). Finally, 1.3-cm bullets were cut from tubing and stored in 4°C with silica gel beads to prevent rehydration.

Slices for DiOlistics were prepared as follows: Mice were perfused with 20 ml 4% PFA/PBS, and brains were isolated and postfixed 30 min in 4% PFA/PBS. Then, brains were washed 1–3 h in PBS and 20 min in 15% sucrose/PBS following another 20 min in 30% sucrose/PBS. 250 μm coronal slices were prepared using vibratome Leica 2000S. Prior to shooting, slices were treated 5 min in 15% sucrose and 5 min in 30% sucrose. Dye was carried using pressure 120 Psi and modified filter as described [84]. After shooting, slices were washed 3× in PBS quickly and dye was let to diffuse 40 min at 4°C. Slices were then mounted onto glass slice in 0.5% n-propyl gallate/90% glycerol/PBS (NPG) and imaged by CARV II/Nikon Ti-E spinning disk.

For carbocyanine dye tracing, mice were perfused transcardially with PBS and fixed with 4% PFA/PBS. Next, either small DiI crystal was placed or 0.1 μl of DiI solution was injected into target area. We used 2.5 mg/100 μl concentration, and DiI was dissolved in DMSO. Slices were prepared in vibratome and scanned by Leica TCS SP8. Details are as follows.

Corpus callosum tracing

DiI solution was injected into superficial layers of cortex. Brains were maintained in 4% PFA/PBS in 37°C for 3–4 weeks. Then, brains were cut in oblique (horizontal + 20°) direction (Appendix Fig S1A), 150-μm-thick sections were prepared. Slices with traced axons were mounted onto glass slide in NPG mounting solution.

Hippocamposeptal axon tracing

After fixation, brains were trimmed to expose septum. DiI crystals were inserted into the medial septum and brains were maintained in 4% PFA/PBS for 1–2 weeks. 100 μm (P0–1) or 150 μm (P8) coronal slices were prepared. We found a strong labeling of septohippocampal projections (e.g., axons arising from the septum entering the hippocampus) and also subicular neurons projecting to the medial septum in both WTs and knockouts. We screened for retrogradely labeled CA1 neuron bodies in the hippocampus, whose presence at P8 indicates incomplete pruning.

Visual corticospinal axon tracing

DiI solution was injected into primary visual area. After 2–3 weeks, brains were cut sagitally to 150–180-μm slices that were mounted in NPG with Hoechst. The tracing pattern was compared with data from Allen brain atlas connectivity studies to ensure that we targeted correct area. We observed two axon branches in the diencephalon: first branch growing into pyramidal tract (corticospinal axons) and second to superior colliculus (collicular axons). To quantify the axonal growth into the pyramidal tract, we compared fluorescence intensity of corticospinal axons vs. intensity of axons before branching. We refer to this ratio as visual pruning index (VP index), with its lower values indicating the presence of refinement.

In utero electroporations

In utero electroporations were done as previously described [85]. Briefly, pregnant mice were anaesthetized by 2.5% isoflurane. Anesthesia was maintained by 2% isoflurane. We injected pCAGGS-EGFP plasmid (3 μg/μl) into ventricles of E14.5 embryos (migration assay, analysis at E17.5) or E15.5 embryos (callosal axons, analyzed at P6). Electroporation was carried out by small paddle electrodes (35 V, five pulses, 950-ms interval) to target sensory cortex. For migration assays, embryos were harvested at E17.5, and brains were fixed in 4% PFA/PBS, sliced (150-μm vibratome sections), counterstained with Hoechst, and scanned by Leica TCS SP8. In this case only, both WTs and *crmp2*$^{+/-}$ embryos were used as controls. Callosal axons were analyzed at P6. After birth, pups were nurtured by a foster mother. At P6, mice were sacrificed, and brains were fixed in 4% PFA/PBS, sliced (150 μm vibratome sections), and analyzed by CARV II/Nikon Ti-E spinning disk.

Semaphorin assays and live imaging

Mouse E16.5 hippocampal neurons were prepared and cultured as described [14]. Briefly, pregnant mice were sacrificed, and embryos isolated and decapitated in cold HBSS with 10 mM Hepes. Hippocampi were isolated, moved to Neurobasal medium (Neurobasal (Gibco) with 2.5% B27 supplement (Gibco), 2.5 mM glutamine, and 1% penicillin/streptomycin solution), and triturated. Subsequently, solution was strained through a 40-μm strainer (Biologix) and spun down (300 *g*, 2 min, 4°C). The supernatant was removed, and the remaining cells were resuspended in a fresh Neurobasal medium and counted. Neurons were plated into 24-glass bottom plates (100,000 cells/well) coated with laminin (1 μg/ml) and poly-D-lysine (50 μg/ml) and cultured in Neurobasal medium that was refreshed every 2–3 days. Neurons were transfected with pCAGGS-EGFP using Lipofectamine 2000 (Invitrogen), 24 h after plating (axon retraction assay) or at DIV14 (dendritic spine analysis). Mouse semaphorin 3A and 3F (carrier free) or control Fc were purchased from R&D systems and were diluted to 1 mg/ml stock concentration. For axon retraction assay at DIV 7, medium volume was adjusted to 300 μl in each well. Neurons were photographed three times (with 20 min gaps), and then, 50 μl of fresh medium with Fc or Sema3A (final concentration 1 nM) or Sema3F (final concentration 5 nM) was added. Subsequently, neurons were imaged every 20 min for 16 h by Leica DMI6000 equipped with a heating box and CO_2 atmosphere. For analysis of dendritic spines, the same segments were photographed at DIV21 and DIV25. At DIV25, neurons were stimulated with Sema3F (5 nM) for 3 h and photographed again.

Microfluidic chambers and DRG collapse assay

Microfluidic chambers were prepared as described before [31,86]. E11.5–E12.5 spinal cord explants were dissected in cold HBSS and placed into laminin (3 μg/ml)- and poly-L-ornithine (1.5 μg/ml)-coated proximal well. After 3–4 days, axons entered the distal compartment. Then, explants were labeled by Alexa 647-conjugated cholera toxin subunit B. 5 nM Sema3A of control Fc was applied distally, and axons were photographed by Leica DMI6000 microscope every 10 min during 14-h interval. Axons growing at least 50 μm were analyzed. Growth cone collapse was analyzed in DRG explants isolated at E11.5–E12.5. DRGs were plated on coverslips coated with laminin (1 μg/ml) and poly-D-lysine (50 μg/ml) and cultured in Neurobasal medium supplemented with NGF (R&D systems, 25 ng/ml). The day after plating, explants were stimulated with various Sema3A concentrations for 30 min, fixed, and stained with antibodies against actin (to label growth cones) and β-3 tubulin (to label axons). DRGs were imaged by Nikon spinning disk.

Analysis of developmental motor axon pruning

WT and *crmp2*$^{-/-}$ pups (both sexes) were sacrificed on P11, and the thorax was excised as previously described [87–90] and fixed in 4% PFA in 0.1 M phosphate buffer (PB) for 1 h on ice. The triangularis sterni muscle was dissected and incubated overnight (4°C) in anti-βIII-tubulin antibody conjugated to Alexa 488 (BioLegend 801203; 1:200)- and Alexa 594-conjugated α-bungarotoxin (Invitrogen B13423; 50 μg/ml; 1:50) in blocking solution (5% BSA, 0.5% Triton X-100 in 0.1 M PB). Muscles were then washed in 0.1 M PB and mounted in Vectashield (Vector Laboratories). *Z*-stacks were recorded using a confocal microscope (FV1000, Olympus) equipped with a 20×/0.8 N.A. oil-immersion objective and analyzed for the percentage of doubly innervated NMJs using Fiji (cell counter plugin) [91].

Behavioral tests

1 Ultrasonic vocalizations were recorded from P6, P8, and P12 pups (WT n = 14, *crmp2*$^{-/-}$ n = 13). Each pup was taken from its home cage, put into Styrofoam box, and recorded for 5 min with microphone (Dodotronic Ultramic 250K, Italy) placed at the top of the box. Audacity software (freely available) was used for recordings with sampling frequency set to 250 kHz. The vocalizations were analyzed automatically using Avisoft-SASLab Pro; however, the automatic analysis was checked and manually corrected if necessary. Main parameters measured were number of vocalizations and its total length.

2 Sociability and social novelty preference were tested in three-chambered apparatus (54 × 20 × 33 cm) made from clear plexiglass. The chambers were divided by transparent walls with squared openings (5 × 5 cm) and sliding doors. Each mouse (WT n = 11, *crmp2*$^{-/-}$ n = 13) was first placed in the middle compartment for 10 min. After the habituation, unknown male mice (stranger 1) were enclosed in a little wire cage and placed in either left or right compartment. Black plug (4.5 cm in diameter) was used as an object and placed in the opposite compartment inside identical wire cage. The position of stranger mouse and object was counterbalanced between trials, and stranger mice were previously habituated to the cage. Sliding doors were then opened, and the test mouse was allowed to freely explore the apparatus for 10 min. After end of this part of experiment, the object was removed and another unknown mouse (stranger 2) was put inside the same chamber. The test mouse was then allowed to explore all chambers for another 5 min. The behavior was recorded by a camera placed above the apparatus. Time spent in each chamber and time spent sniffing the wire cages were analyzed manually in BORIS software.

3 The elevated plus maze (EPM) is a cross-shaped maze elevated 40 cm above the floor level, with all four arms (30 cm long, 5 cm wide, 16 cm high) accessible from the central platform. Two opposite arms were enclosed by opaque walls (closed arms), while the other two were without walls (open arms). The test assesses spontaneous and anxiety-like behaviors of the animals. The closed arms are perceived as safer by the animals, as they are darker, more protected, and without risk of falling. Anxious animals are expected to spend most of the time in the closed arms, while less anxious and more explorative individuals explore the open arms more often. The behavior of the animals during each 5-min session was recorded by a web camera placed above the apparatus. Locomotor activity (total distance) and time spent in different compartments were analyzed offline by digital tracking software (EthoVision, Noldus). Numbers of animals: n = 10 for both WT and knockouts, aged 31–44 weeks.

4 Spontaneous alternation was tested in three-armed maze (Y-maze), with each arm 35 cm long, 6 cm wide, and 18 cm high. The mice were left free to explore the empty apparatus for 8 min. Between trials, the apparatus was cleaned by ethanol and then wiped clean and dry to erase any scent marks. Number of arm visits was counted, indicating the exploratory activity (a visit was counted if the mouse placed all paws into the arm). Spontaneous alternation was measured as the ratio of actual triads (three different arms entered in three subsequent visits) to potential triads (theoretical maximum performance). In the Y-maze task, 17 male mice (9 WT, 8 KO), aged 31–44 weeks, were tested.

5 The active place avoidance task, or AAPA [92,93] (for review, see Ref. [94]), is a rodent cognitive task testing hippocampal functions, including spatial navigation, cognitive coordination, and flexibility. As a dry-arena task, it is more suitable for mice than the Morris water maze, as mice are worse swimmers than rats and tend to be overtly stressed by water immersion [95]. We used a carousel maze (circular arena 56 cm in diameter) with electrified grid floor, surrounded by a transparent plexiglass wall, rotating at approximately 1 rotation per minute. The apparatus was located in a dimly lit room with abundant extramaze cues, with and additional, highly contrast cue card in close proximity (1.5 m) of the arena. A computer-based tracking system (Tracker, Biosignal Group, USA) recorded the positions of the mouse and the arena at a sampling rate of 25 Hz. A 60-deg unmarked to-be-avoided sector was defined in the coordinate frame of the room by tracking software. Each entrance into the sector was punished by mild electric foot shocks (scrambled; 100 Hz alternating current; 40–80 V) delivered by the tracking system into the grid floor. Each shock lasted 0.5 s and was

repeated after 0.9 s if the mouse failed to escape the to-be-avoided sector in time. Intensity of the shock was individualized for each mouse (0.2–0.4 mA), to ensure escape reaction while avoiding excessive pain. The training schedule consisted of five acquisition sessions and four reversal sessions, where the sector position was changed by 180°. Two 10-min sessions were scheduled for each experimental day, separated by approximately 3 h of rest in the home cage. The arena rotated while the sector remained fixed in the reference frame of the room; therefore, the mice had to move actively away from the sector in the direction opposite to arena rotation; otherwise, they would be carried into the sector. For successful avoidance, the animal had to separate the distant room-frame cues, which could be used to locate and avoid the sector, from the irrelevant, arena-frame cues. Selection of the correct spatial cues and achievement of the correct behavioral strategy requires segregation of spatial frames, a skill that is considered equivalent of human cognitive coordination [96]. Furthermore, cognitive flexibility was tested in reversal sessions, to adjust the behavioral response to reversed sector location. The trajectory of the mice was analyzed offline using the custom-made and freely available Carousel Maze Manager 4.0 [97]. Total distance walked, a measure of locomotor activity of the mouse, and the number of entrances, a measure of its ability to avoid entering the to-be-avoided sector, were used as the most important output parameters. Active place avoidance performance was evaluated by two consecutive RM-ANOVA analyses, with sessions taken as repeated measures, and genotype as a between-subject factor. In this task, 21 male mice (11 KO, 10 WT), 12–14 weeks old, were tested.

Light microscopy

Five types of microscopes were used in this study: (i) Leica TCS SP8 confocal equipped with 405-nm laser (Hoechst), 488-nm laser (DiO, EGFP excitation), 552-nm laser (DiI excitation), 10×/0.3 dry, and 25×/0.75 immerse-oil objectives (Figs 2G, 4, 6D, F, EV1F, EV3B, and EV5B, D, Appendix Fig S1C). (ii) Inverted fluorescent microscope Leica DMI6000 equipped with 20×/0.4 dry objective, 37°C incubator, and CO_2 chamber for live imaging (Figs 1F and 5). (iii) CARV II/Nikon Ti-E spinning disk equipped with 20×/0.5 dry, 40×/1.3, and 100×/1.4 immerse-oil objectives (Figs 1B, 2C, D, 3, 6A, B, F, EV1A, F, EV2G, EV3A, EV4A, D, and EV5A, F). (iv) Olympus FV1000 confocal microscope equipped with 20×/0.8 objective (Fig EV3C). (v) Nikon SMZ18 stereomicroscope for microdissections and whole-mount analysis equipped with 1× and 2× SHR Plan Apo objectives (Figs 1C, 2A, EV1C, D, EV2A, B, E, F, and EV4B). Microscopy images from Figs 1–4 and EV1, EV3, and EV4 are compositions of more fields automatically generated by Leica LAS X software or NIS elements software. Maximum projections were generated in ImageJ.

Image processing and statistics

We used Neurolucida 360 software to reconstruct callosal axons from both *in utero* electroporation and DiI-tracing experiments. In case of oblique sections, we picked only midline regions (approximately 100 μm from midline to each side) and traced axons semi-automatically using AutoNeuron algorithm. To display overall axon growth direction, polar histograms and fan-in diagrams were generated using Neurolucida explorer. Polar histograms show total axon length in a specific degree range. We counted lengths in each 20° of histogram. Fan-in diagrams represent the same in another graphical view when all traced axons rise from a single point. Dendrites and dendritic spines were analyzed either with Neurolucida360 or with NeuronJ plugin in ImageJ. Spine head diameter was measured after 3D reconstruction of spines in Neurolucida 360. Images from whole-mount preparations were processed in Helicon focus to create sharp projections. Growth of peripheral nerves and all data from time-lapse imaging series were analyzed in ImageJ. Neuron migration was analyzed in ImageJ using cell counter plugin. Measurements of axon pruning from immunohistochemistry and DiI-tracing experiments were done in ImageJ. In all figures, different channels of image series were combined in pseudo-color using the "screen" function in Adobe Photoshop and adjusted to enhance low-intensity objects. GraphPad Prism was used for statistical analysis. For comparison of two independent groups, unpaired *t*-test was used unless stated otherwise. Multiple comparisons were performed using two-way ANOVA. Data from behavioral experiments were analyzed by unpaired *t*-test (P6, P8 vocalization, sociability, Y-maze, EPM), ANOVA (AAPA), or Mann–Whitney test (P12 vocalization). All data are presented as means ± SD, unless stated otherwise.

Expanded View for this article is available online.

Acknowledgements

The work of MB, JZ, MJ, TP, BP, and AS was supported by Czech Health Research Council grant no. NV18-04-00085. MB, RW, BP, JZ, and MK were supported by Czech Science Foundation grant no. 16-15915S. The work of JZ, RW, and BP was supported by Grant Agency of the Charles University grant nos. 682217, 524218, and 1062216, respectively. MJ, TP, and AS were supported by Czech Science Foundation grant no. 19-03016S and Czech Health Research Council grant no 17-30833A. MW, MSB, and TM were supported by the ERC (FP/2007-2013; ERC Grant Agreement No. 616791), the German-Israeli Foundation, SFB 870, DFG grant CRC870-A11, and the Munich Cluster for Systems Neurology (SyNergy; EXC2145). RS was supported by RVO 68378050 by Academy of Sciences of the Czech Republic. Czech Centre for Phenogenomics infrastructure, used during the project, was supported by grants LM2015040, CZ.1.05/2.1.00/19.0395, and CZ.1.05/1.1.00/02.0109 funded by the Ministry of Education, Youth and Sports and the European Regional Development Fund. We are grateful to Dr. Jan Krůšek from the Department of Cellular Neurophysiology, Institute of Physiology, CAS, Prague, for his help with preparation of glass micropipettes. We acknowledge the Microscopy Centre—Light Microscopy Core Facility, IMG ASCR, Prague, Czech Republic, supported by MEYS (LM2015062), OPPK (CZ.2.16/3.1.00/21547) and (LO1419), and Light Microscopy Core Facility, IPHYS ASCR, Prague, Czech Republic, supported by MEYS (LM2015062 Czech-BioImaging) for their support with confocal and live imaging.

Author contributions

Study design: MB, JZ; data acquisition and analysis: JZ, MB, RW, KJ, MJ, RM, TP, BP, MW, MSB, MK, PK, XZ; supervision: MB, EP, AS, RS, TM, GA-B; writing—original draft: JZ, MB, MSB; writing—review and editing: JZ, MB, GA-B, TM, RM, AS, TP, MSB; project administration: MB.

Conflict of interest

The authors declare that they have no conflict of interest.

References

1. Riccomagno MM, Kolodkin AL (2015) Sculpting neural circuits by axon and dendrite pruning. *Annu Rev Cell Dev Biol* 31: 779 – 805
2. Johnston MV (2004) Clinical disorders of brain plasticity. *Brain Dev* 26: 73 – 80
3. Vanderhaeghen P, Cheng HJ (2010) Guidance molecules in axon pruning and cell death. *Cold Spring Harb Perspect Biol* 2: a001859
4. Van Battum EY, Brignani S, Pasterkamp RJ (2015) Axon guidance proteins in neurological disorders. *Lancet Neurol* 14: 532 – 546
5. Yu F, Schuldiner O (2014) Axon and dendrite pruning in *Drosophila*. *Curr Opin Neurobiol* 27: 192 – 198
6. Bagri A, Cheng HJ, Yaron A, Pleasure SJ, Tessier-Lavigne M (2003) Stereotyped pruning of long hippocampal axon branches triggered by retraction inducers of the semaphorin family. *Cell* 113: 285 – 299
7. Low LK, Liu XB, Faulkner RL, Coble J, Cheng HJ (2008) Plexin signaling selectively regulates the stereotyped pruning of corticospinal axons from visual cortex. *Proc Natl Acad Sci USA* 105: 8136 – 8141
8. Goshima Y, Nakamura F, Strittmatter P, Strittmatter SM (1995) Collapsin-induced growth cone collapse mediated by an intracellular protein related to UNC-33. *Nature* 376: 509 – 514
9. Byk T, Dobransky T, Cifuentes-Diaz C, Sobel A (1996) Identification and molecular characterization of Unc-33-like phosphoprotein (Ulip), a putative mammalian homolog of the axonal guidance-associated unc-33 gene product. *J Neurosci* 16: 688 – 701
10. Minturn JE, Fryer HJ, Geschwind DH, Hockfield S (1995) TOAD-64, a gene expressed early in neuronal differentiation in the rat, is related to unc-33, a *C. elegans* gene involved in axon outgrowth. *J Neurosci* 15: 6757 – 6766
11. Fukata Y, Itoh TJ, Kimura T, Menager C, Nishimura T, Shiromizu T, Watanabe H, Inagaki N, Iwamatsu A, Hotani H *et al* (2002) CRMP-2 binds to tubulin heterodimers to promote microtubule assembly. *Nat Cell Biol* 4: 583 – 591
12. Uchida Y, Ohshima T, Sasaki Y, Suzuki H, Yanai S, Yamashita N, Nakamura F, Takei K, Ihara Y, Mikoshiba K *et al* (2005) Semaphorin3A signalling is mediated via sequential Cdk5 and GSK3beta phosphorylation of CRMP2: implication of common phosphorylating mechanism underlying axon guidance and Alzheimer's disease. *Genes Cells* 10: 165 – 179
13. Yuasa-Kawada J, Suzuki R, Kano F, Ohkawara T, Murata M, Noda M (2003) Axonal morphogenesis controlled by antagonistic roles of two CRMP subtypes in microtubule organization. *Eur J Neurosci* 17: 2329 – 2343
14. Balastik M, Zhou XZ, Alberich-Jorda M, Weissova R, Ziak J, Pazyra-Murphy MF, Cosker KE, Machonova O, Kozmikova I, Chen CH *et al* (2015) Prolyl isomerase Pin1 regulates axon guidance by stabilizing CRMP2A selectively in distal axons. *Cell Rep* 13: 812 – 828
15. Yoshimura T, Kawano Y, Arimura N, Kawabata S, Kikuchi A, Kaibuchi K (2005) GSK-3beta regulates phosphorylation of CRMP-2 and neuronal polarity. *Cell* 120: 137 – 149
16. Arimura N, Menager C, Kawano Y, Yoshimura T, Kawabata S, Hattori A, Fukata Y, Amano M, Goshima Y, Inagaki M *et al* (2005) Phosphorylation by Rho kinase regulates CRMP-2 activity in growth cones. *Mol Cell Biol* 25: 9973 – 9984
17. Zhang H, Kang E, Wang Y, Yang C, Yu H, Wang Q, Chen Z, Zhang C, Christian KM, Song H *et al* (2016) Brain-specific Crmp2 deletion leads to neuronal development deficits and behavioural impairments in mice. *Nat Commun* 7: 11773
18. Makihara H, Nakai S, Ohkubo W, Yamashita N, Nakamura F, Kiyonari H, Shioi G, Jitsuki-Takahashi A, Nakamura H, Tanaka F *et al* (2016) CRMP1 and CRMP2 have synergistic but distinct roles in dendritic development. *Genes Cells* 21: 994 – 1005
19. Nakata K, Ujike H, Sakai A, Takaki M, Imamura T, Tanaka Y, Kuroda S (2003) The human dihydropyrimidinase-related protein 2 gene on chromosome 8p21 is associated with paranoid-type schizophrenia. *Biol Psychiatry* 53: 571 – 576
20. Liu Y, Pham X, Zhang L, Chen PL, Burzynski G, McGaughey DM, He S, McGrath JA, Wolyniec P, Fallin MD *et al* (2014) Functional variants in DPYSL2 sequence increase risk of schizophrenia and suggest a link to mTOR signaling. *G3 (Bethesda)* 5: 61 – 72
21. Clark D, Dedova I, Cordwell S, Matsumoto I (2006) A proteome analysis of the anterior cingulate cortex gray matter in schizophrenia. *Mol Psychiatry* 11: 459 – 470, 423
22. Quach TT, Honnorat J, Kolattukudy PE, Khanna R, Duchemin AM (2015) CRMPs: critical molecules for neurite morphogenesis and neuropsychiatric diseases. *Mol Psychiatry* 20: 1037 – 1045
23. Braunschweig D, Krakowiak P, Duncanson P, Boyce R, Hansen RL, Ashwood P, Hertz-Picciotto I, Pessah IN, Van de Water J (2013) Autism-specific maternal autoantibodies recognize critical proteins in developing brain. *Transl Psychiatry* 3: e277 .
24. De Rubeis S, He X, Goldberg AP, Poultney CS, Samocha K, Cicek AE, Kou Y, Liu L, Fromer M, Walker S *et al* (2014) Synaptic, transcriptional and chromatin genes disrupted in autism. *Nature* 515: 209 – 215
25. Lord C, Elsabbagh M, Baird G, Veenstra-Vanderweele J (2018) Autism spectrum disorder. *Lancet* 392: 508 – 520
26. Bourgeron T (2015) From the genetic architecture to synaptic plasticity in autism spectrum disorder. *Nat Rev Neurosci* 16: 551 – 563
27. Kitsukawa T, Shimizu M, Sanbo M, Hirata T, Taniguchi M, Bekku Y, Yagi T, Fujisawa H (1997) Neuropilin-semaphorin III/D-mediated chemorepulsive signals play a crucial role in peripheral nerve projection in mice. *Neuron* 19: 995 – 1005
28. Taniguchi M, Yuasa S, Fujisawa H, Naruse I, Saga S, Mishina M, Yagi T (1997) Disruption of semaphorin III/D gene causes severe abnormality in peripheral nerve projection. *Neuron* 19: 519 – 530
29. Chen H, Bagri A, Zupicich JA, Zou Y, Stoeckli E, Pleasure SJ, Lowenstein DH, Skarnes WC, Chedotal A, Tessier-Lavigne M (2000) Neuropilin-2 regulates the development of selective cranial and sensory nerves and hippocampal mossy fiber projections. *Neuron* 25: 43 – 56
30. Cheng HJ, Bagri A, Yaron A, Stein E, Pleasure SJ, Tessier-Lavigne M (2001) Plexin-A3 mediates semaphorin signaling and regulates the development of hippocampal axonal projections. *Neuron* 32: 249 – 263
31. Maimon R, Ionescu A, Bonnie A, Sweetat S, Wald-Altman S, Inbar S, Gradus T, Trotti D, Weil M, Behar O *et al* (2018) miR126-5p downregulation facilitates axon degeneration and NMJ disruption via a non-cell-autonomous mechanism in ALS. *J Neurosci* 38: 5478 – 5494
32. Brown M, Jacobs T, Eickholt B, Ferrari G, Teo M, Monfries C, Qi RZ, Leung T, Lim L, Hall C (2004) Alpha2-chimaerin, cyclin-dependent Kinase 5/p35, and its target collapsin response mediator protein-2 are essential components in semaphorin 3A-induced growth-cone collapse. *J Neurosci* 24: 8994 – 9004
33. Zhou J, Wen Y, She L, Sui YN, Liu L, Richards LJ, Poo MM (2013) Axon position within the corpus callosum determines contralateral cortical projection. *Proc Natl Acad Sci USA* 110: E2714 – E2723
34. Wu KY, He M, Hou QQ, Sheng AL, Yuan L, Liu F, Liu WW, Li G, Jiang XY, Luo ZG (2014) Semaphorin 3A activates the guanosine triphosphatase

Rab5 to promote growth cone collapse and organize callosal axon projections. *Sci Signal* 7: ra81

35. Wang CL, Zhang L, Zhou Y, Zhou J, Yang XJ, Duan SM, Xiong ZQ, Ding YQ (2007) Activity-dependent development of callosal projections in the somatosensory cortex. *J Neurosci* 27: 11334 – 11342
36. Penzes P, Cahill ME, Jones KA, VanLeeuwen JE, Woolfrey KM (2011) Dendritic spine pathology in neuropsychiatric disorders. *Nat Neurosci* 14: 285 – 293
37. Garey L (2010) When cortical development goes wrong: schizophrenia as a neurodevelopmental disease of microcircuits. *J Anat* 217: 324 – 333
38. Liu XB, Low LK, Jones EG, Cheng HJ (2005) Stereotyped axon pruning via plexin signaling is associated with synaptic complex elimination in the hippocampus. *J Neurosci* 25: 9124 – 9134
39. Linke R, Pabst T, Frotscher M (1995) Development of the hippocamposeptal projection in the rat. *J Comp Neurol* 351: 602 – 616
40. Sahay A, Molliver ME, Ginty DD, Kolodkin AL (2003) Semaphorin 3F is critical for development of limbic system circuitry and is required in neurons for selective CNS axon guidance events. *J Neurosci* 23: 6671 – 6680
41. Basarsky TA, Parpura V, Haydon PG (1994) Hippocampal synaptogenesis in cell culture: developmental time course of synapse formation, calcium influx, and synaptic protein distribution. *J Neurosci* 14: 6402 – 6411
42. Tran TS, Rubio ME, Clem RL, Johnson D, Case L, Tessier-Lavigne M, Huganir RL, Ginty DD, Kolodkin AL (2009) Secreted semaphorins control spine distribution and morphogenesis in the postnatal CNS. *Nature* 462: 1065 – 1069
43. Yamashita N, Morita A, Uchida Y, Nakamura F, Usui H, Ohshima T, Taniguchi M, Honnorat J, Thomasset N, Takei K *et al* (2007) Regulation of spine development by semaphorin3A through cyclin-dependent kinase 5 phosphorylation of collapsin response mediator protein 1. *J Neurosci* 27: 12546 – 12554
44. Petanjek Z, Judas M, Simic G, Rasin MR, Uylings HB, Rakic P, Kostovic I (2011) Extraordinary neoteny of synaptic spines in the human prefrontal cortex. *Proc Natl Acad Sci USA* 108: 13281 – 13286
45. Bian WJ, Miao WY, He SJ, Qiu Z, Yu X (2015) Coordinated spine pruning and maturation mediated by inter-spine competition for cadherin/catenin complexes. *Cell* 162: 808 – 822
46. Garey LJ, Ong WY, Patel TS, Kanani M, Davis A, Mortimer AM, Barnes TR, Hirsch SR (1998) Reduced dendritic spine density on cerebral cortical pyramidal neurons in schizophrenia. *J Neurol Neurosurg Psychiatry* 65: 446 – 453
47. Ey E, Torquet N, Le Sourd AM, Leblond CS, Boeckers TM, Faure P, Bourgeron T (2013) The Autism ProSAP1/Shank2 mouse model displays quantitative and structural abnormalities in ultrasonic vocalisations. *Behav Brain Res* 256: 677 – 689
48. Hung AY, Futai K, Sala C, Valtschanoff JG, Ryu J, Woodworth MA, Kidd FL, Sung CC, Miyakawa T, Bear MF *et al* (2008) Smaller dendritic spines, weaker synaptic transmission, but enhanced spatial learning in mice lacking Shank1. *J Neurosci* 28: 1697 – 1708
49. Schmeisser MJ, Ey E, Wegener S, Bockmann J, Stempel AV, Kuebler A, Janssen AL, Udvardi PT, Shiban E, Spilker C *et al* (2012) Autistic-like behaviours and hyperactivity in mice lacking ProSAP1/Shank2. *Nature* 486: 256 – 260
50. Binder MS, Lugo JN (2017) NS-Pten knockout mice show sex- and age-specific differences in ultrasonic vocalizations. *Brain Behav* 7: e00857
51. Reynolds CD, Nolan SO, Jefferson T, Lugo JN (2016) Sex-specific and genotype-specific differences in vocalization development in FMR1 knockout mice. *NeuroReport* 27: 1331 – 1335
52. Nakamura H, Yamashita N, Kimura A, Kimura Y, Hirano H, Makihara H, Kawamoto Y, Jitsuki-Takahashi A, Yonezaki K, Takase K *et al* (2016) Comprehensive behavioral study and proteomic analyses of CRMP2-deficient mice. *Genes Cells* 21: 1059 – 1079
53. Kjelstrup KG, Tuvnes FA, Steffenach HA, Murison R, Moser EI, Moser MB (2002) Reduced fear expression after lesions of the ventral hippocampus. *Proc Natl Acad Sci USA* 99: 10825 – 10830
54. Luo L, O'Leary DD (2005) Axon retraction and degeneration in development and disease. *Annu Rev Neurosci* 28: 127 – 156
55. Riccomagno MM, Hurtado A, Wang H, Macopson JG, Griner EM, Betz A, Brose N, Kazanietz MG, Kolodkin AL (2012) The RacGAP beta2-Chimaerin selectively mediates axonal pruning in the hippocampus. *Cell* 149: 1594 – 1606
56. Tapia JC, Wylie JD, Kasthuri N, Hayworth KJ, Schalek R, Berger DR, Guatimosim C, Seung HS, Lichtman JW (2012) Pervasive synaptic branch removal in the mammalian neuromuscular system at birth. *Neuron* 74: 816 – 829
57. Brill MS, Kleele T, Ruschkies L, Wang M, Marahori NA, Reuter MS, Hausrat TJ, Weigand E, Fisher M, Ahles A *et al* (2016) Branch-specific microtubule destabilization mediates axon branch loss during neuromuscular synapse elimination. *Neuron* 92: 845 – 856
58. Xu NJ, Henkemeyer M (2009) Ephrin-B3 reverse signaling through Grb4 and cytoskeletal regulators mediates axon pruning. *Nat Neurosci* 12: 268 – 276
59. Cocchi E, Drago A, Serretti A (2016) Hippocampal pruning as a new theory of schizophrenia etiopathogenesis. *Mol Neurobiol* 53: 2065 – 2081
60. Sanes JR, Lichtman JW (1999) Development of the vertebrate neuromuscular junction. *Annu Rev Neurosci* 22: 389 – 442
61. Venkova K, Christov A, Kamaluddin Z, Kobalka P, Siddiqui S, Hensley K (2014) Semaphorin 3A signaling through neuropilin-1 is an early trigger for distal axonopathy in the SOD1G93A mouse model of amyotrophic lateral sclerosis. *J Neuropathol Exp Neurol* 73: 702 – 713
62. De Winter F, Vo T, Stam FJ, Wisman LA, Bar PR, Niclou SP, van Muiswinkel FL, Verhaagen J (2006) The expression of the chemorepellent Semaphorin 3A is selectively induced in terminal Schwann cells of a subset of neuromuscular synapses that display limited anatomical plasticity and enhanced vulnerability in motor neuron disease. *Mol Cell Neurosci* 32: 102 – 117
63. Demyanenko GP, Mohan V, Zhang X, Brennaman LH, Dharbal KE, Tran TS, Manis PB, Maness PF (2014) Neural cell adhesion molecule NrCAM regulates Semaphorin 3F-induced dendritic spine remodeling. *J Neurosci* 34: 11274 – 11287
64. Schwarting GA, Kostek C, Ahmad N, Dibble C, Pays L, Puschel AW (2000) Semaphorin 3A is required for guidance of olfactory axons in mice. *J Neurosci* 20: 7691 – 7697
65. Friedel RH, Plump A, Lu X, Spilker K, Jolicoeur C, Wong K, Venkatesh TR, Yaron A, Hynes M, Chen B *et al* (2005) Gene targeting using a promoterless gene trap vector ("targeted trapping") is an efficient method to mutate a large fraction of genes. *Proc Natl Acad Sci USA* 102: 13188 – 13193
66. Pozas E, Pascual M, Nguyen Ba-Charvet KT, Guijarro P, Sotelo C, Chedotal A, Del Rio JA, Soriano E (2001) Age-dependent effects of secreted Semaphorins 3A, 3F, and 3E on developing hippocampal axons: *in vitro* effects and phenotype of Semaphorin 3A (-/-) mice. *Mol Cell Neurosci* 18: 26 – 43
67. Schwarz Q, Waimey KE, Golding M, Takamatsu H, Kumanogoh A, Fujisawa H, Cheng HJ, Ruhrberg C (2008) Plexin A3 and plexin A4 convey semaphorin signals during facial nerve development. *Dev Biol* 324: 1 – 9

68. Bretin S, Reibel S, Charrier E, Maus-Moatti M, Auvergnon N, Thevenoux A, Glowinski J, Rogemond V, Premont J, Honnorat J *et al* (2005) Differential expression of CRMP1, CRMP2A, CRMP2B, and CRMP5 in axons or dendrites of distinct neurons in the mouse brain. *J Comp Neurol* 486: 1 – 17
69. Niisato E, Nagai J, Yamashita N, Abe T, Kiyonari H, Goshima Y, Ohshima T (2012) CRMP4 suppresses apical dendrite bifurcation of CA1 pyramidal neurons in the mouse hippocampus. *Dev Neurobiol* 72: 1447 – 1457
70. Yamane M, Yamashita N, Hida T, Kamiya Y, Nakamura F, Kolattukudy P, Goshima Y (2017) A functional coupling between CRMP1 and Nav1.7 for retrograde propagation of Semaphorin3A signaling. *J Cell Sci* 130: 1393 – 1403
71. Giger RJ, Cloutier JF, Sahay A, Prinjha RK, Levengood DV, Moore SE, Pickering S, Simmons D, Rastan S, Walsh FS *et al* (2000) Neuropilin-2 is required *in vivo* for selective axon guidance responses to secreted semaphorins. *Neuron* 25: 29 – 41
72. Ip JP, Fu AK, Ip NY (2014) CRMP2: functional roles in neural development and therapeutic potential in neurological diseases. *Neuroscientist* 20: 589 – 598
73. Tobe BTD, Crain AM, Winquist AM, Calabrese B, Makihara H, Zhao WN, Lalonde J, Nakamura H, Konopaske G, Sidor M *et al* (2017) Probing the lithium-response pathway in hiPSCs implicates the phosphoregulatory set-point for a cytoskeletal modulator in bipolar pathogenesis. *Proc Natl Acad Sci USA* 114: E4462 – E4471
74. Dominguez-Iturza N, Lo AC, Shah D, Armendariz M, Vannelli A, Mercaldo V, Trusel M, Li KW, Gastaldo D, Santos AR *et al* (2019) The autism- and schizophrenia-associated protein CYFIP1 regulates bilateral brain connectivity and behaviour. *Nat Commun* 10: 3454
75. Silva AI, Haddon JE, Ahmed Syed Y, Trent S, Lin TE, Patel Y, Carter J, Haan N, Honey RC, Humby T *et al* (2019) Cyfip1 haploinsufficient rats show white matter changes, myelin thinning, abnormal oligodendrocytes and behavioural inflexibility. *Nat Commun* 10: 3455
76. Liu X, Malenfant P, Reesor C, Lee A, Hudson ML, Harvard C, Qiao Y, Persico AM, Cohen IL, Chudley AE *et al* (2011) 2p15-p16.1 microdeletion syndrome: molecular characterization and association of the OTX1 and XPO1 genes with autism spectrum disorders. *Eur J Hum Genet* 19: 1264 – 1270
77. Weimann JM, Zhang YA, Levin ME, Devine WP, Brulet P, McConnell SK (1999) Cortical neurons require Otx1 for the refinement of exuberant axonal projections to subcortical targets. *Neuron* 24: 819 – 831
78. Li Z, Jagadapillai R, Gozal E, Barnes G (2019) Deletion of semaphorin 3F in interneurons is associated with decreased GABAergic neurons, autism-like behavior, and increased oxidative stress cascades. *Mol Neurobiol* 56: 5520 – 5538
79. Degano AL, Pasterkamp RJ, Ronnett GV (2009) MeCP2 deficiency disrupts axonal guidance, fasciculation, and targeting by altering Semaphorin 3F function. *Mol Cell Neurosci* 42: 243 – 254
80. Cermak T, Doyle EL, Christian M, Wang L, Zhang Y, Schmidt C, Baller JA, Somia NV, Bogdanove AJ, Voytas DF (2011) Efficient design and assembly of custom TALEN and other TAL effector-based constructs for DNA targeting. *Nucleic Acids Res* 39: e82
81. Doyle EL, Booher NJ, Standage DS, Voytas DF, Brendel VP, Vandyk JK, Bogdanove AJ (2012) TAL Effector-Nucleotide Targeter (TALE-NT) 2.0: tools for TAL effector design and target prediction. *Nucleic Acids Res* 40: W117 – W122
82. Kasparek P, Krausova M, Haneckova R, Kriz V, Zbodakova O, Korinek V, Sedlacek R (2014) Efficient gene targeting of the Rosa26 locus in mouse zygotes using TALE nucleases. *FEBS Lett* 588: 3982 – 3988
83. Magiera MM, Bodakuntla S, Ziak J, Lacomme S, Marques Sousa P, Leboucher S, Hausrat TJ, Bosc C, Andrieux A, Kneussel M *et al* (2018) Excessive tubulin polyglutamylation causes neurodegeneration and perturbs neuronal transport. *EMBO J* 37: e100440
84. Sherazee N, Alvarez VA (2013) DiOlistics: delivery of fluorescent dyes into cells. *Methods Mol Biol* 940: 391 – 400
85. Haddad-Tovolli R, Szabo NE, Zhou X, Alvarez-Bolado G (2013) Genetic manipulation of the mouse developing hypothalamus through *in utero* electroporation. *J Vis Exp* e50412
86. Ionescu A, Zahavi EE, Gradus T, Ben-Yaakov K, Perlson E (2016) Compartmental microfluidic system for studying muscle-neuron communication and neuromuscular junction maintenance. *Eur J Cell Biol* 95: 69 – 88
87. Kleele T, Marinkovic P, Williams PR, Stern S, Weigand EE, Engerer P, Naumann R, Hartmann J, Karl RM, Bradke F *et al* (2014) An assay to image neuronal microtubule dynamics in mice. *Nat Commun* 5: 4827
88. Brill MS, Marinkovic P, Misgeld T (2013) Sequential photo-bleaching to delineate single Schwann cells at the neuromuscular junction. *J Vis Exp* e4460
89. Marinkovic P, Godinho L, Misgeld T (2015) Imaging acute neuromuscular explants from Thy1 mouse lines. *Cold Spring Harb Protoc* 2015: pdb prot087692
90. Kerschensteiner M, Reuter MS, Lichtman JW, Misgeld T (2008) *Ex vivo* imaging of motor axon dynamics in murine triangularis sterni explants. *Nat Protoc* 3: 1645 – 1653
91. Schindelin J, Arganda-Carreras I, Frise E, Kaynig V, Longair M, Pietzsch T, Preibisch S, Rueden C, Saalfeld S, Schmid B *et al* (2012) Fiji: an open-source platform for biological-image analysis. *Nat Methods* 9: 676 – 682
92. Bures J, Fenton AA, Kaminsky Y, Zinyuk L (1997) Place cells and place navigation. *Proc Natl Acad Sci USA* 94: 343 – 350
93. Burghardt NS, Park EH, Hen R, Fenton AA (2012) Adult-born hippocampal neurons promote cognitive flexibility in mice. *Hippocampus* 22: 1795 – 1808
94. Stuchlik A, Petrasek T, Prokopova I, Holubova K, Hatalova H, Vales K, Kubik S, Dockery C, Wesierska M (2013) Place avoidance tasks as tools in the behavioral neuroscience of learning and memory. *Physiol Res* 62 (Suppl 1): S1 – S19
95. D'Hooge R, De Deyn PP (2001) Applications of the Morris water maze in the study of learning and memory. *Brain Res Brain Res Rev* 36: 60 – 90
96. Wesierska M, Dockery C, Fenton AA (2005) Beyond memory, navigation, and inhibition: behavioral evidence for hippocampus-dependent cognitive coordination in the rat. *J Neurosci* 25: 2413 – 2419
97. Bahník Š (2014) *Carousel Maze Manager (Version 0.4.0)* Software. Retrieved from https://github.com/bahniks/CM_Manager_0_4_0

Paper 2: *Prolyl Isomerase Pin1 Regulates Axon Guidance by Stabilizing CRMP2A Selectively in Distal Axons.*

In this paper, we showed for the first time that Pin1, a phospho-specific peptidyl-prolyl isomerase well known for its regulation of the cell growth, mitosis and cancerogenesis, is involved in nervous system development and regulates axon guidance in Sema3A gradients. We herein demonstrated that Pin1 stabilizes Cdk5-phosphorylated CRMP2A. Decreasing Pin1 levels (knockdown or knockout) inhibits axon growth and decreases CRMP2A levels. We also found that decreased Pin1 levels increases sensitivity to Sema3A-induced growth cone collapse *in vitro*, thus suggesting that Pin1 is involved in buffering of Sema3A to control axon growth in the gradient. We finally showed that knockdown of Pin1 in zebrafish embryos is capable to rescue motor neuron axon defects induced by Neuropilin1 (Sema3A receptor) knockdown. Together, our data demonstrated that Pin1 regulates Sema3A signaling both *in vitro* and *in vivo*.

For this paper, I analyzed fasciculation of callosal axons in *Pin1*$^{-/-}$ mice by DiI tracing method. Consistently with our hypothesis (that Pin1 deficiency potentiates Sema3A signaling), these experiments showed that fasciculation is unaffected by Pin1 deletion. I prepared the corresponding figures and text of the manuscript.

Article

Cell Reports

Prolyl Isomerase Pin1 Regulates Axon Guidance by Stabilizing CRMP2A Selectively in Distal Axons

Graphical Abstract

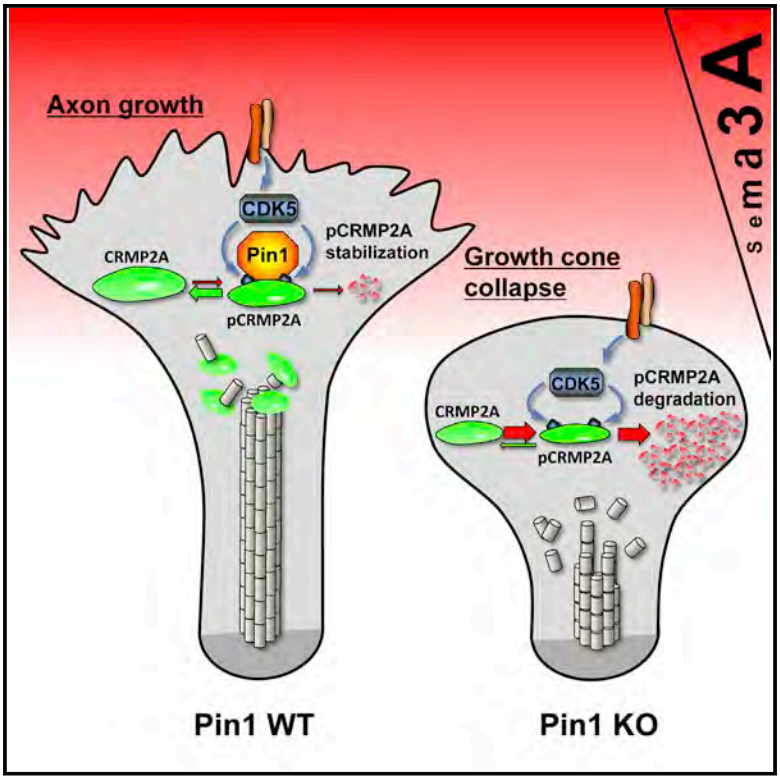

Highlights

- CRMP2A, but not CRMP2B, is the dominant isoform of CRMP2 in distal axons
- Pin1 specifically interacts with CDK5-phosphorylated CRMP2A in distal axons
- Pin1 stabilizes CRMP2A to buffer growth cone collapse induced by low levels of Sema3A
- Pin1 regulates Sema3A-driven axon guidance in embryonic development in vivo

Authors

Martin Balastik, Xiao Zhen Zhou, Meritxell Alberich-Jorda, ..., Calum Sutherland, Rosalind A. Segal, Kun Ping Lu

Correspondence

martin.balastik@fgu.cas.cz (M.B.), klu@bidmc.harvard.edu (K.P.L.)

In Brief

The molecular mechanisms controlling the precise response of growing axons to gradients of extracellular guidance cues are largely unknown. Here, Balastik et al. show that the prolyl isomerase Pin1 regulates axon growth by stabilizing CDK5-phosphorylated CRMP2A in distal axons and modulates Sema3A stimulation in growing axons in vitro and in vivo.

Balastik et al., 2015, Cell Reports *13*, 812–828
October 27, 2015
http://dx.doi.org/10.1016/j.celrep.2015.09.026

CellPress

OPEN ACCESS
CellPress

Cell Reports
Article

Prolyl Isomerase Pin1 Regulates Axon Guidance by Stabilizing CRMP2A Selectively in Distal Axons

Martin Balastik,[1,2,3,*] Xiao Zhen Zhou,[1] Meritxell Alberich-Jorda,[1,2] Romana Weissova,[2,3] Jakub Žiak,[2,3] Maria F. Pazyra-Murphy,[4,5] Katharina E. Cosker,[4,5] Olga Machonova,[2] Iryna Kozmikova,[2] Chun-Hau Chen,[1] Lucia Pastorino,[1] John M. Asara,[1] Adam Cole,[6] Calum Sutherland,[6] Rosalind A. Segal,[4,5] and Kun Ping Lu[1,7,*]

[1]Department of Medicine, Beth Israel Deaconess Medical Center, Harvard Medical School, 330 Brookline Avenue, CLS 0408, Boston, MA 02215, USA
[2]Institute of Molecular Genetics, Vídeňská 1083, 142 20 Prague 4, Czech Republic
[3]Institute of Physiology, Vídeňská 1083, 142 20 Prague 4, Czech Republic
[4]Department of Pediatric Oncology and Cancer Biology, Dana-Farber Cancer Institute, Boston, MA 02215, USA
[5]Department of Neurobiology, Harvard Medical School, Boston, MA 02115, USA
[6]Biomedical Research Institute, University of Dundee, Ninewells Hospital, Dundee DD1 9SY, Scotland, UK
[7]Institute for Translational Medicine, Fujian Medical University, Fuzhou 350108, China
*Correspondence: martin.balastik@fgu.cas.cz (M.B.), klu@bidmc.harvard.edu (K.P.L.)
http://dx.doi.org/10.1016/j.celrep.2015.09.026

SUMMARY

Axon guidance relies on precise translation of extracellular signal gradients into local changes in cytoskeletal dynamics, but the molecular mechanisms regulating dose-dependent responses of growth cones are still poorly understood. Here, we show that during embryonic development in growing axons, a low level of Semaphorin3A stimulation is buffered by the prolyl isomerase Pin1. We demonstrate that Pin1 stabilizes CDK5-phosphorylated CRMP2A, the major isoform of CRMP2 in distal axons. Consequently, Pin1 knockdown or knockout reduces CRMP2A levels specifically in distal axons and inhibits axon growth, which can be fully rescued by Pin1 or CRMP2A expression. Moreover, Pin1 knockdown or knockout increases sensitivity to Sema3A-induced growth cone collapse in vitro and in vivo, leading to developmental abnormalities in axon guidance. These results identify an important isoform-specific function and regulation of CRMP2A in controlling axon growth and uncover Pin1-catalyzed prolyl isomerization as a regulatory mechanism in axon guidance.

INTRODUCTION

During nervous system development, axonal growth is tightly regulated by an array of extracellular secreted and membrane-bound cues that interact with their receptors at active growth cones. These interactions trigger signaling cascades that alter microtubule dynamics, resulting in axonal growth, turn, stop, or retraction. While many extracellular cues and their receptors have been discovered within the last two decades (Culotti and Kolodkin, 1996; Tessier-Lavigne and Goodman, 1996), little is known about how the signaling cascades they trigger are integrated into a single unified response.

A key player in translating upstream signaling cascades into axon growth and collapse is collapsin response mediator protein 2 (CRMP2), a tubulin heterodimer-binding protein that promotes microtubule assembly (Fukata et al., 2002) and axon growth (Fukata et al., 2002; Inagaki et al., 2001; Yoshimura et al., 2005). Importantly, upon its CDK5/GSK-3β- or Rho kinase-mediated phosphorylation, the affinity of CRMP2 to tubulin is dramatically reduced, which shifts the dynamic equilibrium of microtubules toward their disassembly (Arimura et al., 2000, 2005; Uchida et al., 2005; Yoshimura et al., 2005). Consequently, stimulation of growing axons with Sema3A, which activates CDK5 (Sasaki et al., 2002) leading to CRMP2 phosphorylation (Cole et al., 2004; Uchida et al., 2005; Yoshimura et al., 2005), promotes growth cone collapse (Cole et al., 2004; Uchida et al., 2005; Yoshimura et al., 2005).

An alternative splicing of *Crmp2* gene has been recently shown to generate two isoforms that differ in their N terminus: CRMP2B and an ~100-amino-acid-longer CRMP2A (Quinn et al., 2003; Yuasa-Kawada et al., 2003). Little is known about CRMP2A, which has been reported to localize in axons rather than dendrites (Quinn et al., 2003; Yuasa-Kawada et al., 2003) and may be regulated by conformational changes (Schmidt and Strittmatter, 2007).

Conformational changes may represent an important regulatory mechanism in axon guidance, as they enable a rapid change of protein activity, which is vital to ensure the correct response of a growing axon to its changing environment. We have previously shown that pSer/Thr-Pro motifs in certain proteins can exist in two distinct *cis* and *trans* conformations and identified the prolyl isomerase Pin1, which specifically accelerates their conversion to regulate phosphorylation signaling (Yaffe et al., 1997). Furthermore, phosphorylation dramatically slows the already slow rate of isomerization of Ser/Thr-Pro bonds and renders the phosphopeptide bond resistant to the catalytic action of all other PPIases, with the exception of Pin1 (Yaffe et al., 1997). Significantly, Pin1

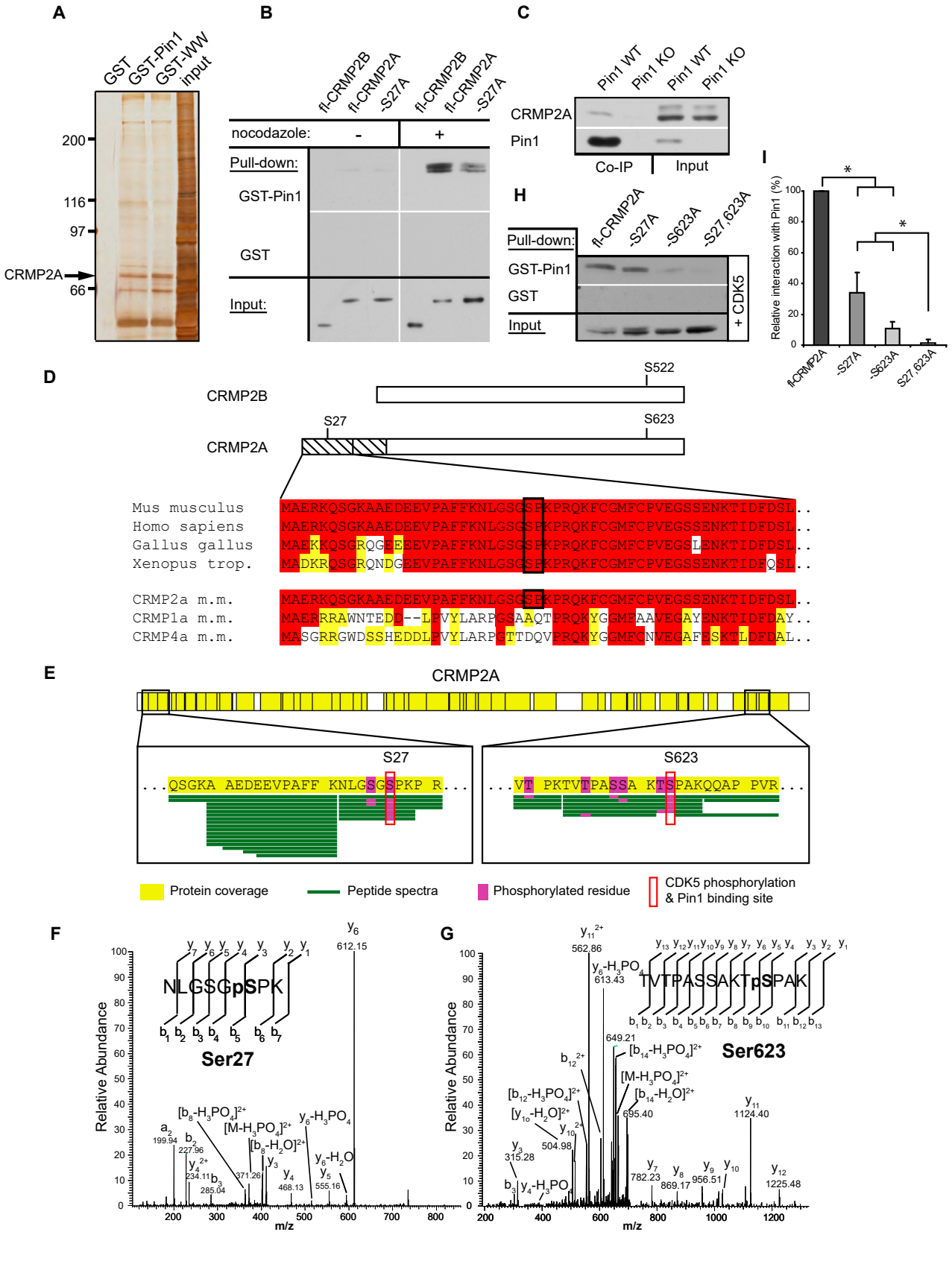

(legend on next page)

is tightly regulated on multiple levels, and its deregulation has an important role in a growing number of pathological conditions such as Alzheimer's disease (AD), where it plays a pivotal role in protecting against age-dependent neurodegeneration (Balastik et al., 2007; Liou et al., 2003; Nakamura et al., 2012; Pastorino et al., 2006). However, little is known about the function of Pin1 in healthy neurons and during development of the nervous system.

Here, using a proteomics approach, we identify CRMP2A as a major Pin1 target in postnatal neurons. Our results not only identify an important isoform-specific function for CRMP2A in regulating axon growth through Pin1-driven conformational stabilization of phosphorylated CRMP2A selectively in distal axons but also uncover a mechanism regulating axon guidance in Sema3A gradients by Pin1 both in vitro and in vivo.

RESULTS

A Proteomics Approach Identifies CRMP2A as a Major Pin1 Substrate in Neurons

To determine the role of Pin1 in healthy neurons, we used a glutathione S-transferase (GST)-Pin1 affinity purification procedure under high-salt and high-detergent conditions to identify Pin1 substrates in postnatal brains. Following SDS-PAGE and liquid chromatography-tandem mass spectrometry (LC-MS/MS), one prominent and reproducibly pulled down protein was identified as collapsin response mediator protein 2 (CRMP2) (Figures 1A and S1). Two splice forms of CRMP2 have been identified: a shorter CRMP2B (~62 kDa) (Fukata et al., 2002; Inagaki et al., 2001) and a longer CRMP2A (~73 kDa) (Yuasa-Kawada et al., 2003). The molecular weight of the Pin1-bound CRMP2 was ~73 kDa (Figure 1A), which is significant given that the shorter CRMP2B is ~20 times more abundant than CRMP2A in brain lysates (Yuasa-Kawada et al., 2003), suggesting that Pin1 might preferentially bind to CRMP2A.

To test this possibility, we overexpressed FLAG-CRMP2A and -CRMP2B in SH-SY5Y neuroblastoma cells and analyzed their binding to Pin1. Given that Pin1 binds its substrates only upon their phosphorylation (Lu et al., 2007; Lu and Zhou, 2007), we arrested the transfected SH-SY5Y cells in mitosis with nocodazole, which increases concentration of mitotic proline-directed kinases (Lu et al., 1999a). The GST-Pin1 pull-down assay confirmed Pin1 binding to CRMP2A (but not CRMP2B) only in the presence of nocodazole (Figure 1B, fl-CRMP2B, fl-CRMP2A), suggesting that phosphorylation of CRMP2A is necessary for the binding. To detect interaction between endogenous Pin1 and CRMP2A in vivo, we immunoprecipitated Pin1 from brain lysates of Pin1 wild-type (WT) and Pin1 knockout (KO) mouse embryos at embryonic day 17.5 (E17.5). CRMP2A co-immunoprecipitated with Pin1 from WT brain lysates, but not Pin1 KO controls (Figure 1C). These results indicate that Pin1 forms stable complexes selectively with CRMP2A in vitro and in vivo.

By analyzing the 5′ sequence of CRMP2A, we found that it contains a single putative Pin1 binding site around Ser27, which is highly evolutionarily conserved, but not present in other CRMP family members (Figure 1D). More importantly, analysis of the sequence with scansite (http://scansite.mit.edu) predicted Ser27 to be a likely CDK5 phosphorylation site. To determine whether Ser27 is indeed phosphorylated in CRMP2A, we overexpressed FLAG-CRMP2A in HEK293T cells together with CDK5/p25 kinase and immunoprecipitated FLAG-CRMP2A with anti-FLAG M2 monoclonal antibody beads. After elution from FLAG-beads with FLAG peptide, the purified CRMP2A was subject to GST-Pin1 pull-down and LC-MS/MS analysis. C-terminal Ser623 in the Pin1-bound CRMP2A fraction was phosphorylated (Figures 1E and 1G), as shown before for analogous Ser522 phosphorylation in CRMP2B (Gu et al., 2000). Importantly, Ser27 in CRMP2A was indeed phosphorylated in the Pin1-bound fraction (Figures 1E and 1F), suggesting that Ser27 phosphorylation might be required for Pin1 binding. To confirm this possibility, we generated S27A mutant of CRMP2A and tested its binding to Pin1 in SH-SY5Y cells. S27A mutation significantly reduced CRMP2A binding to Pin1 (Figures 1B and 1I, -S27A), demonstrating its importance for the Pin1-CRMP2A interaction. In order to test whether the C-terminal CDK5 phosphorylation site also participates on interaction with Pin1, we generated single S623A, and double S27,623A mutants and compared their binding to Pin1 in SH-SY5Y, co-transfected with CDK5/p25 (Figures 1H and 1I). Similar to S27A, single S623A mutation significantly reduced Pin1 binding and S27,623A double mutation totally abolished Pin1 binding to CRMP2A. Notably, CRMP2B is known to be phosphorylated on S522, a site equivalent to S623 of CRMP2A (Gu et al., 2000; Uchida et al., 2005). Thus, our findings that Pin1 binds to

Figure 1. Proteomic Identification of CRMP2A as a Major Pin1-Binding Protein in the Nervous System

(A) Silver staining of proteins pulled down from postnatal mouse brain lysates by Pin1 (GST-Pin1), its WW-domain (GST-WW), or control GST. The CRMP2A band identified by tandem mass spectrometry is indicated.

(B) Pin1 binding to mitotically phosphorylated CRMP2A. SH-SY5Y cells expressing FLAG-CRMP2A (fl-CRMP2A) or its S27A mutant (-S27A) were untreated or treated with nocodazole, followed by pull-down assay with GST-Pin1 (upper panels) or control GST (middle panels).

(C) Endogenous Pin1 and CRMP2A form stable complexes in the brain. Pin1 WT and KO brain lysates were subjected to co-immunoprecipitation with anti-Pin1 antibodies, followed by immunoblotting with anti-CRMP2A antibodies.

(D) CRMP2A differs from CRMP2B due to the presence of a 114-amino-acid-long N-terminal sequence containing a single Pin1-binding/CDK5 phosphorylation site at Ser27. The site is highly conserved among species but is not present in other CRMP family members that have longer forms.

(E–G) Tandem mass spectrometry detected phosphorylation of Ser27 and Ser623 in FLAG-CRMP2A pulled down by Pin1 from HEK293T cells co-transfected with FLAG-CRMP2A and CDK5/p25 (E). Underlining green lines represent peptide sequence coverage, and phosphorylation modifications are highlighted in magenta. The MS/MS spectra are shown for phosphorylation of Ser27 (F) and Ser623 (G).

(H) Ala substitution of either Ser27 (-S27A) or Ser623 (-S623A) reduced, but Ala substitution of both sites completely abolishes, binding to Pin1. SH-SY5Y cells were co-transfected with FLAG-CRMP2A or its mutants and p25/CDK5, followed by GST-Pin1 pull-down assay.

(I) Quantification of Pin1 binding to various CRMP2A mutants.

Values are means ± SEM; * $p < 0.05$. See also Figure S1.

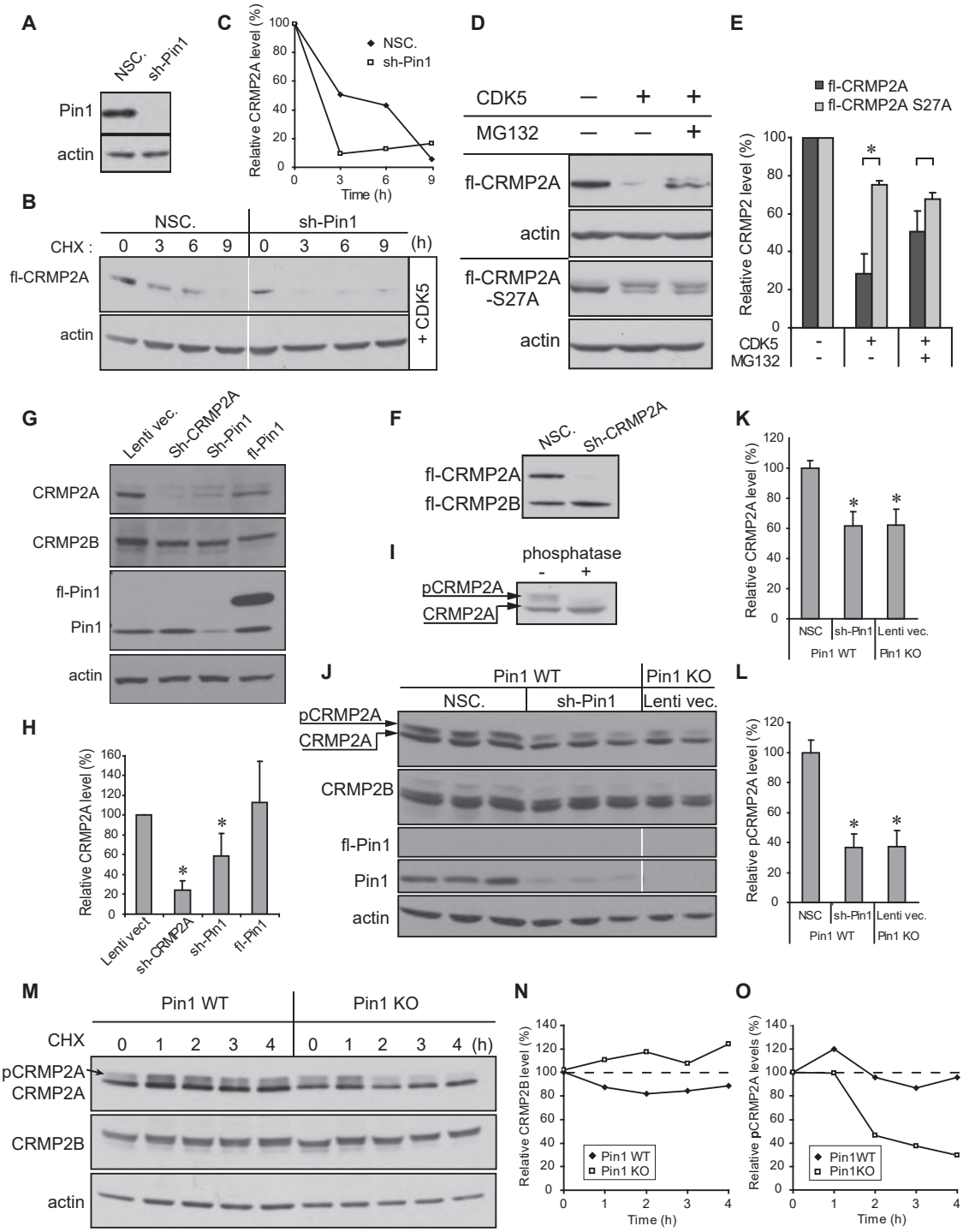

Figure 2. Pin1 Stabilizes CRMP2A Phosphorylated by CDK5.

(A–C) Pin1 KD reduces stability of transfected CRMP2A. SH-SY5Y cells were stably infected with Pin1 silencing (Sh-Pin1) or non-silencing (NSC) lentiviruses (A) and then co-transfected with FLAG-CRMP2A (fl-CRMP2A) and p25/Cdk5, followed by cycloheximide (CHX) chase to measure CRMP2A stability (B), with semiquantitative results of CRMP2A levels shown in (C).

(D and E) Phosphorylation of CRMP2A on Ser27 by CDK5 increases protein turnover. HEK293T cells were transfected with fl-CRMP2A or its Ser27Ala mutant with or without p25/Cdk5 in the absence or presence of MG132 (D), followed by immunoblotting with anti-FLAG antibodies and quantification of CRMP2A levels (E).

(F) Sh-CRMP2A silences CRMP2A, but not CRMP2B. SH-SY5Y cells were infected with Sh-CRMP2A lentiviruses, followed by immunoblotting analysis.

(legend continued on next page)

CRMP2A, but not CRMP2B (Figure 1B), indicate that the critical role in mediating CRMP2A interaction with Pin1 is played by Ser27 phosphorylation.

Pin1 Stabilizes CRMP2A Phosphorylated by CDK5

Given that Pin1 regulates protein stability of many of its substrates (Lu et al., 2007; Lu and Zhou, 2007), we asked whether CDK5 phosphorylation and Pin1 binding affects protein stability of CRMP2A. We generated stable Pin1 knockdown (KD) HEK293T cells using shPin1 or control non-silencing small hairpin RNA (shRNA) (NSC) lentiviruses (Figure 2A) and then introduced FLAG-tagged CRMP2A together with CDK5/p25 into these cells. Cells were treated with cycloheximide to inhibit de novo CRMP2A synthesis, followed by immunoblotting with the anti-FLAG antibody at various times. Under this cycloheximide chase, FLAG-CRMP2A was readily detectable at ~6 hr in NSC control cells (Figures 2B and 2C), but its degradation was greatly accelerated in Pin1 KD cells (sh-Pin1; Figures 2B and 2C). To see whether CDK5 phosphorylation triggers degradation of CRMP2A by proteasome, we analyzed protein stability of FLAG-CRMP2A transfected into HEK293T cells with or without CDK5/p25 in the absence or presence of the proteasome inhibitor MG132. Cotransfection with CDK5 potently reduced CRMP2A levels, which were largely abrogated by MG132 (Figures 2D and 2E). Moreover, S27A mutation significantly stabilized CRMP2A after co-transfection with CDK5/p25, and MG132 treatment did not lead to further stabilization (Figures 2D and 2E). These data indicate that phosphorylation of Ser27 by CDK5 promotes proteasomal degradation of CRMP2A but that Pin1 renders phosphorylated CRMP2A stable.

Next, we tested whether changes in the levels of CRMP2A or Pin1 also affect CRMP2B levels due to CRMP2 tetramerization. We generated a shRNA lentiviral vector specifically targeting CRMP2A, but not CRMP2B (Figure 2F) and examined changes of endogenous CRMP2A and CRMP2B in SH-SY5Y cells after KD of CRMP2A or Pin1. As expected, Sh-CRMP2A lentivirus effectively knocked down endogenous CRMP2A, but did not significantly affect CRMP2B levels (Figures 2G and 2H). Moreover, Pin1 KD also significantly reduced CRMP2A without affecting CRMP2B (Figures 2G and 2H). Next, to examine whether Pin1 also affects CRMP2A level in primary neurons, we cultured E15.5 Pin1 WT primary cortical neurons, infected them with either shPin1 or non-silencing lentiviruses and compared their CRMP2A and CRMP2B levels to those in Pin1 KO primary neurons. Pin1 KD or KO significantly reduced total CRMP2A levels by ~40% (Figures 2J and 2K). Western blotting of primary neuron lysates revealed the presence of multiple CRMP2A bands, suggestive of phosphorylated CRMP2A. Indeed, treating the lysates with λ phosphatase resulted in complete loss of the upper bands (Figure 2I), confirming that the mobility shift is due to CRMP2A phosphorylation. Significantly, Pin1 KD or KO reduced phosphorylated CRMP2A levels even more (~65% reduction) than total CRMP2A levels (Figures 2J and 2L), consistent with the fact that Pin1 acts on its substrates after phosphorylation (Lu et al., 1999b). Neither KO nor KD of Pin1 affected CRMP2B levels (Figure 2G). Finally, using primary cortical neurons at 6 days in vitro (DIV), we detected endogenous phosphorylated CRMP2A levels rapidly decreasing in a cycloheximide chase in Pin1 KO neurons, but not in Pin1 WT neurons (Figures 2M and 2O), and we did not detect a significant change in CRMP2B levels (Figures 2M and 2N). Together, these results indicate that Pin1 specifically binds to CRMP2A phosphorylated by CDK5 and prevents its proteasomal degradation.

CRMP2A Is the Dominant Isoform in the Distal Axons, Where It Is Stabilized by Pin1

Next, we analyzed the distribution of CRMP2A in the primary neuronal cultures. CRMP2A was detected in neuronal cell bodies and to a lesser extent in dendrites, as identified by co-staining with the neuron marker βIII tubulin (Figure S2A) and the dendritic marker MAP2 (Figure S2C). Notably, particularly high levels of CRMP2A were found in WT distal axons close to the growth cones, as detected by the axon marker tau (Figure S2B), but in Pin1 KO neurites CRMP2A was significantly reduced (Figures 3A and 3B). Moreover, similar results were also obtained by knocking down Pin1 in Pin1 WT or Pin1$^{+/-}$ neurons (Figures 3J, 3K, S2D, and S2E). Quantification of the CRMP2A signals in the axon shaft revealed a 64% reduction of CRMP2A levels ($p < 0.0001$) upon Pin1 KD, whereas no significant difference was detected in the neuron cell body ($p = 0.523$) (Figure 3M). Thus, Pin1 KO or KD reduces CRMP2A levels specifically in the axons, with little effect on the perikaryal levels.

Unexpectedly, total CRMP2 signals, as detected by antibodies recognizing both CRMP2A and CRMP2B, were also significantly reduced in distal axons after Pin1 KD (44% reduction, $p = 0.0005$) (Figures 3J, 3K, 3M, and S2). These results are rather surprising given the previous findings that CRMP2B is ~20 times more abundant than CRMP2A in total brain lysates (Yuasa-Kawada et al., 2003). They suggest that CRMP2A could be the dominant isoform of the CRMP2 pool in the vicinity of the growth cone.

In order to gain a better insight into the distribution of the two CRMP2 isoforms in neurons, we used compartmented cultures of dorsal root ganglia (DRG) neurons with Campenot chambers that allow separation of cell bodies and proximal axons (CB + PA) from distal axons (DA) in growing neurons (Figure 3G)

(G and H) KD of CRMP2A or Pin1 significantly reduces endogenous CRMP2A, but not CRMP2B. SH-SY5Y cells were infected with lentiviruses expressing CRMP2A, Sh-Pin1, or full-length Pin1 (Sh-CRMP2A, Sh-Pin1, or fl-Pin1) (G), followed by immunoblotting analysis (H).

(I) Incubation with λ phosphatase identifies CRMP2A mobility shift caused by phosphorylation. Primary cortical neuron lysates were incubated without or with λ phosphatase followed by immunoblotting analysis, identifying phosphorylated CRMP2A (pCRMP2A).

(J–L) Pin1 KD reduces CRMP2A to levels detected in Pin1-KO cells without affecting CRMP2B in primary neurons. Primary cortical neuron cultures derived from three different Pin1 WT embryos and two Pin1 KO embryos at E15.5 were infected with Sh-Pin1 lentiviruses, NSC control, or lentiviral vector control, followed by immunoblotting analysis (J) with semi-quantification of total (K) or phosphorylated (L) CRMP2A and CRMP2A levels normalized to CRMP2B.

(M–O) Pin1 KO reduces stability of endogenous phosphorylated CRMP2A in primary neurons. Cycloheximide chase was performed on primary cortical neurons at 6 DIV (M), with semiquantitative results of CRMP2B and phospho-CRMP2a levels shown in (N) and (O), respectively (means ± SD are shown; *$p < 0.05$).

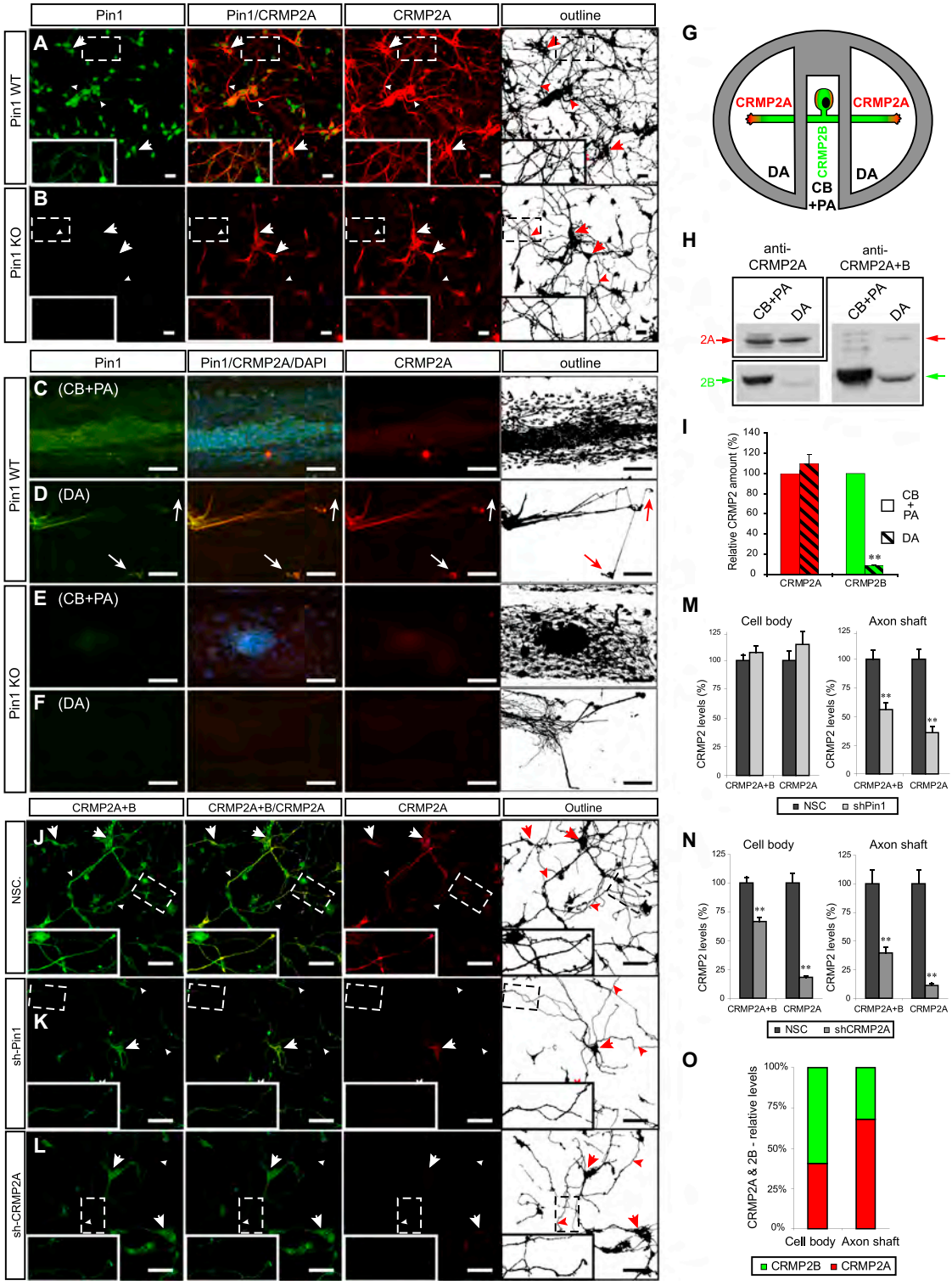

Figure 3. Pin1 Stabilizes CRMP2A Selectively in the Distal Neurites of Primary Neurons

(A and B) Pin1 KO reduces CRMP2A selectively in the distal neurites of primary neurons. CRMP2A (red) and Pin1 (green) immunostaining in Pin1 WT and KO primary cortical neurons at 3 DIV. (A) CRMP2A is expressed strongly in the soma (arrows) as well in the neurites (arrowheads) and co-localizes with Pin1 in the neurites (insets). In the Pin1 KO neurons (B), CRMP2A levels are lower in the neurites (arrowheads), but its levels in the somas are comparable to WT (arrows). (C–F) Pin1 KO reduces CRMP2A in axons. Using rat Pin1 WT DRG compartmental cultures, Pin1 was detected both in the cell body and proximal axon (CB + PA) compartment (C) and in distal axons (DA) (D) by double immunostaining, while higher expression of CRMP2A (co-localizing with Pin1) was detected in DA close to

(legend continued on next page)

(Pazyra-Murphy and Segal, 2008). First, we analyzed the distribution of Pin1 and CRMP2A in DRG neurons isolated from Pin1 WT and Pin1 KO mouse E12.5 embryos by double immunostaining. A weak CRMP2A signal was detected in the CB + PA compartments of both Pin1 WT and KO DRG neurons (Figures 3C and 3E), but a strong expression of CRMP2A was found in the DA of Pin1 WT DRG, which co-localized with Pin1 (Figure 3D). In contrast, in Pin1 KO DRG, there was only a weak CRMP2A signal in the DA compartment (Figure 3F). In order to obtain enough protein lysates to be able to quantify CRMP2A and CRMP2B levels in DA and CB + PA compartments by western blotting, we prepared DRG compartmented cultures from WT rat E14.5 embryos. Analysis of protein lysates isolated from the two compartments revealed that while CRMP2A levels were not significantly different between DA and CB + PA ($p < 0.38$) (Figures 3H and 3I), the levels of CRMP2B in DA were significantly lower ($p < 8.5E-06$) in CB + PA compartments (more than 11 times; Figures 3H and 3I), suggesting an increased role of CRMP2A in distal axons (Figure 3G). In order to estimate the relative content of CRMP2A and CRMP2B directly in the vicinity of growth cones, we used CRMP2A-specific shRNA lentiviruses to specifically silence CRMP2A in primary cortical neurons and calculated the relative contribution of CRMP2A and CRMP2B in the axon shaft and neuron cell bodies indirectly from changes of CRMP2A and total CRMP2 signals. CRMP2A KD reduced CRMP2A signals both in the cell body and the neurite by 89% and 82%, respectively ($p < 0.0001$), confirming the specificity of both the shCRMP2A construct and the CRMP2A antibodies (Figures 3J, 3L, 3N, 3O, and S2). Interestingly, upon CRMP2A KD, total CRMP2 levels decreased only 33% in neuronal cell bodies ($p < 0.0001$) (Figures 3J, 3L, and 3N) but dropped more than 60% in axon shafts ($p < 0.0001$) (Figures 3J, 3L, 3N, S2D, and S2F). Based on these data, we calculated that although CRMP2A represented only a minority (~40%) of the total CRMP2 level in neuronal cell bodies (Figure 3O) of primary cortical neurons, it accounted for 70% of the total CRMP2 pool in the axon shafts (Figure 3O). To further confirm these results, we performed similar calculations upon Pin1 KD (Figures 3J and 3K), because in our previous experiments, Pin1 KD specifically reduced CRMP2A, but not CRMP2B levels (Figures 2G, 2J, and 2M). Similar results were again obtained, with CRMP2A contributing to 69% of the total CRMP2 pool in the axon shafts. Thus, CRMP2A is the dominant isoform in the growth cone vicinity, where it is stabilized by Pin1.

Pin1 Acts on CRMP2A to Promote Axon Growth In Vitro

Given that Pin1 stabilizes CRMP2A in distal axons, we analyzed whether modulating Pin1 or CRMP2A levels would yield a significant effect on axon growth. We used lentiviral vectors to silence or overexpress Pin1 or CRMP2A in E15.5 primary cortical neurons isolated from Pin1 WT embryos and compared their axon lengths after 3 days in cultures. Whereas Pin1 overexpression did not have a significant effect on axon length (Figures 4A, 4B, and 4F), KD of either Pin1 or CRMP2A led to a significant (~40%) reduction of axon length compared to neurons infected with a non-silencing lentiviral vector (Figures 4C–4F). To confirm these results, we performed similar experiments using Pin1 KO primary cortical neurons. While, as expected, Pin1 KD had no effect (Figure 4J–4L), CRMP2A KD resulted in a small although not statistically significant decrease in axon length (Figures 4I–4L), likely due to the fact that CRMP2A in Pin1-deficient axons is already very low (Figures 3B and 3F). Importantly, re-expression of Pin1 in Pin1 KO neurons fully rescued their axon length to WT levels (Figures 4G, 4H, and 4L).

In order to test whether it is the isomerase activity of Pin1 that plays a role in axon growth, we analyzed the effect of juglone, a specific inhibitor of Pin1 isomerase activity (Hennig et al., 1998). Indeed, treatment of WT primary cortical neurons at 1 DIV for 3 days resulted in a significant ($p < 2e-06$) reduction of axon growth and CRMP2A levels in neurites (Figure S3), similar to the effect observed with Pin1 KO or KD (Figures 4A, 4D, 4G, and 4F).

Next, we tested whether overexpression of CRMP2A can rescue the reduced axon growth in Pin1 KO neurons. E15.5 Pin1 WT and KO primary cortical neurons were transfected with FLAG-CRMP2A or a vector control together with GFP to mark the transfected cells, fixed after 6 days, stained for FLAG-CRMP2A, traced, and quantified for axonal length. Similar to the endogenous CRMP2A (Figures 3 and S2), FLAG-CRMP2A was localized in Pin1 WT and KO neurons primarily in distal axons and cell bodies (Figures S3E and S3G). Pin1 WT cortical neurons transfected with CRMP2A did not show any significant increase in their axon length, as shown before (Yuasa-Kawada et al., 2003) (Figures 4M and 4O). Similar to the above experiments (Figure 4G), Pin1 KO neurons had significantly shorter

growth cones (D, arrows) when compared to the CB + PA (C). In the Pin1 KO DRG neurons, CRMP2A expression in the DA (F), but not in the CB + PA region (E), is significantly reduced.

(G–I) The relative level of CRMP2A increases in distal axon region. Lysates collected from DA and CB + PA compartments of rat primary DRG compartment cultures (G) were analyzed by western blotting using CRMP2A and total CRMP2A+B antibodies (H). Semiquantitative analysis of CRMP2A and CRMP2B levels shows significant reduction of CRMP2B levels in distal axons but no significant reduction of CRMP2A levels (I).

(J–L) Pin1 KD reduces CRMP2A and total CRMP2 selectively in neurites. Pin1 WT primary cortical neurons were infected with non-silencing (NSC), Sh-Pin1, or Sh-CRMP2A lentiviruses and immunostained for CRMP2A (red) or total CRMP2 (CRMP2A+B) (green). In NSC neurons, high levels of CRMP2A and total CRMP2 (CRMP2A+B) were detected in both the neurites (arrowhead) and the soma (arrow) (J). Pin1 KD significantly reduced CRMP2A and total CRMP2 levels in neurites (arrowhead), but not in cell bodies (arrow) (K). CRMP2A KD significantly decreases CRMP2A and total CRMP2 levels in neurites (arrowhead) as well as cell bodies (arrows) (L).

(M and N) Quantification of total CRMP2 and CRMP2A levels in Pin1 KD (shPin1) and non-silencing shRNA (NSC) control neurons in the neuronal cell body and in the axon shafts (M).

(O) Quantification of total CRMP2B and CRMP2A levels in CRMP2A KD (shCRMP2A) and control (NSC) neurons in the neuronal cell body and axon shafts. Relative distribution of CRMP2A versus CRMP2B in the cell body and distal axons calculated from (N).

Scale bars represent 20 μm (A and B) and 50 μm (C–F and J–L). Data are means ± SEM; **$p < 0.0001$. See also Figure S2.

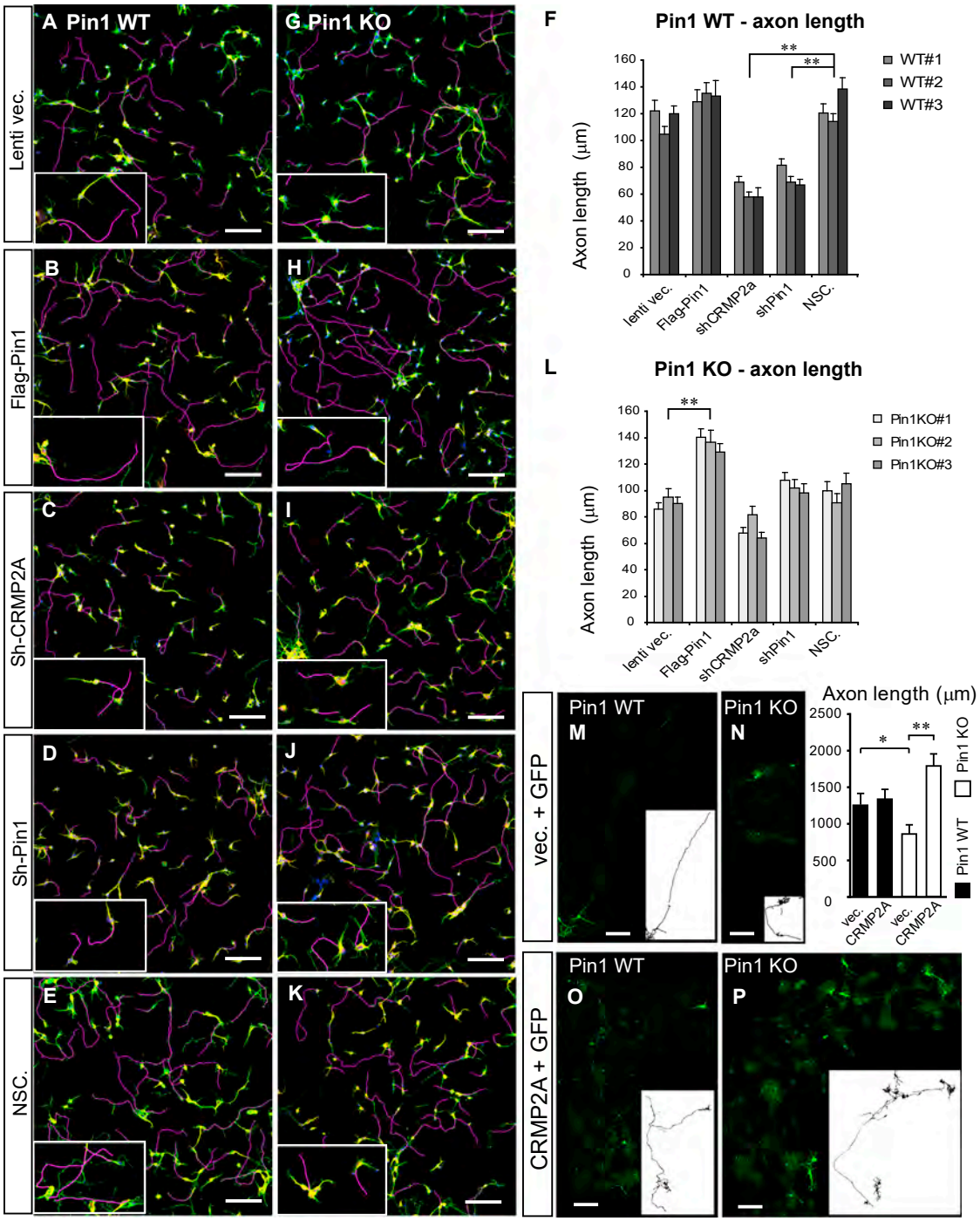

Figure 4. KD/KO of Pin1 Reduces Axon Growth in Primary Neurons and Is Fully Rescued by CRMP2A Overexpression

Primary cortical neuron cultures were derived from embryos of three independent Pin1 WT (A–F) and KO (G–L) mouse littermates and infected with lentiviruses expressing control vector (A and G), FLAG-Pin1 (B and H), Sh-CRMP2A (C and I), Sh-Pin1 (D and J), or non-silencing shRNA (NSC) (E and K) lentiviruses. Their axon length was determined at 3 DIV by immunostaining for the axon marker tau (green) and the dendrite marker MAP2 (yellow). Axon tracings are shown in violet. (F) and (L) show the means ± SEM values calculated from quantification of at least two optical fields and at least 50 neurons in each experiment. In Pin1 WT neurons, while overexpression of Pin1 had no significant effect, KD of CRMP2A or Pin1 in Pin1 WT neurons significantly reduced axon length (**$p < 0.0001$). In Pin1 KO neurons, overexpression of Pin1 completely rescued axon length, but KD of CRMP2A or Pin1 did not significantly reduce axon length, although Sh-CRMP2A neurons had slightly shorter axon. (M–P) CRMP2A overexpression fully rescues shortened axon length in Pin1 KO neurons.

(legend continued on next page)

axons, but their axon growth was fully rescued by CRMP2A overexpression (Figures 4N, 4P, and S3) even beyond the WT length, which is likely due to overcompensation. These results together indicate that Pin1 stabilizes CRMP2A in distal axons to promote axon growth.

Pin1 Buffers Semaphorin 3A-Induced Growth Cone Collapse In Vitro

Activation of CDK5 and subsequent phosphorylation and inactivation of CRMP2 has been shown to be a necessary step in Semaphorin 3A (Sema3A)-induced growth cone collapse (Cole et al., 2004; Uchida et al., 2005). In a broader context, Pin1-dependent regulation of CRMP2A upon CDK5 phosphorylation may therefore represent a regulatory mechanism in Sema3A signaling and axon guidance. To examine this possibility, we first analyzed Pin1 distribution in the active growth cones of primary DRG neurons after stimulation with Sema3A. Interestingly, Sema3A stimulation led to a rapid increase of Pin1 concentration in the vicinity of growth cones (Figures 5A, 5C, and 5D), which may reflect Pin1 binding to CRMP2A upon its Sema3A-induced phosphorylation, because Pin1 subcellular localization is driven by its binding to the substrate (Lu et al., 2002). Indeed, CRMP2A strongly colocalized with Pin1 in Sema3A-stimulated DRG axons (Figure 5A), and axons containing high levels of Pin1 also showed strong CRMP2A staining (Figure 5A). In contrast, lower levels of CRMP2A were detected in the Pin1 KO DRG axons upon Sema3A stimulation (Figure 5B), suggesting that Pin1 could be stabilizing CRMP2A in the growth cone vicinity.

Next, we examined sensitivity of Pin1 KO DRG neurons to Sema3A stimulation. Pin1 WT and KO DRGs were treated at 1 DIV with different concentrations of Sema3A, fixed, and immunostained for Pin1, β-actin (to label active growth cones), and β-tubulin (to label axons), and the number of collapsed axons was counted. Significantly, growth cone collapse was detected in Pin1 KO DRG neurons treated with 0.01 nM Sema3A (Figures 5F–5H and 5J), whereas in Pin1 WT DRG neurons, after treatment with Sema3A, concentrations more than an order of magnitude higher (Figures 5C–5E and 5J). Moreover, Pin1 levels in the growth cones significantly increased ($p < 4e\text{-}06$) in Pin1 WT DRG neurons upon stimulation with 0.05 nM Sema3A, which did not induce collapse of Pin1 WT neurons but which was already collapsing Pin1 KO neurons (Figures 5C, 5D, and 5I). Furthermore, Pin1 levels significantly ($p < 0.0374$) dropped in Pin1 WT DRGs stimulated with high Sema3A concentrations inducing collapse of most of the growth cones (Figures 5E and 5I). These results indicate that Pin1 levels in the growth cone vicinity change during Sema3A stimulation and regulate the sensitivity of the growth cones to Sema3A induced collapse.

To test whether the role of Pin1 in growth cone collapse is specific for Sema3A signaling, growth cone collapse was analyzed in Pin1 WT and KO DRGs upon treatment with lysophosphatidic acid (LPA), which has been shown to induce collapse through activation of Rho-kinase and subsequent phosphorylation of CRMP2 at Thr555 (Arimura et al., 2000). Using the same method of analysis as in the previous Sema3A experiment, treatment with 0.1, 1, 10, and 100 μM LPA produced no significant difference in the number of collapsed growth cones between Pin1 WT and KO DRGs (Figures 5L and S4), and no significant change of Pin1 levels in the growth cones was measured (Figures 5K and S4). These results indicate that Pin1 is not involved in LPA-induced growth cone collapse and further support that the effect of Pin1 on Sema3A signaling is specific.

Finally, since the effects of the guidance cues depend in vivo on their gradient rather than a particular concentration, we tested whether the increased sensitivity of Pin1 KO neurons to Sema3A collapse can be detected also by its gradient application. Mouse E12.5 DRG explants were co-cultured in collagen/Matrigel 3D cultures with SH-SY5Y cells expressing Sema3A for 44 hr, fixed, and immunostained for NF-M to trace DRG axons, and the average distance of the collapsed axons from the source of the Sema3A gradient was measured. Indeed, while no collapse was detected in Pin1 WT or KO DRG explants co-cultured with vector transfected SH-SY5Y cells (Figures 5M and 5O), a significant increase (2.1 times, $p < 2.2e\text{-}05$) of the average distance of the collapsed neurons from the gradient source was detected in Pin1 KO DRG explants as compared to Pin WT neurons (Figures 5N, 5P, and 5Q). Thus, our data demonstrate in multiple systems that Pin1 specifically buffers low levels of Sema3A stimulation, likely via stabilizing CRMP2A in the vicinity of the active growth cones.

Pin1 Regulates Sema3A-Driven Axon Guidance in Embryonic Development In Vivo

To examine whether Pin1 KO mice display any developmental abnormalities in axon guidance that might be opposite to those in Sema3A- or Nrp-1 KO mice in the peripheral nervous system (Behar et al., 1996; Gu et al., 2003), we performed whole-mount neurofilament immunostaining of Pin1 WT and KO embryos at E12.5. In contrast to Pin1 WT controls, the cranial nerves in Pin1 KO embryos displayed stunted neurite processes and a profound lack of arborization in the axons of the ophthalmic branch of the trigeminal nerve (three out of four Pin1 KO embryos, one out of five Pin1 WT) (Figures 6A–6D). Similarly, Pin1 KO spinal nerves in the cervical region also exhibited stunted and less branched projections (two out of four Pin1 KO embryos and none out of four Pin1 WT) (Figures 6E–6H). Next, to characterize the role of Pin1 in development of the CNS, we analyzed entorhino-hippocampal projections (Gu et al., 2003; Pozas et al., 2001) by staining horizontal sections of E15.5 embryonic brains with neurofilament antibodies as a marker. While the entorhinal perforant pathway projections in Pin1 heterozygous embryos at E15.5 had already reached stratum lacunosum-moleculare of the developing hippocampus proper, growth of the Pin1 KO entorhinal projections was significantly slower, reaching the border of subiculum (Figures 6I–6M, three out of three Pin1 KO embryos, none out of three $Pin1^{+/-}$), which is

Pin1 WT (M and O) and KO (N and P) primary cortical neurons were co-transfected with GFP and vector control (M and N) or GFP and FLAG-CRMP2A (O and P) and axon growth was analyzed at 7 DIV in GFP-positive neurons. Outlines of the neurons are shown in lower right boxes. Upper right panel indicates quantification of the axon lengths as mean ± SEM (*$p < 0.05$, **$p < 0.001$). Scale bars, 100 μm. (M, O, and P) are composite images of four, six, and seven images, respectively. See also Figure S3.

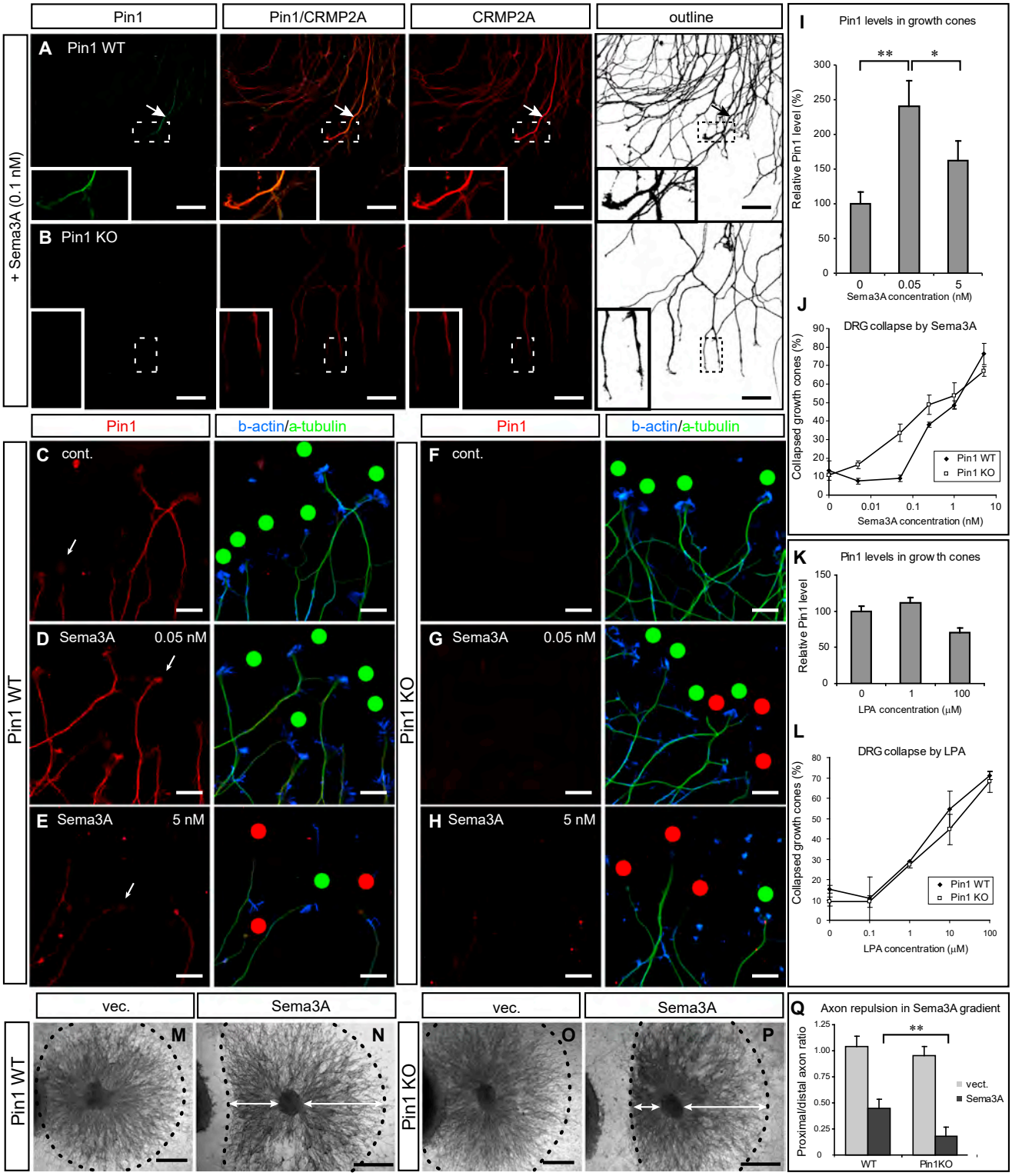

Figure 5. Pin1 KO Increases Sensitivity to Sema3A-Induced Growth Cone Collapse in Primary Dorsal Root Ganglia Neurons

(A and B) Sema3A induces colocalization of high levels of Pin1 and CRMP2A in the vicinity of growth cones (arrows) in Pin1 WT, but not Pin1 KO, DRG axons. Pin1 WT (A) and KO (B) primary DRG neurons were treated with 0.1 nM Sema3A for 30 min, followed by double immunostaining for Pin1 (green) and CRMP2A (red). (C–J) Pin1 KO increases sensitivity to Sema3A-induced growth cone collapse. Pin1 WT (C–E) and KO (F–H) primary DRG neurons were treated with different concentrations of Sema3A for 30 min, fixed, and triple immunostained with anti Pin1, β-actin, and β-tubulin antibodies, followed by growth cone collapse analysis,

(legend continued on next page)

consistent with the reduced axon growth (Figure 4) and increased sensitivity to Sema3A (Figure 5) of Pin1 KO neurons. In addition, WT entorhinal projections showed high levels of CRMP2A, but lower CRMP2A levels were found in Pin1 KO axons (Figures 6K and 6L), again corroborating the view that Pin1 is a regulator of axon growth through stabilization of CRMP2A.

Many of the pathfinding errors from the early development of Sema3A KO mice are corrected or eliminated later in development (White and Behar, 2000). To examine whether the defects in Pin1 KO embryos are also later corrected, we analyzed the perforant pathway of the entorhino-hippocampal projection in newborn (postnatal day 0 [P0]) and adult (P56) Pin1 WT and KO mice. Indeed, at both postnatal stages, the entorhino-hippocampal projections of Pin1 KO were detected in their proper destination, the stratum lacunosum-moleculare (Figures 6N and 6O; three Pin1 KO mice tested), indicating that they are corrected similar to Sema3A KO mice (White and Behar, 2000).

Apart from the Sema3A-regulated perforant pathway, entorhinal fibers send their projections via alveus (alvear pathway) (Deller et al., 1996). Although little is known about guidance cues regulating development of the alvear pathway, Sema3A likely plays a less important role, since Sema3A KO mice seem to have no alvear pathway defects, even though aberrant projections were found in the perforant pathway (Pozas et al., 2001). Similarly, neurofilament immunostaining revealed that unlike the perforant pathway, development of the alvear pathway is not affected in Pin1 KO mice (Figure S5; three out of three Pin1 KO E15.5 embryos), indicating that the axon growth defects in Pin1 KO mice are not general but rather restricted to some Sema3A-guided projections.

Sema3A deficiency has been shown before to interfere with segregation and fasciculation of somatosensory (S1) and primary motor (M1) cortex neuron projections in corpus callosum (Zhou et al., 2013). In order to characterize the growth and fasciculation of S1 axons in adult Pin1-KO mice, we analyzed DiI-labeled S1 axons in corpus callosum. We found that at corpus callosum midline Pin1-KO S1 axons were fasciculated, with similar fluorescence intensity distributions along the dorsoventral (D-V) axis in Pin1-WT and Pin1-KO mice (~120 μm) (Figure S5), i.e., comparable to the published WT values (Zhou et al., 2013) and significantly more focused than projections in Sema3A-KO or Nrp1-KO mice (~300 μm) (Zhou et al., 2013). These data are consistent with the hypothesis that Pin1 deficiency potentiates Sema3A signaling, since the phenotype of Pin1-KO S1 projections is opposite to the defasciculated S1 neuron growth in Sema3A-KO mice.

Finally, we tested genetic interaction between Pin1 and Sema3A in vivo in developing zebrafish embryos. It has been previously shown that Sema3A controls growth of motor neurons in zebrafish and that reduced Sema3A signaling, through morpholino KD of Sema3A or Neuropilin1 (NRP1), triggers aberrant branching, migration, or growth of the motor neurons in 1-day-old zebrafish embryos (Feldner et al., 2005; Sato-Maeda et al., 2006). Thus, we hypothesized that Pin1 KD could rescue the motor neuron defects induced by reduced Sema3A signaling.

To reduce Sema3A signaling we used morpholinos targeting NRP1 (NRP1-MO) (Lee et al., 2002) and designed specific Pin1-targeting morpholinos. Injection of NRP1 morpholino resulted in a 77% reduction of NRP1 levels (Figures 7A and 7B), and injection of Pin1-targeting morpholino reduced Pin1 levels by 53% by western blotting (Figures 7A and 7B). Co-injection of NRP1-MO and Pin1-MO resulted in similar reductions of Pin1 and NRP1 as a single morpholino injection (Figure 7A, line: NRP1 + Pin1 MOs). Next, we analyzed the growth of motor axons in 1-day-old zebrafish embryos using whole-mount immunostaining against anti-acetylated tubulin. KD of Pin1 did not significantly affect the relative number of zebrafish embryos with defective motor neuron growth (27% versus 17% in control) (Figures 7C and 7D). Similarly, the average number of defective axons per embryo (Figures 7C and 7D) was also not significantly changed in Pin1-MO embryos (0.40 versus 0.22 in control). In contrast, NRP1 KD significantly increased number of embryos with aberrant motor neuron growth (85%), with an average of 2.05 defects per embryo (Figures 7C and 7D). Importantly, simultaneous KD of NRP1 and Pin1 significantly reduced the relative number of defective embryos (44%) as well as the average number of defective motor neurons per embryo (0.95) (Figures 7C and 7D), indicating that Pin1 KD partially rescues the motor neuron defects induced by NRP1 KD. Taken together, our data demonstrate that Pin1 regulates Sema3A signaling both in vitro and in vivo.

DISCUSSION

Using a proteomics approach, we identified CRMP2A as a Pin1 substrate in developing neurons and a regulator of axon growth. Pin1 binds to and stabilizes CRMP2A phosphorylated by CDK5 on the Ser27-Pro motif. As a result, Pin1 KO, KD, or inhibition reduces CRMP2A levels primarily in the vicinity of growth cones, where CRMP2A is surprisingly the dominant isoform. Moreover, KO, KD, or inhibition of Pin1 results in similar inhibition of axon growth that is fully rescued by overexpression of either Pin1 or CRMP2A. Furthermore, stimulation with Sema3A, but not LPA, drives Pin1 to the vicinity of growth cones, where it co-localizes with CRMP2A, and Pin1 KO neurons are more sensitive to Sema3A-induced growth cone

with the percentage of growth cone collapse being shown in (J). Red dots, collapsed growth cones; green dots, intact growth cones. Intensity of Pin1 immunostaining in DRG growth cones (C) significantly increases upon low (non-collapsing) Sema3A stimulation (D) and is reduced upon high Sema3A stimulation (E); the quantification after normalization to β-tubulin levels is shown (I).

(K and L) Stimulation with LPA induces similar growth cone collapse in Pin1 WT and KO DRG neurons (L) and does not affect Pin1 levels in the growth cones (K).

(M–Q) Pin1 KO significantly increases sensitivity to Sema3A-induced growth cone collapse in collagen 3D co-cultures. SH-SY5Y cells were transfected with empty vector (M and O) or Sema3A expression vector (N and P) and co-cultured with Pin1 WT (M and N) or KO (O and P) DRG. Proximal/distal axon length ratio was measured (N and P, arrows) upon NF-M immunostaining and quantified (Q).

Scale bars represent 50 μm (A and B), 20 μm (C–H), and 500 μm (M–P); *$p < 0.05$; **$p < 0.0001$. Values are means ± SEM. See also Figure S4.

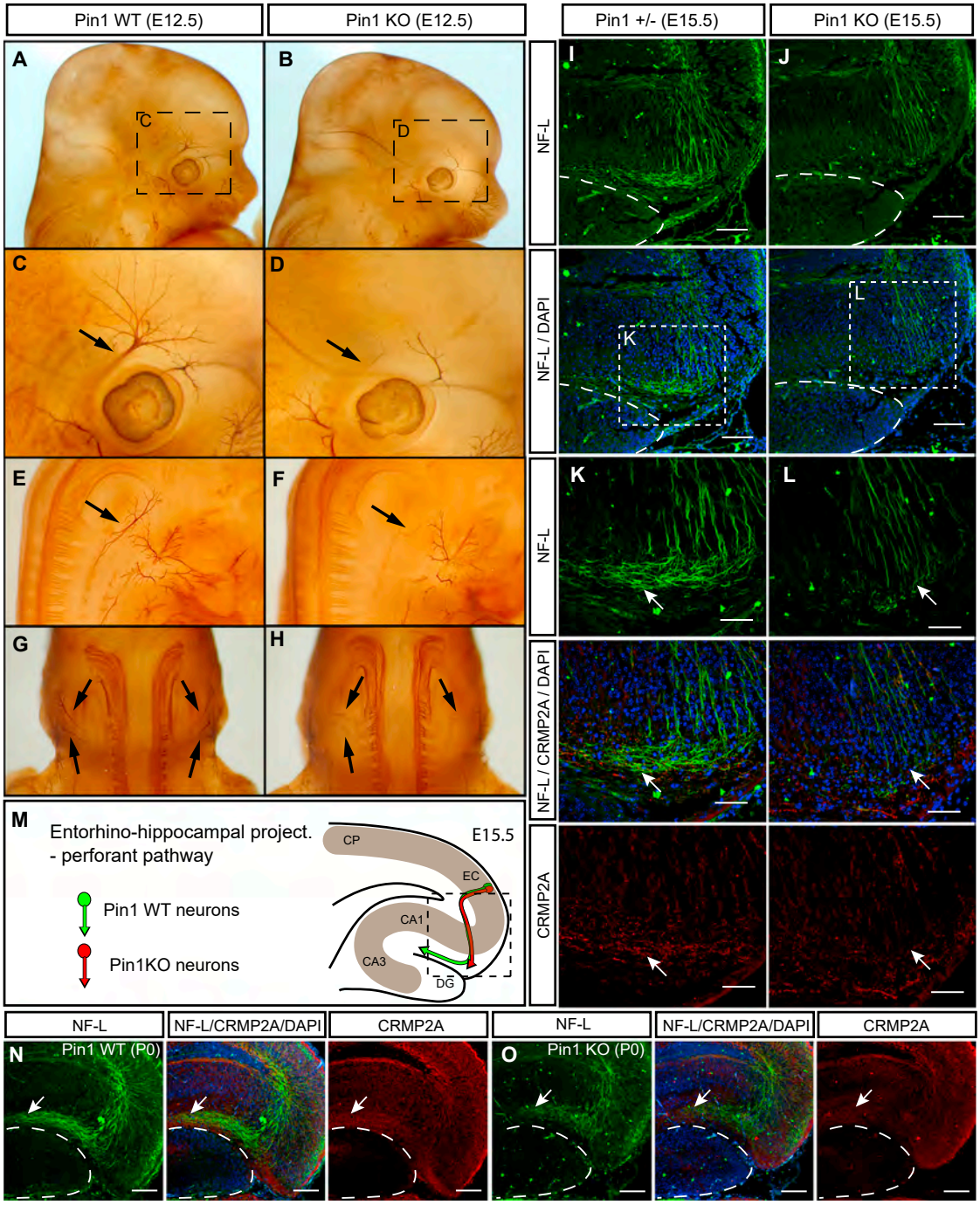

Figure 6. Pin1 KO Leads to Developmental Axon Growth Defects in the Peripheral Nervous System and CNS

(A–H) Axons of the cranial and spinal nerves are less extensive and complex in Pin1 KO embryos. The cranial (A–D) and spinal (E–F) nerves were analyzed in E12.5 Pin1 WT (A, C, E, and G) and KO (B, D, F, and H) embryos by whole-mount immunohistochemistry for neurofilaments. In Pin1 KO embryos, stunted neurite processes are found in the ophthalmic branch of the trigeminal nerve (B and D, arrows) and in the lateral branches of the cervical spinal nerves (F and H, arrows).

(I–M) Entorhino-hippocampal perforant projections are significantly shorter in Pin1 KO embryos at E15.5. Horizontal sections of E15.5 embryos were stained for neurofilament light subunit (NF-L) (green) to trace growth of entorhinal perforant projections toward the stratum lacunosum-moleculare (s.l-m) of the hippocampus proper in Pin1$^{+/-}$ (I) and KO (J) mice. The dashed lines indicate borders of the developing dentate gyrus. (K and L) Pin1 KO shorter perforant projections are associated with reduced CRMP2A level (red) in growth cones, as indicated by arrows. (M) Schematic drawing of the entorhino-hippocampal perforant

(legend continued on next page)

collapse by bath or gradient application. In several regions of the peripheral nervous system and CNS, Pin1 null mice display selective developmental axon growth defects that are associated with reduced CRMP2A and opposite to those found in Sema3A or Nrp-1 mutant mice. Finally, KD of Pin1 partially rescues developmental defects generated in motor neurons by downregulation of Sema3A signaling. These results not only identify an important isoform-specific function for CRMP2A in regulating axon growth but also uncover a regulatory mechanism in which Pin1 promotes axon growth by stabilizing CRMP2A selectively in distal axons and buffers low-level Sema3A stimulation.

Regulation of Axon Growth and Collapse by Pin1

Pin1 is so far the only known prolyl isomerase that specifically catalyzes isomerization of Ser/Thr-Pro bonds upon their phosphorylation. Significantly, proline in the pSer/Thr-Pro motif breaks symmetry of the polypeptide chain and makes it prone to conformational changes. Phosphorylation of the motif significantly restrains the spontaneous isomerization of the pSer/Thr-Pro motif and makes it accessible to Pin1, which can then isomerize the motif to acquire a particular conformation, having a major impact on protein function, localization, and stability (Lu and Zhou, 2007; Pastorino et al., 2006; Yaffe et al., 1997).

Here, we showed that Pin1 binds to and stabilizes CRMP2A in distal axons and that Sema3A stimulation drives Pin1 to the vicinity of growth cones. Thus, the presence of Pin1 in the growth cones might serve as a buffer for Sema3A-induced CDK5 activation and help to maintain an active, intact growth cone until a certain threshold concentration of Sema3A is reached. Consequently, depletion of Pin1 leads to reduced axon growth or premature growth cone collapse. Thus, Pin1 levels in axons may play an important role in the fine-tuning of axon guidance. Importantly, we see that some neuronal projections in Pin1 KO mice (e.g., the ophthalmic branch of the trigeminal nerve) are particularly stunted, less brunched, or misguided, whereas other neurons are not affected. Moreover, while the distribution of the phenotypical changes of Pin1 KO neurons follows in many areas (e.g., ophthalmic branch, entorhino-hippocampal projections) the phenotypical pattern of Sema3A KO mice (although with an opposite effect on axonal growth), the patterns are different in some regions. For example, in the developing DRG, Sema3A or Nrp1 deficiency leads to a loss of segmentation and increased growth and defasciculation of lateral branches of spinal neurons (Kitsukawa et al., 1997). In Pin1 KO embryos, DRG segmentation is preserved (in agreement with the opposite effects of Pin1 and Sema3A deficiencies; data not shown), but the growth of the spinal nerves is more variable. While lateral branches of spinal nerves showed reduced growth in the cervical area (Figures 6F–6H; two out of four Pin1 KO and zero out of five Pin1 WT embryos), the innervation of forelimbs, which is also defasciculated in Sema3A- or Nrp1-deficient mice, was not affected in Pin1 KO mice (zero out of four Pin1 KO embryos, not shown). The discrepancy indicates that the Pin1-KO phenotype is not simply the opposite of the Sema3A-KO or NRP1-KO phenotype in every part of the developing nervous system. This could be due either to different abilities of various neurons to compensate for Pin1 deficiency (e.g., by other, non-phospho-specific isomerases) or to other members of the CRMP family rescuing the CRMP2A insufficiency, all resulting in a different vulnerability of different neurons to Pin1 deficiency. Consistent with this hypothesis, we found that the levels of Pin1 in distal DRG axons in vitro are highly variable and correlate with CRMP2A levels (Figure 5A). These results indicate that expression and/or distribution of Pin1 in the growing DRG axons is regulated, giving some neurons a growth advantage in a Sema3A-rich environment and at the same time making these neurons more vulnerable to Pin1 deficiency. Similarly, it has been shown in human and mouse that various levels of Pin1 expression in different brain regions inversely correlate with their vulnerability to neurofibrillary degeneration in AD (Liou et al., 2003).

In order to test genetic interaction between Sema3A signaling and Pin1 in vivo, we utilized the model of motor neuron development in zebrafish. It has been shown before that downregulation of Sema3A signaling results in defective growth of motor neurons (Feldner et al., 2005; Sato-Maeda et al., 2006). Interestingly, KD of Sema3A homologs in zebrafish produced contradictory results in terms of their effect on motor neuron growth, likely due to compensation by other Sema3A homologs (zebrafish has two) or by other guidance/signaling molecules. For this reason, in order to silence Sema3A signaling in motor neurons, we chose KD of Nrp1, which has been reproducibly shown to induce motor neuron growth defects (Feldner et al., 2005; Sato-Maeda et al., 2006). However, Nrp1 has also been shown to serve also as VEGF receptor (Gu et al., 2003), indicating that by knocking down Nrp1, we also interfere with the VEGF pathway. Importantly, in zebrafish, VEGF KD has been shown per se not to induce significant motor neuron defects in motor neurons, while it did have a clear effect on vascular development (Feldner et al., 2005). Thus, while VEGF could play a minor role in the Pin1 rescue experiments in zebrafish, the major effect was via Sema3A signaling.

Based on our data, we propose a model for the role of Pin1 in regulating Sema3A-driven axonal growth and retraction (Figures 7E–7H). In the absence of Sema3A, CRMP2A present in distal axons is not phosphorylated, promoting tubulin assembly and axon growth in both Pin1 WT and KO neurons (Figure 7E). Low levels of Sema3A stimulation activate CDK5, which phosphorylates CRMP2A at Ser27 and Ser623, attracting Pin1 to the vicinity of the growth cones, where it binds and stabilizes phosphorylated CRMP2A (Figure 7F). In the dynamic equilibrium between phosphorylation and dephosphorylation, Pin1-dependent stabilization of phoshpo-CRMP2A sustains the pool of active CRMP2A in the growth cone. In the absence of Pin1, low levels

pathway at E15.5 in the presence or absence of Pin1 as shown in (I)–(L). CP, cortical plate; EC, entorhinal cortex; DG, dentate gyrus; CA1, CA3, hippocampal regions.

(N and O) Developmental defects are corrected later during development of Pin1 KO mice. Entorhinal perforant projections are detected in s.l-m of both Pin1 WT (N, arrow) and KO (O, arrow) newborn mice. Lower levels of CRMP2A are present in perforant projections in s.l-m in Pin1 KO mice (O).

Scale bars represent 100 μm (I, J, N, and O) and 50 μm (K and L). See also Figure S5.

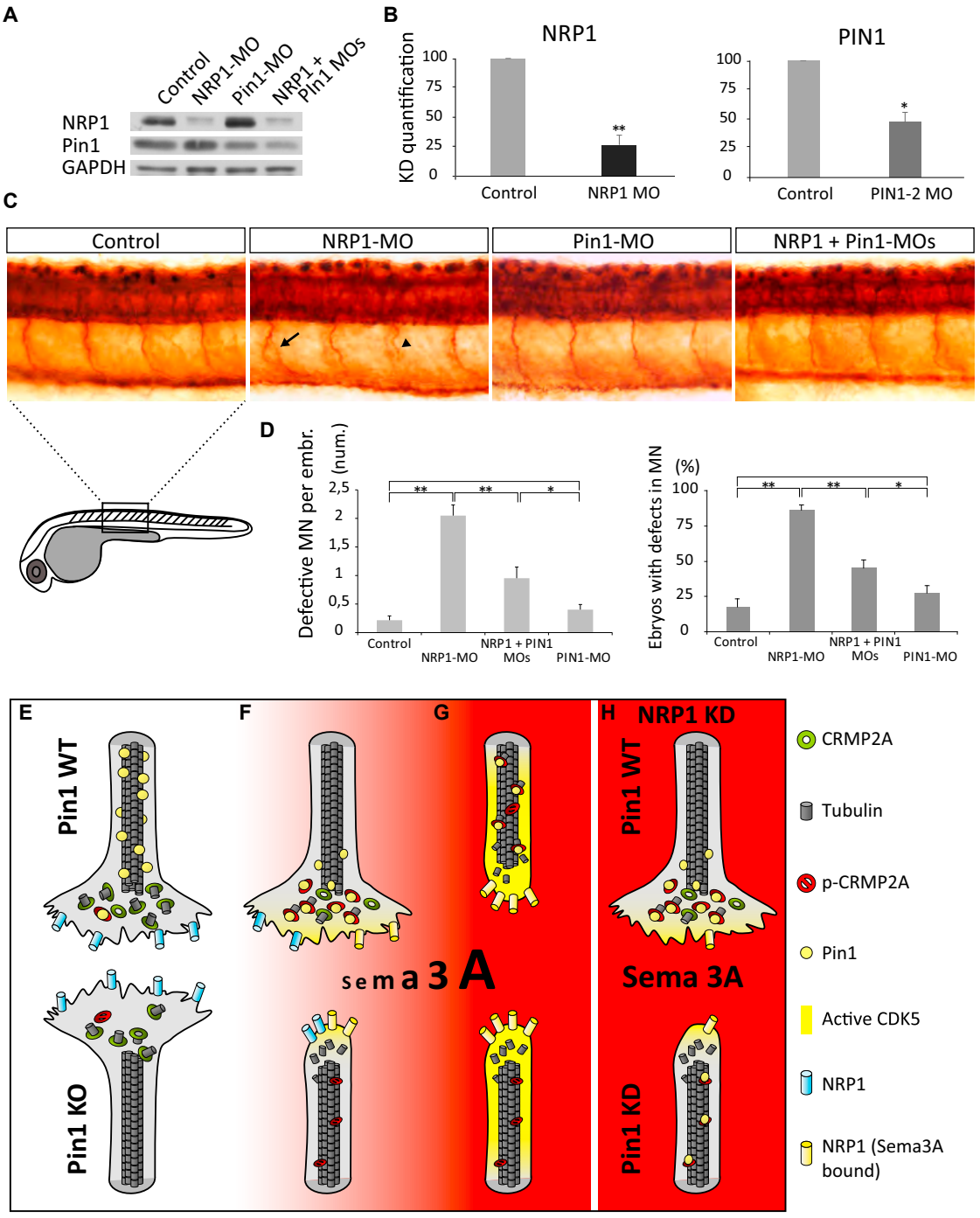

Figure 7. Pin1 Regulates Sema3A Signaling In Vivo

(A and B) Efficiency of single- and double-morpholino KD of zPin1 and NRP1 in 24-hr zebrafish embryos analyzed by immunoblotting (A), with quantification in (B).

(C) Whole-mount immunostaining of acetylated tubulin in 1-day-old zebrafish embryos demonstrates increased incidence of developmental motor neurons defects, e.g., aberrant branching (arrow) or truncated growth (arrowhead), upon NRP1 KD, which is reduced upon co-injection of Pin1-MO.

(D) Quantification of developmental defects in morpholino-injected zebrafish embryos. Control embryos and Pin1-MO injected do not significantly differ in percentage of defective embryos (17% versus 27%, respectively) or average number of defects per embryo (0.22% versus 0.4%, respectively). NRP1 KD induces defective development in 85% of embryos, with an average of 2.05 defects per embryo. Co-injection of Pin1-MO significantly reduces number of defective embryos (44%) as well as the average number of defects per embryo (0.95).

(E–H) A model of Pin1's role in Sema3A-driven axonal growth and retraction.

Values are means ± SEM.

of CRMP2A phosphorylation eventually deplete the growth cone of the active CRMP2A pool, which shifts the dynamic microtubule equilibrium toward growth cone collapse. In the presence of high levels of Sema3A (Figure 7G), activated CDK5 and GSK-3β hyperphosphorylate CRMP2A to reduce its affinity for tubulin heterodimers, leading to growth cone collapse in both Pin1 WT and KO neurons. Reduction of Sema3A signaling (e.g., by KD of NRP1) (Figure 7H) triggers aberrant growth of axons in Sema3A gradients, but simultaneous KD of Pin1 increases sensitivity to Sema3A signaling and partially rescues the defective growth of NRP1 KD axons.

EXPERIMENTAL PROCEDURES

Detailed descriptions of experimental procedures can be found in the Supplemental Experimental Procedures.

Animals

All experimental procedures were performed in compliance with animal protocols approved by the Institutional Animal Care and Use Committee (IACUC) at Beth Israel Deaconess Medical Center. Zebrafish were mated, staged, and raised as described previously (Westfield, 2000) in accordance with IACUC guidelines.

GST Pull-Down Assays and Co-immunoprecipitations

GST pull-down, immunoprecipitation, and immunoblotting analyses were performed as described previously (Lu et al., 1999b; Yaffe et al., 1997) using SH-SY5Y or HEK293T cell lysates incubated with either GST or GST-Pin1 or a specific antibody and then glutathione agarose beads or protein Agarose, followed by washing elution and western blotting analysis.

Histology, Immunohistochemistry, and Immunocytochemistry

Histology, immunohistochemistry, immunocytochemistry, and quantification were carried out as described previously (Lee et al., 2009; Liou et al., 2003; Pastorino et al., 2006). Briefly, mice were intracardially perfused with PBS and ice-cold fixative solution (4% paraformaldehyde [PFA] in PBS) and embedded in paraplast, and 8-μm-thick horizontal sections were cut. For immunohistochemistry, sections were incubated with primary antibodies in PBS with 10% fetal calf serum (FCS) and 0.2% Tween 20 overnight at 4°C and washed three times for 10 min with 0.2% Tween 20 in PBS. Secondary antibodies were then applied and incubated for 1 hr at room temperature, washed twice with 0.2% Tween/PBS, and embedded in Mowiol with 1 μg/ml DAPI. Whole-mount immunohistochemistry of E12.5 embryos was performed as described previously (Klymkowsky and Hanken, 1991). Briefly, embryos were fixed with 4% PFA in PBS overnight at 4°C and soaked in 80% methanol. Endogenous peroxidase activity was quenched with 3% H_2O_2 in Dent's fixative (80% methanol and 20% DMSO) for 3 hr, then embryos were washed with PBS with 1% Tween 20 and incubated with the anti-neurofilament antibody clone 2H3 (1:100) for 2 days at room temperature. Detection of 2H3 was performed with the Vectastain ABC elite kit (Vector). Horseradish peroxidase (HRP) activity was detected with diaminobenzidine. For immunocytochemistry, cells grown on coverslips coated with poly-D lysine (Invitrogen) and laminin (BD Biosciences) were fixed in ice-cold 4% PFA/PBS (15 min) and methanol (−20°C, 6 min), washed in PBS, and incubated with primary antibodies overnight at 4°C. Fluorescence secondary antibodies were then applied and incubated for 1 hr at room temperature, washed twice with PBS, and embedded in Mowiol with 0.5 μg/ml DAPI. Fluorescent images were taken using a confocal microscope (Zeiss, LSM510), and outlines were generated using ImageJ software. For quantification of total CRMP2 versus CRMP2A levels upon CRMP2A or Pin1 KD, a median signal intensity was measured in each soma and axon shaft of all neurons within at least four randomly picked optical fields using ImageJ software. Mean relative values ± SEM were then calculated for either of the two neuron parts in all experimental conditions. Phase-contrast microscopy images were taken using a Nikon eclipse TS100.

S1 neuron anterograde tracing was performed in 4-month-old Pin1 KO and Pin1 WT animals by inserting carbocyanide dye DiI crystals into the 4% PFA-fixed brains in the S1 region as described previously (Niquille et al., 2009). The DiI was left to penetrate for 3–4 weeks in 4%PFA/PBS at 37°C. 100 μm coronal brains sections were cut on vibratome (Leica), images taken using Nikon eclipse TS100 and Leica SP8 microscopes, and analyzed by ImageJ software.

Axon Length and Indirect CRMP2A/B Content Measurement

Primary neurons transduced with lentiviral vectors or treated with Juglone were fixed at 4 DIV and immunostained for MAP2 (dendritic) and tau (axonal) markers. The length of the longest neurite showing specific tau but no MAP2 signal was traced and measured as that of an axon using NeuroJ software. Axon length of neurons in at least 2 randomly selected optical fields and at least 50 neurons in total were counted for each construct and mean axon length ± SEM was calculated. In Pin1 KO rescue experiments, neurons co-transfected with GFP and FLAG-CRMP2A (or empty vector) were fixed at 7 DIV and co-immunostained for βIII tubulin to distinguish primary neurons and FLAG to visualize distribution of FLAG-CRMP2A in the neurons. The length of the longest neurite showing (in the FLAG-CRMP2A-transfected neurons) specific CRMP2A localization close to the growth cones was traced and measured as that of an axon at 7 DIV using the NeuronJ plugin of ImageJ software.

For indirect measurement of CRMP2A/B levels, the median intensity of CRMP2A and total CRMP2(A+B) were measured in the axon shafts using ImageJ software in primary cortical cultures at 4 DIV (3 days after infection with silencing or control lentiviral vectors), with the longest neurite considered as axon. Average CRMP2A and total CRMP2(A+B) intensity of axons from at least three optical fields was calculated and used to quantify the relative CRMP2A/B levels.

Morpholino KD in Zebrafish

Morpholinos targeting NRP1 and Pin1 were synthesized by Gene Tools and injected into one- to two-cell-stage embryos. 1-day-old zebrafish embryos were immunostained using acetylated-tubulin antibodies (Sigma) and analyzed.

Cell Cultures, Transfection, and Infection

Human neuroblastoma SH-SY5Y and human embryonic carcinoma HEC293T cell lines were cultured in DMEM with 10% FCS and transfected using PEI 25 kDa, linear (Polysciences, 1 μg/ml in H_2O). Primary cortical neurons were prepared and cultured as described previously (Nikolic et al., 1996). Briefly, cortices were dissected from E15.5 embryonic brains in Hank's balanced salt solution (HBSS; Invitrogen) supplemented with 20 mM HEPES (pH 7.3). Cells were dissociated with trypsin, plated onto laminin- and poly-D-lysine-coated glass coverslips, and maintained in neurobasal media supplemented with factor B27 (Invitrogen) and 2 mM L-glutamine (Invitrogen). Primary neuron transfection was performed 1 day after plating using Lipofectamine 2000 (Invitrogen) as described elsewhere (Ohki et al., 2001).

pLKO.1 lentiviral vector (Open Biosystems) was used for gene silencing experiments with the following target sequences: human Sh-Pin1, 5′-CCA CCGTCACACAGTATTTAT-3′; mouse Sh-Pin1, 5′-CCGGGTGTACTACTTCA ATCA-3′; non-silencing control, 5′-ATCTCGCTTGGGCGAGAGTAAG-3′; and Sh-CRMP2A, 5′-TGGAAGGGTCCTCGGAGAA-3′. For lentiviral overexpression FLAG-Pin1 was subcloned into pLenti6/V5-GW/lacZ vector (Invitrogen). HEK293T cells were co-transfected with lentiviral construct, a Gag-Pol construct and a VSV-G envelope construct using PEI. Virus containing supernatants was collected at 48 and 72 hr after transfection, filtered though 0.45-μm filter, and concentrated using a Centricon Plus-70 100,000 MWCO column (Millipore). Primary neurons were infected 18 hr after plating; 4 hr after infection, the media was replaced, and infected neurons were selected 1.5 days after infection with 1 μg/ml puromycin.

Pin1 inhibition in primary cortical neurons was performed 1 day after plating by adding 4 μM Juglone into the media.

Compartmented chamber cultures were prepared from rat E15.5 DRG neurons.

Statistics

The Student's t test and nonparametric Man-Whitney test were used to determine the statistical significance of the experimental results.

SUPPLEMENTAL INFORMATION

Supplemental information includes Supplemental Experimental Procedures and five figures and can be found with this article online at http://dx.doi.org/10.1016/j.celrep.2015.09.026.

ACKNOWLEDGMENTS

We are grateful to G. Finn and M.-L. Luo for Pin1 KO mice, A. Kolodkin for AP-Sema3A plasmid, G. Alvarez-Bolado for comments on the manuscript, and O. Svoboda and Z. Kozmik for advice regarding the work with the zebrafish model. We also thank S. Hagen for Confocal Microscopy Core (NIH grant S10 RR017927). The work was supported by MŠMT Návrat grant LK11213 and Marie Curie CIG grant PCIG12-GA-2012-334431 (to M.B.), MŠMT Návrat grant LK21307 and the Czech Science Foundation (GACR, project 15-03796S) (to M.A.-J.), MŠMT grant LO1419 (to O.M. and I.K.), and NIH grants R01AG039405 and R01AG046319 and National Natural Science Foundation of China grant U1205024 (to K.P.L.).

Received: January 22, 2015
Revised: July 21, 2015
Accepted: September 8, 2015
Published: October 15, 2015

REFERENCES

Arimura, N., Inagaki, N., Chihara, K., Ménager, C., Nakamura, N., Amano, M., Iwamatsu, A., Goshima, Y., and Kaibuchi, K. (2000). Phosphorylation of collapsin response mediator protein-2 by Rho-kinase. Evidence for two separate signaling pathways for growth cone collapse. J. Biol. Chem. *275*, 23973–23980.

Arimura, N., Ménager, C., Kawano, Y., Yoshimura, T., Kawabata, S., Hattori, A., Fukata, Y., Amano, M., Goshima, Y., Inagaki, M., et al. (2005). Phosphorylation by Rho kinase regulates CRMP-2 activity in growth cones. Mol. Cell. Biol. *25*, 9973–9984.

Balastik, M., Lim, J., Pastorino, L., and Lu, K.P. (2007). Pin1 in Alzheimer's disease: multiple substrates, one regulatory mechanism? Biochim. Biophys. Acta *1772*, 422–429.

Behar, O., Golden, J.A., Mashimo, H., Schoen, F.J., and Fishman, M.C. (1996). Semaphorin III is needed for normal patterning and growth of nerves, bones and heart. Nature *383*, 525–528.

Cole, A.R., Knebel, A., Morrice, N.A., Robertson, L.A., Irving, A.J., Connolly, C.N., and Sutherland, C. (2004). GSK-3 phosphorylation of the Alzheimer epitope within collapsin response mediator proteins regulates axon elongation in primary neurons. J. Biol. Chem. *279*, 50176–50180.

Culotti, J.G., and Kolodkin, A.L. (1996). Functions of netrins and semaphorins in axon guidance. Curr. Opin. Neurobiol. *6*, 81–88.

Deller, T., Adelmann, G., Nitsch, R., and Frotscher, M. (1996). The alvear pathway of the rat hippocampus. Cell Tissue Res. *286*, 293–303.

Feldner, J., Becker, T., Goishi, K., Schweitzer, J., Lee, P., Schachner, M., Klagsbrun, M., and Becker, C.G. (2005). Neuropilin-1a is involved in trunk motor axon outgrowth in embryonic zebrafish. Dev. Dyn. *234*, 535–549.

Fukata, Y., Itoh, T.J., Kimura, T., Ménager, C., Nishimura, T., Shiromizu, T., Watanabe, H., Inagaki, N., Iwamatsu, A., Hotani, H., and Kaibuchi, K. (2002). CRMP-2 binds to tubulin heterodimers to promote microtubule assembly. Nat. Cell Biol. *4*, 583–591.

Gu, Y., Hamajima, N., and Ihara, Y. (2000). Neurofibrillary tangle-associated collapsin response mediator protein-2 (CRMP-2) is highly phosphorylated on Thr-509, Ser-518, and Ser-522. Biochemistry *39*, 4267–4275.

Gu, C., Rodriguez, E.R., Reimert, D.V., Shu, T., Fritzsch, B., Richards, L.J., Kolodkin, A.L., and Ginty, D.D. (2003). Neuropilin-1 conveys semaphorin and VEGF signaling during neural and cardiovascular development. Dev. Cell *5*, 45–57.

Hennig, L., Christner, C., Kipping, M., Schelbert, B., Rücknagel, K.P., Grabley, S., Küllertz, G., and Fischer, G. (1998). Selective inactivation of parvulin-like peptidyl-prolyl cis/trans isomerases by juglone. Biochemistry *37*, 5953–5960.

Inagaki, N., Chihara, K., Arimura, N., Ménager, C., Kawano, Y., Matsuo, N., Nishimura, T., Amano, M., and Kaibuchi, K. (2001). CRMP-2 induces axons in cultured hippocampal neurons. Nat. Neurosci. *4*, 781–782.

Kitsukawa, T., Shimizu, M., Sanbo, M., Hirata, T., Taniguchi, M., Bekku, Y., Yagi, T., and Fujisawa, H. (1997). Neuropilin-semaphorin III/D-mediated chemorepulsive signals play a crucial role in peripheral nerve projection in mice. Neuron *19*, 995–1005.

Klymkowsky, M.W., and Hanken, J. (1991). Whole-mount staining of Xenopus and other vertebrates. Methods Cell Biol. *36*, 419–441.

Lee, P., Goishi, K., Davidson, A.J., Mannix, R., Zon, L., and Klagsbrun, M. (2002). Neuropilin-1 is required for vascular development and is a mediator of VEGF-dependent angiogenesis in zebrafish. Proc. Natl. Acad. Sci. USA *99*, 10470–10475.

Lee, T.H., Tun-Kyi, A., Shi, R., Lim, J., Soohoo, C., Finn, G., Balastik, M., Pastorino, L., Wulf, G., Zhou, X.Z., and Lu, K.P. (2009). Essential role of Pin1 in the regulation of TRF1 stability and telomere maintenance. Nat. Cell Biol. *11*, 97–105.

Liou, Y.C., Sun, A., Ryo, A., Zhou, X.Z., Yu, Z.X., Huang, H.K., Uchida, T., Bronson, R., Bing, G., Li, X., et al. (2003). Role of the prolyl isomerase Pin1 in protecting against age-dependent neurodegeneration. Nature *424*, 556–561.

Lu, K.P., and Zhou, X.Z. (2007). The prolyl isomerase PIN1: a pivotal new twist in phosphorylation signalling and disease. Nat. Rev. Mol. Cell Biol. *8*, 904–916.

Lu, P.J., Wulf, G., Zhou, X.Z., Davies, P., and Lu, K.P. (1999a). The prolyl isomerase Pin1 restores the function of Alzheimer-associated phosphorylated tau protein. Nature *399*, 784–788.

Lu, P.J., Zhou, X.Z., Shen, M., and Lu, K.P. (1999b). Function of WW domains as phosphoserine- or phosphothreonine-binding modules. Science *283*, 1325–1328.

Lu, P.J., Zhou, X.Z., Liou, Y.C., Noel, J.P., and Lu, K.P. (2002). Critical role of WW domain phosphorylation in regulating phosphoserine binding activity and Pin1 function. J. Biol. Chem. *277*, 2381–2384.

Lu, K.P., Finn, G., Lee, T.H., and Nicholson, L.K. (2007). Prolyl cis-trans isomerization as a molecular timer. Nat. Chem. Biol. *3*, 619–629.

Nakamura, K., Greenwood, A., Binder, L., Bigio, E.H., Denial, S., Nicholson, L., Zhou, X.Z., and Lu, K.P. (2012). Proline isomer-specific antibodies reveal the early pathogenic tau conformation in Alzheimer's disease. Cell *149*, 232–244.

Nikolic, M., Dudek, H., Kwon, Y.T., Ramos, Y.F., and Tsai, L.H. (1996). The cdk5/p35 kinase is essential for neurite outgrowth during neuronal differentiation. Genes Dev. *10*, 816–825.

Niquille, M., Garel, S., Mann, F., Hornung, J.P., Otsmane, B., Chevalley, S., Parras, C., Guillemot, F., Gaspar, P., Yanagawa, Y., and Lebrand, C. (2009). Transient neuronal populations are required to guide callosal axons: a role for semaphorin 3C. PLoS Biol. *7*, e1000230.

Ohki, E.C., Tilkins, M.L., Ciccarone, V.C., and Price, P.J. (2001). Improving the transfection efficiency of post-mitotic neurons. J. Neurosci. Methods *112*, 95–99.

Pastorino, L., Sun, A., Lu, P.J., Zhou, X.Z., Balastik, M., Finn, G., Wulf, G., Lim, J., Li, S.H., Li, X., et al. (2006). The prolyl isomerase Pin1 regulates amyloid precursor protein processing and amyloid-beta production. Nature *440*, 528–534.

Pazyra-Murphy, M.F., and Segal, R.A. (2008). Preparation and maintenance of dorsal root ganglia neurons in compartmented cultures. J. Vis. Exp. *20*, 951.

Pozas, E., Pascual, M., Nguyen Ba-Charvet, K.T., Guijarro, P., Sotelo, C., Chédotal, A., Del Río, J.A., and Soriano, E. (2001). Age-dependent effects of secreted Semaphorins 3A, 3F, and 3E on developing hippocampal axons: in vitro effects and phenotype of Semaphorin 3A (-/-) mice. Mol. Cell. Neurosci. *18*, 26–43.

Quinn, C.C., Chen, E., Kinjo, T.G., Kelly, G., Bell, A.W., Elliott, R.C., McPherson, P.S., and Hockfield, S. (2003). TUC-4b, a novel TUC family variant, regulates neurite outgrowth and associates with vesicles in the growth cone. J. Neurosci. *23*, 2815–2823.

Sasaki, Y., Cheng, C., Uchida, Y., Nakajima, O., Ohshima, T., Yagi, T., Taniguchi, M., Nakayama, T., Kishida, R., Kudo, Y., et al. (2002). Fyn and Cdk5 mediate semaphorin-3A signaling, which is involved in regulation of dendrite orientation in cerebral cortex. Neuron *35*, 907–920.

Sato-Maeda, M., Tawarayama, H., Obinata, M., Kuwada, J.Y., and Shoji, W. (2006). Sema3a1 guides spinal motor axons in a cell- and stage-specific manner in zebrafish. Development *133*, 937–947.

Schmidt, E.F., and Strittmatter, S.M. (2007). The CRMP family of proteins and their role in Sema3A signaling. Adv. Exp. Med. Biol. *600*, 1–11.

Tessier-Lavigne, M., and Goodman, C.S. (1996). The molecular biology of axon guidance. Science *274*, 1123–1133.

Uchida, Y., Ohshima, T., Sasaki, Y., Suzuki, H., Yanai, S., Yamashita, N., Nakamura, F., Takei, K., Ihara, Y., Mikoshiba, K., et al. (2005). Semaphorin3A signalling is mediated via sequential Cdk5 and GSK3beta phosphorylation of CRMP2: implication of common phosphorylating mechanism underlying axon guidance and Alzheimer's disease. Genes Cells *10*, 165–179.

Westfield, M. (2000). The Zebrafish Book. A Guide for the Laboratory Use of Zebrafish (Danio rerio), Fourth Edition (University of Oregon Press).

White, F.A., and Behar, O. (2000). The development and subsequent elimination of aberrant peripheral axon projections in Semaphorin3A null mutant mice. Dev. Biol. *225*, 79–86.

Yaffe, M.B., Schutkowski, M., Shen, M., Zhou, X.Z., Stukenberg, P.T., Rahfeld, J.U., Xu, J., Kuang, J., Kirschner, M.W., Fischer, G., et al. (1997). Sequence-specific and phosphorylation-dependent proline isomerization: a potential mitotic regulatory mechanism. Science *278*, 1957–1960.

Yoshimura, T., Kawano, Y., Arimura, N., Kawabata, S., Kikuchi, A., and Kaibuchi, K. (2005). GSK-3beta regulates phosphorylation of CRMP-2 and neuronal polarity. Cell *120*, 137–149.

Yuasa-Kawada, J., Suzuki, R., Kano, F., Ohkawara, T., Murata, M., and Noda, M. (2003). Axonal morphogenesis controlled by antagonistic roles of two CRMP subtypes in microtubule organization. Eur. J. Neurosci. *17*, 2329–2343.

Zhou, J., Wen, Y., She, L., Sui, Y.N., Liu, L., Richards, L.J., and Poo, M.M. (2013). Axon position within the corpus callosum determines contralateral cortical projection. Proc. Natl. Acad. Sci. USA *110*, E2714–E2723.